The Host-Microbiota Axis in Chronic Wound Healing

Amber Rose Stafford, BSc. (Hons), MRes, University of Hull

Thesis submitted for the degree of Doctor of Philosophy (PhD)

The University of Hull and The University of York

Hull York Medical School

May 2023

Abstract

Chronic, non-healing skin wounds represent a substantial area of unmet clinical need, leading to debilitating morbidity and mortality in affected individuals. Due to their high prevalence and recurrence, chronic wounds pose a significant economic burden. Wound infection is a major component of healing pathology, with up to 70% of wound-associated lower limb amputations preceded by infection. Despite this, the wound microbiome remains poorly understood. Studies outlined in this thesis aimed to characterise the wound microbiome and explore the complex interactions that occur in the wound environment. Wound samples were analysed using a novel long-read nanopore sequencing-based approach that delivers quantitative species-level taxonomic identification. Clinical wound specimens were collected at both the point of lower-extremity amputation and via a pilot clinical trial evaluating extracorporeal shockwave therapy (ESWT) for wound healing. Combining microbial community composition, host tissue transcriptional (RNAseq) profiling, with clinical parameters has provided new insight into healing pathology. Specific commensal and pathogenic organisms appear mechanistically linked to healing, eliciting unique host response signatures. Patient- and site-specific shifts in microbial abundance and community composition were observed in individuals with chronic wounds versus healthy skin. Transcriptional profiling (RNAseq) of the wound tissue revealed important insight into functional elements of the host-microbe interaction. Finally, ESWT was shown to confer beneficial effects on both cellular and microbial aspects of healing. High-resolution long-read sequencing offers clinically important genomic insights, including rapid wide-spectrum pathogen identification and antimicrobial resistance profiling, which are not possible using current culture-based diagnostic approaches. Thus, data presented in this thesis provides important new insight into complex host-microbe interactions within the wound microbiome, providing new and exciting future avenues for diagnostic and therapeutic approaches to wound management.

Table of Contents

List of Figures

List of Tables

Abbreviations

AGE - Advanced glycosylation product

AMP - Antimicrobial peptide

AMR - Antimicrobial resistance

ANOSIM - Analysis of similarities

ANOVA - Analysis of variance

αSMA - α-smooth muscle actin

AST - Antimicrobial susceptible testing

ATCC - American Type Culture Collection

bFGF - Basic fibroblast growth factor

CDC - Centre for Disease Control

Anti IFN-γ – Anti Interferon-γ

APS - Ammonium persulfate

bFGF – Basic Fibroblast Growth Factor

CAMP/LL-37 - Cathelicidin antimicrobial peptide

CD31 - Cluster of differentiation 31

CD68 - Cluster of Differentiation 68

CLSM - Confocal laser scanning microscopy

CoNS - Coagulase-negative *Staphylococci*

DAMP - Damage-associated molecular pattern

DAPI - 4’,6-diamidino-2-phenylindole

DEJ - Dermal-epidermal junction

DFU - Diabetic foot ulcer

DM - Diabetes mellitus

DNA - Deoxyribonucleic acid

DPBS - Dulbecco's phosphate-buffered saline

EGF - Epidermal growth factor

CE – Cornified Envelope

CFU - Colony forming units

REC - Research Ethics Committee

REDOX - Reduction-oxidation

CHROMagar - Chromogenic Staphylococcus selective agar

CLEC7A - C-type lectin domain family 7 member A

CLEC7A - Dectin-1

COG - Clusters of Orthologous

DbS - Diabetic skin

DEFB1 - Defensin beta 1

DEFB103A - Defensin beta 103A

DEFB104A - Defensin beta 104A

DEFB4A - Defensin beta 4A

DFD - Diabetic foot disease

DMT1 – The Divalent Metal Transporter 1

ECM – Extracellular Matrix

EDF - Energy flux density

EGF – Epidermal Growth Factor

FB - Flush Buffer

FGF – Fibroblast Growth Factor

FGF-2 – Fibroblast Growth Factor 2

FLT - Flush Tether

Fmoles – Femtomoles

GAPDH - Glyceraldehyde 3-phosphate dehydrogenase

GBP- British pound sterling

GO - Gene Ontology

GPAC - Gram-positive anaerobic cocci

HaCaT - Immortalized human keratinocytes

HB-EGF – Heparin-Binding EGF-Like Growth Factor

HbA1c - Glycated haemoglobin

HDF – Human Dermal Fibroblast

HMP - Human Microbiome Project

HPC - High Performance Computing

HS – Healthy Skin

IDF - International Diabetes Federation

IFN-γ - Interferon-γ

IL-1 – Interleukin 1

IL-13 – Interleukin 13

IL-4 – Interleukin 4

IL-6 – Interleukin 6

K1 – Keratin 1

K10 – Keratin 10

K14 – Keratin 14

K5 – Keratin 5

K6 – Keratin 6

KB - Kilobase

KGF – Keratinocyte Growth Factor

KO – Knockout

LB - Loading Beads

LPS – Lipopolysaccharides

M0 – Unpolarised Macrophage

M1 – Classically Activated Macrophage

M2 – Alternatively Activated Macrophage

Mb - Mega bases

MCP-1 – Monocyte Chemoattractant Protein 1

MF – Myofibroblasts

MG- Meggitt-Wagner

MHA - Mueller Hinton agar

MIC - Minimum inhibitory concentration

mJ/mm2 - mJ per millimetre square

mm^{2-} Millimetre squared

MMPs - Matrix metalloproteinases

MRSA - Methicillin-resistant *Staphylococcus aureus*

MSSA - Methicillin-susceptible *Staphylococcus aureus*

MTS - Tetrazolium Assay

MYD88 - Myeloid differentiation primary response 88

NDbS - Non-diabetic skin

NE – Neutrophil Elastase

NET – Neutrophil extracellular trap

NFKB1 - Nuclear factor kappa B subunit 1

NFW - Nuclease free water

Ng – Nanogram

nm - Nanometer

NHS – National Health Service

NI – Non-infected

NLRs - Nod-like receptors

NOD1 - Nucleotide binding oligomerization domain containing 1

NOD2 - Nucleotide binding oligomerization domain containing 2

Nos2 – Nitric Oxide Synthase

OD - Optical density

ONT - Oxford Nanopore Technology

OTU - Operational taxonomic unit

PAMP - Pathogen-associated molecular pattern

PBS - Phosphate-buffered saline

PC - Principal component

PDGF - Platelet-Derived Growth Factor

PDGF-BB - Platelet-Derived Growth Factor Subunit B

pEMT - Partial epithelial–mesenchymal transition

PERMANOVA - Permutational multivariate analysis of variance

PERMDISP - Permutational analysis of multivariate dispersions

PKC - Protein kinase C

PCoA - Principal coordinate analysis

PCR - Polymerase chain reaction

PDE - Phosphodiesterase

PDGF - Platelet-derived growth factor

PN - Peripheral neuropathy

PRR - Pattern recognition receptor

PSMα - Phenol-soluble modulin alpha

PVC - Polyvinyl chloride

PVD - Peripheral vascular disease

QC - Quality control

QIIME - Quantitative Insights into Microbial Ecology

qPCR - Quantitative polymerase chain reaction

qPCR - Quantitative polymerase chain reaction

RAP - Rapid Sequencing Adapter

RCF - Relative centrifugal force

RIPK2 - Receptor interacting serine/threonine kinase 2

RNASE7 - Ribonuclease A family member 7

RNAseq - RNA sequencing

RNS - Reactive nitrogen species

RONS - Reactive oxygen and nitrogen species

ROS - Reactive oxygen species

rRNA - Ribosomal ribonucleic acid

RT - Room temperature

ROS – Reactive Oxygen Species

RRM - Revolutions per minute

RAP - Rapid sequencing adapter

RCA - Resazurin colourimetric agar

rCFU - Relative colony forming units

S100A7 - S100 calcium binding protein A7(S100A7)

S100A7 – Psoriasin

S100A8 - S100 calcium binding protein A8(S100A8)

S100A8/A9 – Calprotectin

S100A9 - S100 calcium binding protein A9(S100A9)

SA10757 - *S. aureus* strain 10757

SAMtools - Sequence Alignment/Map

SB – Stratum Basale

SC – Stratum Corneum

SCF - Sample collection fluid

SD - Seborrheic dermatitis

SEM - Standard error of the mean

SG - Stratum granulosum

SQB - Sequencing buffer

SS - Stratum spinosum

TGF-β - Transforming growth factor-beta

SDS - Sodium dodecyl sulphate

SG – Stratum Granular

SQB - Sequencing Buffer

SS – Stratum Spinosum

TEMED – Tetramethylethylenediamine

TF - Transferrin

TFR1 – Transferrin Receptor 1

TGF-β – Transforming Growth Factor Beta

TGF-β1 – Transforming Growth Factor Beta 1

TGFα – Transforming Growth Facotr Alpha

TGFβ1 - transforming growth factor beta 1

TICAM1 - Toll like receptor adaptor molecule 1

TIRAP - TIR domain containing adaptor protein

TLR - Toll-like receptor

TNF - Tumour Necrosis Factor

TRAM1 - Translocation associated membrane protein 1

Tsp1 – Thrombospondin 1

TSS - Total sum scaling

TUNEL - Terminal deoxynucleotidyl transferase dUTP nick end labelling

USB - Universal serial bus

USD - United States dollar

UT - University of Texas

UV - Ultraviolet

VBNC - Viable but non culturable

VEGF - Vascular endothelial growth factor

VLU - Venous leg ulcer

VSMC - Vascular smooth muscle cell

VST - Variance stabilising transformation

WHO - World Health Organisation

WT - Wild type

ZOI - Zone of inhibition

3D - Three-dimensional

Thesis Associated Presentations

2023, Oxford Nanopore Technologies Scientific Meeting - Newcastle, UK. "*Scratching the surface of the skin microbiome.*"

2022, International PhD Student Scientific Conference - Hradec Kralove, Czech Republic. 'Application of long-read sequencing to profile the chronic wound microbiota'.

2022, Infection Disease Hull University Teaching Hospitals Academic Meeting – Hull, UK.

'Application of long-read sequencing to profile the chronic wound microbiota'.

2021, Vascular Societies Annual Scientific Meeting - Manchester, UK. "*The mechanistic effects of shockwave therapy on an ex-vivo human wounded skin model.*"

2021, Allam Lecture - University of Hull, UK *"*Chronic wound microbiota profiling using long-read sequencing*."*

2019, Nanopore Community Meeting - New York, USA. *"Optimisation of* long-read nanopore-based sequencing technology for chronic wound microbiome profiling*."*

2019, Northern Bioinformatics User Group, Bradford, UK. *"Optimisation of a Bioinformatic pipeline for analysis of Nanopore data."*

2018, School of Life Sciences, Annual Research Conference, University of Hull, UK. *"The Impact of Ferric Iron on Cell Populations in the Cutaneous Wound Healing Environment."*

Thesis Associated Publications

Tissue Iron Promotes Wound Repair via M2 Macrophage Polarization and the Chemokine (C-C Motif) Ligands 17 and 22" – Wilkinson, Roberts, **Stafford** et al., (2019)

Thesis Associated Awards

Annual (2017) Highest Achieving Human Biology/ Biomedical Science Student (£250 GBP)

Oxford Nanopore Bursary ($674 USD)

University of Hull Doctoral Conference Fund (£200 GBP)

Ann Watson Employability Grant (£500 GBP)

HYMS Student Research Conference Bursary (£200 GBP)

Acknowledgements

Thank you to my clinical and academic supervisory team, Prof. Mat Hardman, Dr Holly Wilkinson, Dr Angela Oates, Mr George Smith and Mr Daniel Carradice for their encouragement and supervision throughout this journey. Thanks to all team members of the Hardman Lab and Daisy building, including Dr Sammi Iveson, Sophie Upson, Kayleigh Banyard, Dr Michelle Rudden and Dr Victoria Green for their friendship, technical expertise, and overall support.

Declaration

I confirm that this work is original and that if any passage(s) or diagrams(s) have been copied from academic papers, books, the internet or any other sources these are clearly identified by the use of quotation marks and the reference(s) is fully cited. I certify that, other than where indicated, this is my own work and does not breach the regulation of HYMS, the University of Hull or the University of York regarding plagiarism or academic conduct in examinations. I have read the HYMS Code of Practice on Academic Misconduct, and state that this piece of work is my own and does not contain any unacknowledged work from any other sources'.

1 Introduction

1.1 Skin Structure and Function

The human skin functions as a specialised interface between the internal body and the harsh external environment (Gallo et al., 2017). The dynamic structure of the skin, and its consequent physicochemical properties, allow it to act as an efficient mechanical barrier, providing defence against exogenous agents such as chemicals, pathogens and UV light (Lee et al., 2008) (Figure 1.1). In addition, this barrier role extends multiple immune-related functions, including the maintenance of the commensal skin microflora (Byrd et al., 2018). Collectively, these functions are conducted by the combined activity of two distinct layers that compose the overall skin structure, the epidermis, and the dermis (Gallo et al., 2017).

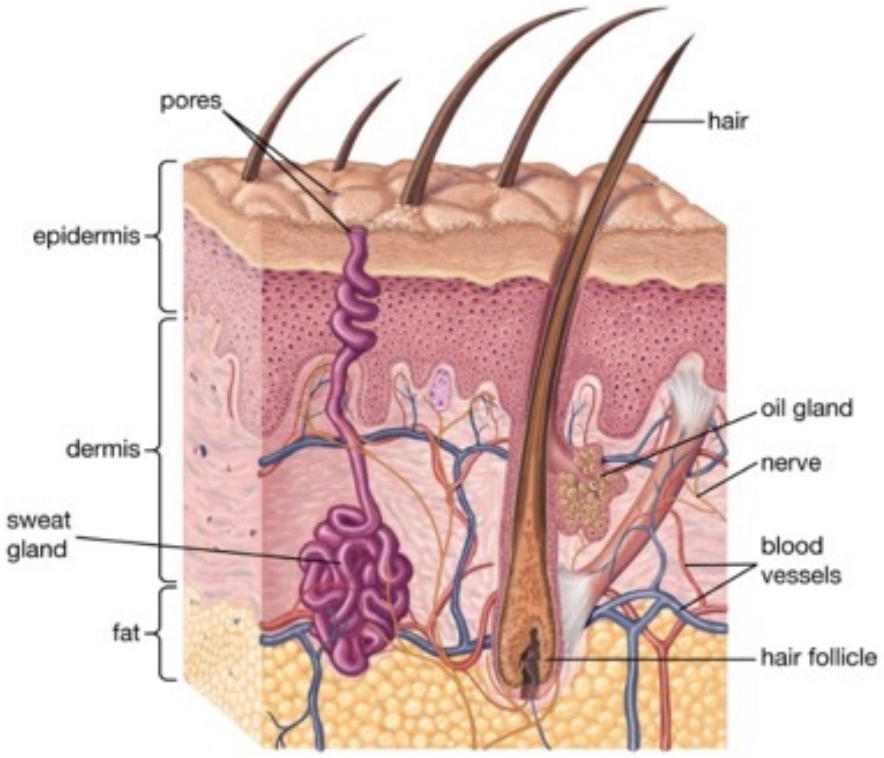

Figure 1. 1: Anatomy of human skin. Human skin is composed of three principal layers, the epidermis, the dermis, and the hypodermis. The dermis connects to the epidermis via the basement membrane and contains hair follicles and sweat glands. Image taken from Wong and Chang, 2009.

1.1.1 Epidermis

The epidermis exists as the outermost superficial portion of the skin, enduring constant exposure to the harsh external environment (Fore et al., 2006). The epidermal structure can be categorised into five distinct layers, the stratum basal, stratum spinosum, stratum granulosum, stratum lucidum and the stratum corneum (Koster et al., 2009) (Figure 1.2). The stratum basal exists as the deepest innermost epidermal layer, interconnected with the dermis via the basal lamina and action of connecting hemidesmosomes (Boer et al., 2016). Cells found residing in this layer include melanocytes and mitotically active cuboidal to columnar epidermal stem cells (Ojeh et al., 2015). Daughter keratinocytes produced by these rapidly proliferating cells begin to differentiate, withdrawing from the cell cycle and migrating upwards towards the outermost epidermal surface (Boer et al., 2016). Directly above the stratum basal exists the stratum spinosum (Ojeh et al., 2015; Simpson et al., 2011). Referred to as the prickle layer, this 8-10 cell dense layer includes irregular, polyhedral keratinocytes with cytoplasmic protrusions that connect with neighbouring cells (Ojeh et al., 2015; Simpson et al., 2011). Keratinocytes of the stratum granulosum adopt a flatter diamond shape, enclosing both lamellar and keratohyalin granules (Boer et al., 2016). Within these granules are keratin precursors and glycolipids, components that facilitate cellular aggregation, keratin filament crossing linking and ultimately epidermal barrier maintenance (Boer et al., 2016).

Located between the stratum granulosum and stratum corneum layers, the stratum lucidum is a clear cellular deposit layer consisting mainly of eledin, an intermediate transformation product of keratin (Koster, 2009). Finally, the outmost layer of the epidermal surface layer is the stratum corneum (Koster, 2009). Approximately 20-30 cell layers thick, the stratum corneum is comprised of cornified anucleate keratinocytes forming horny keratin-rich scales that eventually slough off to the environment (Falconer et al., 2001). Keratinocytes contained within this epidermal layer function to secrete defensins, host peptides which play a key role in initial cutaneous innate immunity (Falconer et al., 2001).

Overall, keratinocytes compose approximately 90-95% of the cellular component of the epidermis (Boer et al., 2016). Keratin, the main protein component of this population, is

expressed by epidermal keratinocytes in a site-specific and differentiation-dependent manner (Celli et al., 2010). As keratinocytes differentiate and migrate up to join the stratum corneum (Celli et al., 2010), tight regulation of the intracellular keratin network is essential for effective epidermal turnover and successful skin barrier function (Gutowska-Owsiak et al., 2020). Basal keratinocytes of progenitor status, eventually differentiate to form layers of the epidermis (Cohen et al., 2022). The expression of Keratin 14 (K14) and Keratin 5 (K5) occurs in mitotically active basal layer keratinocytes (Figure 1.2) (Cohen et al., 2022). As these cells commit to terminal differentiation, cells of the basal layer stop dividing, migrating upward into the suprabasal compartment and initiating the expression of Keratin 1 (K1) and Keratin 10 (K10) (Celli et al., 2010). As the process of vertical migration continues, markers of late keratinocyte differentiation are expressed, including involucrin, filaggrin, and loricrin (Koster, 2009). These differentiation-dependent proteins support and protect the stratum corneum by reinforcing the cornified envelope (Gutowska-Owsiak et al., 2020; Cohen et al., 2022).

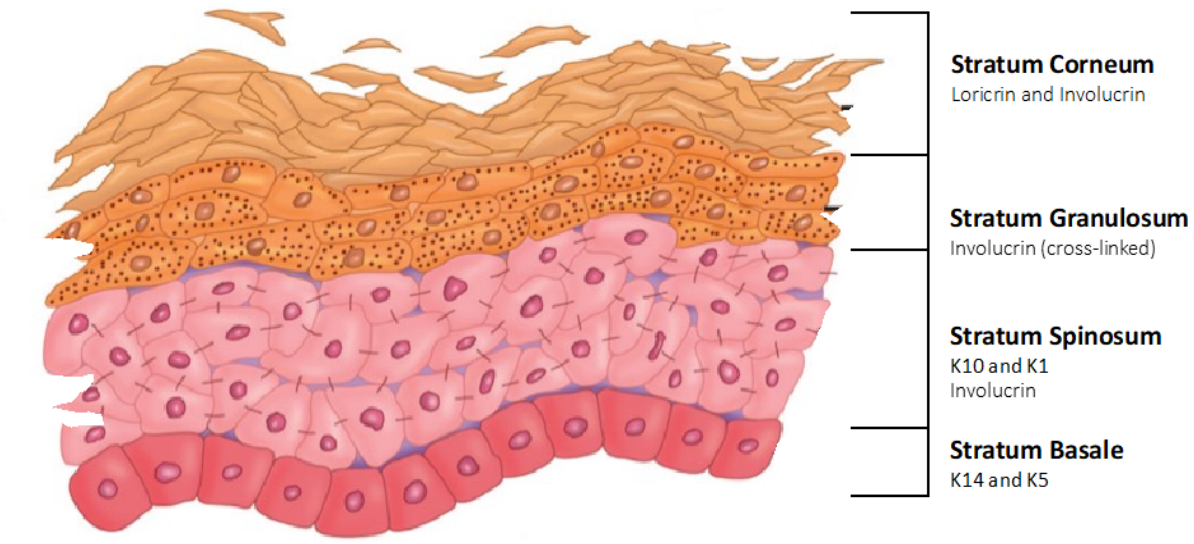

Figure 1.2: Structure of the human epidermis. The epidermis is composed of five distinct layers, the stratum basal, stratum spinosum, stratum granulosum, stratum lucidum and the stratum corneum. Image adapted from Baumann, 2009.

1.1.2 Dermis

The dermis is a connective tissue layer of mesenchymal origin, located deep to the epidermis and superficial to the subcutaneous fat layer (Fore, 2006). The human dermis contains multiple cellular and matrix components, including fibroblasts, collagen, blood vessels and elastic fibres (Menon et al., 2012). This fibrous dermal layer can be further broken down into two morphologically distinct forms of connective tissue, the papillary and reticular layers (Menon et al., 2012).

The papillary layer is the uppermost layer of the dermis, lying deep to the epidermis and intertwining with the rete ridges (Koster., 2009). This highly vascularised layer is composed of fine and loosely arranged collagen fibres (Green et al., 2014). The reticular dermis, however, exists as a thicker, deeper layer of dense irregular connective tissue (Ojeh et al., 2015). The reticular layer constitutes the bulk of the overall dermal volume and is essential for providing skin with strength and elasticity (Ojeh et al., 2015). Two forms of collagen, type I and type II exist within the dermis (Green et al., 2014). In addition to collagen, elastic fibres composed of both elastin and fibrillin microfibrils function to allow stretching, gliding, and recoiling within this layer (Green et al., 2014). Two subtypes of this connective tissue component are predominant in the dermis: elaunin and oxytalan fibres (Uitto et al., 2013). In the papillary dermis, oxytalan fibres are organised in a perpendicular formation (Koster., 2009). In contrast, elaunin fibres are arranged in a horizontal formation in proximity to the papillary and reticular dermal junction (Uitto et al., 2013).

1.2 Wound Repair

Constant exposure of the skin to the harsh external environment frequently results in cutaneous injury (Wilkinson and Hardman, 2020). In response, any disturbance that leads to a change in the ordinary anatomic structure of the skin, is, by definition, considered a wound (Lazarus et al., 1994). These disturbances may range from a minor disruption of the epithelial layer to extensive subcutaneous wounding (Demidova-Rice et al., 2012). Regardless of the severity, any breach in tissue integrity is rapidly followed by the onset of a biological wound-healing response (Wilkinson and Hardman, 2020). This reparative process requires extensive

communication between both cellular constituents of the skin, and the underlying extracellular matrix (ECM) (Lazarus et al., 1994).

1.2.1 Phases of Wound Healing

Classically, wound healing is accomplished through four highly dynamic and tightly regulated phases: haemostasis, inflammation, proliferation and tissue remodelling (Demidova-Rice et al., 2012). To achieve complete physiological and architectural tissue restoration, this repair cascade must progress at optimal intensity through a timely sequencing of repair (Wilkinson and Hardman, 2020).

1.2.1.1 Haemostasis

Immediately after injury, the initiation of tissue haemostasis marks the onset of wound repair (Figure 1.3). In response to vascular disruption, this initial phase encompasses the rapid contraction of damaged blood vessels and the coagulation of leaked blood constituents (Velnar et al., 2009). Circling platelets, which act as critical components of the haemostatic system, are activated by exposure to subendothelial matrix proteins (Serra et al., 2017; Levinson et al, 2013). Activation of this cellular population leads to coagulation and the formation of an insoluble clot (eschar), or 'platelet plug', aggregated from platelets, fibrin, fibronectin and thrombospondin (Reinke and Sorg, 2012). Whilst the primary function of this plug is to inhibit blood loss, this eschar also performs a collection of secondary functions, including the secretion of immune cell recruiting cytokines and stimulation of neighbouring fibroblasts and keratinocytes (Childs and Murphy, 2017). Additionally, the eschar plays an early antimicrobial role, acting as a physical barrier while also expressing several host defence peptide recognition receptors (Wilkinson and Hardman, 2020).

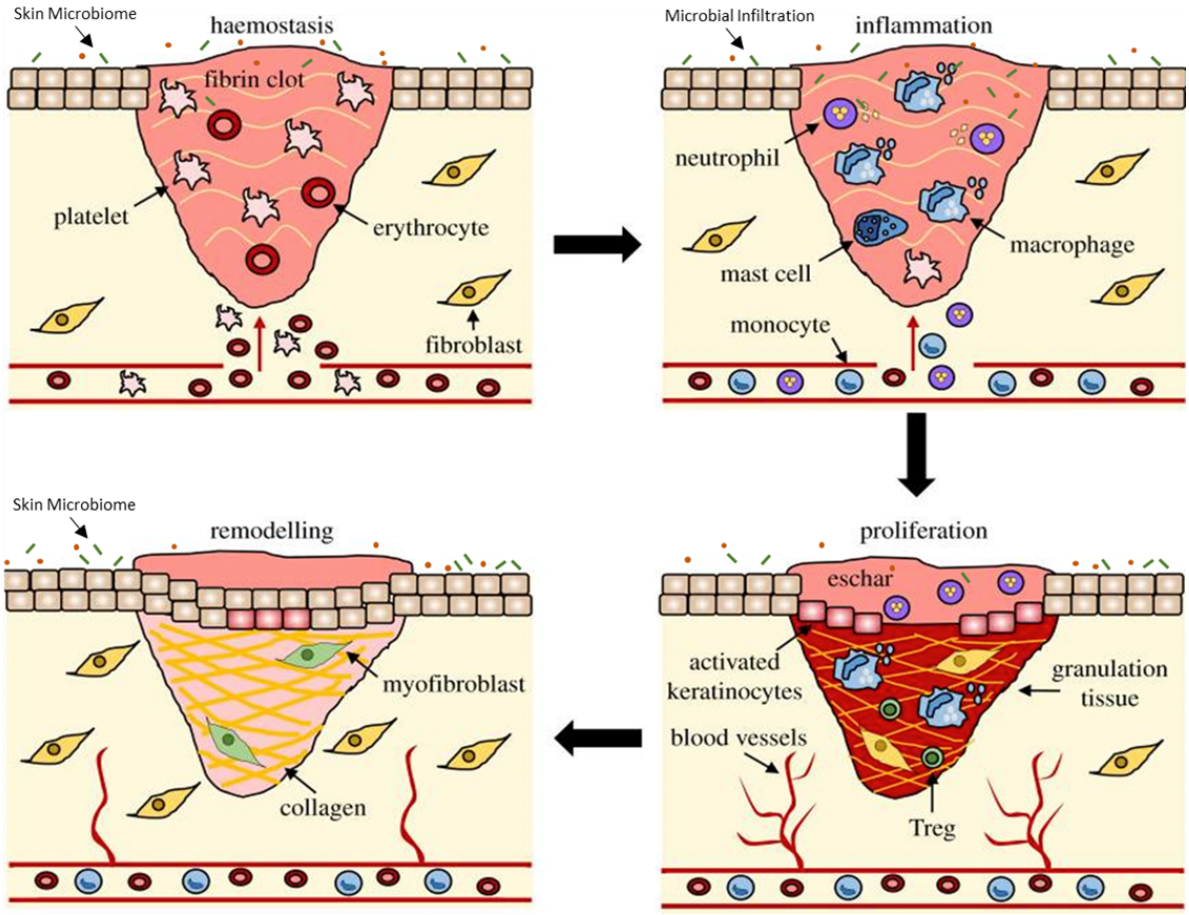

Figure 1.3: The four dominant stages of wound healing. Initially, wound repair initiates during the process of haemostasis, where a 'platelet plug' inhibits the loss of blood from damaged vasculature. The onset of host inflammation acts as the first line of defence, preventing pathogenic invasion, via the influx and activity of neutrophils and macrophages. During the proliferative phase, keratinocytes migrate to re-epithelise the wound bed, while resident fibroblasts produce granulation tissue with angiogenic support. Finally, matrix remodelling, and maturation are conducted by resident fibroblasts. Image adapted from Wilkinson and Hardman, 2020.

1.2.1.2 Inflammation

Host innate inflammation constitutes the primary defence against invading microbial species (Wilkinson and Hardman, 2020). Activation of innate inflammation relies on the host identification of conserved pathogenic structures termed pathogen-associated molecular patterns (PAMPs), or endogenously released danger molecules termed damage-associated molecular patterns (DAMPs) (Bin-Hafeez et al., 2021). The binding of host pattern recognition

receptors (PRRs) to their corresponding molecular pattern ligands initiates a downstream inflammatory signalling cascade, resulting in the release of pro-inflammatory cytokines, host defence peptides and the activation of resident immune cells (Kolimi et al., 2022). In parallel, pro-inflammatory molecules stimulate increased capillary vasodilation (Serra et al., 2017), which aids the infiltration of circulating leucocytes into the wound microenvironment (Reinke and Sorg, 2012). Within 12 hours of injury, neutrophils rapidly mobilise into the wound site (Raja et al., 2007), preventing pathogenic invasion through phagocytosis, and the release of host defence peptides, reactive oxygen species (ROS), proteolytic enzymes and extracellular traps (NETs) (Serra et al., 2017).

Wound macrophages, which differentiate from infiltrating circulating monocytes, reach peak presence at 3-4 days after post-injury (Deng et al., 2022). Macrophages, which function as master effector cells, exhibit strong phagocytic capabilities, internalising pathogenic debris, apoptosed neutrophils and components of the extracellular matrix (Serra et al., 2017). Additionally, macrophages within the wound environment release a reservoir of cytokines and pro-angiogenic, inflammatory and fibrogenic factors (Velnar et al., 2009). In the wound environment, macrophages are conventionally segregated into two dominant phenotypes, including both M1 (classically activated) or M2 (alternatively activated) categories (Snyder et al., 2016). Whilst this dichotomous classification is now considered to exist as more of a phenotypic spectrum than strict categories, wound macrophages do exhibit diverse transcriptional and behavioural responses to specific stimuli (Wilkinson and Hardman, 2020). Classically activated macrophages are commonly induced by pro-inflammatory stimuli including LPS and interferon-gamma (IFN-γ) (Snyder et al., 2016). The primary function of this population is to phagocytose apoptotic neutrophils and promote overall inflammation by releasing ROS and inflammatory cytokines (e.g. IL-1, IL-6 and TNF-α) (Gurevich et al., 2018). As inflammation starts to resolve, macrophages generally transition to an alternatively activated state, expressing pro-resolutory cytokines (IL-4, IL-10, IL-13) and arginase. Anti-inflammatory macrophages also release numerous growth factors to promote re-epithelialisation and angiogenesis (Gurevich et al., 2018). At this stage, both resident T cells and mast also play a critical role in wound repair, however, their influence is often masked by

the overwhelming presence of neutrophil and macrophage populations (Wilkinson and Hardman, 2020).

1.2.1.3 Proliferation

As local inflammation subsides, the proliferative repair phase is characterised by the onset of wound re-epithelialisation, granulation tissue formation and the onset of angiogenesis (Shah et al., 2015). During this stage of repair, leading-edge keratinocytes undergo partial epithelial–mesenchymal transition (pEMT), adopting an invasive migratory phenotype (Wilkinson and Hardman, 2020). In response to stimulation from epidermal and keratinocyte growth factors (EGF) (KGF), keratinocytes undergo PCKα-mediated dissociation from their cellular and basal lamina desmosome-based adhesions (Trinh et al., 2022). Shifts from vertical, to front-to-rear cellular polarity, allow lateral epidermal migration into the provisional fibrin-rich matrix (Cangkrama et al., 2020). In the presence of wound bed debris, keratinocytes secrete matrix metalloproteinases (MMPs), degrading necrotic tissue and facilitating integrin receptor dissociation between cells (Trinh et al., 2022). Eventually, as opposing leading edges meet, migration signals are terminated. Neo-epidermal keratinocytes then reconstitute the basement membrane, fully regenerating the stratified epidermis (Kolimi et al., 2022).

During the proliferative phase, resident fibroblasts also secrete MMPs, degrading and replacing the preliminary matrix with new connective granulation tissue (Kolimi et al., 2022). This new provisional tissue, rich in fibronectin, immature collagens and proteoglycans, provides a biological scaffold for cell migration, differentiation and mature matrix deposition (Akbarian et al., 2022). Simultaneously, the restoration and development of new blood vessels from pre-existing vasculature is required to meet the enhanced metabolic demands of regenerating tissue (Eming et al., 2014). This process of ‘angiogenesis’, is initiated by endogenous proangiogenic mediators such as vascular endothelial growth factor (VEGF), basic fibroblast growth factor (bFGF) and transforming growth factor β (TGF-β) (Shah et al., 2015). In response to stimulation, endothelial cells of existing vessels secrete proteolytic

enzymes, proliferating and mobilising towards the source of the angiogenic stimulus (Trinh et al., 2022). As they migrate, angiogenic capillary sprouts invade the fibrin-rich eschar, establishing an extensive underlying microvascular network throughout the granulation tissue (Akbarian et al., 2022).

1.2.1.4 Remodelling

In wound repair, the extracellular matrix (ECM) remodelling stage commences at the point of haemostatic fibrin clot formation, reaching completion in the significant future, upon the establishment of a mature cutaneous scar, rich with type I collagen deposits (Cangkrama et al., 2020). The primary function of the remodelling stage is to restore physiological tissue structure through ECM reorganisation, degradation, and resynthesis (Bao et al., 2009). These compositional ECM changes are achieved via the carefully balanced helical collagen-cleaving activities of tissue MMPs. Initially, granulation tissue is comprised largely of embryo-associated type III collagen deposits, which eventually undergo partial replacement by type I collagen deposits (Akbarian et al., 2022). While collagen remodelling acts to directly increase tensile strength, new collagen fibrils are unable to restore their previous physiological weave orientation, instead adopting a post-wounding weaker parallel alignment (Kolimi et al., 2022). In this new architecture, the ECM achieves only 50-80% of its original pre-wounded tissue strength (Wilkinson and Hardman, 2020).

1.2.2 Aberrant Wound Healing

Wounds can generally be classified based on specific criteria, including the length of time taken to completely regenerate (Whitney, 2005). Whilst the human skin possesses significant reparative ability, derangement in wound-linked cellular behaviours, as seen in diabetes, can lead to impaired healing (Wilkinson and Hardman, 2020). Typically, when an insult fails to progress through a timely sequence of repair, within approximately 12 weeks, it is defined as a chronic wound (Han and Ceilley, 2017). Unfortunately, these chronic wounds, including diabetic foot ulcers (DFUs), venous leg ulcers (VLUs) and pressure sores are currently an area of major unmet clinical need (Tipton et al., 2020). In the UK alone, the annual wound management financial healthcare burden is estimated at £8.3 billion (Guest et al., 2020), of

which £5.6 billion is associated specifically with the treatment of persistent non-healing wounds (Guest et al., 2020)

1.3 The Diabetic Foot

One direct consequence of aberrant wound healing is the onset of diabetic foot disease (DFD) (Guest et al., 2020). Foot-related disorders including infection, ulceration and gangrene, are one of the most common causes of hospitalisation in the diabetic community (Bowers and Franco, 2020). In 2017/2018, the NHS provided direct wound care treatment for 3.8 million individuals, an increase of 71% from 2012/2013 (Guest et al., 2020). Within this wound population, there were an estimated 326,000 diabetic foot ulcers, equating to 9% of the overall UK adult diabetic population (Guest et al., 2020).

1.3.1 Diabetes

Diabetes mellitus (DM) is defined as a group of metabolic diseases, characterised by prolonged hyperglycaemia in response to defective insulin secretion and/or action (American Diabetes Association, 2010; Khattoubi and Darwish, 2015). In the UK alone, another individual receives a positive diabetic diagnosis every two minutes (Lin et al., 2020). Globally, diabetes mellitus is now considered as one of the most challenging public healthcare issues of the 21st century (Singer et al., 2022). Associated with a significant global increase in physical inactivity and obesity, adult-onset (type 2) diabetes is regarded as the leading cause of this 'modern preventable pandemic' (Singer et al., 2022). In 2017, the International Diabetes Federation (IDF) estimated that 451 million adults live with diabetes worldwide, a figure that without the rapid adoption of effective preventative measures, is expected to increase to 693 million by 2045 (Lin et al., 2020).

1.3.1.1 Signs and Symptoms

Individuals with diabetes typically begin to express classical signs of the disease, including excessive urination (polyuria) and thirst (polydipsia) (Kolimi et al., 2022). Depending on the exact form of diabetes present, the onset of these symptoms may develop rapidly or may

progress at a much slower rate (American Diabetes Association, 2010). Typically, symptoms arise as a physiological response to prolonged hyperglycaemia (American Diabetes Association, 2010). For example, excessive glucose filtering by the kidneys results in the production of a greater volume of urine (Ramachandran, 2014), consequently inducing dehydration and extreme thirst due to fluid loss (Javeed and Matveyenko, 2018). In the case of type 2 diabetes, individuals often present with a dormant, symptomless stage, resulting in delayed clinical diagnosis (Javeed and Matveyenko, 2018). Therefore, in many of these patients, the consequences of micro and macrovascular complications are already present at the time of diagnosis (Aberti et al., 2007). Following diagnosis, continued chronic hyperglycaemia may also be accompanied by increased susceptibility to infections and impaired wound healing (Singer et al., 2022). Additionally, prolonged uncontrolled diabetes may lead to immediate life-threatening consequences, such as ketoacidosis or nonketotic hyperosmolar syndrome (Galtier, 2010).

1.1.1.1 Aetiology and Diagnosis

Diabetes is a complex metabolic disorder that may develop as a result of numerous pathogenic events (Viigimaa et al., 2020). These processes vary from autoimmune pancreatic beta-cell destruction to progressive insulin resistance (Viigimaa et al., 2020). Based on these two events, diabetes can generally be classified into two main etiopathogenetic categories (American Diabetes Association., 2010). Accounting for only 5-10% of overall cases of diabetes, juvenile or type 1 diabetes, typically results from the autoimmune destruction of insulin-secreting pancreatic β-cells (American Diabetes Association., 2010). While the degree of β-cell destruction fluctuates significantly, individuals with this form of diabetes are typically insulin-dependent (Atkinson et al., 2014). Overall, the diagnosis of type 1 diabetes typically demonstrates a biphasic pattern, frequently presenting between the ages of 5-7 or at the point of puberty (Singer et al., 2022). Disease onset also demonstrates autumn/winter seasonal distribution, supporting the theory of viral involvement in disease initiation (Atkinson et al., 2012).

Type 2 diabetes, which accounts for 90% of overall cases, describes those that generally do not, at least initially, require insulin administration in order to survive (Belle et al., 2011). Type 2 diabetes is marked by a combination of defective pancreatic β-cell insulin secretion and the progressive inability of insulin-sensitive tissues to effectively respond to insulin (Singer et al., 2022). In prolonged disease, endogenous insulin secretions become unable to support glucose homeostasis, ultimately resulting in hyperglycaemia (Singer et al., 2022). Typically, type 2 diabetes is primarily attributed to lifestyle factors, with 90% of diagnosed individuals being defined as medically obese (Scott et al., 2013). Individuals not classified as obese commonly demonstrate a high percentage of adipose tissue in the visceral fat depots and high subcutaneous truncal/abdominal adipose tissue distribution (Patel and Abate., 2013). This form of diabetes is also commonly associated with a predisposing genetic factor, and, while the involvement of genetics in type 2 diabetes is poorly defined, a family history of the disease remains a strong and significant risk factor for disease onset throughout life (Scott et al., 2013).

1.3.1.2 Complications

The presence of diabetes mellitus has a profound effect on the structure and function of all peripheral organs and tissues, leading to life-changing complications (Singer et al., 2022). Within this range, the most debilitating effects include cardiovascular disease, retinopathy, nephropathy, and neuropathy (Gandhi et al., 2016). Typically, these long-term complications begin after many years of chronic hyperglycaemia, however, occasionally these dysfunctions occur as the first symptom, prior to the diagnosis of diabetes mellitus (Papatheodorou et al., 2016).

1.3.2 Pathophysiology of the Diabetic Foot

Diabetic foot disease (DFD) is considered a leading healthcare complication of DM. Yet, the pathological tissue breakdown of the diabetic foot does not occur spontaneously, but in response to multiple underlying components that associate with the hyperglycemic state (Reardon et al., 2020). Briefly, dominant risk factors in the pathway to ulceration and

amputation include a combined triad of diabetic peripheral neuropathy (DPN), peripheral vascular disease (PVD) and secondary tissue infection (Figure 1.4) (Lepäntalo et al., 2011).

Commonly regarded as the lead cause of DFU development, DPN describes the onset of distal-to-proximal neurodegeneration, encompassing sensory, motor, and autonomic impairment (Pouget et al., 2021). Pathological causes of peripheral nerve damage include exposure to chronic hyperglycemia, increased oxidative stress, advanced glycosylation product (AGE) formation, activation of protein kinase C (PKC) isoforms, segmental demyelination and axonal loss (Feldman et al., 2019). Often demonstrating a "stocking and glove" pattern of distribution, DPN contributes heavily towards longstanding diabetic complications, including muscular atrophy, loss of protective sensation, postural and co-ordinational deviation, increased metatarsal head prominence and vulnerability to unconscious traumas (Figure 1.4) (Juster-Switlyk & Smith, 2016). Deformities in the anatomical foot structure, such as hammer-toe contracture or high plantar surface pressure, induce a 32-fold increase in the likelihood of ulceration (Bandyk et al., 2018).

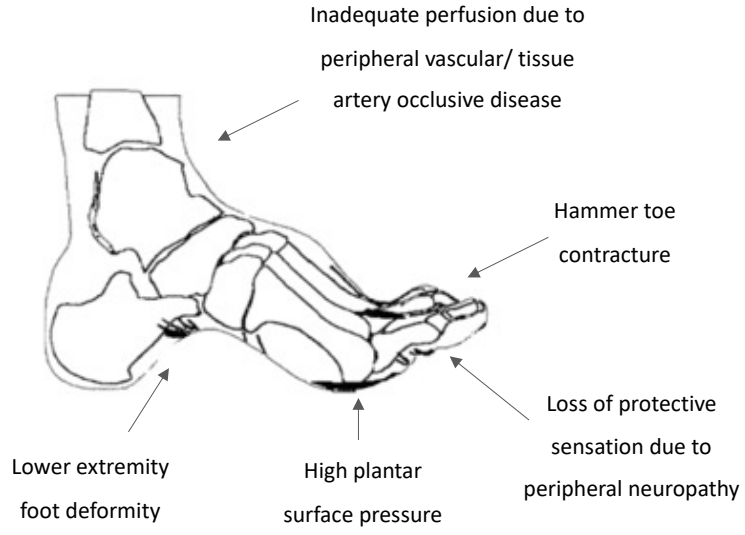

Figure 1.4: Mechanisms of diabetic foot disease. A combination of neuropathy and arterial occlusive disease leads to the initial formation of a diabetic foot ulcer. Neuropathy-induced muscular atrophy leads to anatomical deformities, such as hammer-toe formation and the development of high planar pressure zones. Decreased sensation and repetitive unconscious

trauma may eventually lead to ulceration and infection. Image adapted from Bandyk et al., 2018.

Whilst the pathway from neuropathy to ulceration is considered the leading cause of tissue breakdown, the presence of peripheral vascular disease (PVD) is equally important (Reardon et al., 2020). PVD is primarily driven by progressive atherosclerotic disease, resulting in the partial or complete occlusion of peripheral lower-limb vessels and subsequent diminished blood flow and tissue ischemia (Balta et al., 2021). Several pathogenetic mechanisms have been identified in the initiation of atherosclerosis, including hyperlipidaemia, dysfunction of the vascular endothelium, increased pro-inflammatory mediators, elevated platelet activation factors and vascular smooth muscle cell (VSMC) dysfunction (Felipe et al., 2021). The anatomical dissemination of lower-extremity atherosclerotic disease differs according to patient diabetic status (Bandyk et al., 2018). In diabetes, occlusion preferentially involves the infrageniculate leg posterior and anterior tibial arteries, with less frequent inclusion of the femoropopliteal arterial and aortoiliac artery segment (Bandyk et al., 2018). In the presence of diffuse tibial artery occlusive disease, inadequate low-extremity perfusion ultimately obstructs blood flow to the point of critical limb ischemia, resulting in the impaired healing of wounds/ulcers and lower-extremity gangrene (Figure 1.5) (Bandyk et al., 2018).

In the presence of damaged or poorly perfused tissue, bacterial communities rapidly penetrate the area, leaving neuroischaemic ulcers highly susceptible to invasive limb-threatening infection (Bandyk et al., 2018). Diabetic foot infection phenotypes range from simple cellulitis to high-mortality necrotizing fasciitis (Perez-Favila et al., 2019). In parallel, the presence of a prolonged hyperglycaemic state induces host innate and immune cell dysfunction, further contributing towards the onset of infection, excessive inflammation and perturbated wound repair (Jalilian et al., 2020). Briefly, wound bed neutrophils become resistant to apoptosis and macrophage clearance, whilst also increasing their production of cytotoxic extracellular traps (NETs) (Bandyk et al., 2018). Excessive inflammation, which maintains wound chronicity may also be attributed to altered macrophage activity (Jalilian et al., 2020). Chronic wound macrophages generally maintain a pro-inflammatory state, also demonstrating impaired neutrophil and bacterial phagocytosis (Olsson et al., 2019). In

addition to immune cells, leading-edge keratinocytes are often hyperkeratotic and parakeratotic, presenting an increased number of non-proliferative senescent cells (Wilkinson and Hardman, 2020). In combination with increased fibroblast senescence, high wound protease levels further compromise ECM deposition and inhibit keratinocyte migration (Haalboom, 2018). These wound bed cells also fail to elicit an appropriate host response in the presence of pathogens, due to the altered expression of pattern recognition receptors (Jones et al., 2018). Therefore, while infection is rarely considered a direct cause of ulceration, wound microbial composition, defective host wound repair mechanisms and the presence of clinical infection are significantly associated with healing response, wound chronicity and the likely hood of future amputation (Kiefer and Mazzeffi, 2022)

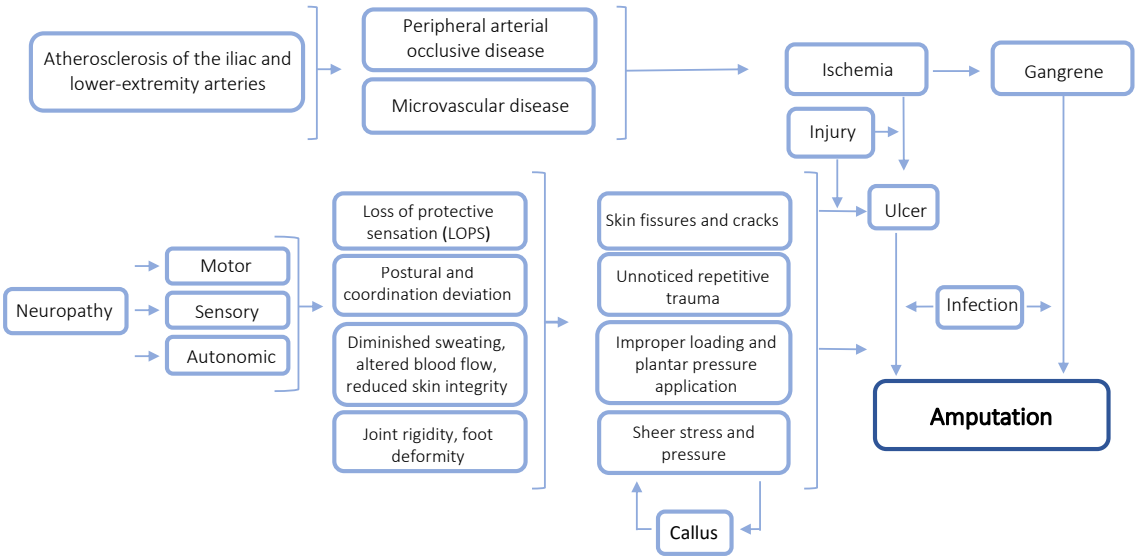

Figure 1.5: Pathway to diabetic foot ulceration and subsequent amputation. Diabetic peripheral neuropathy and ischemia are considered the leading causes of foot ulceration and subsequent amputation. (Bandyk et al., 2018; Balta et al., 2021).

1.3.3 Diabetic Foot Classification

Methods of classification and scoring are commonly used for the description and clinical management of diabetic foot ulcers (Perez-Favila et al., 2019). To date, several classification systems have been implemented, yet no single method has been widely adopted as the gold

standard (Table 1.1) (Game, 2015). Regardless of the precise methods, the predominant focus of each system is to guide appropriate therapeutic strategies and predict clinical risk outcomes for each unique DFU (Jalilian et al., 2020).

The first DFU classification system to be widely accepted, the Meggitt-Wagner (MW) method, is a numerical (0-5) linear scoring system, that focuses on assessing ulcer penetration depth and the existence of osteomyelitis/gangrene (Wagner, 1981; Pendsey, 2010). However, this method has received extensive criticism, as it fails to consider the ischemic status of the wound (Jalilian et al., 2020). In contrast, the University of Texas (UT) system accounts for not only ulcer depth and wound infection, but also clinical signs of lower extremity ischaemia (Lavery et al., 1996). Gradings range from pre-ulcerative sites (Grade 0) to an ischemic and infected ulcer that penetrates to bone (Grade 3, D) (Jalilian et al., 2020). Comparative studies have reported that while both UT and MW classification systems accurately predict the likelihood of major amputation, the enhanced descriptive power of the UT system allows improved prediction of cutaneous healing and minor amputations (Jalilian et al., 2020).

Additional wound classification systems include the DUSS, DEPA and SINBAD scoring methods (Singer et al., 2020) (Table 1.1). The DUSS mechanism considers four dichotomous DFU variables including insult location and palpable pedal pulse to assign a score between 0 and 4 (Beckert et al., 2006). However, while clinically very simple, the DUSS system also fails to consider the impact of wound neuropathy or infection (Singer et al., 2020). In contrast, both DEPA and SINBAD systems deliberate bacterial involvement, with DEPA considering ulcer depth, bacterial contamination/infection, the phase of healing and associated underlying aetiology (Younes and Albsoul, 2004). Yet, whilst DEPA fails to consider ulcer area, SINBAD simultaneously considers ulcer location, the presence of either ischemia or neuropathy, bacterial involvement and ulcer area and depth (Ince et al., 2008)

Table 1.1: Classification system grading mechanisms of the diabetic foot ulcer.

Classification System	Classification Mechanisms
Wagner (Grading) (Wagner, 1981)	**Grade 0**: No ulcer in a high-risk foot. **Grade 1**: Superficial ulcer involving the full skin thickness but not underlying tissues. **Grade 2**: Deep ulcer, penetrating down to ligaments and muscle, but no bone involvement or abscess formation. **Grade 3**: Deep ulcer with cellulitis or abscess formation, often with osteomyelitis. **Grade 4**: Localized gangrene. **Grade 5**: Extensive gangrene involving the whole foot.
University of Texas (Grading and staging) (Lavery et al., 1996)	**Grade 0-A**: non-infected, non-ischemic pre- or post-ulcerative lesion completely epithelized **Grade 0-B**: infected, non-ischemic pre- or post-ulcerative lesion completely epithelized **Grade 0-C**: ischemic, non-infected pre- or post-ulcerative lesion completely epithelized **Grade 0-D**: ischemic and infected pre- or post-ulcerative lesion completely epithelized **Grade I-A**: non-infected, non-ischemic superficial ulceration (not involving tendon or bone) **Grade I-B**: infected, non-ischemic superficial ulceration (not involving tendon or bone) **Grade I-C**: ischemic, non-infected superficial ulceration (not involving tendon or bone) **Grade I-D**: ischemic and infected superficial ulceration (not involving tendon or bone) **Grade II-A**: non-infected, non-ischemic ulcer that penetrates to capsule or bone **Grade II-B**: infected, non-ischemic ulcer that penetrates to capsule or bone **Grade II-C**: ischemic, non-infected ulcer that penetrates to capsule or bone **Grade II-D**: ischemic and infected ulcer that penetrates to capsule or bone **Grade III-A**: non-infected, non-ischemic ulcer that penetrates to bone or a deep abscess **Grade III-B**: infected, non-ischemic ulcer that penetrates to bone or a deep abscess **Grade III-C**: ischemic, non-infected ulcer that penetrates to bone or a deep abscess **Grade III-D**: ischemic and infected ulcer that penetrates to bone or a deep abscess
SINBAD (Scoring between 0-6) (Ince et al., 2008)	**Site:** forefoot: 0; midfoot/hindfoot: 1 I**schemia**: blood flow intact, at least one pulse palpable: 0; clinical evidence of ischaemia: 1 **Neuropathy**: protective sensation intact, neuropathy defined as being absent: 0; protective sensation diminished, neuropathy present: 1 **Bacterial Infection**: based on clinical features absent: 0; present: 1 **Ulcer Area**: ulcer < 1 cm^2: 0; ulcer ≥ 1 cm^2: 1 **Ulcer Depth**: Insult confined to skin and subcutaneous tissue: 0; reaching muscle, tendon or deeper: 1
DEPA (Scoring between 3-12) (Younes and Albsoul, 2004)	**Depth of Ulcer**: superficial skin ulcers: 1; subcutaneous tissues and tendon involvement: 2; bone involvement: 3. **Extent of bacterial colonization**: Contamination: 1; Active infection: 2; Sepsis or necrotising infection. **Phase of Ulcer**: granulating phase: 1; inflammatory phase: 2; non-healing phase: 3. **Associated Etiology**: Neuropathy: 1; bone (structural) deformity: 2; lower limb ischaemia: 3.
DUSS (Scoring between 0-4) (Beckert et) al., 2006	**Palpable Pedal Pulses:** Yes: 0; No: 1. **Probing to bone**: No: 0; Yes: 1. **Ulcer Site**: Toes: 0; Foot: 1. **Ulcer Number**: Single: 0; Multiple: 1.

1.3.4 Treatment and Management

The treatment of diabetic foot ulcers accounts for approximately one-third of the total cost of diabetic care (Everett et al., 2018). Optimal ulcer management typically involves a multi-disciplinary team of primary care physicians, podiatrists, vascular surgeons, wound care nurses and infectious disease specialists, that communicate to design a personalised care plan (Pouget et al., 2021). Current treatment regimen options include mechanical debridement, peak pressure offloading, infection control, restoration of local tissue perfusion, wound dressings and multiple alternative therapies (Cascine et al., 2021). Additionally, patient blood glucose levels must be tightly controlled to improve wound healing and limit future adverse effects on cellular activity and infection (Cascine et al., 2021). Overall, the focus of any treatment is to achieve complete healing and maintain patient ambulation (Pouget et al., 2021).

1.3.4.1 Alternative Therapies (Extra Corporeal Shockwave Therapy)

In addition to standard practices in diabetic foot care, there is currently a wide range of novel approaches being studied as adjuvant therapies (Jalilian et al., 2020; Cascine et al., 2021). One of these therapies, extracorporeal shockwave therapy (ESWT), has gained increasing popularity over the past decade, due to its highly rated clinical efficacy, ease of use, cost-effectiveness and non-invasive nature (Cascine et al., 2021). While initially used in the field of orthopaedic repair, the early successful application of shockwave therapy began to encourage studies investigating alternative areas of clinical need, such as cutaneous wound healing (Schaden et al., 2007). In the clinic, therapeutic devices produce transient interim acoustic pulses (shockwaves), that propagate rapidly to reach high peak pressure within the targeted tissue (Yan et al., 2009). Accounting for specific parameters, such as peak pressure vs. time plot and maximum pressure, treatment intensity is commonly described as calculated total energy and energy flux density (EDF), with EDF given in mJ per millimetre square (mJ/mm^2) (Cascine et al., 2021).

Studies investigating the biological mechanisms of ESWT in wound healing have reported increased angiogenesis, upregulated proliferation, reduced apoptosis, and broad anti-microbial activity (Cascine et al., 2021). In the tissue, *in-vivo* studies have demonstrated enhanced post-treatment perfusion following shockwave therapy (Yan et al., 2009; Meirer et al., 2007). *In ex-vivo* rat models of ischemic skin flaps, both Yan et al., 2009 and Meirer et al., 2007 reported significantly reduced skin flap necrosis following shockwave therapy, with enhanced local perfusion, pre-existing vessel vasodilation and elevated tissue VEGF and NOS gene expression. Alternatively proposed mechanisms include modifications to immune cell function (Kuo et al., 2009). In combination, Kuo et al., 2009 and Davis et al., 2009 observed that in ESWT-treated mice, post-surgical early local leukocyte and macrophage inflammatory responses were mitigated, suggesting anti-inflammatory properties. Regarding anti-microbial efficacy, ESWT has reported activity against both planktonic *Staphylococcus aureus* cultures *in-vitro* and in multispecies biofilms *in-vivo* (Qi et al., 2016; Datey et al., 2019*).* In the clinic, shockwave therapy has been applied to wounds of multiple clinical phenotypes. Schaden et al., 2007 treated burn wounds, post-traumatic tissue, atrial insufficiency ulcers, and venous stasis ulcers, demonstrating the safety and efficacy of low-energy shockwave therapy for therapeutic use.

1.3.4.2 Surgical Intervention

In circumstances where insults fail to respond to standard treatment, surgical intervention may be required (Pouget et al., 2021). The presence of diabetic foot ulcer infection is currently the leading cause of diabetes-related hospitalisations and non-traumatic lower extremity amputations (Everett et al., 2018). In response to current treatment regimes, it is estimated that 70-80% of DFU patients are able to achieve complete wound closure (Pouget et al., 2021). However, in the remaining 20-30% of patients, minor distal to ankle surgical resection is required to remove necrotic tissue and prevent the further spread of infection (Pouget et al., 2021). In approximately 15% of this surgical population, further minor amputations are required due to the failure of previous surgical intervention techniques (Cascine et al., 2021). Within this further subpopulation, approximately 9% of patients will further progress to require a major lower extremity amputation (Singh and Chawla, 2006). Following major

amputation, patient mortality is high, with 5-year survival rates ranging from 20% to 50% (Cascine et al., 2021).

1.4 The Wound Microbiome

The microbiome is typically defined as the assemblage of microorganisms, including bacteria, fungi, viruses, and archaea present in a defined environment (Grice and Segre, 2011). A microbiome is present amongst almost every surface exposed to an external environment, including the human body and the cutaneous wound environment (Grice and Segre, 2011). Recent evidence now suggests that the species-level microbiome of each wound environment plays a key role in its ability to effectively repair (Loesche et al., 2019). Therefore, characterising the role of the microbiome in the initiation or persistence of chronic wounds remains a key area of research interest (Cho and Blaser, 2012).

1.4.1 Contamination, Colonisation and Infection

All wounds are naturally exposed to the commensal skin microbiota; it is, therefore, important to differentiate between contamination, colonization and infection (Figure 1.6) (Farhan and Jeffery, 2021). Wound contamination is ordinarily defined as the presence of non-proliferating microbes on the wound surface (Bowler et al., 2001). Colonisation, however, is described as the existence of multiplying bacteria with the absence of an observable immunological host reaction (Johnson et al., 2018). Both wound contamination and colonisation have a polymicrobial aetiology and are considered conditions common in all healing wounds (Bowler, 2003).

In contrast, infection of the wound occurs when the virulence factors of invading organisms overcome host resistance, resulting in the multiplication and invasion of microbial populations and subsequent resident tissue damage (Negut et al., 2018). It has been long proposed that a transition from colonisation to infection in the chronic wound environment occurs solely as a consequence of increasing microbial load (Johnson et al., 2018). Wound care practitioners generally adhere to growth guidelines, suggesting that 10^5 colony-forming units (CFUs) per gram of viable tissue are indicative of a critical colonisation level (Farhan and

Jeffery, 2021). At this threshold, it is believed that the bacterial burden acts to overwhelm host defence mechanisms and impair wound healing (Daltrey et al., 1981; Krizek and Robson, 1975) However, this guideline provides no insight into species diversity, polymicrobial interactions and the pathogenicity of individual microbial populations (Farhan and Jeffery, 2021).

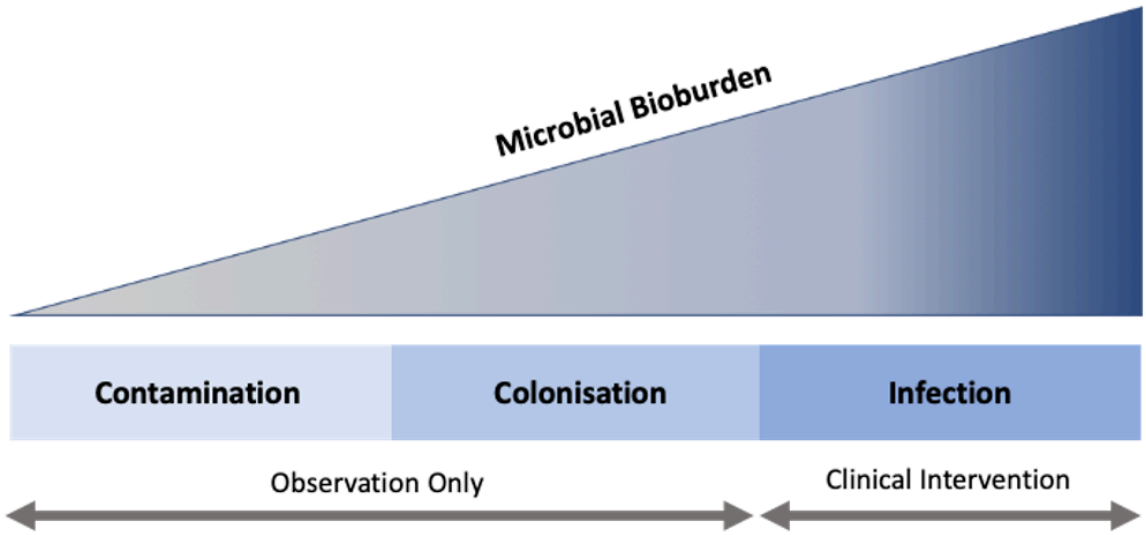

Figure 1. 6: The Wound Contamination, Colonisation and Infection Continuum. As tissue microbial load exceeds colonisation levels, intervention is required to prevent the onset of infection. Imaged adapted from Farhan and Jeffery, 2021.

One example of deviation from this clinical guideline is the toxin-producing bacterium, B-haemolytic *Streptococcus* (Khosravi et al., 2018). This microbe alone is capable of inducing infection and local tissue damage at the bacterial load of approximately 10^2 CFUs per gram of tissue, significantly lower than the 10^5-growth guideline (Khosravi et al., 2018). This concept is further complicated by the ability of polymicrobial interactions to alter the virulence capabilities of one another (Johnson et al., 2018). For example, commensal strains of *Staphylococcus* and *Corynebacterium* typically will not maintain a chronic infection alone, yet may co-aggregate symbiotically to maintain polymicrobial multi-layered biofilm structures (Wong and Santiago, 2017, Omar et al., 2017). Such biofilm structures are estimated to exist in over 90% of chronic wounds, surviving as polymicrobial communities that are encircled by

dense extracellular polymeric substances (EPS) (Singh et al., 2017). Groups of microorganisms contained within a biofilm construct frequently adopt a multicellular behavioural pattern, contributing to the augmented survival abilities of such communities across a wide range of invaginations and specialised environmental niches (Singh et al., 2017).

1.4.2 The Microbial Profile of Chronic Wounds

In recent years, increasing evidence suggests that microbial composition plays a key role in the transition of an acute wound into a chronic state (Verbanic et al., 2020). Culture-independent methods for bacterial detection and analysis have revealed the wound microbiome to be much more diverse and complex than previously revealed by culture-based methods (Park et al., 2019). To date, there have been several studies attempting to profile the microbiome of a variety of chronic wounds, including venous insufficiency ulcers, pressure ulcers, and diabetic foot ulcers (Han et al., 2011). Major bacterial genera found include *Staphylococcus, Streptococcus, Corynebacterium, Pseudomonas*, and various anaerobes (Figure 1.7) (Gardner et al., 2013; Loesche et al., 2017). However, the exact role of the microbiome in wound healing remains poorly understood. While current research is promising, studies are very heterogeneous, hindering the comparison of findings across different research groups (Table 1.2) (Tipton et al., 2020). In addition, more studies are needed to correlate microbiome findings with clinical factors, as well as in the relatively unexplored fields of nonbacterial microbiomes, such as the wound mycobiome and virome (Verbanic et al., 2020).

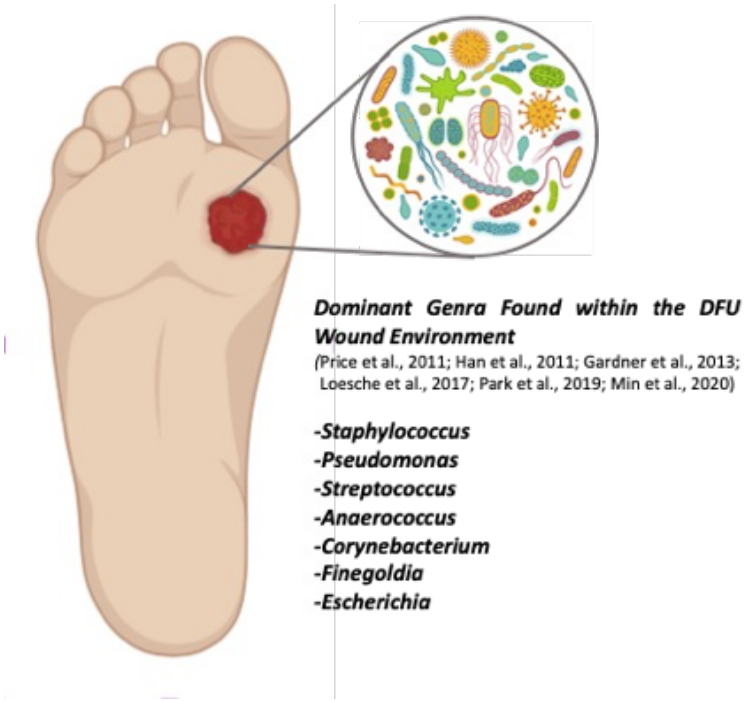

Figure 1.7: Dominant genera found within the DFU wound environment. Using culture-independent methods to analyse DFUs at a genus level, a wide combination of studies determined, *Staphylococcus, Pseudomonas, Streptococcus, Anaerococcus, Corynebacterium, Finegoldia and Escherichia* to be the most dominant microbes present within the wound environment (Price et al., 2011; Han et al., 2011; Gardner et al., 2013; Loesche et al., 2017; Park et al., 2019; Min et al., 2020).

Table 1.2: Summary findings of recent wound microbiome studies.

Study	Gardner et al., 2013	Loesche et al., 2017	Park et al., 2019	Min et al., 2020	Tipton et al., 2020	Verbanic et al., 2020
Wound Aetiology	Neuropathic nonischaemic diabetic foot ulcers (n=52)	Heterogenous diabetic foot ulcer (n=100)	Heterogenous diabetic foot wound (n=20)	Plantar Diabetic Foot Ulcer (n=10)	Plantar Chronic Wounds (n=190)	Diabetic ulcers Venous wounds Arterial wounds Pressure ulcers (n=5 per wound type)
Collection Method	Wound swab (Levine technique)	Wound swab (Levine technique)	Debridement of necrotic/ unhealthy granulation tissue	Wound bed swab (Levine technique)	Buccal swabs	Wound bed swab (Levine technique)
Analysis Platform	Roche 454 FLX Titanium Instrument (16S rRNA gene sequencing) (5,634 sequenced reads per sample)	Illumina MiSeq system (300-bp paired ends, V1-V3 chemistry, 16S sequencing) This generated a dataset of 7,702,607 sequences.	Illumina MiSeq system (300-bp paired ends) (16S metagenomic sequencing) The V1–V3 regions of the 16S rRNA gene 2,161,104 from 20 tissue samples = analysed reads)	Illumina MiSeq system (300-bp paired ends) (V4 conserved regions of bacterial 16S rRNA) (6.4 million overall sequenced reads, n=10)	454 Titanium Instrument 454 Life Sciences - Roche, Ion Torrent PGM (16S sequencing)	Illumina MiSeq with PE300 V3 (5,931,472 total reads) (16S sequencing)
Dominant Phyla	Firmicutes (67%), Actinobacteria (14%) Proteobacteria (9.8%) Bacteroidetes (7.3%) Fusobacteria (1.4%)	N/A	*Firmicutes Actinobacteria* *Proteobacteria* *Bacteroidetes* *Fusobacteria*	*Firmicutes* (44.7%) *Actinobacteria* (35.1%) *Proteobacteria*(14.5%) *Bacteroidetes* (4.6%) *Fusobacteria* (0.9%)		*Firmicutes* *Proteobacteria* *Actinobacteria Bacteroidetes*
Dominant Genera	*Staphylococcus* (29.6%) (Staphylococcus species: 96.5% S. aureus, 0.4% S. epidermidis) Streptococcus (8.8%) Lactococcus (3.9%)	*Staphylococcus* (22.7%) (Staphylococcus species: 13.3% S. aureus, 5.3% S. pettenkoferi, 4% unclassified) Streptococcus (11.98%) Corynebacterium (11.46%) Anaerococcus* (7%)	*Staphylococcus* Prevotella Finegoldia* Corynebacterium Escherichia Anaerococcus* Streptococcus Pseudomonas Porphyromonas*	*Staphylococcus* (21.1%) *Corynebacterium* (20.3%) *Arthrobacter* (6.9%) *Finegoldia* *(6.1%) *Brevibacterium* (6.0%) *Peptoniphilus** (4.7%) *Oligella* (4.7%) *Anaerococcus** (3.9%) *Alcaligenes* (3.4%) *Streptococcus* (2.7%)	*Pseudomonas aeruginosa* *Staphylococcus epidermidis* *Staphylococcus aureus*	*Staphylococcus* *Corynebacteria* *Pseudomonas* *Proteus* *Enterobacter* *Campylobacter* *Porphyromonas* *Streptococcus* *Bacteroides*

In previous studies attempting to characterise the wound microbiome, both Gardner et al., 2013 and Loesche et al., 2017 surveyed plantar neuropathic diabetic foot ulcers, independently identifying *Staphylococcus* as the dominant wound bacterial genera (29.6% and 22.7% relative abundance). Of the total *Staphylococcus* population identified by Gardner et al., 2013, 96.5% of reads were assigned to the genus *Staphylococcus aureus*, while only 0.4% of reads were identified as skin commensal *Staphylococcus epidermidis* (Figure 1.8). In parallel, both Loesche et al., 2017 and Verbanic et al., 2020 also reported *S. aureus* as the most abundant *Staphylococcal* wound species. In relation to the remaining microbiome, Loesche et al., 2017 reported *Streptococcus* (11.98%), *Corynebacterium* (11.46%) and *Anaerococcus* (7%) to be the second, third, and fourth most dominant bacterial genera present in the DFU samples, with remaining genera contributing to less than 5% of the total relative bacterial abundance. Gardner et al., 2013 showed brief consistency with these findings, with *Streptococcus* (8.8%) and *Lactococcus* (3.9%) reported as the second and third dominant genera (Figure 1.8). One common finding across Gardner et al., 2013 and Loesche et al., 2017 was that the presence of S. *aureus* was both negatively associated with the abundance of anaerobic populations, and positively with the relative abundance of *Corynebacterium*.

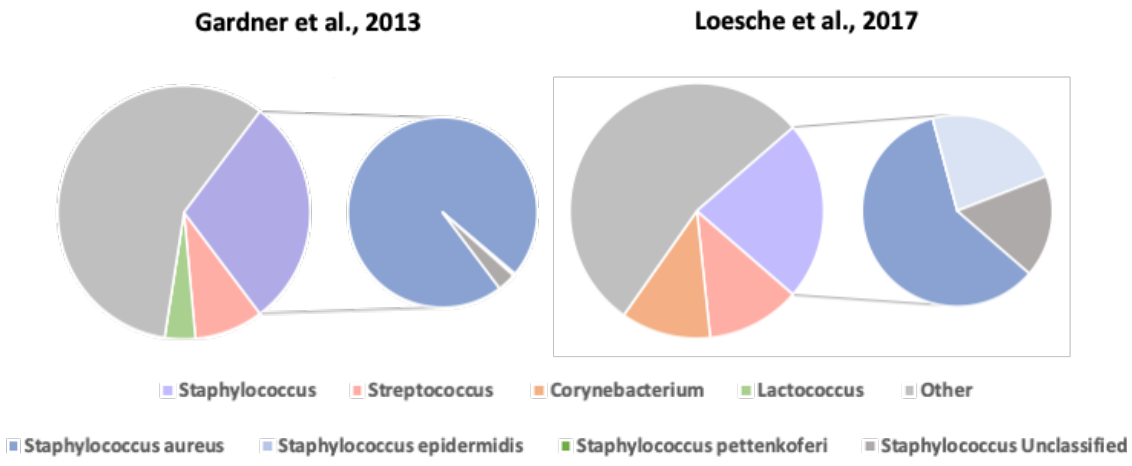

Figure 1.8: Dominant wound microbiome profiling. Dominant genus and the relative species contributions of the *Staphylococcus* genus (Gardner et al., 2013; Loesche et al., 2017).

While *Staphylococcal* dominance is frequently reported across wound microbiome studies, extensive variation in abundance is observed. Han *et al.,* 2011 confirmed that while *Staphylococcus* is present in over 90% of wound specimens, relative abundance varies from 9.6%–97%. In addition to *Staphylococcal species*, Min et al., 2020 also listed other significant members of the microbial community, including *Corynebacterium* (20.3%), *Arthrobacter* (6.9%), *Finegoldia* (6.1%), *Brevibacterium* (6.0%), *Peptoniphilus* (4.7%), *Oligella* (4.7%), *Anaerococcus* (3.9%), *Alcaligenes* (3.4%), *Streptococcus* (2.7%), *Porphyromonas* (1.7%) and *Pseudomonas* (1.0%). In a similar study, Park et al., 2019 acted to compare the corresponding wound bed and skin samples of DFU patients, observing that the abundance of *Pseudomonas*, *Bacteroides*, and *Enterococcus* was significantly increased in the wound tissue.

While culture-independent studies have attempted to characterise the bacterial fraction of the wound environment, the fungal wound mycobiome remains virtually unexplored (Kalan and Grice, 2018). Chellen et al., 2010 used culture-based methods to assess the prevalence rate and spectrum of fungal species infecting the deep tissues of diabetic lower-limb wounds (n=512). Fungal communities, spanning 18 individual species, were detected in 27.2% of all lower limb wound specimens (Figure 1.9). Of this population, over 60% of wounds presented with mixed fungal and bacterial species, while the remaining wounds contained only fungal flora. Dowd et al., 2011 was the first study to employ culture-independent techniques for fungal community analysis in the chronic wound environment. The study identified that 40.8% of DFUs were fungal-positive, exhibiting a total fungal to bacterial ratio of >50%. Across this study, the predominant detected pathogenic fungal communities included *Candida* species *Trichosporon asahii,* and *Rhodotorula species* (Dowd et al., 2011). Further highlighting the importance of these novel findings, recent research has demonstrated how the presence of fungi in multi-kingdom biofilms may provide structural scaffolding and enhanced protection for bacterial communities (Schlecht et al., 2015).

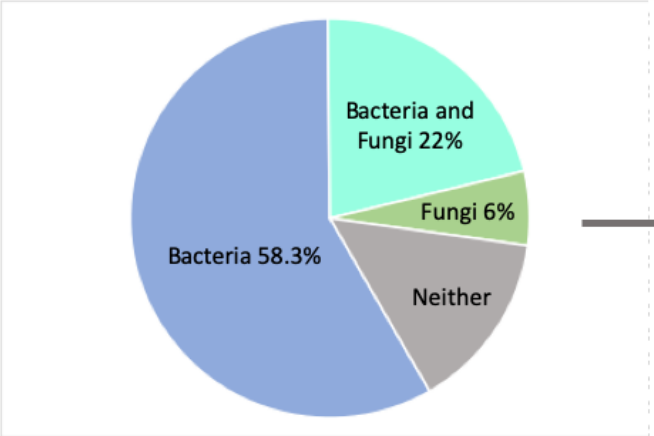

Species ID	Species Name	Percentage of Detection
1	*Candida parapsilosis*	25.5
2	*C. tropicalis*	22.7
3	*T. asahii*	12.8
4	*C. albicans*	10.6
5	*Aspergillus* sp.	5
6	*C. guilliermondii*	2.8
7	Non-*albicans Candida* sp.	2.8
8	*C. glabrata*	2.8
9	*Fusarium* sp.	2.8
10	*Candida sake*	2.8
11	*Zygosaccharomyces* sp.	2.1
12	*Kodamaea ohmeri*	2.1
13	*Candida globosa*	1.4
14	*C. krusei*	0.7
15	*Penicillium* sp.	0.7
16	*C. lusitaniae*	0.7
17	*Candida famata*	0.7
18	*Candida melibiosica*	0.7

Figure 1.9: Wound mycobiome profiling. The spectrum of frequency of fungal species isolated from deep tissue of diabetic foot wounds (n=512), using culture-based methods (Chellen et al., 2010).

1.4.2.1 The Impact of Clinical Covariates on the Chronic Wound Microbiome

In addition to community profiling, current studies have attempted to assess the relationship between microbial composition and clinical parameters. One covariable that these studies have focused on is patient glycated haemoglobin (HbA1c), a measurement of patient glycaemic control. Gardner et al., 2013 found that poor control of blood glucose was strongly correlated with the increased abundance of both *Staphylococcus* and *Streptococcus* species (Gardner et al., 2013). In parallel, Park et al., 2019 also revealed that higher proportions of not only *Streptococcus*, but also *Bacteroidetes* and *Peptoniphilus* were present in the wounds of participants demonstrating elevated HbA1c levels. In the investigation of the chronic wound fungal microbiome, Grice et al., 2018 found that elevated HbA1C levels and heightened white blood cell numbers were associated with the presence of pathogenic fungal communities, such as *Candida* and *Trichosporon* species.

In addition to glycaemic control, Gardner et al., 2013 reported associations between microbial diversity and ulcer depth/duration. In contrast to deeper and longer-lasting ulcers, a higher relative abundance of *S. aureus* was consistently observed in ulcers of a shallow nature and shorter duration. Additionally, Gardner et al., 2013 revealed that deeper ulcers and those

present for a longer duration generally demonstrated not only a higher relative abundance of anaerobic bacteria and Gram-negative Proteobacteria, but also greater overall bacterial diversity. However, these findings are not consistent across all studies, as Min et al., 2020 also analysed wound microbial diversity, identifying that microbial diversity across both healing and non-healing DFUs shared a large degree of similarity.

1.4.2.2 Association of the Wound Microbiome with Clinical Outcomes

Following the collection of wound microbiome profiling data, research groups now focus on how wound microbial composition may be used to predict clinical risk outcomes (Verbanic et al., 2020). So far, results have been highly heterogenous, reporting multiple correlations based on overall community stability and the presence of specific bacterial genera, species and strains (Loesche et al., 2017).

In relation to population stability, Loesche et al., 2017 observed that microbial permanence was associated with delayed healing, while community temporal instability was associated with enhanced healing. Whilst impaired healing generally correlated with *Streptococcus* or *Staphylococcus* community dominance, positive healing outcomes were associated with wounds exhibiting a highly diverse and heterogeneous microbial population (Loesche et al., 2017). In addition to community diversity and instability, the investigation of microbial community environmental oxygen requirements has also shown clinical importance. In Min et al., 2020, the most noteworthy study association was related to the abundance of Gram-positive anaerobic cocci (GPAC), in which the genera *Peptoniphilus* was significantly elevated in the wounds of DFUs with an impaired healing phenotype. This correlation has also been partially demonstrated within findings from other research groups. For example, Verbanic et al., 2020 also identified that facultative anaerobes, specifically the genus *Enterobacter*, acted as a negative prognostic factor of clinical wound outcomes.

In an attempt to study the microbiome in further depth, Kalan et al., 2019 investigated the abundance of wound bacteria at the strain level. The study identified that while S. *aureus* was

the most abundant *Staphylococcal* species, multiple strains of this pathogen were delineated, each with distinctive clinical associations. Whilst numerous *S. aureus* strains exhibited similar abundance profiles across all healing categories, a unique strain, *S. aureus* 10757 (SA10757), was exclusively associated with non-healing wounds. In another study aiming to understand the wound microbiome in extensive detail, Tipton et al., 2020 investigated how patient-specific processes may shape the wound microbiome. Overall, this study identified specific host genotypes associated with distinct involvement in host cell migration and focal adhesions. In relation to the microbiome, these host phenotypes were associated with inter-patient variations in the presence of wound pathogens, including *Pseudomonas aeruginosa* and *Staphylococcus epidermidis*, with subsequent associations to wound healing outcomes (Tipton et al., 2020).

In addition to bacterial community composition, the influence of fungal species on the process of wound healing should also be considered (Sandoval-Denis et al., 2016). Kalan et al., 2016 employed a fungal ITS1 region-based sequencing approach to accurately delineate the prevalence, frequency and structure of fungal communities commonly residing in DFUs. Fungi-positive wounds could be categorised based on the presence of either 'pathogenic' or 'allergenic' species. Throughout the study, pathogenic fungal species, including *Candida*, *Trichosporon asahii*, and *Rhodotorula* species were strongly linked with adverse clinical outcomes, such as perturbated cutaneous healing and subsequent major amputations (Kalan et al., 2016).

1.4.3 The Host-wound Microbiome Interaction

The recent advancement of culture-independent profiling techniques have revolutionised our understanding of the microbial world (Tang et al., 2022). In response, advanced characterisation of the wound microbiome provides critical insight into interactions that occur between the wound microbiota and host innate immune system (Tipton et al., 2020). Host-microbiome interactions that occur in the wound environment undoubtedly play an important role in wound repair, specifically in the activation of the host defence response (Duan et al., 2022). One important component of this host defence response is the production

of antimicrobial peptides (AMPs), natural antibiotics recognized for their potent antibacterial activity that act to modulate inflammatory and immune responses (Gera et al., 2022). As a first line of defence, these proteins are essential for preventing bacterial invasion and promoting cutaneous wound healing (Duan et al., 2022).

Host defence proteins are commonly classified according to their protein structure, with most clinically relevant proteins belonging to either α-helical or β-sheet groups (Nguyen et al., 2011). Under physiological conditions, α-helical peptides exist as unstructured proteins, assuming amphipathic helical structures upon exposure to pathogenic protein stimuli (Nguyen et al., 2011). Cathelicidin (LL-37), the most extensively studied α-helical peptide, is produced by numerous cell types including neutrophils, mast cells and keratinocytes, promoting immune responses via the stimulation of cytokine and chemokine production (Bandurska et al., 2015; Fabisiak et al., 2016). In contrast, β-sheet peptides maintain a consistent protein structure, declining any extensive physiological conformational change (Gera et al., 2022). Human β-defensins, expressed by keratinocytes, neutrophils and epithelial cells, exist as the most intensely studied β-sheet antimicrobial peptides in human wound repair (Yeaman and Yount, 2003).

1.4.3.1 Pattern Recognition Receptors

Stimulation of AMPs and related host defence peptide production is regulated predominantly by the activation of pattern recognition receptors (PRRs), including toll-like receptors (TLRs), nod-like receptors (NLRs) and C -type lectin receptors (Gera et al., 2022). Activation is instigated by the binding of each receptor to its corresponding ligand. This in turn initiates downstream inflammatory signalling cascades, including nuclear factor kappa B (NF-κB), leading to the production of host defence proteins and proinflammatory cytokines (Aluri et al., 2022). Investigation of host PRRs and their ability to regulate components of innate immunity is essential to characterise host-microbiome interactions that occur in the wound environment (Tang et al., 2022). To date, 10 TLRs have been identified in humans (TLR1–TLR10), many of which play a critical role in innate immunity and host defences-related gene

expression (Aluri et al., 2022). TLRs present at the cell surface prominently bind with microbial cell membrane components such as lipids and lipoproteins, including the lipopolysaccharide (Aluri et al., 2022). Intracellular TLRs mainly recognise nucleic acids derived from pathogens or self-nucleic acids associated with specific disease states (Figure 1.10) (Raziyeva et al., 2021). Overall, TLR-mediated signalling and initiated host defence responses play a critical role in optimal cutaneous wound healing, with multiple studies reporting delayed wound healing, reduced granulation tissue formation and impaired neutrophil recruitment in TLR2, TLR3, TLR4, or TLR2 and 4 double-deficient mice (Suga et al., 2014, Chen and DiPietro, 2017).

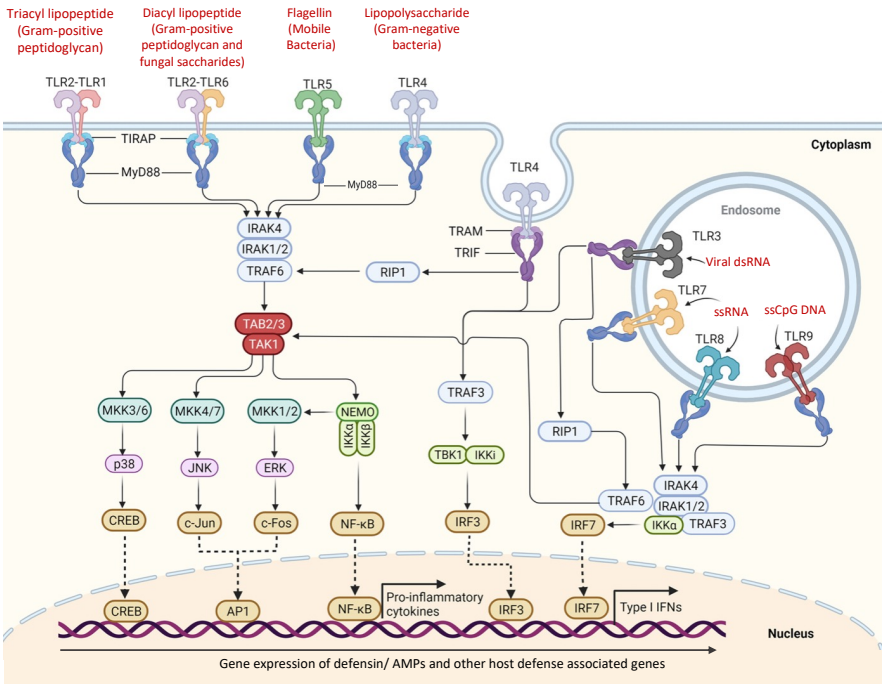

Figure 1.10: TLR signalling pathway in innate immune cells. The ligand affinity of human TLRs in the host defence response. Membrane pattern recognition receptors (PRRs), TLR5, TLR4, and heterodimers of TLR2/TLR1 or TLR2/TLR6 recognise pathogenic components at the cell surface (Duan et al., 2022). Transmembrane PRR, TLR4 resides at the cell membrane but is endocytosed into endosomes upon stimulation. Intracellular PRRs, TLR3, TLR7–TLR8, and TLR9 localise to cytoplasmic endosomes, where they have an affinity for recognising both pathogenic and host nucleic acids (Duan et al., 2022). Upon binding to their respective ligands, TLR signalling is initiated by receptor dimerization and interaction of TIR domains of TLRs with MyD88, TIRAP/MyD88, TRIF or TRAM/TRIF. Activation of these pathways stimulates downstream signalling molecules including IRAK4 and IRAK1/2, ultimately leading to the activation factor NF-κB. TAK1, which also results in the activation of MAPKs, results in the activation of critical transcription factors, CREB, AP1 (Duan et al., 2022). These transcription

factors cooperate with NF-κB to promote the induction of pro-inflammatory cytokines. Transcription factors activated throughout this pathway cooperate with NF-κB to promote the induction of pro-inflammatory cytokines, defensin, AMP and host defence gene expression. Image adapted from Duan et al., 2022.

Other critical players in host defence pattern recognition include both C -type lectin and Nod-like receptors (NLRs). In cutaneous human wound healing, Dectin-1 (*CLEC7A*) functions as a critical C-type lectin signalling pattern recognition receptor, innating antifungal immunity (Tang et al., 2018). Parallel to both the TLR and NOD-like receptors, activation of the C-type lectin receptors in turn triggers the downstream recruitment of TRAF6 and NF-κB activation, ultimately leading to the stimulation of AMP production and recruitment of tissue macrophages and neutrophils (Tang et al., 2018).

In contrast to the predominantly membrane-situated TLR and CLEC7A receptors, NOD-like receptors exist as essential intracellular sensors of the bacterial PAMPs and host DAMP-associated molecules (Trindade and Chen, 2020). In addition, NOD signalling also contributes towards type I interferon expression, an integral component of host antiviral immunity (Sabbah et al., 2009), with *Nod2*−/− mice demonstrating increased susceptibility to viral pathogens (Wu et al., 2020). An important function of the NOD proteins is to act synergistically with toll-like receptors (TLRs), both stimulating immune response and amplifying immune function in the presence of pathogen-induced TLR ligand tolerisation (Kim et al., 2008). This function can be demonstrated *in-vivo*, in which *Nod1*−/−*Nod2*−/− mice previously infected with *E. coli* exhibit decreased bacterial clearance and survival in the presence of subsequent infection (Lee et al., 2016). In studies of the skin microbiome, Nod2−/− mice display altered skinmicrobial composition, presenting increased pathogenic contribution and associated delayed wound closure (Williams et al., 2017).

1.4.3.2 Host Defence Peptides

A key function of cellular PRRs is to stimulate the production of host defence peptides, including beta-defensins (Contreras et al., 2020). In human wound healing, β-defensins 1-4

are known to play a critical role in bacterial clearance and restoration of the skin barrier (Contreras et al., 2020). While the exact mechanisms vary between individual defensins, antibacterial activity largely revolves around the attachment of defensins to negatively charged intermediate peptidoglycan synthesis lipids, leading to bacterial cell wall permeation and irreversible osmolytic damage (Figure 1.11) (Piipponen and Landén., 2020). Through these mechanisms, β-defensins have potent antimicrobial activity against a range of common wound pathogens, including hospital-acquired strains of *S. aureus, E. coli, P. aeruginosa, S. pyogenes,* and *C. albicans* (Bruggeman et al., 2019; Bolatchiev, 2020; Li et al., 2022). In addition to direct growth inhibition, the application of defensin molecules to patient implants has been shown to inhibit methicillin-resistant *Staphylococcus aureus* (MRSA) biofilm formation (Shen et al., 2020). In relation to host functions in human wound healing, human β-defensins are known to positively influence multiple aspects of the host repair processes (Contreras et al., 2020). Specifically, β-defensin-1 is known to stimulate the keratinocyte secretion of matrix metalloproteinase-9 (MMP-9), facilitating cellular migration (Bucekova et al., 2017). In addition, β-defensin-3 has been shown to promote angiogenesis and enhance fibroblast migration and proliferation through the activation of FGFR/JAK2/STAT3 pathways (Takahashi et al., 2021).

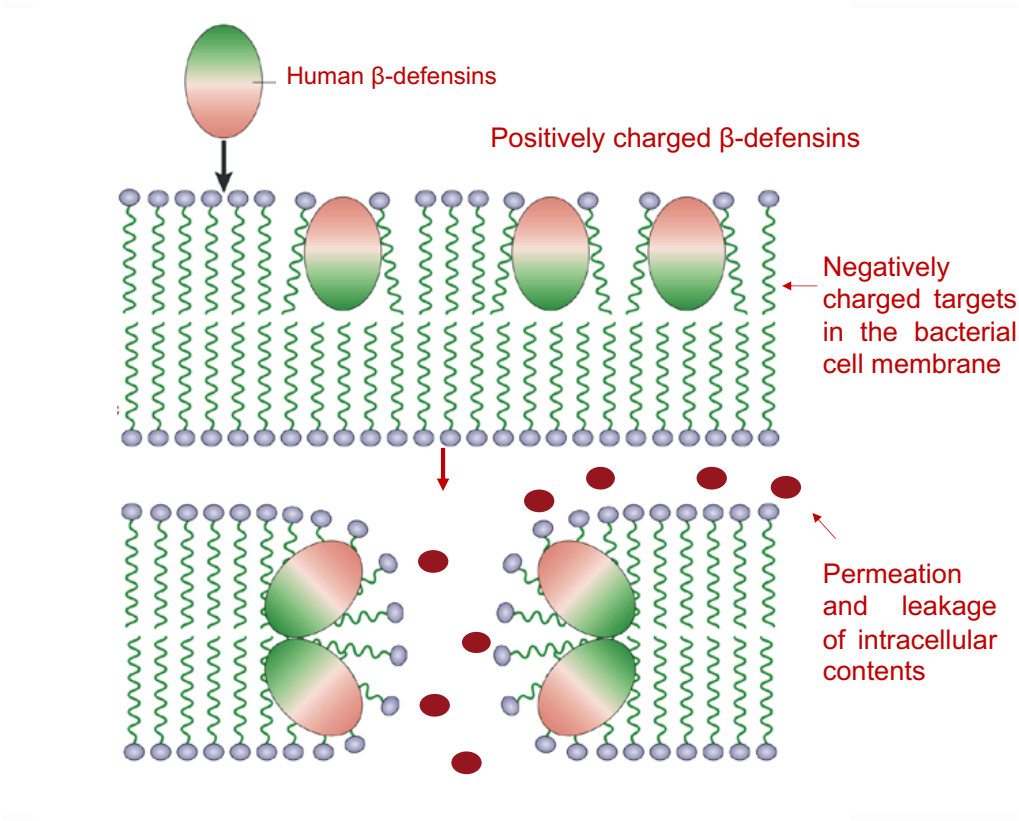

Figure 1.11: Mechanism of antimicrobial action of human beta-defensins. Image adapted from Ganz et al., 2003.

Supplementary to the β-defensins, additional antimicrobial molecules also function to provide immunity in response to bacterial stimulation, including proteinase inhibitors, chemokines, and enzymes (Gera et al., 2022), with one key example being the antimicrobial ribonuclease 7 (RNase 7) (Harder & Schröder, 2002; Petkovic et al., 2021). While the complete antimicrobial mechanisms of RNase 7 action are not fully understood, the expression of this peptide is primarily induced by the activity of pathogenic microbial stimuli and proinflammatory cytokines (Fritz, 2012, Gera et al., 2022). In the gut microbiota, RNase 7 is highly effective at repressing the growth of *Enterococcus faecium* (Köten et al., 2009), a function similarly replicated in the stratum corneum (Rademacher et al., 2016). Specifically, multiple studies exist reporting the potent antimicrobial activity of RNase 7 against the opportunistic pathogen *Staphylococcus* (Nasseri and Sharifi, 2021; Gera et al., 2022). In human skin explants, the deliberate inoculation of skin with *S. aureus* cultures induces the rapid expression and production of cutaneous RNase 7 (Simanski et al., 2010, Ahmad-Mansour et al., 2021). Independently, Zanger et al., 2010 also observed that relative *RNase7*

gene expression is significantly elevated in the tissue of those harbouring *S. aureus* as a colonising member of the skin microflora (Zanger et al., 2010). In studies inhibiting RNase 7 (Simanski et al., 2010, Spencer et al., 2010: Gera et al., 2021), reduced RNase 7 activity on the skin was shown to promote colonisation and accelerated growth of cutaneous *S. aureus* (Simanski et al., 2010). In parallel, inhibition of RNase 7 activity in clinical urine samples significantly increases the growth of uropathogenic genera including, *Pseudomonas, Klebsiella and Proteus* (Spencer et al., 2010).

Among the collection of additional host defence-related molecules, the S100 proteins have also recently gained increased interest, largely due to their emerging role in the modulation of host inflammation (Zackular et al., 2015). While constitutive basal expression is present, the presence of bacterial stimuli induces the biphasic TLR-5 mediated expression of the S100 AMP proteins in human skin (Ingram et al., 2018) Both Psoriasin (S100A7) and calprotectin (S100A8/A9) exist as fundamental regulators of keratinocyte migration, whilst also possessing the ability to directly stimulate the production of chemotactic agents involved in tissue neutrophil and T-lymphocytes recruitment (Zackular et al., 2015). In the host defence response, both Psoriasin (S100A7) and calprotectin (S100A8/A9) have been shown to harbour antimicrobial activity, sequestering environmental metal-ions as a mechanism of inducing antimicrobial nutrient competition (Rangaraj et al., 2017). Interestingly, S100A7 has reported pathogenic selectivity, eradicating the growth of *E. coli, P. aeruginosa and S. aureus*, while contributing to the maintenance of commensal microbial populations (Gla¨ser et al., 2005). Due to the strong response of calprotectin to bacterial stimuli, the S100A8/A9 protein is currently being investigated as part of an inflammatory biomarker algorithm to predict the underlying severity of diabetic foot ulcer infection prior to the onset of clinical symptoms (Ingrim et al., 2019).

1.5 Microbiome Analysis Techniques

Increasing literature now provides evidence that the microbial community composition of a wound environment may have a significant impact on the healing process (Johnson et al., 2018). In accordance with this, the development of new and effective microbial community

analysis methods in wound care remains an area of intense research (Xu and Hsia, 2018). Previous investigations have utilised both culture-based and culture-independent methods for bacterial detection and analysis, both of which, despite distinctive limitations, remain invaluable techniques in microbial research (Chapman et al., 2022). Overall, while this research has revealed a wealth of information, the significance of the cutaneous microbiome in the processes of wound repair and chronic wound formation remains poorly defined (Johnson et al., 2018).

1.5.1 Culture Based Methodology

Traditional culture-based testing techniques have been the mainstay for bacterial identification and isolation in clinical laboratory investigations for generations (Youseif et al., 2021). Such techniques were the first established methods used for the investigation of the human cutaneous/wound microbiota, with many of our frequent wound pathogens being previously identified and isolated via this approach (Bowler et al., 2001). Culture-based techniques have many distinct advantages, providing a vast quantity of microbial cells from a single clonal community (Emerson et al., 2017). Such populations can be utilised to yield data about clinically collected microbes in relation to bacterial growth, biochemistry and antimicrobial resistance (Emerson et al., 2017). Furthermore, culture-based methods benefit from the capability to selectively investigate the truly viable wound microbiota (Emerson et al., 2017). As culture-independent techniques are based on DNA sequencing, such methods typically do not distinguish between viable and nonviable DNA from microbial cells (Emerson et al., 2017). However, while microbial culture is still considered the 'gold standard' for specific microbial applications, these approaches also present a range of limitations (Wang et al., 2020).

Inherently, culture-dependant methods predominantly select for the most numerically dominant microorganisms, amenable to growth under the precise nutritional and physiological conditions provided by traditional diagnostic laboratory conditions (Youseif et al., 2021). As chronic wounds sustain complex poly-microbial populations, encompassing a selection of bacterial phyla, genera and species, wound microbial diversity is likely to have

been historically underestimated (Wang et al., 2020). One specific example is the identification of anaerobes, a bacterial subset commonly referred to as 'the secret pathogens of wound care' (Pitocco et al., 2019). While both acute and chronic wounds are susceptible to colonisation and potential damage by anaerobic microorganisms, the prevalence of these bacteria in the wound environment is often underappreciated (Johnson et al., 2018). This failure has been attributed to previous diagnoses that the presence of anaerobes is not determinantal to the wound repair process (Youseif et al., 2021). Moreover, the culture and identification of anaerobes from tissue samples is significantly more labour-demanding, costly and time-consuming than the frequent colonisers, a process which is often deemed too challenging for many diagnostic laboratories (Emerson et al., 2017). Additionally, while still commonly utilised, clinical cultures have limited diagnostic value in the absence of clinical signs of infection, as wounds are naturally contaminated by polymicrobial communities (Youseif et al., 2021). Therefore, it is now widely accepted that culture-based techniques have several limitations, offering data on only a restricted selection of microbial taxa (Bonnet et al., 2019).

1.5.2 Next Generation Sequencing Platforms

The previous decade has witnessed a revolutionary increase in the use of DNA sequencing platforms (Figure 1.12) (Gautam et al., 2019). This change has occurred predominantly due to the development of low-cost increased throughput sequencing methods, improvements which have allowed the analysis of microbial community composition in areas of clinical interest (Gautam et al., 2019). Numerous next and third-generation sequencing approaches have been developed and are continuing to advance the field of wound microbiology (Malla et al., 2019) (Figure 1.12). These platforms include 454 Roche, Illumina (MiniSeq & HiSeq), ABI SOLiD, ION Torrent, Pacific BioSciences, Qiagen Gene Reader and Oxford Nanopore Technologies (Malla et al., 2019).

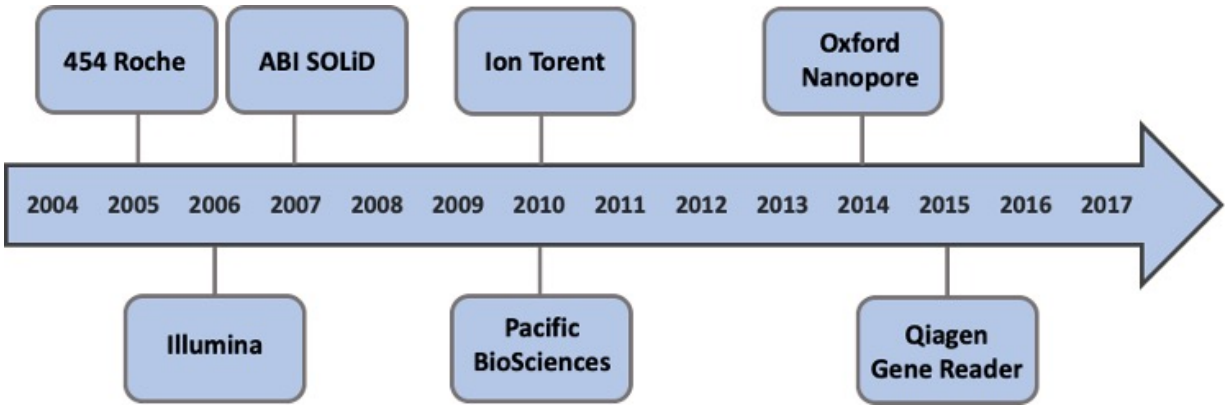

Figure 1.12: Timeline of the introduction of the next and third-generation DNA sequencing technologies and platforms. Image adapted from Malla et al., 2019.

Previous next-generation platforms have typically involved sequencing by synthesis (SBS) methods (Table 1.3) (Malla et al., 2019). For example, founded upon the principle of pyrophosphate release, Roche 454 produced the first form of SBS next-generation technology in 2005 (Thakkar et al., 2017). This approach involves the attachment of adaptors to fragmented genomic DNA, which are then amplified in water droplets immersed in oil (Thakkar et al., 2017). At the time of production, this sequencing method proved advantageous over other present sequencing platforms (Thakkar et al., 2017). In 2010, Ion torrent released the personal genome machine (PGM), which differed significantly from other methods of SBS, as this platform focused on the detection of enzymatic, rather than optical signals (Malla et al., 2019). As target DNA strands are submerged with a single nucleotide, complementary dNTPs are incorporated into the DNA template (Chapman et al., 2022). A hydrogen ion is released upon DNA polymerisation, producing a detectable change in the local PH. One further SBS platform that later became emphasised in the field due to its integrated workflow, is the Qiagen 'Gene Reader', which demonstrates an all-in-one platform (Garrido-Cardenas et al., 2017).

Yet, despite the introduction of multiple NGS platforms, the development of Illumina sequencing has previously dominated the field as the most widely used sequencing

technology for microbial genomics (Malla et al., 2019). Illumina incorporates a sequencing-by-synthesis method in which reversible dye terminators for all four bases are used to label and identify single bases as they are introduced into DNA strands (Weirather et al., 2017). DNA strands are cut into short fragments, followed by the attachments of adaptors to either end of the segments (ligation). As the DNA enters the flow cell, terminal sequences adaptors added to the DNA fragments before this step hybridize to specific oligonucleotides, holding the DNA strands in place during the sequencing process (Weirather et al., 2017). Once attached, fluorescently tagged nucleotides are added by DNA polymerase to the growing complementary DNA strand. Each base emits a unique colour, allowing the base added to be recognised. Once this stage is complete; all nucleotides are distinguished, and the added bases are recorded (Malla et al., 2019).

The emergence of these new techniques has allowed us to overcome many of the limitations characteristic of studies based on traditional culturing methods (Johnson et al., 2019), with the rapid development of next-generation sequencing (NGS) technologies remarkably augmenting our basic understanding of the microbial world (Johnson et al., 2019). However, at present, the wealth of research focusing on microbial populations using these sequencing platforms has focused on amplicon sequencing (Chapman et al., 2022). For example, the study of wound-related bacterial phylogeny and taxonomy has previously taken advantage of the 16S ribosomal RNA (rRNA) gene as a common genetic marker (Srinivasan et al., 2014). The 16S rRNA gene (approximately 1.5 Kbp) encodes a structurally essential component of the 30S small subunit prokaryotic ribosome, functioning as a highly conserved marker gene for the specific identification and classification of different bacterial genera (Srinivasan et al., 2014). This bacterial rRNA gene encompasses nine species-specific hypervariable regions, flanked by conserved evolutionary stable stretches. Such hypervariable regions can be used the identify bacterial genera and perform taxonomic studies (Malla et al., 2019). The highly conserved regions allow for broad-range amplicons, targeting individual 16S rRNA genes from poly-microbial populations using bacterial kingdom-specific primers (Srinivasan et al., 2014).

However, while 16S rRNA gene sequencing platforms such as 454 Roche, Illumina, ION Torrent and Qiagen Gene Reader have become a cornerstone of sequence-based bacterial

analysis, the use of short-read sequencing technologies demonstrates significant limitations (Srinivasan et al., 2014). For example, short-read paired-end sequencing technologies usually do not allow discrimination between closely related species, allowing only genus-level classification (Malla et al., 2019). Fortunately, the recent development of novel long-read third generation sequencing platforms acts to further combat these limitations. While many sequencing platforms have focused on adapting and improving current methods of polymerase-mediate DNA synthesis, most third-generation sequencing approaches have adopted a drastically different methodology (Table 1.3) (Malla et al., 2019).

Table 1.3: Characteristics of next and third-generation sequencing platforms

Method (Sequencing Reaction)	Advantages	Disadvantages	Current Platforms	Maximum Read Length	Number of Reads	Throughput
Sequencing by Ligation	Low Cost	Slow and low palindromic accuracy	SOLiD 5500 Wildfire	50-75 (Single End Sequencing)	700 M	80 -160 Gb
Sequencing by Synthesis: Cyclic Reversible Termination	High sequencing yield Potential for extremely high accuracy	Costly Equipment Low read length	Qiagen Gene Reader, Illumnia (MiSeq v2, v3, HiSeq2500 v4, 3000/4000)	50 (Single End Sequencing) 150 (Paired End Sequencing)	Up to 4B	Up to 700Gb
Sequencing by Synthesis:	Less equipment cost than other platforms		454 GS Junior, GS FLX, Titanium XLR70, 454 GS FLX + Ion PGM 314	1000 (Paired End Sequencing, 400 Single End Sequencing)	0.1-1M	Up to 700 Mb
Single Molecule Real Time Sequencing	Rapid Clinically useful sample Insight Extremely Long reads enhance metagenomic identification of closely related species Resolve complex structural variants and repetitive regions Portable Sequencing With the direct elimination of PCR bias.	Costly Equipment Not currently as readily adopted SMRTS have high raw error rates	Oxford Nanopore	Nanopores will read the length of the DNA fragment presented to them 200 Kb (Individual Read)	7-12 M NA	Up to 4 Tb
	Extremely Long reads		Pacific Biosciences	20 Kb	55,000 350,000	Up to 7 Gb

1.5.2.1 Oxford Nanopore Sequencing

Oxford Nanopore Technologies (ONT) is currently a principal company in the development and commercialisation of third-generation sequencing technology, making significant progress in previous years (Malla et al., 2019; Chapman et al., 2022). In 2014, the MinION, the first commercial sequencer was released, and the company now offers a range of devices that provide single-molecule real-time- sequencing (Mikheyev and Tin, 2014). This sequencing process is achieved by electrophoretically manipulating DNA molecules in a set solution through a nano-scale pore (Figure 1.13) (Mikheyev and Tin, 2014). Briefly, protein nanopores are embedded in an electrically resistant polymer membrane over an electrical detection grid (Chapman et al., 2022). A membrane voltage is then set, distributing an ionic current through each microscopic nanopore. The present DNA strands are threaded through microscopic protein nanopores by a molecular motor protein (Chapman et al., 2022). This motor protein is bound to the double-stranded DNA samples, functioning to both unwind the DNA molecules and maintain the position of DNA nucleotides long enough for base identification. As each DNA base passes through the pore structure, characteristic and measurable disruptions in the ionic correct are produced (Bowden et al., 2019). Using a base-calling algorithm, this process reveals specific characteristics of the molecule, which can then be translated in real-time to identify the order of nucleobases passing through the nanopore structure (McNaughton et al., 2019).

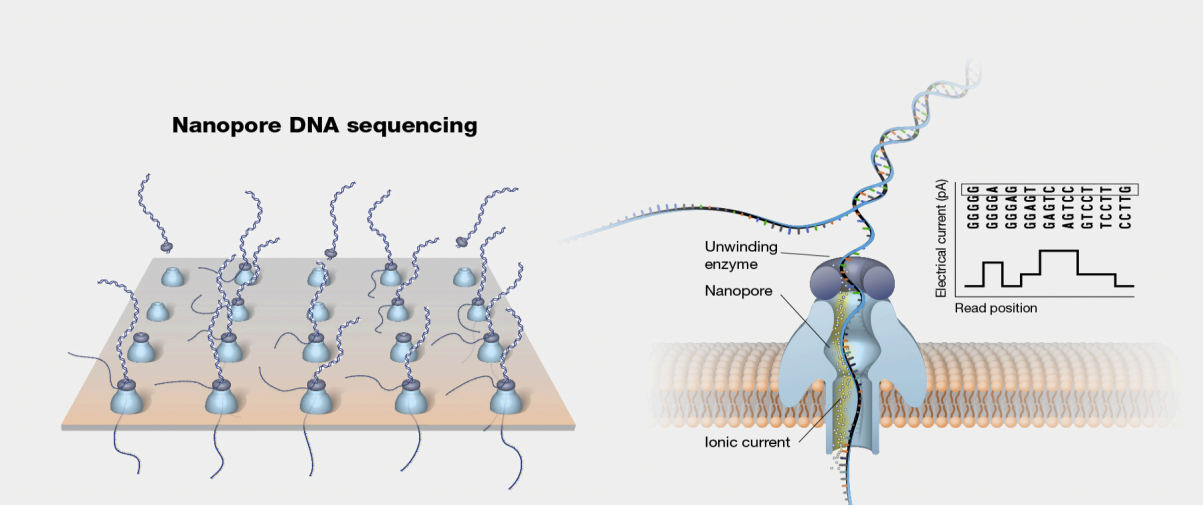

Figure 1.13: The mechanism of Nanopore sequencing. Initially, protein nanopores are embedded into an artificial electrically resistant polymer membrane inside the sequencing flow cell. A current is then applied across the membrane, prompting the negatively charged DNA strands to move through the set nanopores. The obstruction of a nanopore by a passing DNA fragment leads to characteristic changes in the current, which is then measured by electronic chips contained within the flow cell. A base-calling algorithm then uses these signals to determine the original DNA sequence. Image adapted from the national human genome research institute (NIH), 2023.

While DNA sequencing using protein membrane nanopores has been proposed for several decades, ONT remains the first to advance this concept into commercial development (McNaughton et al., 2019; Chapman et al., 2022). Using this technology, the combined advantages of enhanced data output, increased read lengths, speed and low equipment cost highlight this platform as an extremely attractive method of sequencing (Bowden et al., 2019). One of the principal advantages of nanopore sequencing is the ability to eliminate the requirements for nucleotides, polymerases or ligases during the sequencing process (Malla et al., 2019). Additionally, unlike parallel approaches (e.g., 454 Roche, Illumina, SOLiD or Helico Biosciences), nanopore sequencing removes the use of purified fluorescent reagents (Malla et al., 2019). This third-generation platform also functions to sequence unamplified sample material, including microbial genomic DNA, further eliminating the need for enzymes, cloning and amplification during the read-out process (Malla et al., 2019). In addition to allowing unbiased assembly, current research has reported that complete microbial genomes are generally assembled with long nanopore technologies using 10-fold fewer contigs than

previously demonstrated with next-generation short-read sequencing approaches (Sereika et al., 2022) The generation of significantly enhanced N50 values produced from third generation sequencing methods emphasises the ability of nanopore sequencing to produce an improved quality complete microbial genome assembly (Bowden et al., 2019). In accordance with this, MinION reads have been used to successfully enhance metagenomic identification, resolve challenging repeat regions, identify structural variants, discriminate between closely related species and determine the presence of genomic AMR genes, providing rapid sample insight (Bowden et al., 2019). Overall, this third-generation approach has the ability to revolutionise the analysis of microbial samples, with very few other approaches being capable of providing a point-of-care testing method with this level of species identification (Chapman et al., 2022). Recent advancement of nanopore-based sequencing products from ONT has been described by many as impressive, with the further adoption of ONT in the area of wound management providing an opportunity to characterise microbial communities in unprecedented detail (McNaughton et al., 2019; Chapman et al., 2022). When used in a clinical setting, the combination of advanced microbial analysis techniques and research into host-microbiome interactions holds significant clinical promise for the future of chronic wound care.

1.6 Project rationale, Hypothesis & Aims

Hypothesis: The overarching research hypothesis for this PhD is that in combination with host factors, species-level alterations in the human wound microbiome contribute to poor healing. In addition, new wound treatments, such as extracorporeal shockwave therapy (ESWT) may beneficially modify the wound microbiome to promote healing. The broad project aims are as follows:

Aim 1) To characterise the species-level microbiota profile of human skin and wounds. This aim will address the hypothesis that species-level alterations in the human wound microbiome contribute towards healing pathology. Specifically, skin and wound swabs will be collected from both healthy donors and those presenting with an active non-healing wound. Novel long-read sequencing approaches will be used to profile participant microbial community composition.

Aim 2) To explore the host-wound microbiome axis, by correlating host response, microbiome and related drivers of wound chronicity. Global transcriptional profiling (RNAseq) of wound related tissue samples from a selection of donors will be examined to identify distinct gene expression signatures in key wound healing-associated pathways. Next, species-level microbial composition profiles will be directly compared to host tissue transcriptional profiles, histological and clinical parameters to gain critical insight into the functional elements of host-microbe interaction.

Aim 3) To test the effects of extracorporeal shockwave therapy (ESWT) on both microbiome and healing. The effects of ESWT on proliferation, scratch assay closure, cutaneous repair and angiogenesis will be evaluated in human cell populations and/or in a human *ex-vivo* wound model. Antimicrobial efficacy of ESWT will be assessed against clinical wound isolates *in-vitro*. The direct effects of ESWT on diabetic foot ulcer microbiome will be evaluated as part of a clinical pilot study.

2 Materials and Methods

2.1 Ethics statement

All human tissue samples were obtained from surgical theatres at Hull Royal Infirmary (Hull, UK) or Castle Hill Hospital (Cottingham, UK) with full local research ethics committee (LREC) approval (REC: 17/SC/0220) (REC: 19/NE/0150) (IRAS: 311664, R&D R2743). All participants provided written informed consent. Identifiable participant information was anonymised to protect patient data. For comparative 'healthy skin; specimens, participants undergoing swabbing procedures provided written informed consent, under University Research Ethics Committee approval (Ref: FHS12).

2.2 Tissue Processing

Skin specimens collected from participant samples were incubated in Dulbecco's modified eagle media (DMEM) (Gibco™, Thermo Fisher Scientific, Loughborough, UK) with 2% antibiotic-antimycotic solution, (Gibco™) for a minimum of 30 minutes. Skin samples were washed thoroughly in Hanks' Balanced Salt Solution (HBSS) (Gibco™) with 4% antibiotic-antimycotic solution while undergoing continuous agitation. Tissue samples were then rinsed twice with Dulbecco's phosphate-buffered saline (DPBS) (Gibco™), and fully dried using sterile gauze. Following tissue processing, skin sections were either used immediately for experimentation (*ex-vivo* wounding/ histological processing) or used to harvest primary human skin cells.

2.3 Primary Human Dermal Fibroblast Isolation

Post-processing, human skin samples were incubated at 4ºC for 16 hours on a 0.2% neutral protease (dispase) (Gibco™), maintaining an upward epidermal orientation. Skin strips were then transferred to a sterile Petri dish (Thermo Fisher Scientific, Loughborough, UK), rinsed in DPBS and separated with sterile forceps into two distinct layers, the epidermis, a pale semi-transparent and the dermis, a thicker pinker layer (Boer et al., 2016). Dermal skin was then further dissected using a sterile surgical scalpel (No 22) and incubated at 37ºC, 5% CO2

and >95% relative humidity (standard culture conditions) for 3 hours in dermal enzyme-dissociation solution (Whole Skin Dissociation Kit, Miltenyi Biotec, Germany). Post incubation, the dissociation solution was diluted using 500µl of cold human dermal fibroblast growth medium (Gibco^{TM}) and ran on the 'h_skin_01' program setting of the gentleMACs dissociateor (Miltenyi Biotec).

Following program completion, sample tubes were detached from the gentleMACs dissociateor and centrifuged at 750 relative centrifugal force (RCF) for five minutes. The pelleted material was then resuspended in human dermal fibroblast growth media and filtered using a 70-micron pore cell strainer (Thermo Fisher Scientific). The primary human dermal fibroblast suspension was then centrifuged again at 750 (RCF) for five minutes, resuspended and seeded into a T25 cell culture vessel (Thermo Fisher Scientific) at a density of $5x10^5$ cells per flask· Primary cultures were then left undisturbed in standard culture conditions for approximately 48 hours before further culture.

2.4 Cell Maintenance and Passage

Throughout the remaining studies, human dermal fibroblasts (HDFs) were cultured in high glucose, no glutamine, no phenol red, Dulbecco's Modified Eagle Medium (DMEM) (Gibco™). HDF media was further supplemented with 10% heat-inactivated foetal bovine serum (Gibco™), 1% L-glutamine (Gibco™) and 1% Penicillin-streptomycin (Gibco™) (standard HDF media- Appendix 8.8). HaCaT cells (CLS Cell Line Service, Eppelheim, Germany), were cultured in high glucose, no glutamine, no calcium DMEM (Gibco™) supplemented with 10% heat-inactivated foetal bovine serum, 1% L-glutamine, 1% Penicillin-streptomycin and 1mM calcium chloride (Gibco™) (standard HaCaT media – Appendix 8.8). Throughout this thesis, all mammalian cell populations were maintained in standard culture conditions at 37ºC, 5% CO2 and >95% relative humidity.

For cell passage, adherent cultures were dissociated using 0.25% Trypsin solution (Gibco™). One dissociation was complete, proteases were neutralised using cell specific standard culture media (Appendix 8.8) and cell suspensions were centrifuged at 300 RCF for five

minutes, pelleted and resuspended in standard media. For primary cell populations not undergoing immediate experimental use, cellular cryopreservation methods were introduced to store cell populations without the possibility of ageing associated genetic or behavioural changes. Following the detachment and pelleting of each cell population, the supernatant of each tube was discarded, and cells were resuspended in standard culture media to a concentration of 5 x 10^6 cells/mL. The total volume of standard cell culture media was then combined with 10% (V/V) dimethylsulfoxide (DMSO) (Sigma-Aldrich) and immediately aliquoted into cryogenic storage vials (Scientific Laboratory Supplies) to start the freezing procedure within five minutes. Storage cryovials were insulated in several layers of embossed centrefold paper roll and place in the –80°C freezer. For long term storage, cells were transferred to liquid nitrogen storage after 48 hours. In culture, primary cells can only replicate and divide between forty to sixty times (Hayflick and Moorhead, 1961). At this point, cells will reach the Hayflick Limit, where breakdown will occur via programmed cell death or apoptosis due to telomere shortening and subsequent DNA damage (Hayflick and Moorhead, 1961; van Batenburg et al., 2021). Cells were used between their third and tenth passage for the studies described throughout this thesis.

2.5 Chemicals, Media & Plasticware

All chemical reagents used within this remaining study were of certificated analytical grade quality (Sigma-Aldrich, Poole, UK). Microbial culture media and agar supplied were provided by Oxoid (Basingstoke, UK) and reconstituted using the manufacture protocol (Appendix 8.8). General plasticware was acquired from STARLAB (Milton Keynes, UK) or Fisher Scientific (Loughborough, UK).

2.6 Bacterial Stocks & Storage

Bacterial clinical healthcare isolates were stored until collection on nutrient agar bijoux slopes (Oxoid, UK). After sample collection, permanent glycerol-based stocks were produced using Microbank bead cryovials (Pro-Lab Diagnostics, Canada), produced according to the manufacturer's protocol. Long-term bacterial bead stocks were stored at -80ºC until required.

2.7 Statistical Analysis

Generally, all data within this thesis is described as mean +/- the standard error of the mean (SEM). Unless otherwise presented, all statistical analysis was performed using GraphPad Prism version 8.1.1 for Mac (GraphPad Software, California, USA). Throughout, all generated data was checked for normality visually using the quantile-quantile (Q-Q) plot function. Specific statistical tests used across all results did include T-tests and one-way or two-way analysis of variances (ANOVAs). The selection of testing was dependant on the quantity of factors to be tested, followed by Tukey's multiple comparisons post hoc tests where required. All *p*-values of less than 0.05 were determined to be significant and delineated using one asterisk (*), while *p*-values < 0.01 are shown by '**', *p*-values < 0.001 by '***' and *p*-values < 0.0001 by '****'.

3 Profiling the Chronic Wound Microbiome

3.1 Introduction

Chronic non-healing wounds result from cutaneous insults, and fail to progress through a timely sequence of repair (Wilkinson and Hardman, 2020). It is estimated that in the UK alone, chronic wounds affect over 3 million people, resulting in an annual financial healthcare burden of approximately £5.3 billion (Guest et al., 2020). Although the magnitude of chronic wound burden is frequently overshadowed by the impact of primary disease (e.g. diabetes; Olsson et al., 2018), those affected experience devastating morbidity and mortality, severely reducing their overall quality of life (Sen et al., 2009). Patients at a high risk of developing chronic wounds include those with established disease, such as diabetes, peripheral atrial disease, and vascular insufficiency (Sen et al., 2009) and those over the age of 65 (Guest et al., 2020). As the worldwide prevalence of chronic wounds continues to rise, improved therapeutic approaches, focused on impeding the growing economic and human costs of this condition, are urgently needed (Verbanic et al., 2020).

The presence of infection and associated pathological inflammation is a major factor in delayed healing (Leaper et al., 2015). While not all chronic wounds are classified as clinically infected, all are subject to microbial colonisation which will likely influence the cutaneous healing process (Min et al., 2019). Previous wound microbiota profiling studies have utilised cultivation-based approaches; however, these techniques introduce severe bias and fail to fully recapitulate the complexity of the wound environment (Leonel et al., 2019). The rapid emergence of culture-independent genomic sequencing methods has remarkably improved our understanding of the human microbiome (Johnson et al., 2019).

Despite these advances, next-generation amplicon sequencing-based approaches (e.g. Illumina) typically offer limited phylogenetic resolution; due to poor discrepancy between highly similar 16S rRNA genes in combination with short-read lengths (<500 bp; Johnson et al., 2019). As a result, the majority of previously published studies are limited by low taxonomic resolution, that precludes accurate microbial identification to the species or strain

level (Kalan et al., 2019). Effectively discriminating between genetically distinct microbial strains and species is of utmost clinical importance, as bacteria of a single genus frequently possess important functional differences which can influence interactions with their host (Leonel et al., 2019). Shotgun metagenomic sequencing approaches can overcome this limitation, by providing further insight into the function and virulence of the wound microbiota (Kalan et al., 2019). One approach, third-generation (Oxford Nanopore) sequencing, utilises long-read sequencing, which can routinely produce reads in excess of 2.5Kb. Such read lengths are capable of sequencing the entire 16s rRNA gene and beyond (Johnson et al., 2019). As a result, Nanopore sequencing delivers enhanced taxonomic resolution at a previously unattainable species and strain level. The use of long-read technology for shotgun metagenomic sequencing, therefore, provides previously unattainable insight into the complexity of the chronic wound microbiome.

Recent studies suggest that the cutaneous wound environment undergoes major host environment-associated changes in microbiota, which contribute to the delayed healing phenotype (Kalan et al., 2019; Tipton et al., 2020; Verbanic et al., 2020). Generating a detailed understanding of how taxonomy associates with healing status is of paramount importance (Tipton et al., 2020). Investigations may determine keystone species that, in combination with host-related and clinical parameters, will promote or impede healing and/or act as biomarkers of healing phenotype. To date, several research groups have utilised culture-independent methods to investigate the microbiome of a variety of chronic wounds, including venous insufficiency ulcers, pressure ulcers, and diabetic foot ulcers (Gardner et al., 2013; Loesche et al., 2017; Min et al., 2020; Kalan et al., 2019; Tipton et al., 2020; Verbanic et al., 2020; Table: 3.1). Major bacterial genera identified include *Staphylococcus*, *Streptococcus*, *Corynebacterium*, *Pseudomonas*, and various anaerobes (Gardner et al., 2013; Loesche et al., 2017; Verbanic et al., 2020). Loesche et al., 2017 observed that improved healing outcomes may be correlated with increased microbial diversity and instability at the wound community level. Conversely, Kalan et al., 2019 and Min et al., 2020 were able to correlate specific microbial populations with negative healing outcomes. Finally, Verbanic et al., 2020 established a link between the relative abundance of wound bed facultative anaerobes and impaired healing.

Table 3. 1: Summary of recent wound microbiome studies

Study	Sample Type	Platform	Observations
Gardner et al., 2013	Neuropathic non-ischemic diabetic foot ulcer (n=52)	Roche 454	Ulcer depth was associated with ulcer cluster, positively correlated with abundance of anaerobic bacteria, and negatively correlated with abundance of Staphylococcus
Loesche et al., 2017	Heterogenous diabetic foot ulcer (n=100)	Illumina MiSeq	Temporal stability in chronic wound microbiota associated with poor healing
Kalan et al., 2019	Plantar Diabetic Foot Ulcer (n=100)	Illumina MiSeq	Several specific strains of *S. aureus* were exclusively associated with unhealed wounds
Min et al., 2020	Plantar Diabetic Foot Ulcer (n=10)	Illumina MiSeq	Increased initial abundance of Gram-positive anaerobic cocci (GPAC), especially Peptoniphilus was associated with impaired healing
Tipton et al., 2020	Chronic Wounds (nonspecific wound type) (n=96)	Roche 454 Ion Torrent	Participant genotypes were significantly associated with inter-patient variation of *Pseudomonas aeruginosa* and *Staphylococcus epidermidis.*
Verbanic et al., 2020	Diabetic, venous, arterial, and pressure ulcers (n=5 each)	Illumina MiSeq	High relative abundance of facultative anaerobes was significantly associated with non-healing wounds

Other than the above studies, there is limited literature exploring the clinical relevance of wound microbiome. In addition, most publications have utilised next generation (Illumina or Roche), short-read sequencing platforms with targeted 16S amplicon sequencing. Therefore, investigations of high taxonomic resolution are urgently needed to deepen our understanding of the wound microbiome and its therapeutic potential. To our knowledge, the characterisation of chronic wound microbial composition in relation to markers of favourable clinical outcomes, is yet to be evaluated by third-generation sequencing methods.

3.1.1 Aims

1) Evaluate species-level taxa, diversity and overall microbial community composition of healthy skin versus skin from an individual with an active wound.

2) Characterise all aspects of the chronic wound microbiome using a novel Nanopore-based sequencing approach.

3) To identify individual taxa (e.g., genera, species, strains) or community features (e.g., diversity, richness) associated with clinical parameters (e.g. wound duration, aetiology).

3.2 Methods

3.2.1 Study Design

Study inclusion criteria: Vascular dysfunction and a lower extremity wound. Principal exclusion criteria: aged 17 or younger; suffering from psychological disorders; participants unable to provide informed consent.

3.2.2 Sample Collection

Surplus tissue was collected from participants undergoing lower extremity surgery at Hull Royal Infirmary (Figure 3.1). Tissue samples were transported to the research laboratory for swab collection and processing. DNA from the wound, peri-wound and intact skin regions of participants was collected using nylon flocked swabs (Figure 3.1) (Copan Diagnostics, USA), pre-moistened in sterile PBS (as in Pondaven-Letourmy et al., 2020; Ok et al., 2020). In accordance with the Human Microbiome Project (HMP) guidelines (NIH HMP Working Group, 2009), swabs were continuously swiped and rotated across a one-inch squared sampling area for 30 seconds. Swabs were then carefully placed into MoBio Power Bead® 2mL collection tubes (MoBio, Carlsbad, California, United States) for immediate DNA isolation.

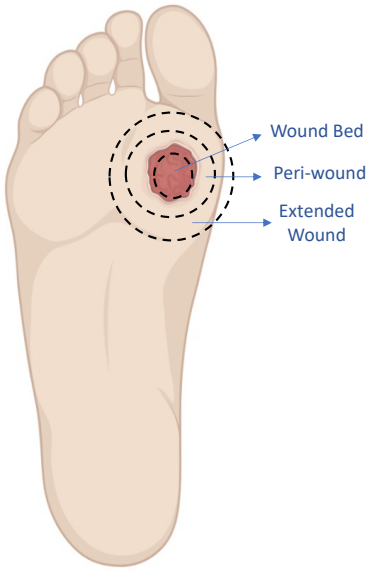

Figure 3.1: Schematic representation of DNA samples collected from lower extremity tissue donors. Participant tissue biopsy specimens were harvested from three wound based locations with increasing proximity to the wound environment, including: extended wound area, peri-wound and wound bed.

3.2.3 Microbial DNA Extraction

Following collection, samples immediately underwent DNA extraction according to the MoBio PowerSoil® DNA Isolation Kit protocol (Figure 3.2). Briefly, 60µL of lysis solution (C1) was added to each MoBio Power Bead® 2mL collection tube, then samples were vortexed and incubated at 70°C for 15 minutes. After lysis, the samples were centrifuged at 10,000 x g for 30 seconds and the supernatant collected. 250µL of solution C2 was then added to the supernatant and samples were incubated at 4°C for 5 minutes. After incubation, samples were spun down and the supernatant collected. 200µL of solution C3 was added to the supernatant and samples were incubated again at 4°C for 5 minutes. Following the collection of this supernatant, samples were combined with 1200µL of a purification solution (C4), transferred into spin columns and centrifuged. Following purification, 500µL of an ethanol based (C5) solution was added to each spin filter prior to centrifugation to complete the sample washing process. 50µL of DNA was then eluted into a separate collection tube and stored at -80°C.

Figure 3.2: Schematic depicting specimen collection procedure. Swabs were collected and processed for downstream DNA isolation and metagenomic sequencing.

3.2.4 Flow Cell Quality Control

Prior to use for sequencing, all flow cells underwent quality control steps using the MinKNOW graphical user interface (GUI; v.2.1-2.4). Flow cells were monitored for the number of active pores, with flow cells containing fewer than 800 pores being returned to Oxford Nanopore technologies as defective. Prior to DNA library loading, the average number of active pores available for sequencing across this study was 1248.

3.2.5 MinION Library Preparation

Preparation of the MinION DNA library was conducted in accordance with the Oxford Nanopore rapid PCR barcoding kit protocol (SQK-RPB004). Initially, 1µL of fragmentation mix (FRM) was added to 3µL of previously isolated template DNA, within a 0.2mL Lo-Bind PCR tube (Eppendorf, Germany). DNA then underwent fragmentation using a thermal cycler (Techne, Essex, UK) to incubate at 30°C for 1 minute, then 80°C for 1 minute. Following this process, 20µL of nuclease free water (NFW; Qiagen, Germany), 1µL of barcode (01-12a, Oxford Nanopore, UK) and 25µL of LongAmp Taq 2X master mix (New England Biolabs, USA) was added to the 4µL of fragmented DNA. The DNA solution then underwent PCR amplification (Table 3.2) to increase DNA yield prior to downstream sequencing.

Table 3.2: DNA library preparation PCR amplification

Function	Duration	Temperature (°C)	Cycle Number
Initial Denaturation	3 mins	95	1
Denaturation	15 secs	95	22
Annealing	15 secs	56	22
Extension	6 mins	65	22
Final Extension	6 mins	65	1

The amplification product was purified to exclude small non-specific fragments using 30µL of AMPure XP magnetic beads (Mag-Bind Total Pure NGS, Omega Bio-Tek, USA). The combined mix of DNA and beads were then washed twice using 200µL of 70% ethanol prepared in NFW (v/v). Collected pellets were resuspended in 10µL of 10 mM Tris-Cl pH 8.0 with 50mM NaCl and left to incubate for 2 minutes at room temperature. Magnetic beads were then pelleted using a magnet, and the DNA eluate removed for downstream sequencing. The DNA samples were then quantified using a Qubit fluorometer (Thermo Scientific™) and calibrated using the dsDNA high sensitivity kit standard protocol (Invitrogen, USA). The Qubit Fluorometer is a tool frequently used to accurately and quickly determine the concentration of either nucleic acids or proteins in a sample (Masago et al., 2021). Highly selective for double-stranded DNA (dsDNA) over RNA, the HS kit incorporates a spectrophotometer-based method to measure the natural absorbance of light at 260 nm for DNA (Masago et al., 2021). Included in the kit is a proprietary working solution buffer containing a fluorescent dye that binds specifically to analytes of interest such as double-stranded DNA (dsDNA) (Masago et al., 2021). This fluorescent based solution is mixed (200:1) with neat samples to emit a fluorescent signal at a strength that is proportional to the concentration of DNA present with each sample. Once quantified, the individual barcoded DNA libraries were then pooled in the desired ratios to a total of 50-100 fmoles. 1µL of Rapid Sequencing Adapter (RAP) was finally added to the pooled library and left to incubate for 5 minutes at room temperature prior to flow cell loading (Figure 3.3).

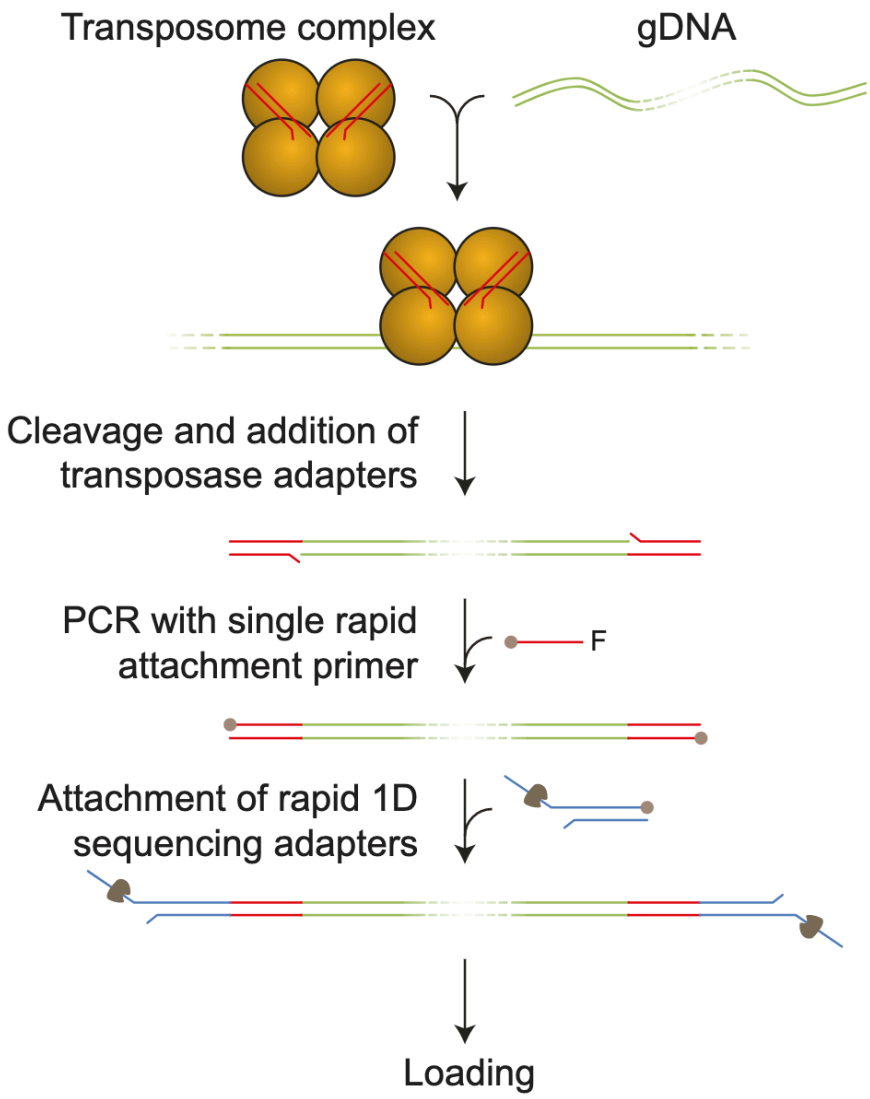

Figure 3.3: Rapid PCR barcoding kit (SQK-RPB004) workflow. A transposase conducts the primary function of the nanopore kit. The transposase complex simultaneously cleaves template DNA and attaches barcoded tags containing primer binding sites, which facilitate the attachments of rapid sequencing adaptors.

Following pooled DNA library preparation, a flow cell priming mixture was created by combining 30µL of Flush Tether (FLT) to a contained tube of Flush Buffer (FB). 800µL of priming mix was inserted into the flow cell priming port and the device was left to incubate for 5 minutes at room temperature. Following incubation, the flow cell sample port was opened and 200µL of priming mix was again added to the priming port (Figure 3.4). After the flow cell had been adequately primed, the sample mix was prepared. For this preparation 34µL of Sequencing Buffer (SQB), 25.5µL of Loading Beads (LB) and 4.5µL of NFW were added to the previously incubated 10µL DNA library and 1µL RAP. The sample solution was

adequately mixed and loaded into the SpotON sample port in a dropwise fashion. The MinION flow cell was then connected to the MinKNOW GUI software (GUI; v.18.12) the appropriate experimental parameters were selected, and DNA sequencing initiated. The exact appropriate experimental parameters include unique sample identification markers, DNA-based sequencing run methods with included PCR amplification and multiplexing kit selection (SQK-RPB004). Total run duration set at 48 hours, with no flow cell target data set. Minimum read length filter of 200 base pairs, with all active sequencing channels selected and no pores reserved. Output folder and high-accuracy base calling selected. No-alignment genome was selected for the current study. Minimum Q score of 7 selected for all DNA sequencing runs.

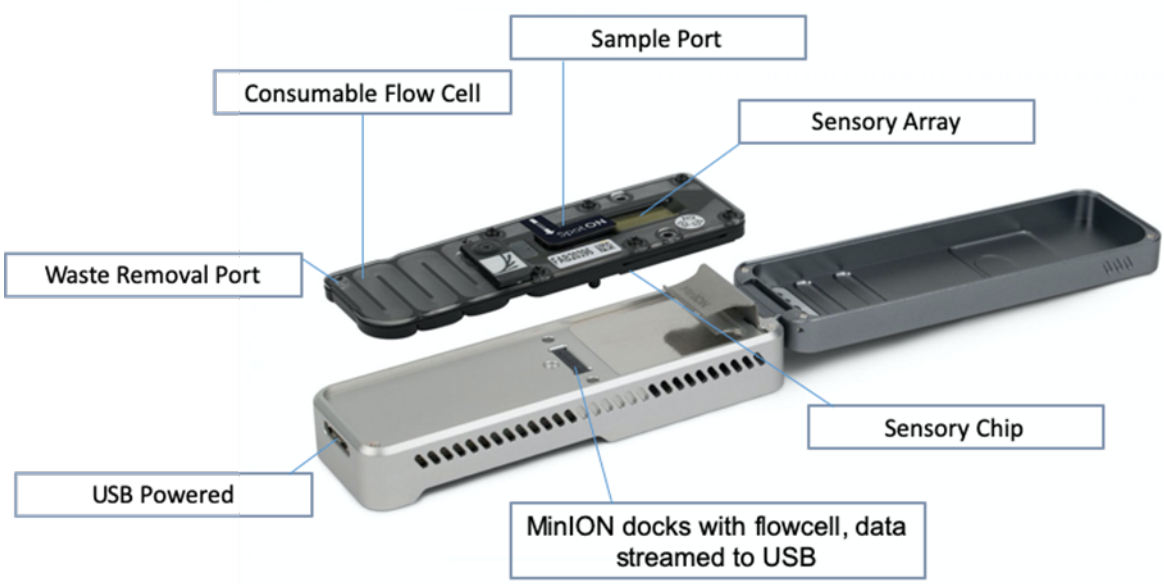

Figure 3.4: MinION DNA/ RNA sequencing device with flow cell. Weighing approximately 103 grams, the MinION device incorporates a consumable flow cell. The prepared DNA library is loaded directly into the sample port, the sample is then drawn by capillary action across the sensor array, where the nanopore sequencing is performed. The device connects to a PC or laptop for real-time sample analysis. Read length is dependent on the fragmentation process during the sample preparation, however, each flow cell can generate up to 12 million individual reads, or 30Gb of DNA sequence data.

3.2.6 Bioinformatic Processing

Bioinformatic-based methods described in this pipeline were performed using enhanced terminal MobaXterm (v.20.1) connected remotely to the University of Hull VIPER High Performance Computing (HPC) sever (Figure 3.5).

Raw data from the sequencing process was outputted in hierarchical data format or 'HDF5/Fast5' format. Each Fast5 file contained 4000 raw signal reads as the original source information for downstream sequencing analysis. For conversion into a readable format, base calling of the raw signal reads was conducted using the data processing toolkit: Guppy (v.4.2.2; Oxford Nanopore Technology, UK). All the data contained in this study was prepared using the SQK-RPB004 library kit and was sequenced on the MIN106D flow cell. Guppy was set to automatically 'fail' reads that demonstrated a Qscore of less than 7, removing them from downstream analysis. The quality score 'Qscore' of a base is an integer value estimating how likely the base identification is to be correct. Within this study, bases were called with a minimum accuracy of 80%.

Demultiplexing was conducted using Qcat (v.1.1.0). This command-line tool enables FASTQ files to be separated based on their barcode assignment. Firstly, FASTQ files were concentrated into one master FASTQ file. Qcat was then employed to output reads, with a single combined FASTQ file for each barcode. Any files unable to be classified by barcode were excluded from downstream analysis.

Further quality control steps were then carried out using Prinseq-lite (v.0.20.4) (Schmieder and Edwards, 2011). This is a form of statistical analysis software that allows the filtering, reformatting and trimming of next-generation sequence data. Within this study, Prinseq-lite was used to mask low-complexity nucleotide regions from downstream data processing. Low-complexity reads are stretches of nucleotides, that upon analysis, provide little content information and have limited biological significance. Within this software, the DUST algorithm approach was used to calculate the sequencing complexity, reads containing scores above 7 were considered low complexity and masked from future analysis.

The experimental tool Minimap2 (v.2.15) was then implemented, utilising the human genome reference database GRCh38 for mapping positions of the human genome alignments in the sequencing reads. Following sequence alignment, reads consistent with the human reference genome were removed using (Sequence Alignment/Map) SAMtools (v.1.3.1).

For microbial classification, centrifuge (v.1.0.4) was the designated engine. This system allowed for sensitive, rapid and accurate labelling of reads using a refined memory-optimised indexing scheme (4.2 GB for 4078 bacterial genomes).

Profiling data was then further transformed and assembled into feature table format using Quantitative Insights Into Microbial Ecology version 2 (QIIME2) software (Caporaso et al., 2010). For profiling community analysis data visualisation, MicrobiomeAnalystR (Chong et al., 2020; et al., 2017) and in RStudio (v.1.3) were used.

3.2.7 Functional Profiling – PICRUSt/COGs

Microbiome Analyst abundance based OTU table (Greengenes OTU ID) outputs were utilised for analysis with Phylogenetic Investigation of Communities by Reconstruction of Unobserved States (PICRUSt) (PICRUSt.V2). PICRUSt uses an extended ancestral-state reconstruction algorithm to predict which gene families are present and then combines gene families to estimate the composite metagenome (Langille et al., 2013). The Clusters of Orthologous Groups of proteins (COGs) database was then utilised to classify proteins from completely sequenced genomes on the basis of the orthology concept. COGs derived from the samples were then assigned to functional categories with accompanying functional predictions.

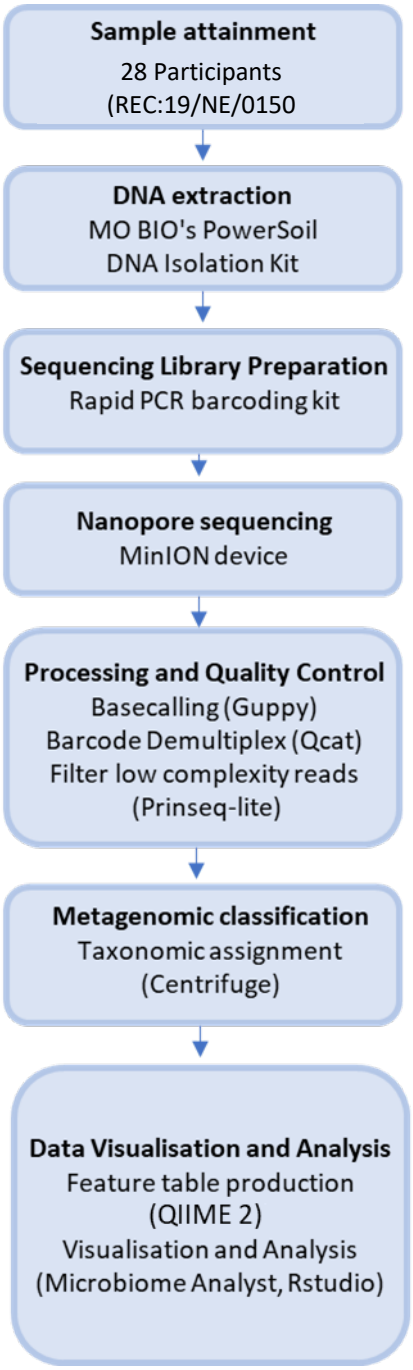

Figure 3.5: Flowchart of nanopore sequencing workflow. Summary flowchart documenting the individual experimental steps of wound microbiome profiling analysis.

3.3 Quality Control

3.3.1 Nanopore Quality Control Checkpoints

The summary statistics of individual nanopore runs provided information on nanopore quality control parameters. A typical summary statistics report is shown in Figure 3.6. In this run, read sequencing was observed for all included sample barcodes, with reasonable distribution of reads between barcodes (Figure 3.6: A). While this is indicative of effective barcoding adaptor attachment, difficulties can arise regarding the equal distribution of reads between demultiplexed samples. Within the run, a significant sum of the sequencing data is generated within the first eight hours (Figure 3.6: B), corresponding to the timeframe in which the first group of pores are actively sequencing (Tyler et al., 2018). Each flow cell has 512 channels, each connected to four individual pores, allowing the simultaneous sequencing of 512 DNA molecules. As each channel provides data from only one well/pore at any given time, the order of pore use is allocated during periodic 'mux scans', in which the most suitable pore is selected for sequencing. Default sequencing scripts initiate MUX scans every eight hours during the sequencing process, at which point many of the in-use pores will have accumulated damage/degraded, allowing pore reallocation (Laver et al., 2015). For this reason, intermittent increases in sequencing yield are often temporarily seen following MUX scans. Throughout all runs conducted within this study a Q score of 7 was used, with the small proportion of reads scoring below this being eliminated from downstream analysis. The average Q score value across the full dataset was between 9-10, with an inferred base call accuracy of around 90%. Finally, library preparation with the RPB004 rapid PCR barcoding kit entails a DNA fragmentation step. Read count lengths present in the summary statistics indicate effective sample fragmentation with a mean read length of around 2.4Kb (Figure 3.6: D).

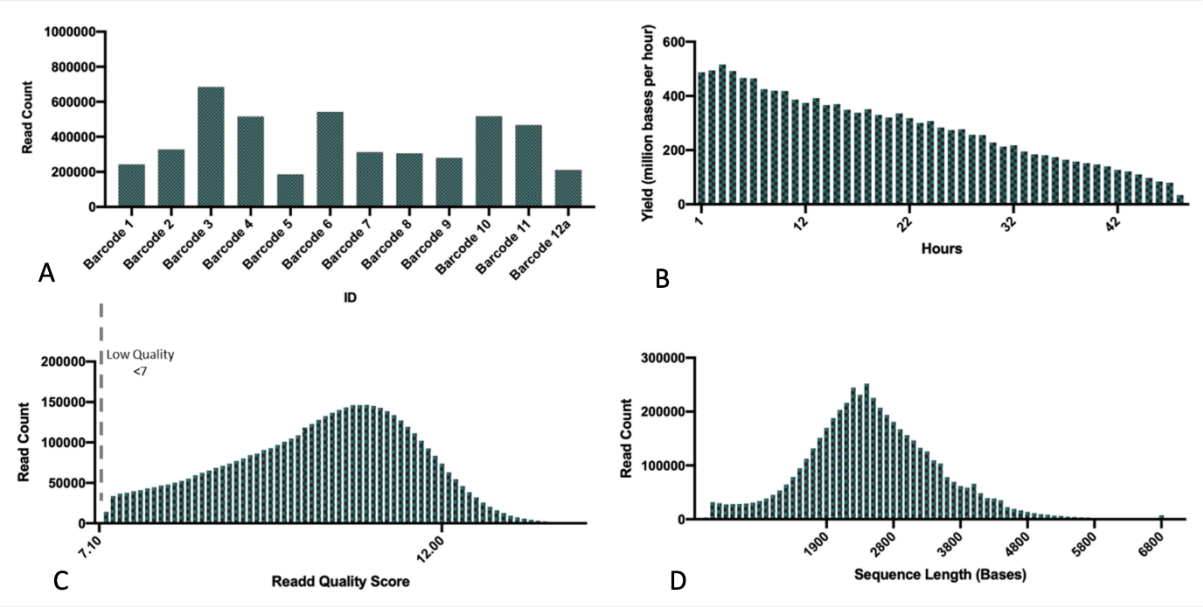

Figure 3.6: Summary statistics of a standard 48-hour Oxford Nanopore MinION (RPB004) sequencing run. Assigned barcode counts show read distribution across samples multiplexed within a single run (A). Yield (per million bases) show sequenced reads gradually decline over a 48-hour run period (B). Read quality scores were generally high, with low quality <7 reads removed (C). Confirmation of DNA fragmentation (2-3K reads) prior to sequencing (D).

3.3.2 Mock Community Validation

To investigate sequencing quality, workflow bias, library preparation and the impact of protocol modifications on data outputs, a ZymoBIOMICS Microbial Community DNA standard (D6305) was sequenced alongside study samples (Zymo Research, USA). Composition following both 14 and 22 PCR amplification cycles was tested and compared to known composition (Figure 3.7). This was to assess whether increasing PCR cycles from 14 to 22, as required due to low sample biomass, influenced community abundance composition.

Theoretical composition of the ZymoBIOMICS Microbial Community DNA based on genomic DNA was defined as: *Listeria monocytogenes - 12%, Pseudomonas aeruginosa - 12%, Bacillus subtilis - 12%, Escherichia coli - 12%, Salmonella enterica - 12%, Lactobacillus fermentum - 12%, Enterococcus faecalis - 12%, Staphylococcus aureus - 12%, Saccharomyces cerevisiae - 2%, and Cryptococcus neoformans - 2%.*

Sequence data from the mock community subject to 14 or 22 PCR cycles showed strong agreement with the theoretical composition expected. It was noted that *Pseudomonas aeruginosa* was underrepresented following Nanopore sequencing, regardless of PCR cycle amplification number. Additionally, only one of the two fungal isolates present in the mock, was successfully identified. *Saccharomyces cerevisiae* was classified and represented at proportions identical to its theoretical abundance however, *Cryptococcus neoformans* was not identified within the mock community sample at either 14 or 22 PCR cycles. This evaluation confirms that cycle number has little influence on sequencing output. It does highlight some discrepancy between sequence data and actual composition, due to unknown factor(s) such as technological limitations of the sequencing platform or potential downstream classification bias. However, overall it confirms the suitability of the nanopore analysis pipeline for species-level metagenomic characterisation of biological samples.

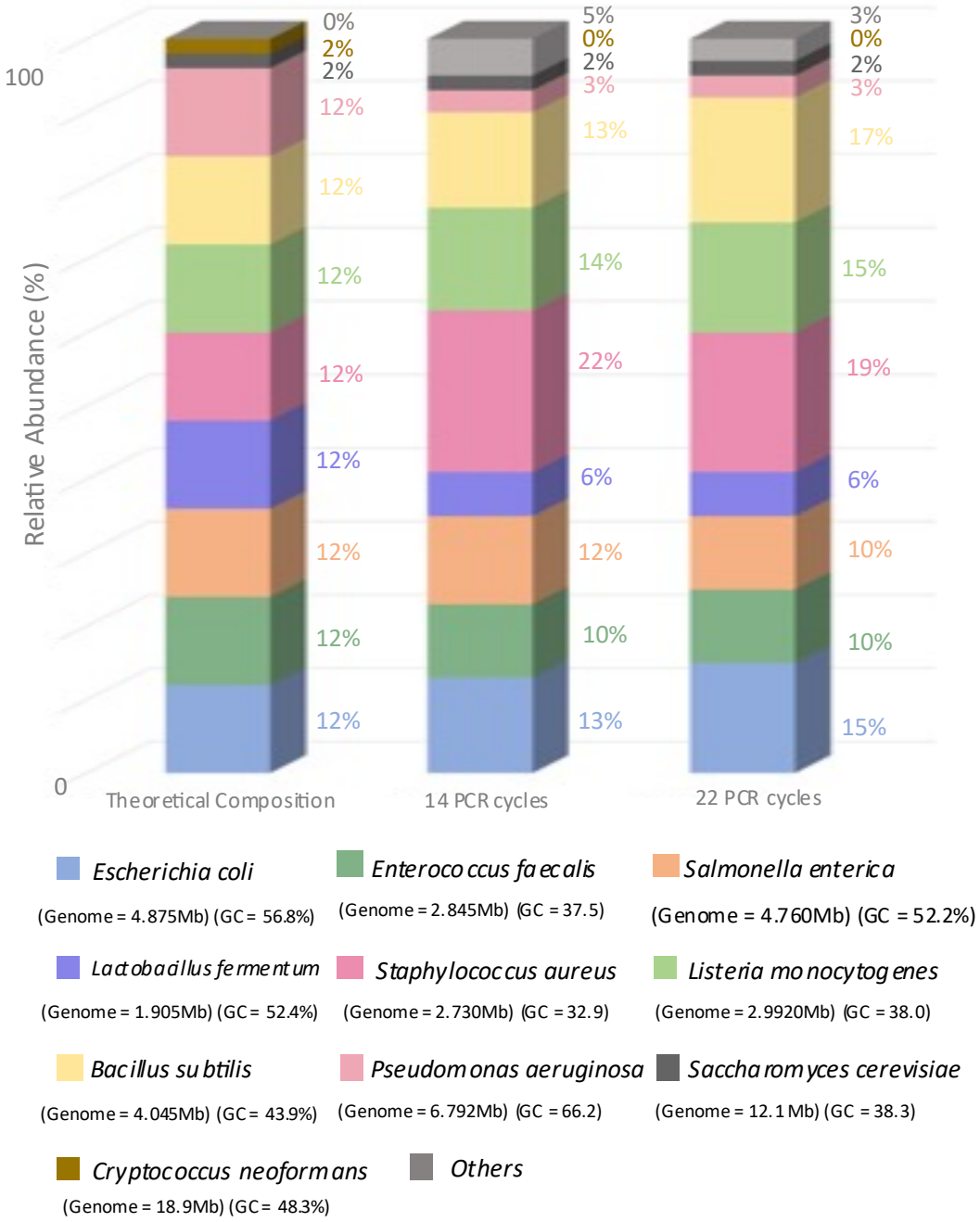

Figure 3.7: Analysis of mock community composition comparing theoretical abundances to data following differential PCR amplification. Relative composition of reads sequenced by Nanopore, including theoretical read composition compared to profiles obtained following 14 and 22 PCR amplification cycles. Percentages represent the measured proportion of reads for each species.

3.4 Microbiome Profiling Overview

In this study, 73 swabs from a total of 34 donors were collected. Of the total 34 donors, 28 presented with a chronic wound, undergoing lower extremity amputation at the time of sample collection. The 67 swabs analysed from this group included DNA from a range of sample sites across the donors. Generally, three sites were chosen for sampling of the post-amputation tissue: 'intact' skin [n=16], peri-wound [n=17] and wound (bed) [n=34]. Alongside DNA collection, corresponding tissue biopsies were collected from 28 donors for differential gene expression and histological analysis. Six swabs from the feet of healthy control donors were collected for comparative analysis.

The samples within this study generated a combined 4,374,041 microbial reads spanning 6768 operational taxonomic units (OTU), from three distinct domains: bacteria (99%) eukaryotes (1%) and archaea (<0.01%). High variation in read number was observed between samples; the lowest sample read number was 48 reads (post-host read removal) and the highest 495,011, with a mean of 50,860 reads per sample. Species accumulation curves (Figure 3.8), reveal variation in sequencing saturations between study samples (Good's coverage estimations – Appendix 8.8). However, as in other published studies sampling diverse microbial communities (Burner et al., 2021), species accumulation curves were still increasing for a select number of samples (Figure 3.8). The total library size of samples varied throughout the study, this was likely due to inherent differences in sample DNA yield and quality, rather than methodological variability.

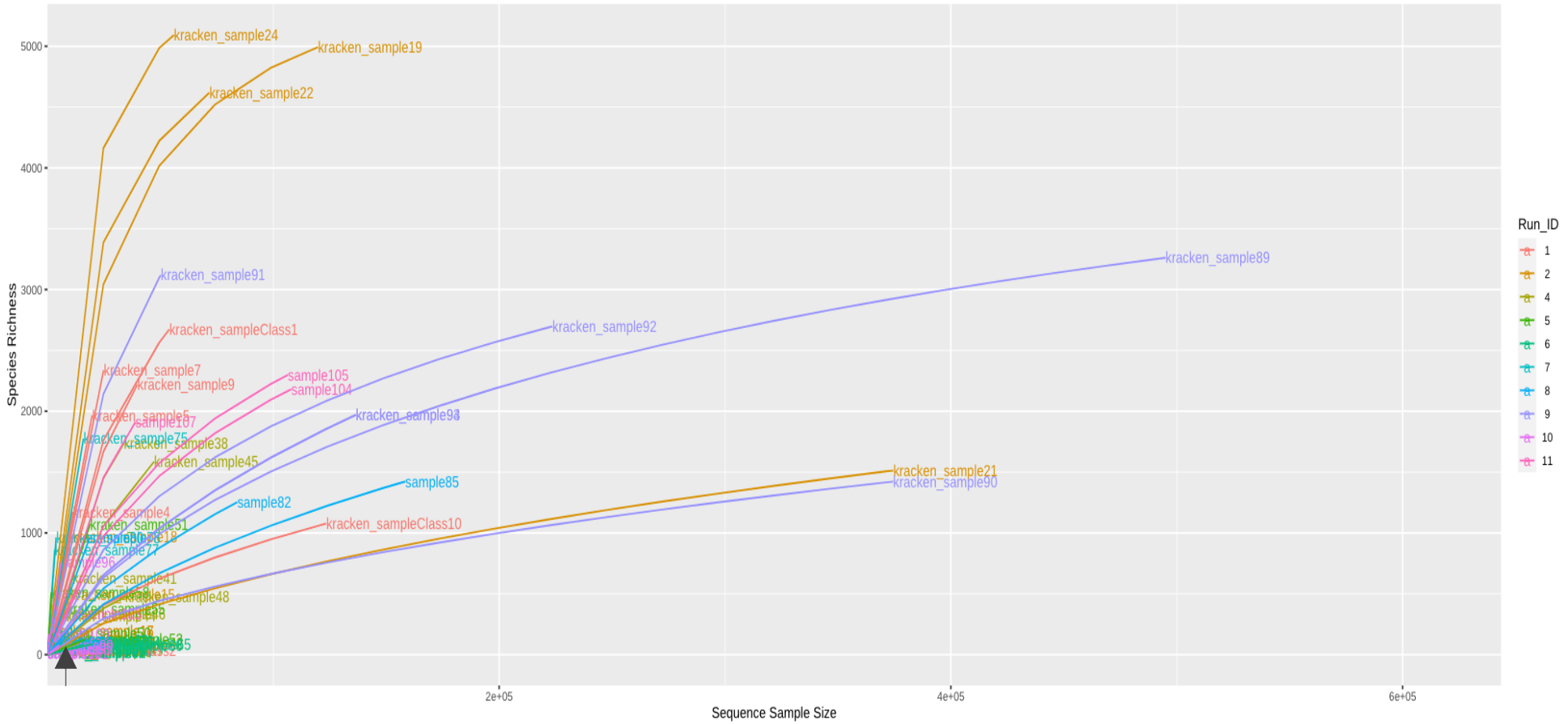

Figure 3.8: Species accumulation curve of all study samples. Samples are coloured according to run ID number. Black arrow indicates the smallest library size produced across all samples. In the instance of library rarefaction, only data/reads situated left of the identifying arrow would be included in the analysis for the current study. Goods coverage for each sample is contained in Appendix 8.8.

The microbiome research community now commonly advocate the avoidance of rarefying altogether for the analysis of complex microbiome-based data sets, due to the potential of excluding valid data (e.g. McMurdie and Holmes, 2014). As a result, data within this study did not undergo rarefaction prior to data visualisation. Instead, total sum scaling (TSS) normalisation was implemented (Lin et al., 2021). This scaling method removes technical bias related to variations in sequencing depth by presenting each feature count according to the total library size, yielding the relative proportion of counts for that feature (OTU; Lin et al., 2021).

In line will other community microbiome profiling studies, subsequent analysis methods included calculation of alpha and beta diversity, while data was visualised by principal coordinates analysis (PCoA) and OTU hierarchal clustering heatmap analysis (Verbanic et al., 2020; Lin et al., 2021). For alpha diversity profiling, a range of diversity metrics were utilised to limit the likelihood of data outcomes being method dependent. For the different metrics, "observed diversity" identifies unique OTUs per sample, while "Chao1" and "ACE" both estimate metrics based on abundance, thus requiring data that includes sample abundance according to class (Chong et al., 2020). "Shannon index" focuses on the equality of OTU proportional abundances, while "Simpson index" focuses on OTU richness and evenness (Chong et al., 2020). For differential expression analysis, data was normalised by the application of variance stabilisation transformation (VST), selected to allow for the simplification of considerations in graphical exploratory data analysis (Kelmansky et al., 2013). Principal coordinates analysis for the visualisation of beta diversity were calculated using the Bray-Curtis dissimilarity index. This statistical measure was used to quantify the compositional dissimilarity between two samples or groups, bounded between 0 and 1, where 0 indicated identical composition and 1 represents a complete lack of similarity (Modin et al., 2020)

3.4.1 Participant Characterisation and Summary Statistics

For the current study, 67 swabs were collected from 28 donors, who presented with a chronic wound, undergoing lower extremity amputation at the time of sample collection (Figure 3.9). Donor metadata and wound summary details are present in Appendix 8.2 and 8.3. 75% of participants received a below knee amputation, 21% received an above knee amputation and a single donor (3.4%) underwent a through-knee amputation. The average donor age was 70 (ranging from 36 to 86) and 75% of participants were male. The majority (69%) of participants were of positive diabetic status, whilst 57% of donors were determined to have clinically infected wounds. Full blood profiles were available for each participant, including haemoglobin, white cell count, platelet, sodium, potassium, albumin, and bilirubin values. The average haemoglobin A1c (HbA1c) level was 78 mmol/mol, ranging from 45 to 149 mmol/mol. The antibiotic status of 82% of the volunteers was known, the remainder were excluded from the any antimicrobial exposure-based analysis, due to their unknown status.

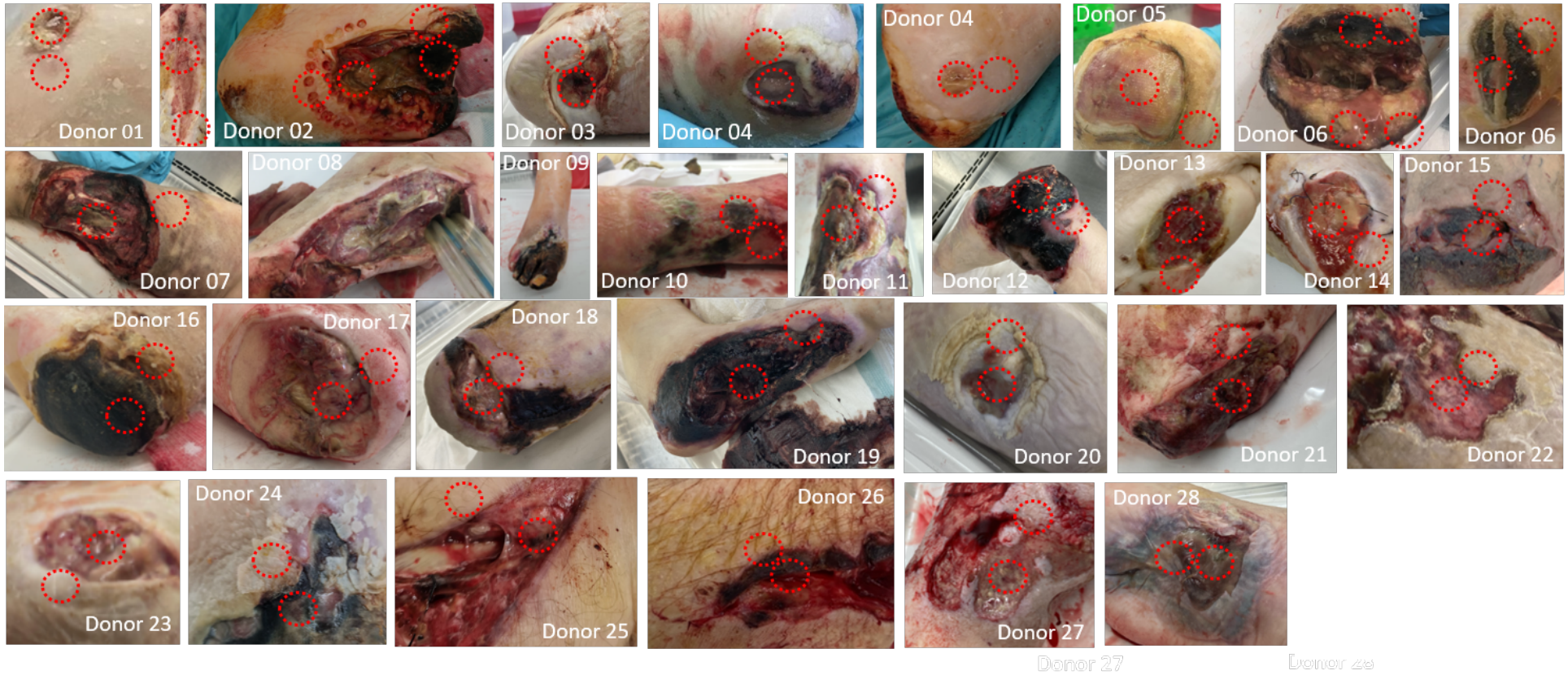

Figure 3.9: Representative images of each wound sample included within the study. Red indicators are markers of exact swabbing location.

3.5 Results

3.5.1 Skin microbial community composition varies significantly between those with and without a non-healing wound.

Initially, microbial community composition was investigated across donor skin samples. Swabs were acquired from intact skin present on the feet/legs of both healthy participants (Healthy Skin - HS), and those undergoing lower extremity amputation with the presentation of a non-healing wound. Participants with a wound were then further classified according to diabetic status, non-diabetic skin (NDbS) and diabetic skin (DbS). Post sequencing, data analysis was performed across all donors and incorporated reads from all kingdoms. Across multiple levels of the taxonomic hierarchy, principal coordinates analysis (PCoA; Figure 3.10: A), revealed significant community grouping based on donor classification. Alpha diversity metrics (Chao1, Observed, Fisher) revealed that, at the species-level, healthy skin samples were significantly more diverse than the skin of those with a chronic wound (*p-value: <0.001*). This trend was not observed with Shannon or Simpson diversity metrics (*p-value: 0.52, 0.57*; Figure 3.10: B). Taxonomic visualisation was then performed to further examine group-specific differences highlighted by PCoA analysis (Figure 3.11).

Proteobacteria were identified as the most abundant phyla (HS:57%, DbS:86%, NdbS:34%) in study samples, primarily the genus Enterobacter (97%) in HS. In NDbS and DbS samples, the Proteobacteria composition was more varied, incorporating multi-genus contribution (NDbS: 42% Proteus, 37% Enterobacter and 18% Escherichia; DbS: 33% Pseudomonas, 29% Proteus, 12% Escherichia and 0.5% Enterobacter). As previously highlighted (PCoA; Figure 3.10: A), specific phyla exhibited distinct donor group association. For example, Actinobacteria were elevated in diabetic skin samples (11.1% DbS, 2% HS, 1.9% NDbS), whilst Bacteroidetes were almost exclusively confined to the skin of those with a chronic wound (2.2% NDbS, 1.8% DbS, <1% HS).

Significant proportions of Firmicutes were also identified within all groups (HS: 41%, NDbs: 7%, DbS: 51%), predominantly accounted for by the genus *Staphylococcus* (HS: 39%, NDbs: 39%, DbS: 84%). However, the individual *Staphylococcal* species comprising this genus varied considerably. Notably, the relative abundance of *Staphylococcus epidermidis* was significantly lower in all patient skin groups compared to that of the healthy skin (Bubble plot; Figure 3.11). The composition of the HS: 43% *epidermidi*s, 26% *capitis* and 17% *pettenkoferi* and 1.6% *aureus*, was very different to the post amputation group: NDbS: 31% *epidermidi*s, 32% p*ettenkoferi* and 6% *aureus*. DbS: 40% a*ureus*, 12% *pettenkoeri* and 10% *epidermidis*. In addition to *Staphylococcus aureus*, taxonomic level resolution revealed numerous other species predominantly identified in DbS samples, including *Pseudomonas aeruginosa* (<1% HS/NDbs, 11% DbS), *Staphylococcus caprae* (<1% HS/NDbs, 11% DbS) and *Corynebacterium striatum* (<1% HS/NDbs, 10% DbS). Whilst *Proteus mirabilis* was observed largely in the wound presenting participant population (HS: <1% HS, NDbS 36%, DbS 10%). Visual analysis of the overall top 12 most abundant taxa (Bubble plot) is presented in Figure 3.11.

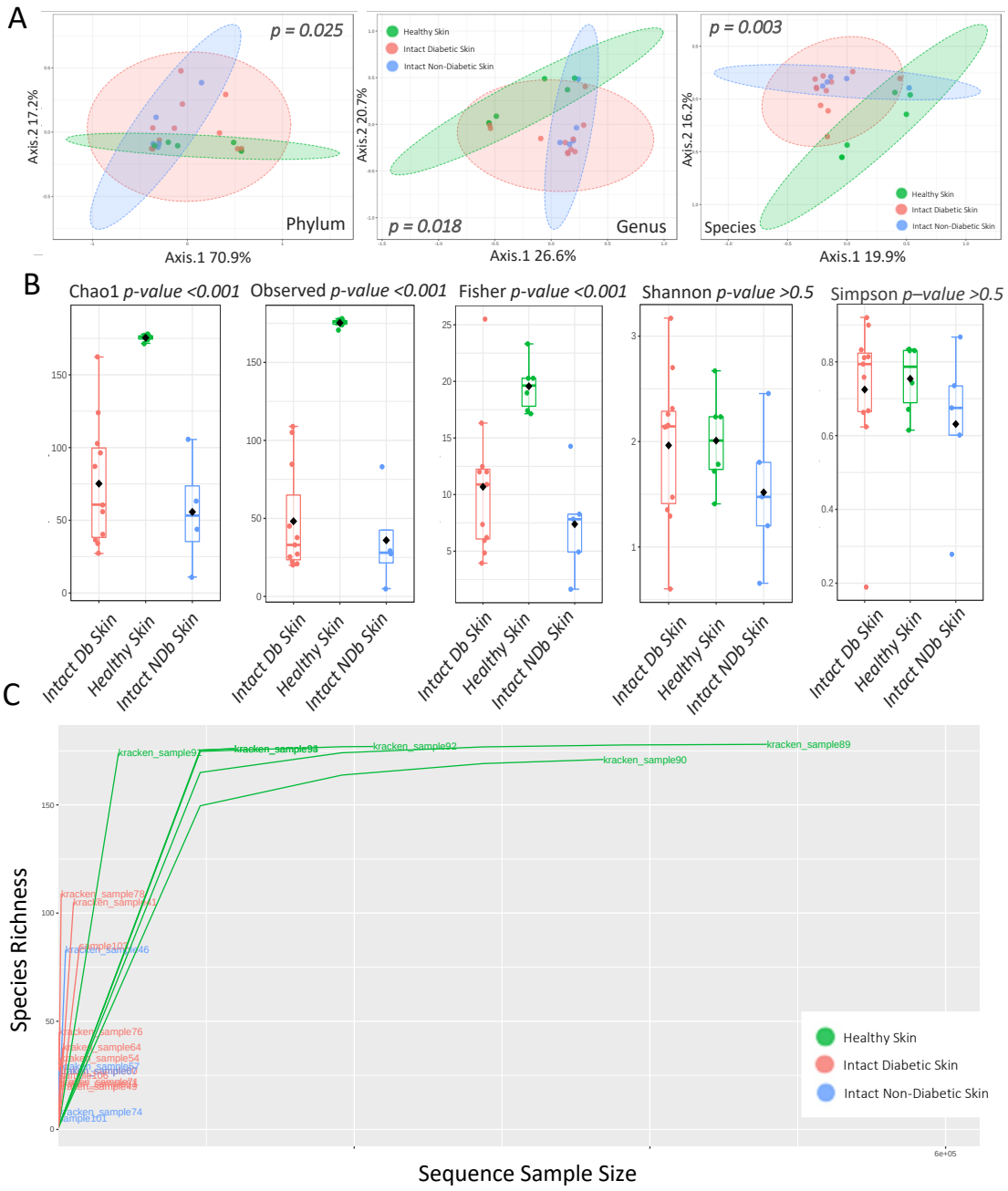

Figure 3.10: Diversity plots visualise community differences in the skin of those with and without a non-healing wound. Beta diversity (A) measured via the Bray-Curtis dissimilarity index shows phylum, genus, and species-level resolution plots (PERMANOVA, p<0.05). Each data point represents an individual participant sample. Alpha diversity (B) measurements, are significant (Chao1, Observed, Fisher, Mann-Whitney: p<0.001) and non-significant (Shannon and Simpson, Mann-Whitney: p>0.05). The lower and upper markers on each box plot represent the 25th and 75th percentiles. The median is identified as a solid line within each box plot and the mean as a black diamond. The extended bar reaches the furthest points up to 1.5x interquartile range (IQR). Species accumulation curves (C) of all samples highlighted differences in species richness within participant groups. Samples are colour coded according to donor classification. [HS n = 6, NDbS n=5, DbS n=11].

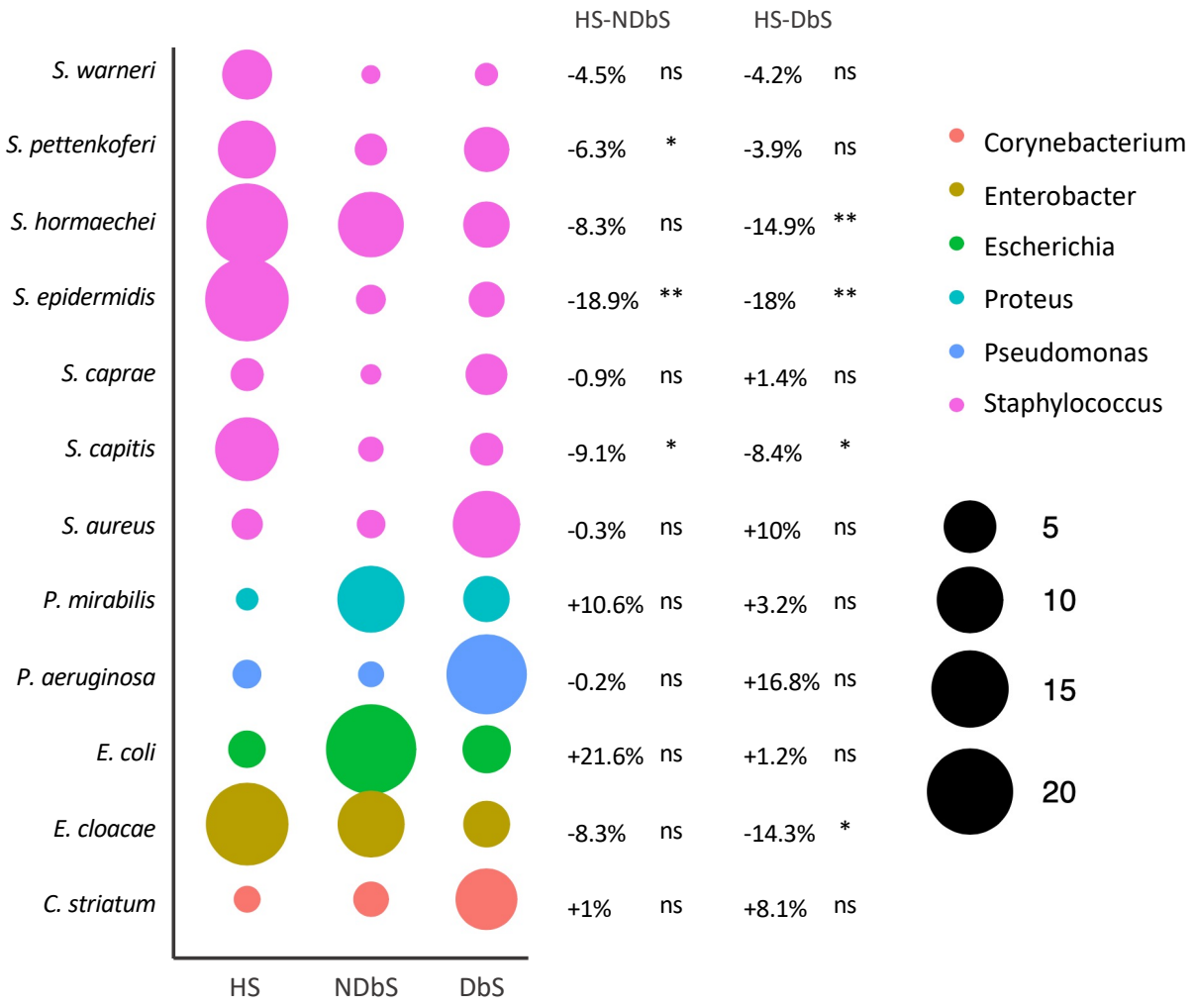

Figure 3.11: Bubble plot of the 12 most abundant species identified in the skin swabs of healthy subjects and those with a non-healing wound. Bubble size denotes relative abundance (%) relative to all listed OTUs. Percent value shows the change in the proportion of that specific OTU from either HS or NDbs to DbS. Bubble colour corresponds to genera. Statistical significance determined via Mann-Whitney test, ns = not significant, *p < 0.05, **p < 0.01, ***p < 0.001. [HS n = 6, NDbS n=5, DbS n=11].

3.5.2 Microbial profiles of the skin, peri-wound and wound site show strong similarities.

Sampling location was next examined for its influence on the microbiome. Samples were collected from intact skin, wound bed, and margin (peri-wound) of those undergoing lower extremity amputation (Figure 3:12). Healthy skin donors, as described previously, were excluded from this analysis. Average alpha diversity (regardless of metric used) revealed high overall dispersion and overlap between sampling sites and was therefore not statistically significant (Figure 3.12: A, $p>0.5$). Beta diversity also showed no statistically significant cluster separation based on sampling location (Figure 3.12: B, PERMANOVA: $p>0.5$).

Again, taxonomic visualization was performed to examine site-specific microbial distribution (Figure 3:13). All three sites exhibited *Corynebacterium striatum, Escherichia coli* and *Pseudomonas aeruginosa* as dominant species. Intact skin also contained *Staphylococcus aureus* as a dominant species. *Escherichia coli* (11.8%) was the most prevalent species in the wound environment, whilst *Corynebacterium striatum* (11.4%) *and Pseudomonas aeruginosa* (11.9%), were the most abundant species in the peri-wound and skin regions respectively. Surprisingly, this data indicates that microbial community composition varies minimally between the skin, peri and wound of those presenting with a non-healing wound.

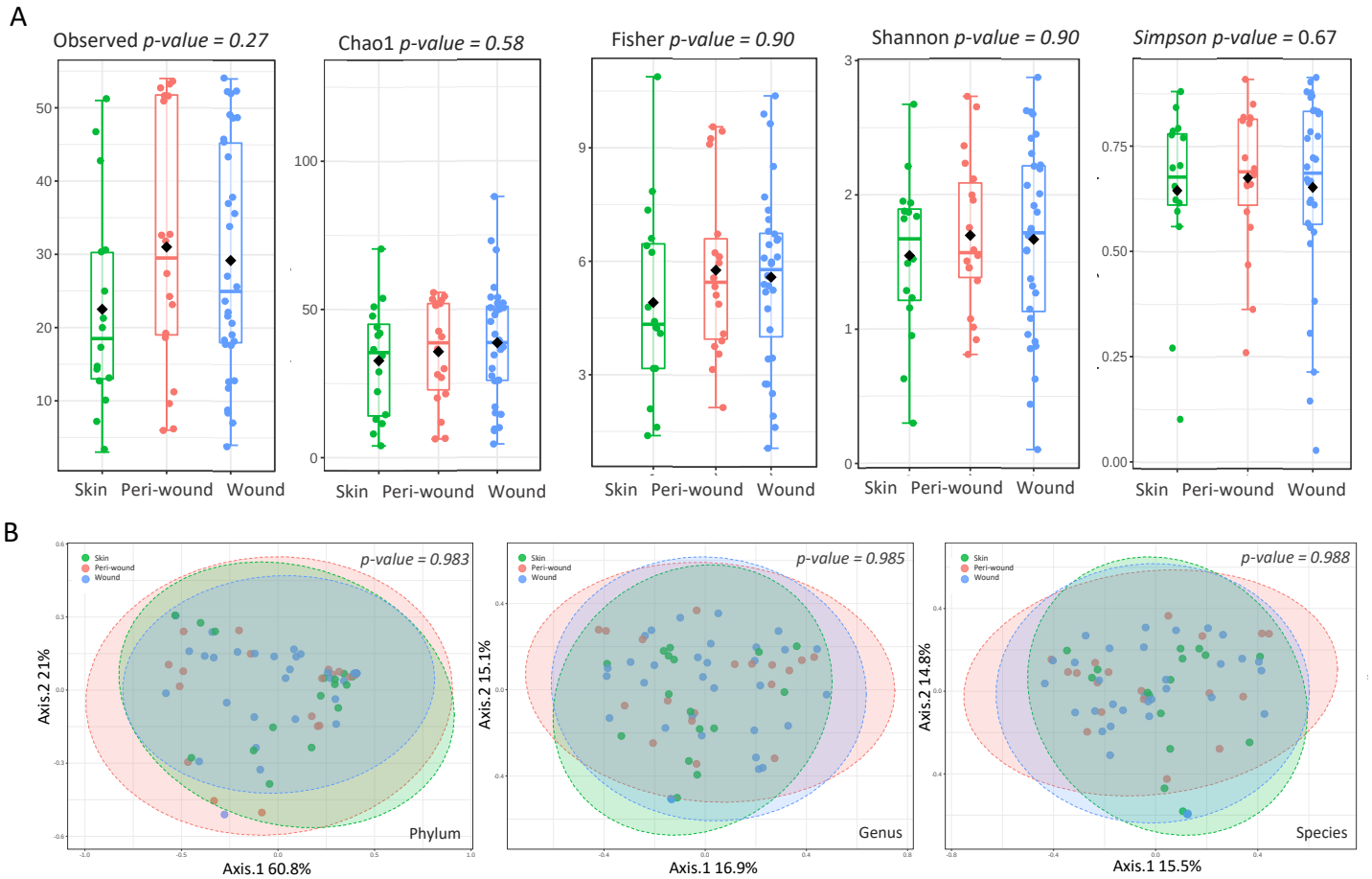

Figure 3.12: Microbial community composition of the skin, peri-wound and wound microbiome. Alpha diversity metrics; Observed, Chao1, Fisher, Shannon, Simpson (A) (Mann-Whitney: *p > 0.05*). Beta diversity measured via Bray-Curtis dissimilarity index presented in a PCoA plot at phylum, genus and species-level resolution (B) (PERMANOVA: *p-value >0.5*). *p < 0.05, **p < 0.01, ***p < 0.001. [Wound n = 34, peri-wound n = 17, intact skin n=16].

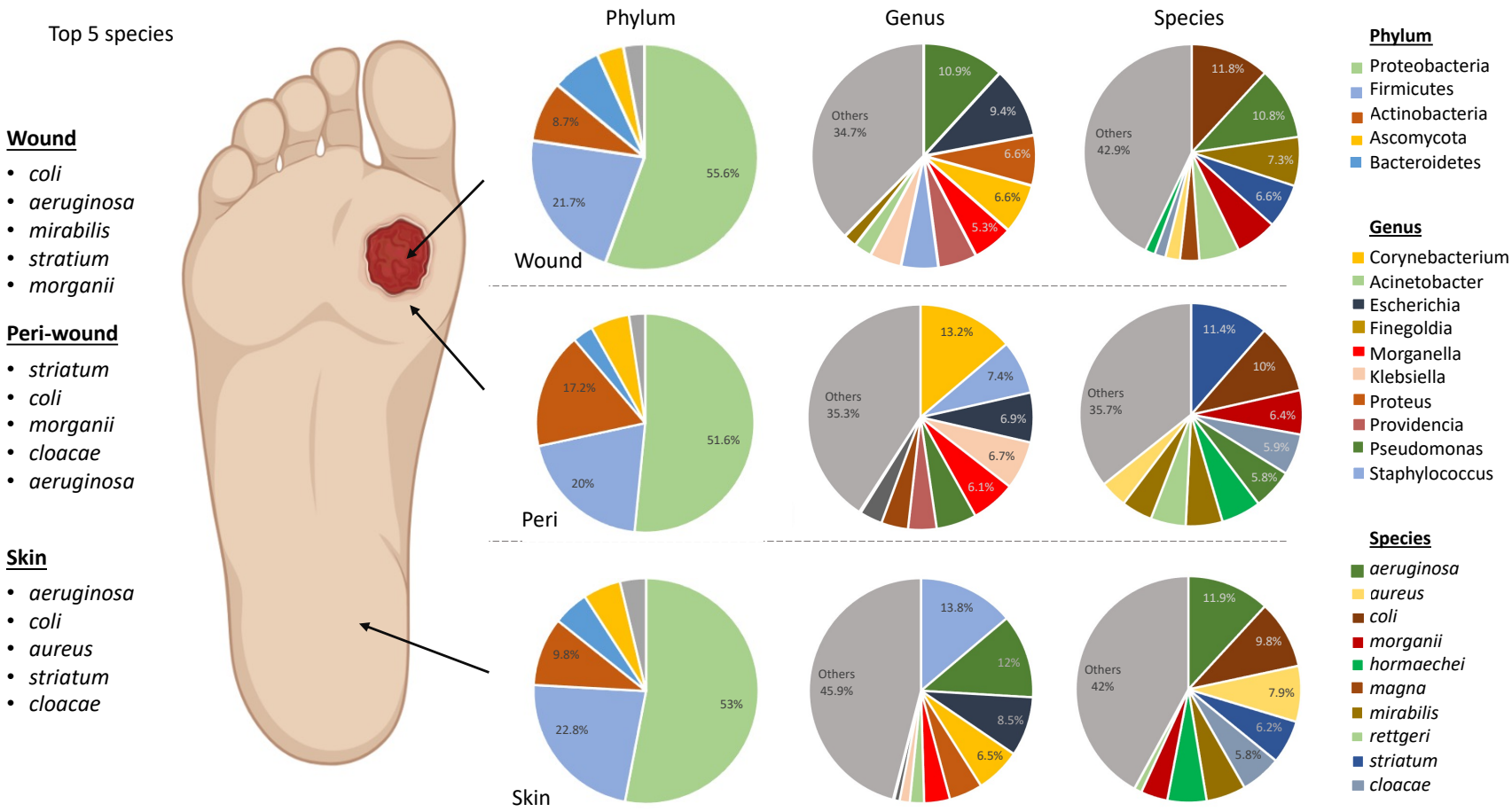

Figure 3.13: Topographical distribution of the most abundant bacterial phylum, genus and species present at the wound, peri-wound and intact skin of those with an active foot wound. Relative proportions of the most abundant phyla, genera and species are displayed in pie charts and the five most abundant species are identified on the left. [Wound n = 34, peri-wound n = 17, intact skin n=16].

3.5.3 Community analysis of individual donor samples revealed distinct clustering between locations.

Community-level clustering between intact skin, peri-wound and wound participant samples was not observed for the full dataset. However, clustering was evident when individual donors were considered at a more granular level. For example, donor 06 presented with two independent foot wounds (anterior and posterior; Figure 3.14: A) with DNA isolated from the wound bed/ peri-wound area of each wound. Moreover, microbial community composition revealed clear grouping across numerous samples collected from single insults (Figure 3.14: B) with high similarities being present between the wound and peri-wound profiles from either the anterior or posterior location.

Within this single donor, 83% of reads could be attributed to 8 dominant taxa, with profile clustering attributed to abundance variations in a limited set of microbial species, including; *Staphylococcus aureus; Corynebacterium striatum; Pseudomonas aeruginosa; Escherichia coli* and *Proteus mirabilis* (Figure 3.14: C). Within these 8 taxa, both wounds exhibited similar levels of *Escherichia coli* (58%; 55%), whilst other species presented greater variation. The relative abundance of *Staphylococcus aureus* was greatly elevated in the wound and peri-wound of the anterior insult (46.9% and 26.35%) compared to that of the posterior wound, peri-wound or intact skin (1.5%. 0.83% and 3.39%, respectively). Intact skin profiles presented higher levels of *Corynebacterium striatum* and *Proteus mirabilis* compared to either of the wound, peri-wound sites.

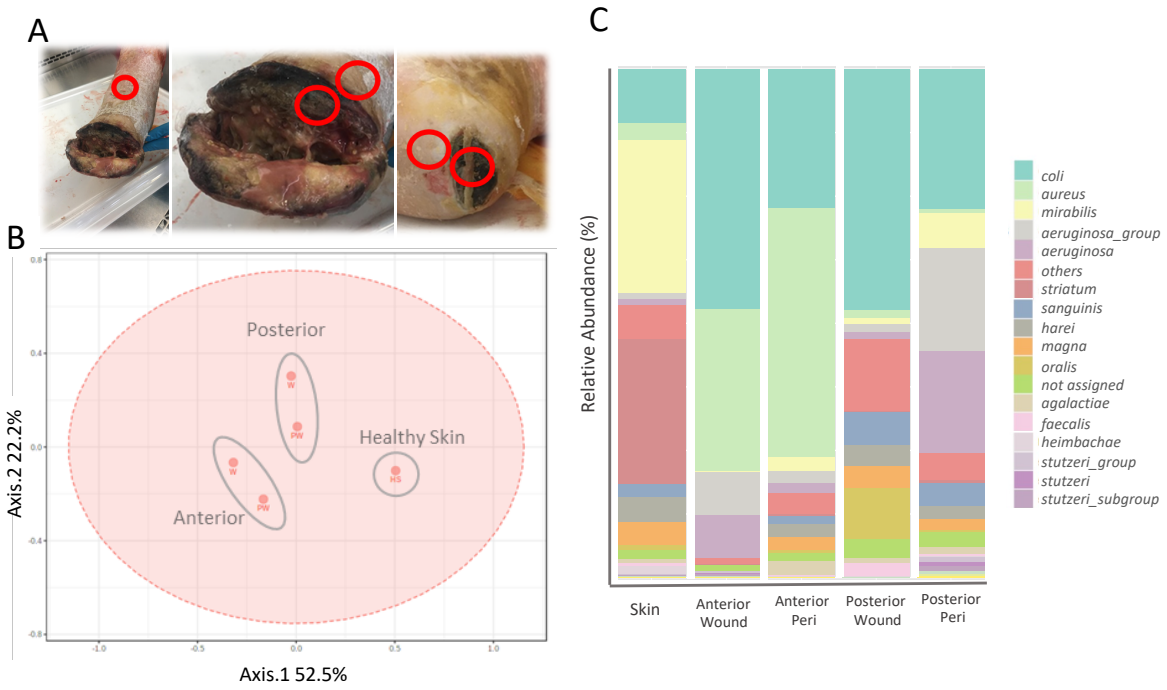

Figure 3.14: Intra-donor microbiome profiling according to unique location. Images captured of different swabbing sites within a single donor (A). Species-level Bray-Curtis dissimilarity index based PCoA (B) of samples according to unique insults sites within a single donor. Relative abundance of the 18 most dominant species present within donor microbial profiles (C). *[Intact skin n=1, anterior wound n=1, anterior peri-wound n=1, posterior wound n=1, posterior peri-wound n=1]*.

3.5.4 Wound microbial composition varies greatly between donors.

Given the observed site-based microbial profile correlation, the individual microbial profiles of participant wounds were investigated further. Wound microbiomes appear to be highly heterogeneous. Community heatmap visualisation was used to compare expression of the top 100 most abundant donor microbial OTUs (Figure 3.15). This data suggests that the chronic wounds investigated in this study did not display a core microbiome signature. In addition, no clear correlations were observed between run ID or clinical factors at this global level.

Analysis of beta diversity (species level) based on the Bray-Curtis distance matrix showed a high degree of dispersion and large overlap between wound samples (Figure 3.16: A). No clear group clustering of samples was observed. To compare the colonising diversity of the chronic wound microbiomes, alpha diversity metrics were investigated. The average index was 54 (6–112) for observed (Figure 3.16: C) and 0.64 (0.01-0.99) for Simpson (Figure 3.16: B) metrics. Overall, these patterns indicate that the chronic-wound exhibits a highly heterogenous microbiome.

Figure 3.15: Community heatmap of 100 most abundant microbial OTUs identified across participant wound swabs. Heatmap visualisation highlights the expression pattern of the 100 most abundant microbial OTUs present across all samples. Heatmap colour showing the row scaled relative presence of each OTU across all samples. Reduced proportions are represented in pink and highly represented OTUs are shown in purple. Heatmap columns correspond to individual samples. Heatmap based on data of complete OTU tables following variance stabilisation transformation (VST). [n=34].

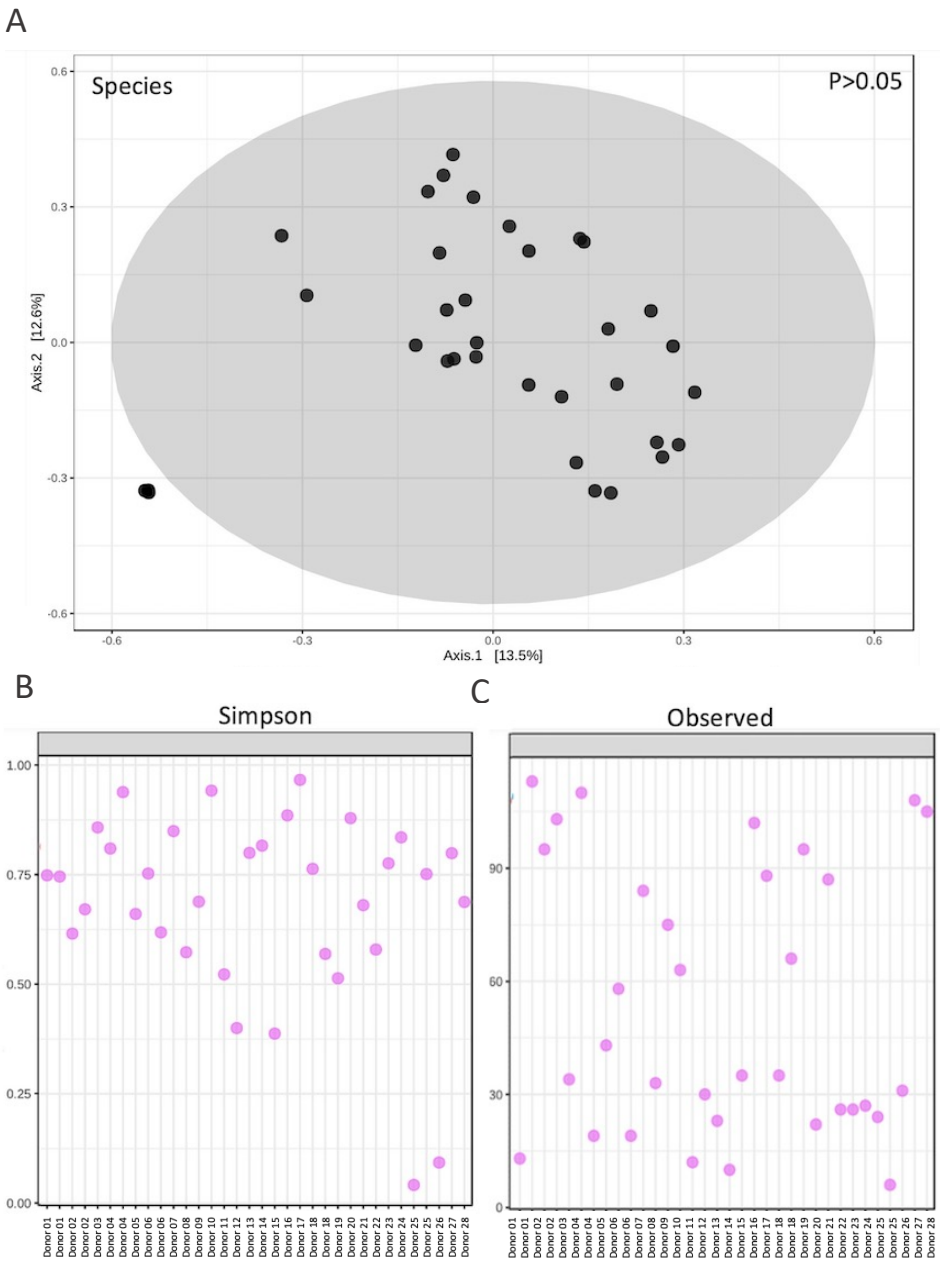

Figure 3.16: Community analysis across all wound swabs. Species-level Bray-Curtis dissimilarity index based beta diversity PCoA (A) and alpha diversity calculated using Observed (C) and Simpson (B) metrics. [n=34]

3.5.5 Relative abundance of the top 12 wound species reveals a high level of variation.

Given the high inter-donor variation in microbial composition observed in both the current study and similar published studies, the relative abundance of the most overrepresented wound species with respect to individual donor contribution was visualised (Figure 3.17). These species included *Escherichia coli, Pseudomonas aeruginosa, Proteus mirabilis, Corynebacterium striatum, Morganella morganii, Providencia rettgeri, Finegoldia magna, Staphylococcus epidermidis, Mycobacterium avium, Porphyromonas asaccharolytica, Staphylococcus aureus* and *Enterococcus faecium*. Across all wound samples*, Escherichia coli* was identified as the most abundant taxa*.* While the average relative abundance was 11.8%, this ranged from 0% to 85.7% (Figure 3.17: A). 70% of overall *Escherichia coli* abundance was identified in donors of positive diabetic status presenting with clinical wound infection. *Pseudomonas aeruginosa* was identified as the second most dominant taxa, with an average relative abundance of 10.8%, varying from 0% to 96% (Figure 3.17: B)*.* Indeed, as for the majority of taxa, a small subset of donors accounted for the majority of this *Pseudomonas aeruginosa* relative contribution, with the top 3 donors accounting for 76.5% of the total abundance from this species. For most of the presented taxa, donors with the highest relative abundance include both diabetic and non-diabetic and a mixture of those with and without the presence of clinical infection. *Porphyromonas asaccharolytica*, presenting an average relative abundance of 2.2%, was the only species in the top 12 where all donors presenting abundance >0% were diabetic (Figure 3.17: J). *Morganella morganii*, with a relative abundance of 6.2%, was the only species in which the highest three donors were both non-infected and diabetic, accounting for 85% of the overall abundance. Interestingly, *Staphylococcus epidermidis* was identified amongst the most common wound isolates, presenting an average relative abundance of 2.4%, and this was the only species where the top three samples belonged to non-diabetic donors.

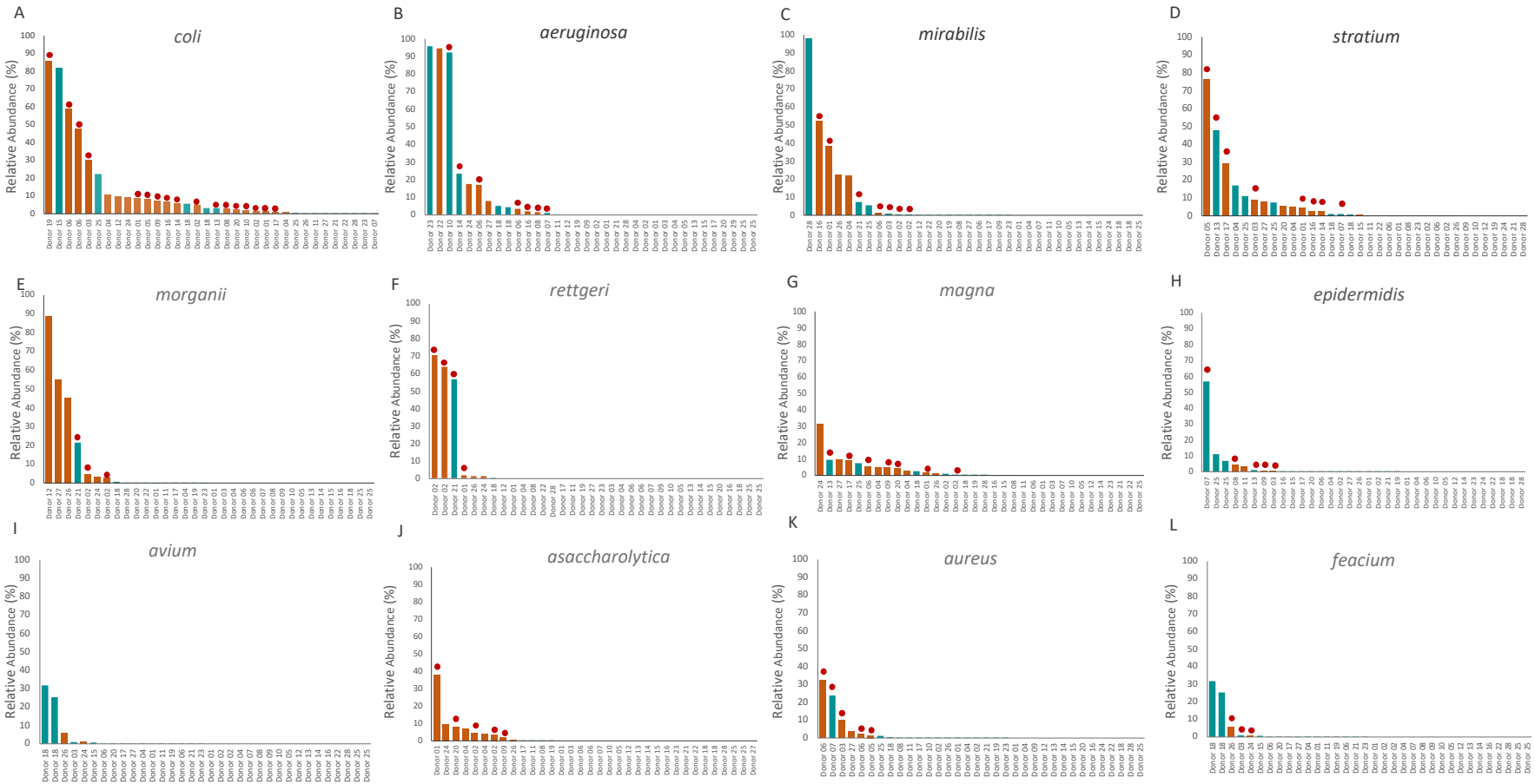

Figure 3.17: Relative abundance of the top 12 species identified in the wound microbiome according to individual samples (descending order). *Escherichia coli* (A), *Pseudomonas aeruginosa* (B), *Proteus mirabilis* (C), *Corynebacterium striatum* (D), *Morganella morganii* (E), *Providencia rettgeri* (F), *Finegoldia magna* (G), *Staphylococcus epidermidis* (H), *Mycobacterium avium* (I) *Porphyromonas asaccharolytica* (J), *Staphylococcus aureus* (K), *Enterococcus faecium* (L). Bar coloring represents diabetic status, blue = ndb, orange = db, red markers indicate the presence of clinical wound infection. *[n=34]*.

The correlation of chronic wound microbiome composition to clinical healing outcomes is a key ongoing objective in the field (Grice et al., 2019). Whilst community-based studies frequently focus on high abundance taxa, members with low abundance are often overlooked. As such, consideration of their significance and contribution to the host repair process has been limited. Therefore, in this subset of wounds, all of which resulted in amputation, we investigated high prevalence low-abundance taxa in the wound microbiome. Inclusion criteria included presence in at least 25% (average = 47%) of samples, with a mean relative abundance below 1.5%. These criteria selected six species commonly present in low abundance throughout the sample population, including: *Peptoniphilus harei, Ezakiella massiliensis, Providencia stuartii, Citrobacter freundii, Pseudomonas fluorescens* and *Pseudomonas putida* (Figure 3.18).

Peptoniphilus harei was most abundant, identified in 56% of samples with a mean relative abundance of 1%. Similar prevalence was observed for *Ezakiella massiliensis* (50%), *Citrobacter freundii* (52%), *Pseudomonas fluorescens* (52%) *and Pseudomonas putida* (44%). The mean relative abundances of these species were 0.2%, 0.13%, 0.07% and 0.04% respectively. *Citrobacter freundii* was the only species in which the top three contributing individuals were all non-diabetic, all other species were predominantly linked to diabetes. Donor 8 presented the highest relative abundance of both *Pseudomonas fluorescens* (0.73%) and *Pseudomonas putida* (0.84%), with a comparatively low relative abundance of *Pseudomonas aeruginosa* (1.37%).

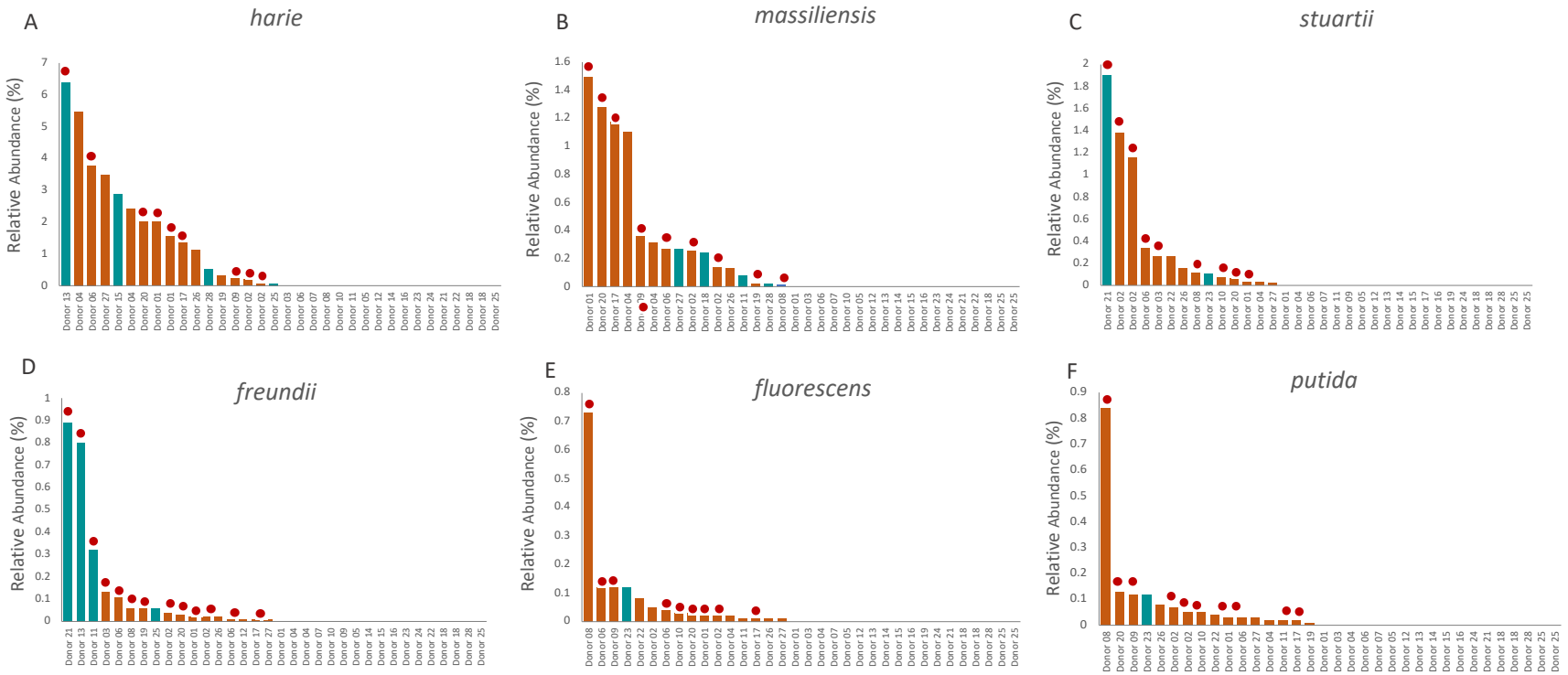

Figure 3.18: Top six low abundance high prevalence species identified in the wound microbiome according to individual samples. *Peptoniphilus harei* (A), *Ezakiella massiliensis* (B), *Providencia stuartii* (C), *Citrobacter freundii* (D), *Pseudomonas fluorescens* (E), *Pseudomonas putida* (F). Bar coloring represents diabetic status, blue = ndb, orange = db. Red markers indicate the presence of clinical wound infection. *[n=34]*.

3.5.6 Species correlation between the diabetic and non-diabetic wound microbiome.

Wound healing is a complex, dynamic process that is essential to efficiently repair damaged tissue (Wilkinson and Hardman, 2020). Derangement in wound-linked physiological behaviours, as seen in diabetes, is a leading risk factor in the formation of non-healing wounds. In this study, wound microbial profiles were separated into diabetic [n=23] and non-diabetic [n=11] participants and evaluated (Figure 3:19).

No significant variance was identified in microbial profiles with respect to diabetes. Analysis of beta diversity based on the Bray-Curtis distance matrix revealed a high degree of cluster overlap at each taxonomic level investigated (Figure 3:19: A). At phylum level, diabetic donors displayed a non-significant (*p=0.379*) tightening of cluster distribution. At the genus and species level, non-diabetic participant profiles consistently demonstrated greater profile dispersion on axis 1, whilst diabetic participant profiles presented greater distribution on axis 2. The mean alpha diversity of microbial species was measured using both Observed and Simpson metrics, to assess the presence of both unique OTUs and OTU evenness between samples. Profiles varied slightly between those with and without diabetes, with samples from diabetic donors exhibiting a trend toward higher multimeric alpha diversity versus non-diabetic donors (Figure 3.19: B). For both indices this failed to reach statistical significance (*p=0.11, 0.13)*.

Next, sparse correlations for compositional data (SparCC) analysis was implemented to search for species-based patterns. SparCC infers correlations in genomic data sets, accounting for a large number of present OTUs and the presence of a sparse correlation network. Interestingly, SparCC analysis identified three wound species that showed a non-significant correlation between the presence or absence of diabetes (Figure 3.19: C). These include *Clostridium difficile*, *Anaerococcus mediterraneensis* and *Staphylococcus epidermidis*. Both *C. difficile* and *A. mediterraneensis* were elevated in the diabetic group, whilst *Staphylococcus epidermidis* was elevated in the non-diabetic group (Figure 3.19: C). In relation to other research studies in the field, many other microbiome-based findings fail to directly compare diabetic and non-

diabetic wound microbial profiles, with each study generally focusing on a small experimental group (e.g diabetic neuropathic foot ulcers) (Gardner et al., 2013; Min et al., 2020).

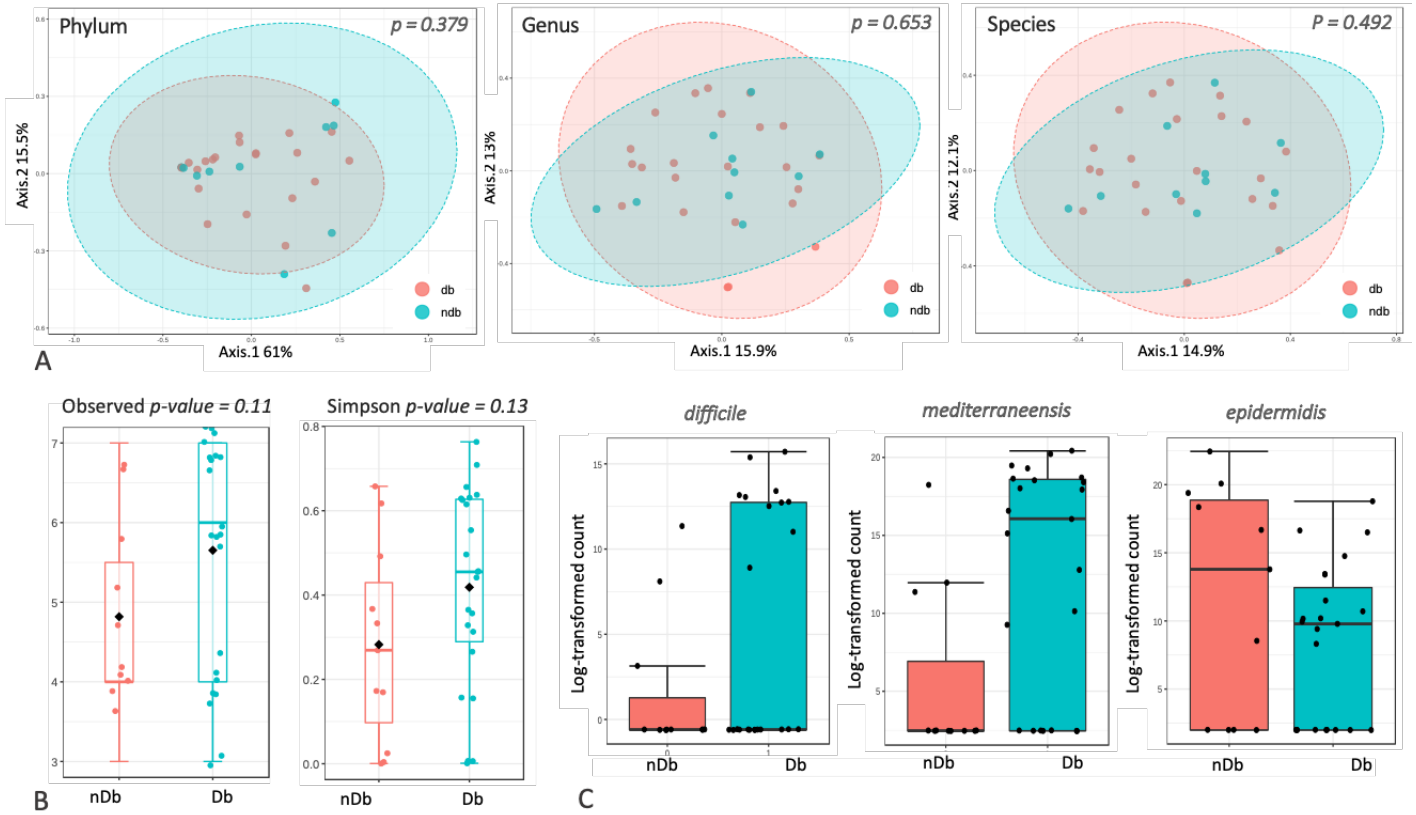

Figure 3.19: Community profiling of wound samples according to diabetic status identified similar profiles. Phylum, genus, and species-level resolution PCoA analysis using the Bray-Curtis dissimilarity index shows differences in bacterial diversity of the wound microbiome in both diabetic and non-diabetic donors (A). Observed and Simpson alpha diversity metrics (B) show minimal variation and large overlap between groups (Kruskal-Wallis test: *p= 0.11, 0.13*). Three individual species were identified using SparCC analysis coefficients, that correlate least between the diabetic and non-diabetic group (C), including *Clostridium difficile*, Anaerococcus *mediterraneensis* and *Staphylococcus epidermidis*. Each data point represents a single donor sample. [Db n=23, nDb n=11].

3.5.7 Microbial profiles of diabetic foot ulcers correlate with clinical infection status.

As the global incidence of diabetes continues to rise, so will the burden of chronic wounds (Kalan et al., 2019, Guest et al., 2020). The presence of infection is one of the leading impediments to effective healing (Guest et al., 2020), suggesting a critical role for the wound microbiome as a driver of chronicity. Therefore, the microbial profiles of both infected [n=16] and non-infected [n=7] diabetic wounds were analysed within this study.

At each level of taxonomy, principal coordinates analysis revealed non-significant participant clustering according to infection status. This trend increased in strength at each lowering taxonomic level, reaching $p<0.55$ at species level (Figure 3.20: A). Generally, infected samples exhibited a greater spread of variation than samples from non-infected donors, (Figure 3.20: A), indicating that the overall community structure of infected samples are more diverse than non-infected donors. Alpha diversity measured using both Observed and Simpson metrics revealed high variability and sample dispersion within both groups (Figure 3.20: C). Diversity profiles between the groups were extremely similar, regardless of diversity metrics (Figure 3.20: B).

Analysis of the top 22 most abundant taxa revealed a selection of species which demonstrated association with infection parameters, contributing to differences seen in microbial profiles (Bubble Plot; Figure 3.21). *Escherichia coli* and *Providencia rettgeri* were more abundant within the infected groups (3.8% vs 15.8%, 0.42% vs 8.3%), however, this was not significant (Mann-Whitney: $p>0.05$). *Morganella morganii* and *Bacteroides fragilis* were most abundant in the non-infected group (0.45% vs 25.5%, 0.3 vs 7%). *Morganella morganii* was the only species to demonstrate a statistically significant difference in abundance (Mann-Whitney: $p = 0.009$).

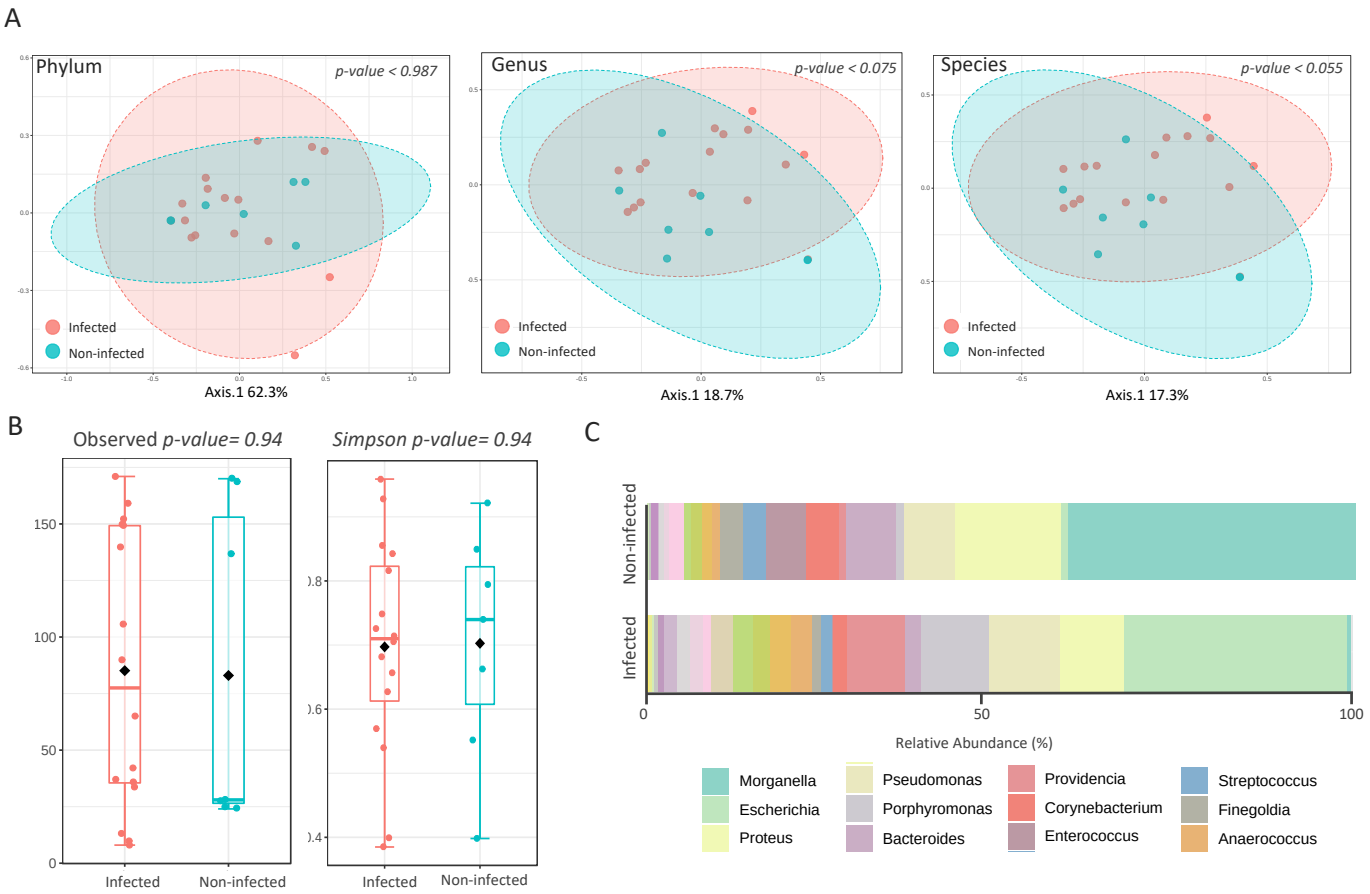

Figure 3.20: Diversity profiling reveals clustering of diabetic participant wound microbiomes according to clinical infection status. PCoA analysis using the Bray-Curtis dissimilarity index at phylum, genus, and species-level based on diabetic wound microbiome profiles according to the clinical infection status (A). Each data point represents an individual wound sample, coloured according to infection status. Observed and Simpson alpha diversity metrics (B) show minimal variation and extensive overlap between groups (Kruskal-Wallis test: *p= 0.9, 0.9).*Merged profiles (C) visualised the distribution of the most abundant bacteria genus. [Infected n=16, non-infection n=7].

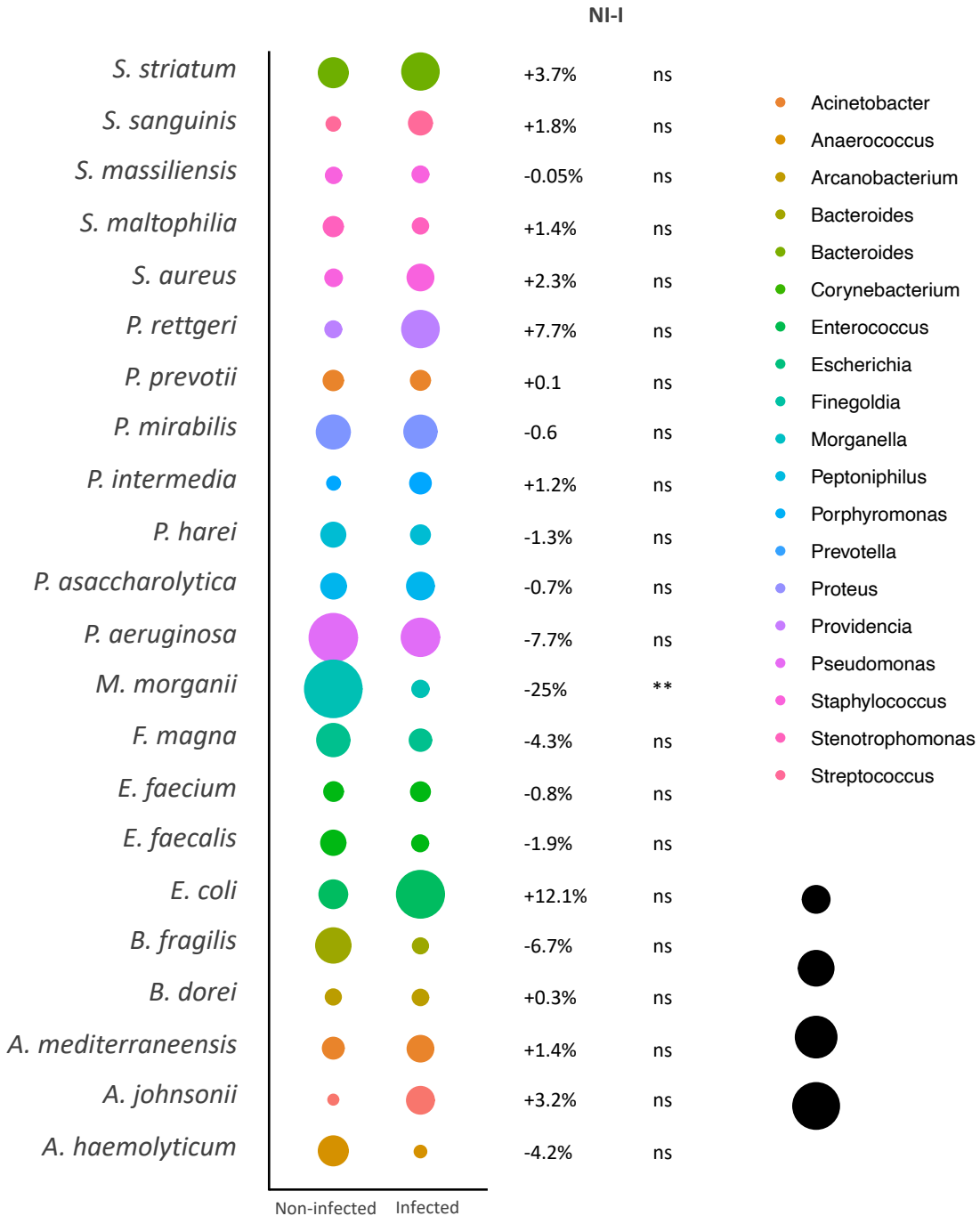

Figure 3.21: Bubble plot of the top 22 most abundant species identified in the microbial profiles of those with and without clinical infection. Bubble size denotes abundance (%) relative to all listed OTUs. The percentage value shows the change in the proportion of that specific OTU from NI-I. Bubble colour corresponds to genera. Statistical significance determined via Mann-Whitney test, ns = not significant, *p < 0.05, **p *< 0.01, ***p < 0.001*. [Infected n=16, non-infection n=7].

3.5.8 Exploration of the wound microbiome reveals clustering based on participant glycaemic control.

HbA1c is an important indicator of long-term glycaemic control and overall diabetes management, reflecting the cumulative glycaemic history of the preceding months (Campbell et al., 2019). Within the study, clinical HbA1c measurements were available for a subset of diabetic patients *[n=12]*. *n=4 participants* presented a 'high' HbA1c reading >100 mmol/mol, indicating a lack of insulin (Campbell et al., 2019), while *n=8* were classified as low <100 group mmol/mol. The primary wound microbial profiles were directly compared between these 'high' and 'low' HbA1c groups.

Across all taxonomic levels, principal coordinates analysis revealed significant global community grouping based on HbA1c classification (Figure 3.22: PERMANOVA, A: Phylum: *p-value < 0.003, B: Genus: p-value < 0.008, C: Species: p-value < 0.008*). In relation to alpha diversity, a multi-metric trend towards reduced species-level diversity was observed with low HbA1c (Figure 3.22: D, E, Mann-Whitney*: p-value = 0.05*). A trend towards higher dispersion of species diversity was observed in the low group, not replicated by metrics aiming to assess species evenness. At the phylum level (Figure 3.22: F), the proportions of Bacteroidetes was significantly higher in the >100 mmol/mol group than in <100 mmol/mol group (*p < 0.05*), whilst Firmicutes were also non-significantly elevated. Proteobacteria was the most abundant phyla in the low HbA1c group (High:24%, Low:76%). These differences at the phylum level could be heavily attributed to changes in the abundance distribution of 11 species (Figure 3.22: G). Species elevated in the high group were, *Porphyromonas asaccharolytica* (High:11.8%, Low:0.9%), *Bacteroides fragilis* (High:9.7%, Low:0.1%), *Anaerococcus mediterraneensis* (High:5.5%, Low:0.4%), *Proteus mirabilis* (High:14.4%, Low:0.3%) and *Corynebacterium striatum (*High:5.4%, Low:1.5%). Differential abundance of *Porphyromonas asaccharolytica* alone achieved statistical significance (*Mann-Whitney: p=0.04*), likely due to high sample variability. In the low group *Pseudomonas aeruginosa (High:0%, Low:14.8%), Escherichia coli* (High:2%, Low:16.3%), *Arcanobacterium haemolyticum* (High:0%, Low:3.6%), *Acinetobacter johnsonii* (High:0%, Low:6.5%),

Morganella morganii (High:0%, Low:8.15) and *Providencia rettgeri* (High:0%, Low:6.9%) all demonstrated a non-significant increase in relative abundance.

To further explore the relationship between microbial profiles and participant glycaemic control, differential expression analysis was employed (DESeq2). The top 100 most variable OTUs across all subjects [*n=12*] were represented in a heatmap (Figure 3:23). Hierarchical clustering centred strongly around two unique groups, as defined by column dendrograms. Therefore, participant samples were grouped into either cluster 1 or 2 (Heatmap; Figure 3:23). Cluster 2 comprised exclusively donors presenting with lower HBA1C measurements (<100 mmol/mol, [n=7 of 8 total 'low' donors]), with reduced expression of the most variable OTUs (orange). Cluster 1 contained all donors presenting >100 mmol/mol HbA1C measurements [n=4], in addition to a single donor [n=1] exhibiting <100 mmol/mol measurements. Cluster 1 was characterised by the high abundance of the most variable OTUs (purple). An OTU subset of most variable zone of OTUs (Zone 1 - Figure 3.23) between the two clusters was selected for further downstream community investigation.

Further examination of OTU 'Zone 1' revealed clear donor clustering [*n=12*]. In total, 'Zone 1' (Figure 3.24) was constructed of 28,027 bacterial reads spanning 17 operational taxonomic units (OTUs). In accordance with the above participant cluster allocation, principal coordinate analysis (PCoA; Figure 3.24: A) revealed distinct community donor grouping according to HbA1c status. Additionally, a multi-metric alpha diversity reading revealed significantly enhanced species diversity in 'cluster 1' in relation to this OTU subset. Collectively, this data reinforces that microbial community composition varies strongly between the OTU subsets according to participant glycaemic status.

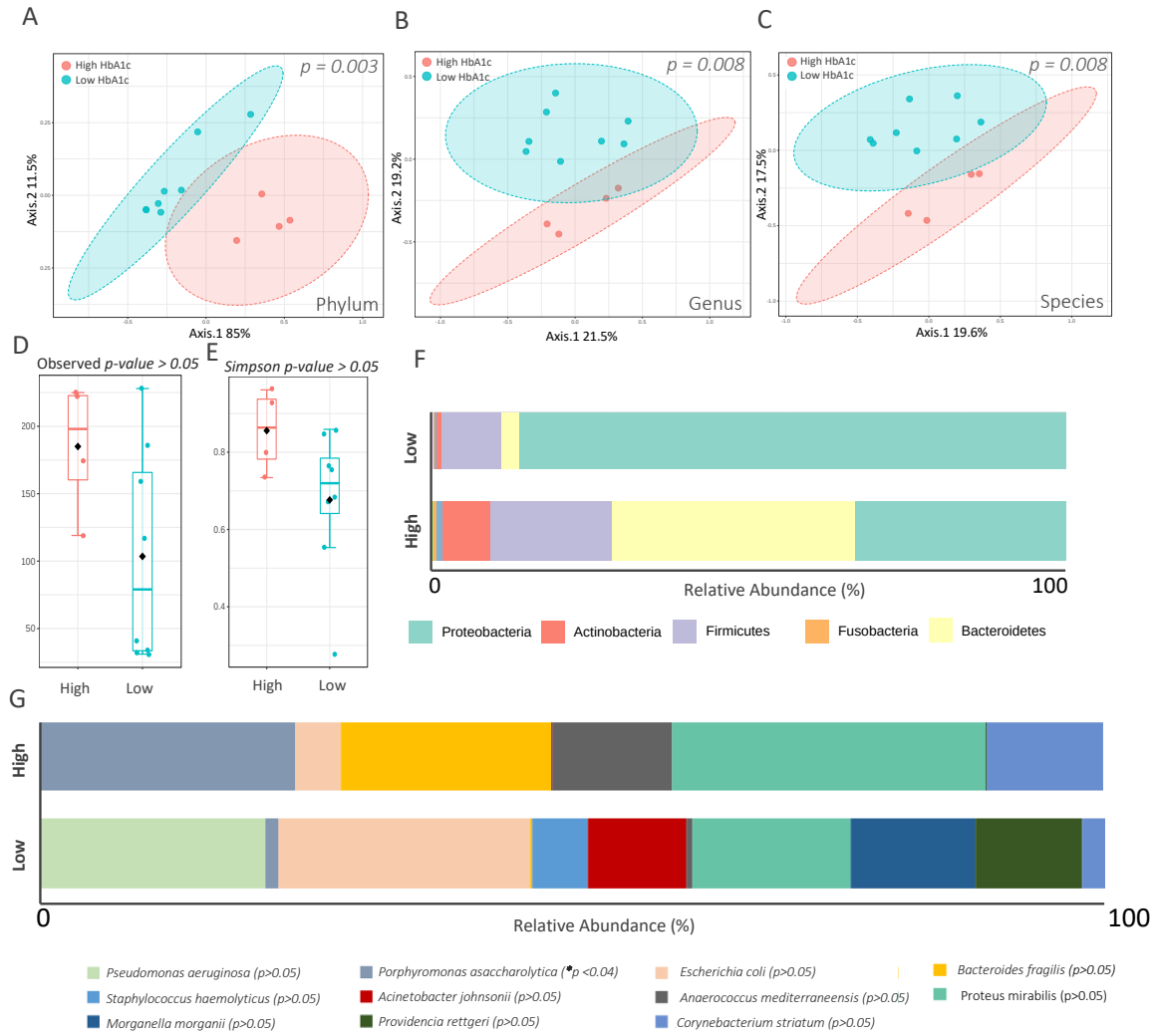

Figure 3.22: Community wound profiling of diabetic participants according to glycaemic control. PCoA analysis using the Bray-Curtis dissimilarity index at phylum (A), genus (B), and species-level (C) identify significant clustering (PERMANOVA: p = < 0.003, <0.008, <0.008). Each data point represents an individual wound sample, colour corresponding to glycaemic status. Observed (D) and Simpson (E) alpha diversity metrics show increased diversity in the 'high' group (*Kruskal-Wallis test: p>0.05, >0.05*). Differential abundance of microbial phyla (F). Relative abundance of the top 11 species (G) across both high and low groups. [High n=4, low n=8].

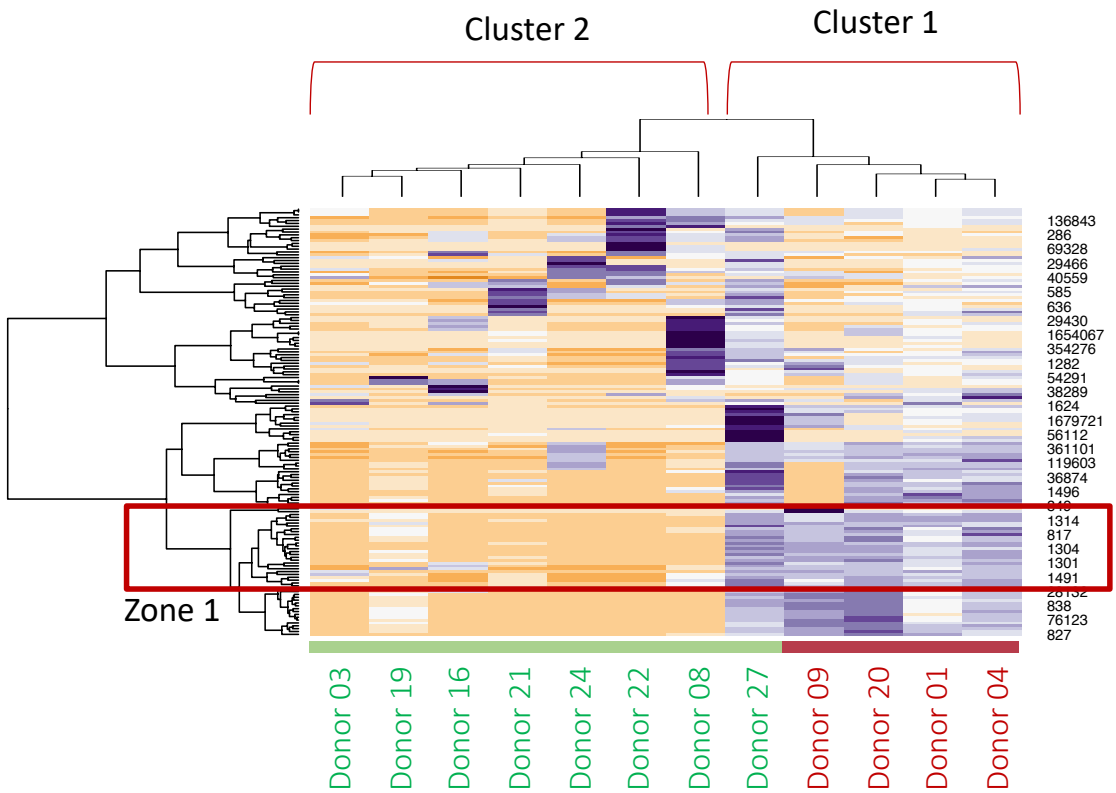

Figure 3.23: Community heatmap of 100 most variable microbial OTUs identified in the primary wound swabs of diabetic participants reveals clustering according to participant HbA1c index. Differential expression analysis highlights clustering patterns within a heatmap. Row dendrograms show hierarchical structure-based on OTU profile similarity between rows as a result of Euclidean clustering. Reduced proportions are represented in orange and highly expressed OTUs are highlighted in purple. Samples within the heatmap were grouped into either cluster 1 or 2 depending on their OTU expression profile. OTUs contained within the highlighted red area (zone 1) were selected, extracted, and processed for further downstream investigation. Supplementary labelling on the horizontal axis reveals Donor ID and HbA1c categorisation across all samples within the heatmap. [High (red) n=4, low (green) n=8].

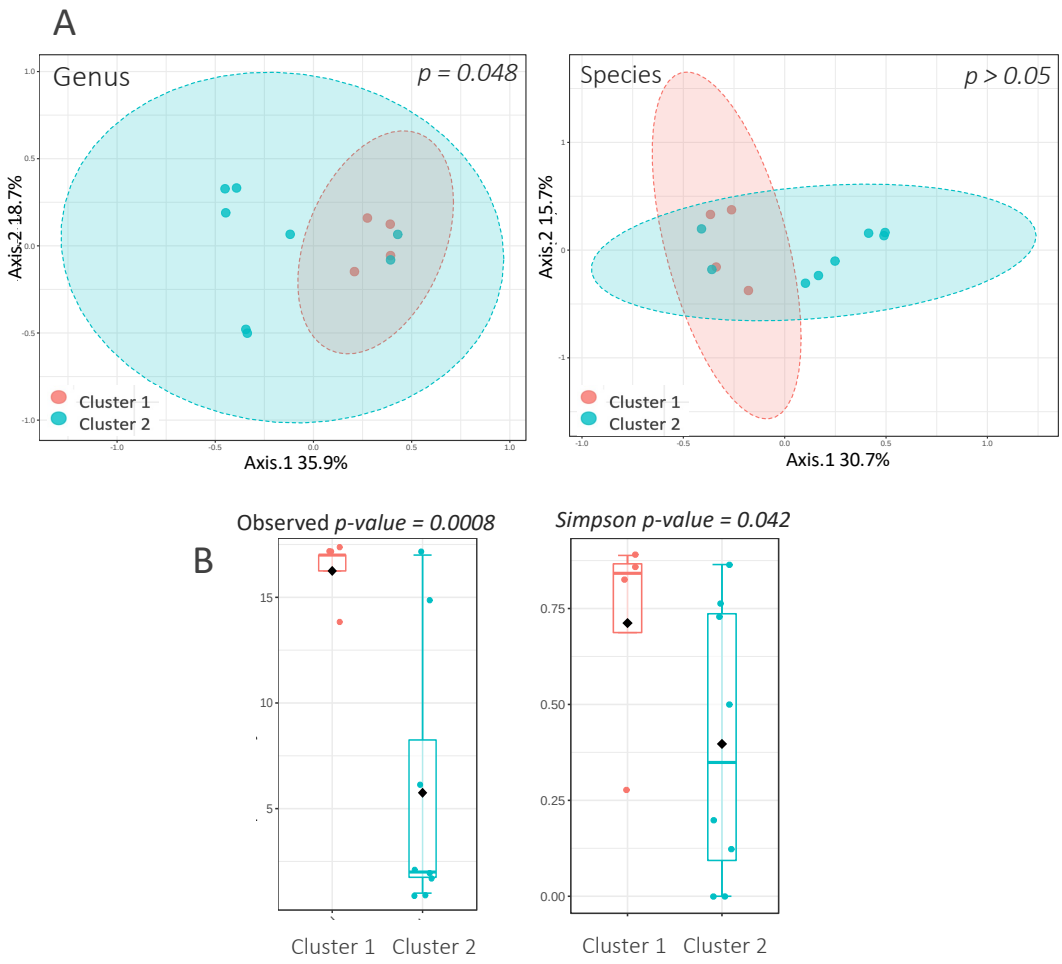

Figure 3.24: Community wound profiling according to participant glycaemic control in the selected 'most variable' OTUs. PCoA analysis using the Bray-Curtis dissimilarity index at both genus (A) and species-level (B) resolution in the differential 'Zone 1' OTUs selected for further in-depth analysis (PERMANOVA: *p = 0.048, > 0.05*). Each data point represents an individual wound sample, point colour corresponding to cluster allocation. Alpha diversity, Observed and Simpson metrics (B), *p= 0.008, 0.042*. [Cluster 1 n=5, Cluster 2 n=7].

To further evaluate expression variation in selected OTUs between the cluster groups, species abundance visualisation was performed (Bubble plot; Figure 3.25), revealing increased overall OTU read relative abundance in donors assigned to cluster 1 compared to that of cluster 2. Within the dominant genus of *Prevotella*, 5 individual species were identified: *intermiedia, jejuni, enoeca, dentalis, meaninogenica.* As with all the species listed in the OTU zoned cluster, *Prevotellla intermedia* was detected only within the high group (2.5%). This pattern was identified across this group of OTUs; Parvimonas micra (1.4%) and *Bacteriodes heparinolyticus* (0.9%), with *Peptoniphilus harei* being the only OTU determined as significantly different between the clusters (*p=0.009*).

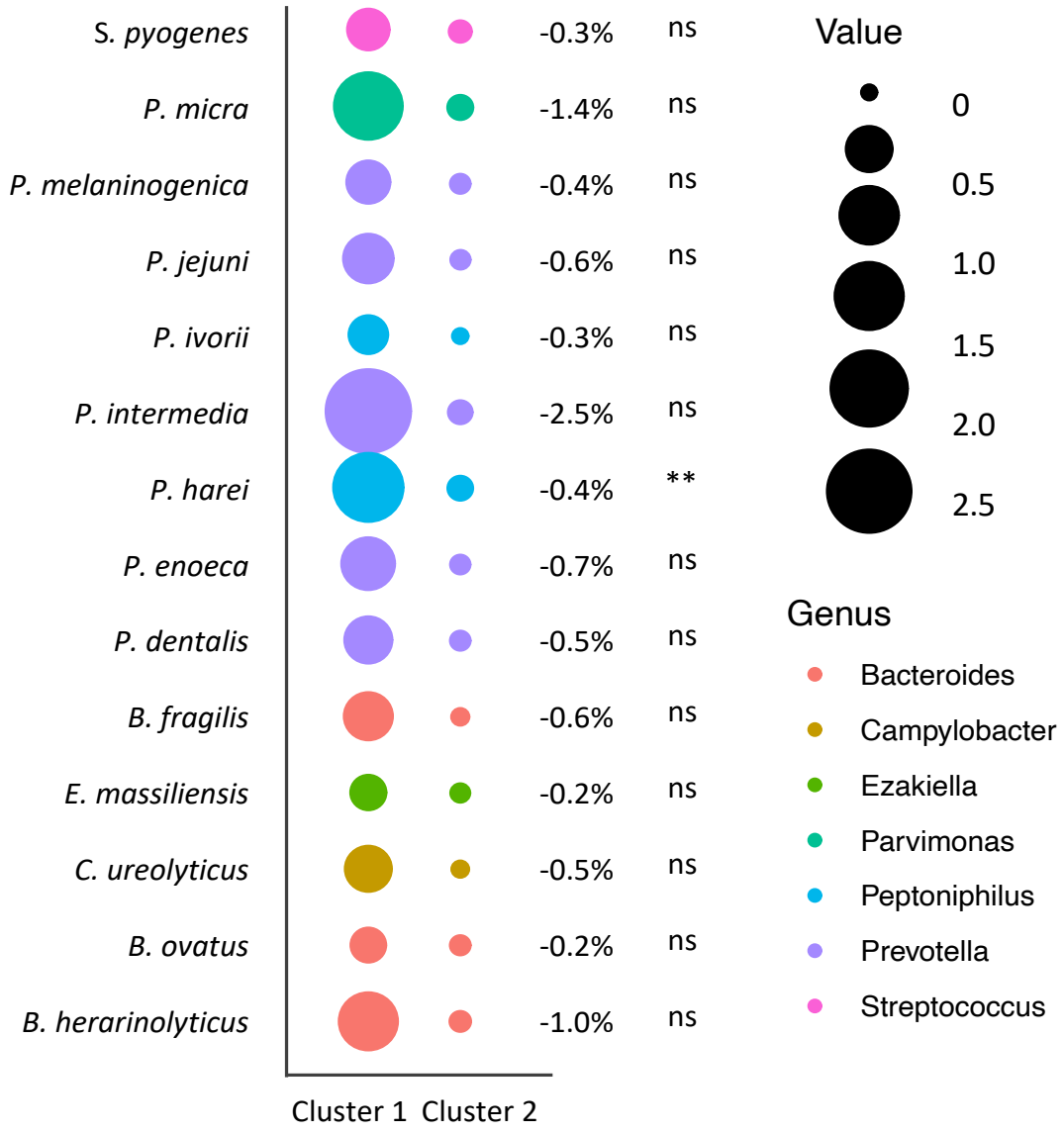

Figure 3.25: Relative abundance of the top most variable Zone 1 bacterial species identified from participants assigned to either 'Cluster 1' or 'Cluster 2'. Bubble size corresponds to relative abundance of selected OTUs contained within a single species. Percent value shows the variation in OTU abundance between cluster zone 1 and cluster zone 2. Bubble colour correlates to individual genera. Statistical significance determined via Mann-Whitney test, ns = not significant, *p < 0.05, **p < 0.01, ***p < 0.001. [Cluster 1 n=5, cluster 2 n=7*].*

3.5.9 Wound duration prior to amputation is associated with phylum-level microbial distribution.

Data from both diabetic and non-diabetic donors was combined and wounds were categorised according to duration. Each wound was assigned into to either short (<3months *n=10), m*edium (3-6 months *n=11)* or long (>6months *n=7)* grouping. Beta diversity metrics revealed highly similar community composition between all durations at both genus and species level (PCoA; Figure 3:26: B, C). At the phylum level, beta diversity exhibited cluster separation based on duration, returning a weakly significant result (Figure 3.26: A, PERMANOVA: $p = 0.049$). To further explore this result, the relative abundance of dominant wound phyla was visualised (Figure 3.26: D). Proteobacteria was identified as the most abundant phyla (Short: 98%, Medium: 84%, Long: 49%), exhibiting the highest abundance in wounds presenting less than three months prior to amputation. Furthermore, the three remaining dominant phyla exhibited a duration-dependent increase in Actinobacteria (Short: 0.3%, Medium: 0.2%, Long: 6.5%), Bacteroidetes (Short: 0.5%, Medium: 4.5%, Long: 24.7%), and Firmicutes (Short: 1.6%, Medium: 11%, Long: 19.9%). In agreement with other research groups, alpha diversity metrics (Figure.26: E, F) revealed that insults with a longer duration prior to amputation contained a more diverse microbiome than those of a shorter duration. Collectively, these findings indicate that wound duration prior to amputation has a weak effect on microbial community composition, particularly at higher taxonomic level.

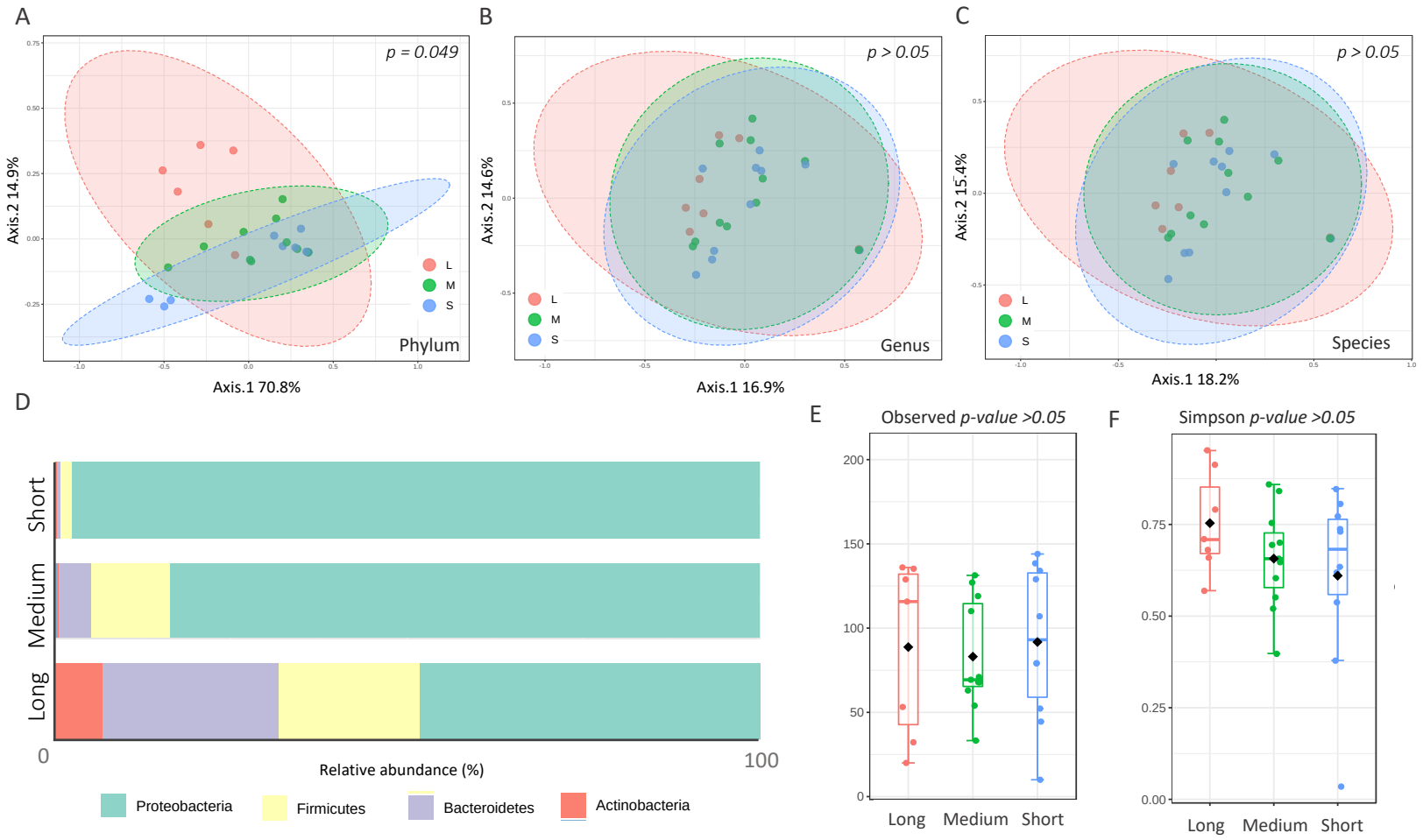

Figure 3.26: Microbial community composition according to wound duration prior to amputation. PCoA analysis calculated using the Bray-Curtis dissimilarity index characterises microbial profiles at phylum (A), genus (B) and species-level (C) (PEROMANOVA: *p= 0.049, p> 0.05, p> 0.05*). Alpha diversity measurements according to wound duration (E)(F). [Short n=10, medium n=11, long n=7].

3.5.10 Antimicrobial treatment has no clear effect on wound microbial composition.

While the microbial composition of a wound has been linked to healing outcomes, little is known about the impact of antimicrobial exposure on the wound microbiota, or subsequent healing (SanMiguel et al., 2017). A subset of participants in the current study had received antibiotics prior to sample collection and metagenomic profiling *[n=12]*. The inclusion of such participants afforded the opportunity to observe the effects of antibiotics on the wound microbiome.

We first compared participants who had received any form of antimicrobial therapy [*n=12*] to those who had not received any antimicrobial therapy 8 weeks prior to surgical preparation [*n=10*]. Beta diversity metrics were utilised to assess overall genus and species-level community variation between the two groups. PCoA revealed wide sample distribution and substantial overlap at all levels of taxonomic investigation (PCoA: Figure 3.27: A, B). Alpha diversity profiling provided additional insight into the impact of antimicrobial treatment on microbial community diversity. Observed and ACE diversity metrics revealed significantly increased diversity following antimicrobial therapy (*p=0.02, p=0.01*). By contrast, Shannon and Simpson metrics showed no association between antimicrobial treatment and wound sample diversity (*p=0.2, 0.3*). Collectively, this data indicates that antimicrobial therapy influences the number of species, including rare taxa, rather than species richness or evenness (Figure 3.27: C).

Following the analysis of microbial profiles according to overall antimicrobial treatment, those with available information were categorised according to antibiotics received based on their class and mechanism of action. These included sulphonamides [*n=2*], aminoglycosides [*n=1*], fluoroquinolones [*n=1*], nitroimidazoles [*n=1*] and beta-lactams [*n=7*]. Samples included both topical and systemic treatment regimes. PCoA analysis revealed a lack of sample similarity according to participant antimicrobial treatment status (Figure 3.27: D). This trend was replicated in alpha diversity, which showed absence of clustering based on the treatment.

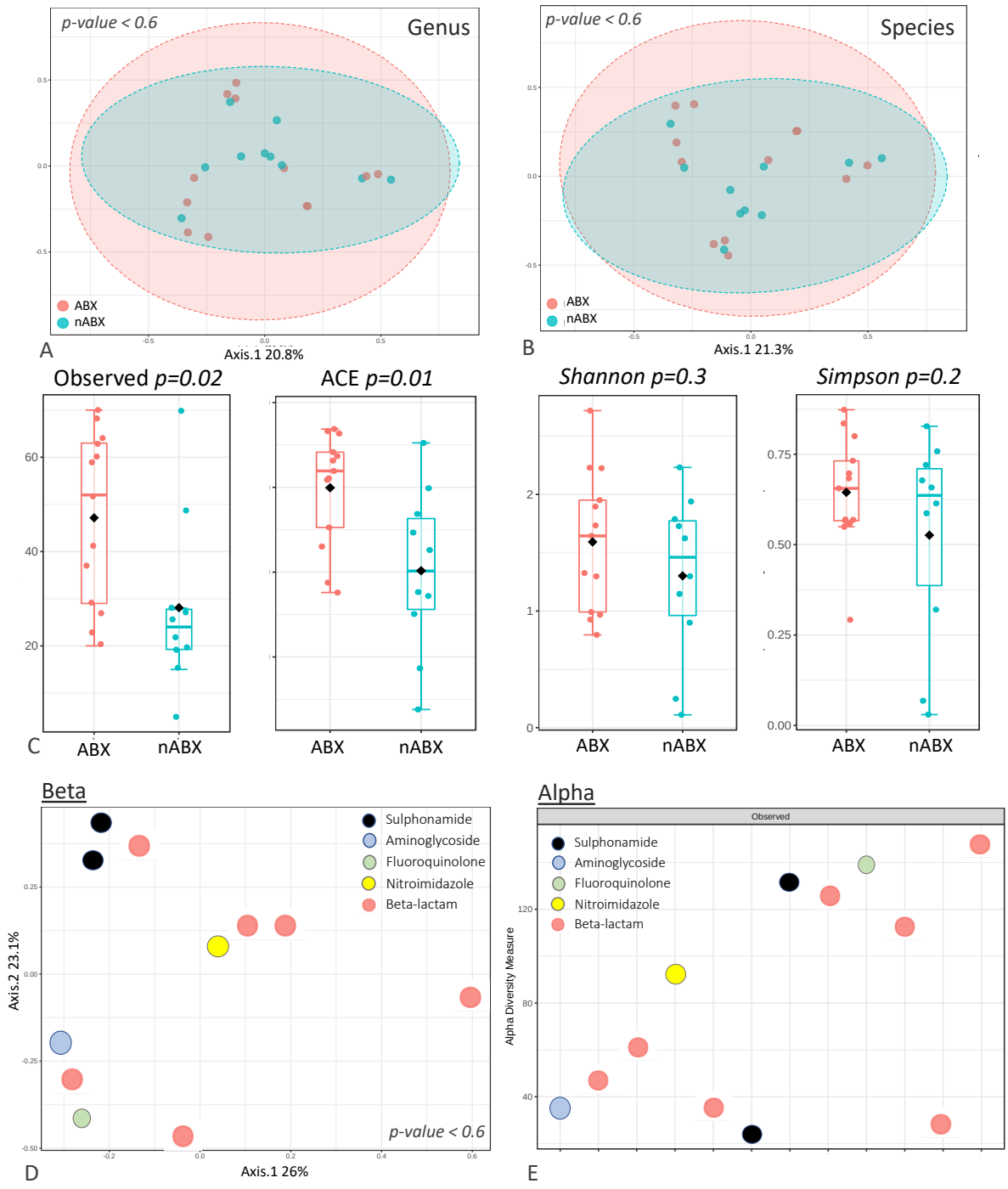

Figure 3.27: Wound microbial profiles are altered by previous antibiotic treatment. PCoA analysis using the Bray-Curtis dissimilarity index characterises microbial profiles at both genus (A) and species-level (B) according to previous antimicrobial treatment. Alpha diversity (C) measurements, show metric dependant significance (Observed, ACE, Mann-Whitney: $p<0.05$) (Shannon, Simpson, Mann-Whitney: $p>0.05$), [ABX n=12, nABX n=10]. PCoA (D) and Observed (E) alpha diversity analysis reveals that patient microbiomes do not cluster based on 'ABX' treatment class. [Sulphonamide n=2, aminoglycosides n=1, fluoroquinolone n=1, nitroimidazole n=1 and beta-lactams n=7].

3.5.11 Characterisation and community analysis of the mycobiome across the healthy skin and wound environment reveals species-specific changes.

Across this study, around 1% of reads were aligned to eukaryotic sequences. Host reads were removed during processing (Section 3.2.6) with remaining eukaryotic reads assigned to fungal OTUs, predominantly the phyla Ascomycota or Basidiomycota. At the eukaryotic community level, all samples from participants presenting with a non-healing wound (skin, peri-wound, wound) displayed very similar profiles. Samples acquired from the feet of healthy participants (HS) were included as a direct comparison.

Comparison of eukaryotic profiles between subjects with a chronic wound (all sites) versus without a chronic wound (alpha and beta diversity metrics) revealed significant differences in fungal community composition (*Mann-Whitney: Observed, p = 0.004, Simpson, p=0.002, PERMANOVA: p = 0.002*). Mean alpha diversity was higher in healthy skin samples, when compared to that of the intact skin, peri-wound and wound patient samples (Figure 3.28: A,B). Similarly, beta diversity (PCoA plots) displayed tight clustering of healthy skin samples, while post-amputation samples showed a larger spread of variation (Figure 3.28: C).

Species-specific distribution was also explored (Figure 3.29; Bubble plot), with statistical significance assessed between healthy donor skin (HS) and intact skin (IS). *Botrytis cinerea* presented as the dominant species present across patient samples (Skin: 69%, PW: 65%, Wound: 64%), a trend not observed in skin from healthy donors (18%) ($p<0.001$). In contrast, healthy donors presented *Malassezia restricta* as the most dominant eukaryotic species (23%). The largest variation in abundance between healthy skin and post-amputation patient samples was in *Thielavia terrestris* (HS: 9.8%, post-amputation: IS:<1%, PW: 1.4%, Wound: 2%) and *Talaromyces regulosus* (HS: 10.5%, post-amputation: IS: <1%, PW: 1.4%, Wound: 5%).

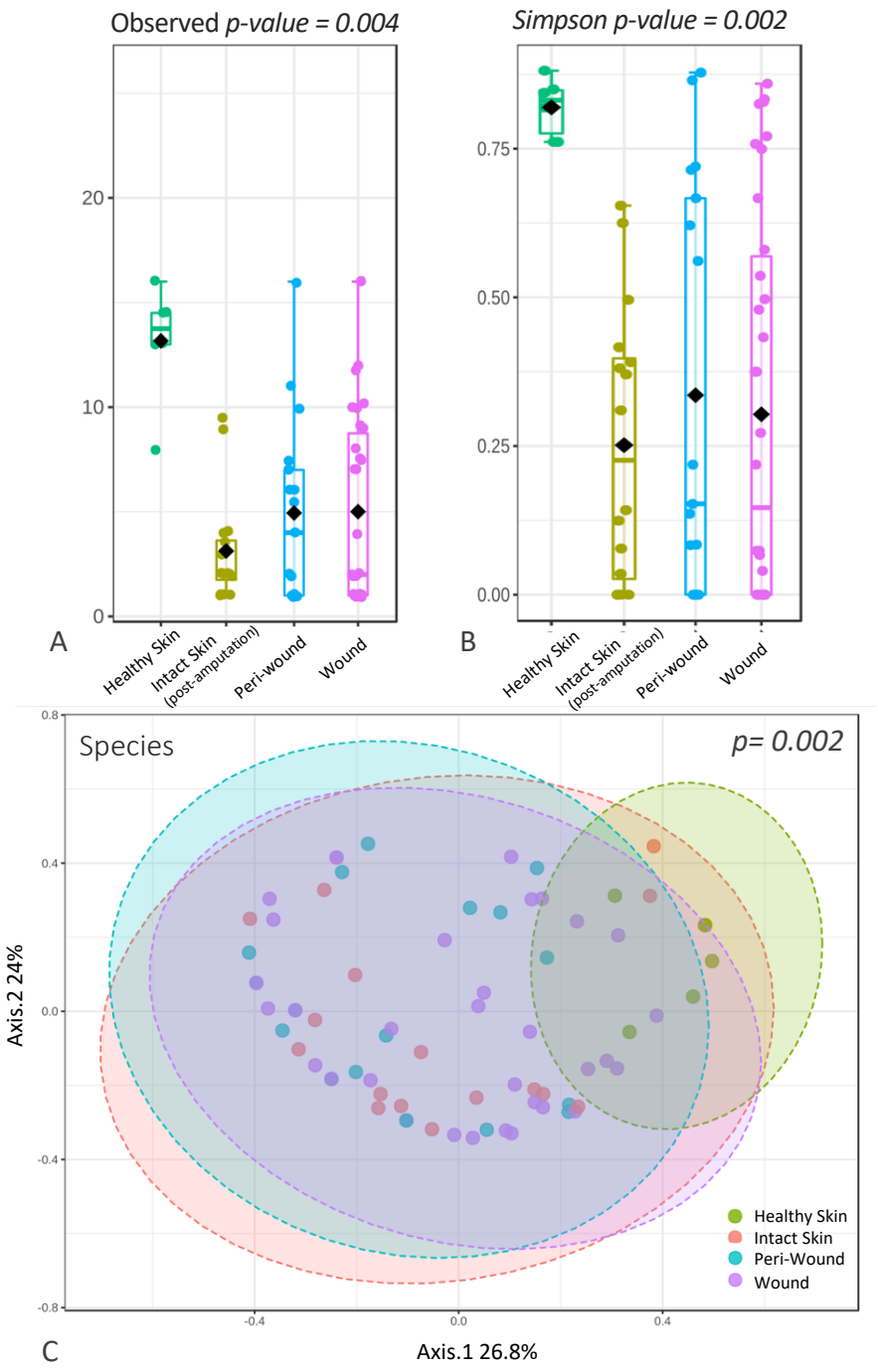

Figure 3.28: Eukaryotic community analysis of the fungal microbiome in both healthy skin donors and the skin, peri-wound and wound site of those presenting with a non-healing wound. Alpha metrics, Observed (A) and Simpson (B) diversity plots visualise community differences in the microbiome from healthy skin and wound environment (Mann-Whitney: *p = 0.004, 0.002*). Beta diversity measured via Bray-Curtis index and presented in a PCoA plot (B) (PERMANOVA, *p = 0.002*). [*HS n=6, IS n=16, PW n=17, W n=34*].

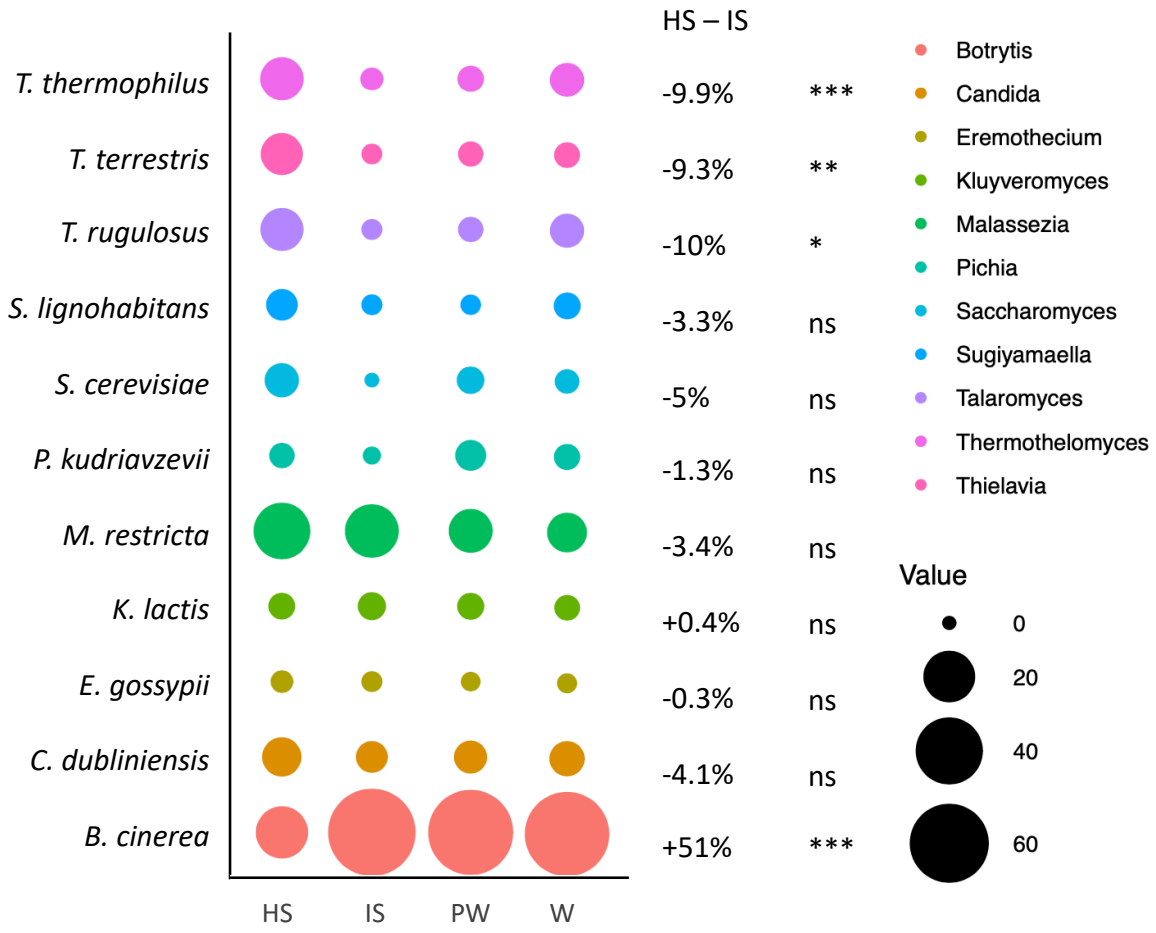

Figure 3.29: Bubble plot of the top 11 most abundant fungal species identified in both healthy skin donors and the skin, peri-wound and wound site of those presenting with a non-healing wound. Bubble size denotes abundance (%) relative to all listed fungal OTUs. Percent value shows the change in the proportion of that specific OTU from healthy skin to the intact skin of wound donors. Bubble colour corresponds to genera. Statistical significance determined via Mann-Whitney test, ns = not significant, *p < 0.05, **p < 0.01, ***p < 0.001. [HS n=6, IS n=16, PW n=17, W n=34].

3.5.12 Culture vs sequencing: Nanopore described microbial profiles correlate with clinical cultivation-dependent methods.

In cases of suspected infection, microbiological samples are sent for routine clinical microbiology, to identify causative infective organisms and guide antimicrobial treatment (Bui et al., 2019). Traditionally, microbiologists have used culture-based methods to assess the wound microbiome, however, these assays are biased toward microorganisms that thrive in isolation under laboratory conditions (Ko et al., 2022). In recent years, culture-independent sequencing techniques have augmented our understanding of complex bacterial communities (Ko et al., 2022). Despite this, culture remains the diagnostic gold standard for many microbial infections and the method against which alternative techniques are often evaluated (Bonnet et al., 2002).

In this study, both routine clinical culture and sequencing-based methods were applied for the microbial analysis of infected wound swabs *[n=13]*. In an attempt to understand the correlation between these two methods, dominant wound species identified using Nanopore-based microbial profiles were compared directly with clinical culture results (Figure 3.30). The comparison of these two methods initiates a collection of fundamental questions. For example, in the cases where results differ, which method is correct? In addition, hypothetically, how many thesis discrepancies alter clinical treatment strategies? In times of species-level ONT based identification, what is the importance of this information? While this section of results will briefly outline the overall findings and correlation between these two methods, questions and clinical application of the findings will be addressed within the discussion.

Interestingly, the two independent methods broadly correlated, with 61% of wounds presenting an organism identified using both genomic and culture techniques. However, there were also clear differences between culture and nanopore-based identification. In donor 10, 93% of microbial reads were assigned to *Pseudomonas aeruginosa*, whilst the genus *Pseudomonas* was also the only microbe identified using culture-based techniques. Again, in donor 14, *Pseudomonas* was identified as a dominant microbe in culture, alongside

Pseudomonas aeruginosa using sequencing techniques. In both donors 06 and 08, *Pseudomonas* was identified as a dominant microbe exclusively in culture results, contributing a relative abundance of only 3.6% and 1.7% according to nanopore-based profiling.

While a range of samples showed a correlation between culture and sequenced profiles, 37% of samples shared no correlation, failing to identify a single corresponding microbe. Additionally, clinical culture results from three individual donors described the presence of 'anaerobes', with a lack of further description. Included in this donor selection, donor 20, revealed the presence of anaerobes and *proteus* in clinical culture investigation. However, nanopore sequencing/analysis revealed the presence of *Anaerococcus mediterraneensis, Prevotella intermedia, Porphyromonas asaccharolytica and Prevotella melaninogenica,* four independent anaerobic species of three separate genus, each with varying clinical implications (Min et al., 2019). Similarly, in donor 01, sequencing analysis revealed *Porphyromonas* asaccharolytica, *Proteus mirabilis*, *Anaerococcus mediterraneensis and Peptoniphilus harei* as dominant species. Based, on culture-based techniques, only *Staphylococcus aureus* and *Streptococcus* were identified as microbes present in the wound environment.

Both donor 06 and donor 19 revealed the mutual identification of *Escherichia coli*. Interestingly, despite the reported issue of over-representation of these species in culture-based results, *Escherichia coli* was also identified in donor 09 and 14 using metagenomic, but not culture-based techniques. Multiple *Staphylococcal* species were also commonly identified within the study. Donor 07 highlighted two different species of *Staphylococcus* as key species in sequencing analysis, dominated initially by *Staphylococcus epidermidis* and then *Staphylococcus aureus*. None of the dominant organisms identified were also identified within the culture data. With this donor, only a selection of Gram-negative microbes were identified using culture-based techniques. In donor 03 and donor 13, *Botrytis cinerea*, a necrotrophic fungus, was identified by molecular methods as a dominant organism. Fungal organisms are not tested for under routine clinical culture-based investigation.

Figure 3.30: Top species identified in the wound profiles of participants using both nanopore metagenomic analysis and clinical swab culture data. Samples are ordered according to individual donors. Blue bars represent species identified using Nanopore-based methods whilst orange bars exhibit the corresponding clinical culture data. Highlighted green areas represent agreement between clinical culture and nanopore sequencing results, whilst bright green signifies agreement with nanopore providing identification to a higher taxonomic resolution.

3.6 Discussion

Chronic nonhealing lower extremity wounds represent a major medical and financial burden (Guest et al., 2020). Those affected report reduced life quality, lack of perceived social support and other socio-economic challenges (Olsson et al., 2019). Chronic wounds are multi-factorial, with diabetes, hyperglycaemia, peripheral neuropathy, vascular disease, and microbial colonisation each potentially contributing to impaired tissue regeneration (Verbanic et al., 2020). The limitations of culture-based and short-read sequencing approaches, mean that microbial communities that colonise wounds remain challenging to characterise, and even more challenging to link with the presence of infection (Verbanic et al., 2020). Current evidence suggests that specific components of the wound microbiota contribute to the delayed healing phenotype observed in chronic wounds (Price et al., 2011; Han et al., 2011; Gardner et al., 2013; Loesche et al., 2017; Park et al., 2019; Min et al., 2020; Kalan et al., 2019). However, further research is required to fully characterise the wound microbiome, and more importantly, to understand how host-microbiome interactions contribute to healing pathology.

Within the current study, swabs from the skin, wound and peri-wound of 28 patients with chronic wounds undergoing lower extremity amputation were utilised for metagenomic sequencing. Both bacterial and fungal taxonomic summaries revealed substantial differences between the skin microbiome of healthy volunteers and the intact skin of individuals presenting with a chronic wound (Figure 3.10). Consistent with previous reports, participant wound profiles were profoundly heterogeneous (Figure 3.15; Gardner et al., 2013; Park et al., 2019). However, individual wound microbial taxa were shown to associate with specific clinical factors. For example, diabetic wounds were more likely to contain pathogenic species, whereas non-diabetic wounds displayed more commensal inhabitants (Figure 3.19). In the diabetic population, glycaemic status was significantly associated with a specific microbial subset. Somewhat surprisingly, infection status, duration prior to amputation and antibiotic exposure had limited association with species-level microbial distribution. This may reflect the small sample number in this study. Finally, participant clinical culture data was compared directly with sequencing results. Here, ONT led to superior taxonomic characterisation while associating with previously established clinical prognosis (Figure 3.30; Min et al., 2020; Wan

et al., 2021). Collectively, the data reinforces that using long-read sequencing technology to deliver quantitative, species-level, taxonomic identification, provides a previously unprecedented insight into the complexity of the human chronic wound microbiome.

Prior to sequencing, sample collection and DNA isolation techniques underwent extensive optimisation. As reported by previous microbiome profiling studies, low sample biomass presented a principal challenge throughout this study (Selway et al., 2020; Verbanic et al., 2019). Multiple extraction kits were assessed for their microbial DNA isolation capabilities, including the DNeasy PowerSoil kit (Qiagen), DNeasy PowerSoil Pro Kit (Qiagen) and the QIAamp DNA Microbiome Kit (Qiagen). While the DNA microbiome kit functions to simultaneously deplete host contamination and purify bacterial DNA, this kit failed to yield sufficient DNA for downstream analysis. Despite small variation amongst the remaining kits, the DNeasy PowerSoil kit was selected for use throughout the study. In addition to genomic isolation kits, ONT offer a range of metagenomic and targeted DNA sequencing approaches, however, the current study was limited by the initial gDNA input required. Multiple kits were screened for optimal protocol sequencing design, including the rapid PCR barcoding kit (SQK-RPB004), the PCR barcoding kit (SQK-PBK004) and the 16S barcoding kit (SQK-RAB204). The latter two kits were found to be unsuitable, with the PCR barcoding kit (SQK-PBK004) requiring high initial gDNA input (100ng) and the 16S kit failing to yield quantifiable amounts of data. The rapid PCR barcoding kit (SQK-RPB004) was selected for use throughout the study.

To mitigate low sample biomass issues experienced during the optimisation process, protocol modifications were incorporated to increase PCR amplification cycle number. Mock community validation was implemented to assess the contribution of workflow bias on accurate microbial community recapitulation. Minor discrepancies were identified, including moderate underrepresentation of the primary pathogen *Pseudomonas aeruginosa.* Recent publications using the same ZymoBIOMICS mock community also report underrepresentation of *Pseudomonas aeruginosa*, in combination with increased detection of *B. subtilis* (Nicholls et al., 2019; Yang et al., 2019). Further analysis revealed that 5% of reads were attributed to 'other' species, potentially assigned to other *Escherichia/Shigella* species. High genome

similarity (>99% sequence identity) between *Escherichia and Shigella species*, once classified as a single species, causes frequent challenges in differentiating between the two organisms (Chattaway et al., 2017). In addition, *Cryptococcus neoformans* was not identified within the mock community sample. Upon further investigation, it became apparent that the fungal portion of the centrifuge classification index contained only the genomes of 29 fungal species at the time of classification, with *Cryptococcus neoformans* not being included in this data set (Kim et al., 2016). Following this discovery, an improved fungal classification genome data set was developed to allow the inclusion of the 285 fungal genome sequences contained in the NCBI Ref Seq database (Marcelino et al., 2020). While this custom database functions as an improvement, many of the 2 million species of fungi are still not accounted for, leaving room for future alterations (Marcelino et al., 2020). The late optimisation of this pipeline unfortunately resulted in it not being able to be implemented in the current study. However, this adapted pipeline will be imperative for future studies, particularly those investigating the fungal mycobiome. Regardless, concordance between theoretical and observed composition indicated that increasing PCR amplification has a negligible effect on community recapitulation.

Community analysis directly compared skin microbial community composition between those presenting with and without a non-healing wound (Figure 3.10). Interestingly, the intact skin microbiome of those with a chronic wound was dissimilar to the healthy skin, showing reduced sample biomass and strong similarities with that of the diabetic wound environment, regardless of diabetic status (Figure 3.10). One hypothesis for this significant shift in microbial composition is the clinical routine of continuous topical washing of the wound (and surrounding skin) with non-specific antimicrobial agents. While not yet fully characterised, Erlund et al., 2021 previously described how in venous stasis ulcers, frequent wound area cleansing causes consistent changes in wound composition and a reduction in microbial biomass. Commensal bacteria, acquired from healthy skin, modulate the immune response and promote barrier restoration, preventing pathogenic colonisation and infection (Tomic-Canic et al., 2020). It is likely that extensive washing dysregulates this process, providing increased opportunity for unchallenged invasion and dominance of the wound environment by opportunistic pathogens (Erlund et al., 2021, Tomic-Canic et al., 2020; Canic et al., 2020).

Investigation of wound bacterial composition was a primary aim of the current research (Figure 3.13). 34 profiled wound samples were included from 28 individual donors. Across all wound samples, 12 species were identified as the most abundant wound microbes: *Escherichia coli, Pseudomonas aeruginosa, Proteus mirabilis, Corynebacterium striatum, Morganella morganii, Providencia rettgeri, Finegoldia magna, Staphylococcus epidermidis, Mycobacterium avium, Porphyromonas asaccharolytica, Staphylococcus aureus,* and *Enterococcus faecium*. This contrasts with other studies (Price et al., 2011; Han et al., 2011; Gardner et al., 2013; Loesche et al., 2017; Park et al., 2019; Min et al., 2020) where *Staphylococcus*, characterised to only the genus level, was consistently identified as the dominant microbe (average relative abundance 25.8%).

Individual analysis of wound composition according to the topmost abundant colonising bacterial taxa present revealed great heterogeneity (Figure 3.17). Examination of sample diversity and overall composition showed extreme relative dispersion and lack of consistency between samples. As a result, many taxonomic associations with clinical features were detected but not deemed to be significant (Mallick et al., 2020). Due to the high number of clinical variables and limited overall sample number, it is likely that only associations of a comparatively sizeable effect could be detected and clinically correlated (Mallick et al., 2020). Whilst sample size was comparable to previous studies: Price et al., 2011 *[n=12]*, Han et al., 2011 *[n=15]*, Gardner et al., 2013 *[n=52]*, Loesche et al., 2017 *[n=100]*, Park et al., 2019 [n=20] and Min et al., 2020 [n=10], heterogeneity will be introduced by the broad types of wounds and participant clinical phenotypes included within our study. Pathophysiologically distinct wounds are likely coupled with different host/wound environments, ultimately confounding the identification of microbial populations associated with clinical features (Kalan and Grice, 2018; Wu et al., 2020). Note, Gardner et al., 2013, also determined wound microbiomes to be extremely heterogeneous, even in the presence of a tightly restricted study population.

One issue that may have contributed to the profile heterogeneity is high levels of host DNA contamination, a well-established challenge in metagenomic analysis (Kerkhof, 2021). Despite this, there is currently no guidance on acceptable levels of host DNA, nor on the depth of sequencing needed to acquire meaningful profiling-based information (Ciuffreda et al., 2021).

Addressing this topic, Pereira-Marques et al., 2019 aimed to assess the impact of host DNA on microbiome analysis using synthetic microbial samples spiked with increasing levels of host DNA. Taxonomic analysis revealed that increasing proportions of host DNA resulted in reduced sequencing depth, reduced detection of low abundance species and overall decreased coverage for microbiome characterisation (Pereira-Marques et al., 2019). Throughout the current study, the percentage abundance of human host DNA within the samples was on average around 92%. Similar studies have also revealed challenges relating to the predominance of host DNA in whole metagenome sample analysis (Pereira-Marques et al., 2019). Data from the Human Microbiome Project (HMP) revealed that while stool samples comprise less than 10% of human DNA, samples such as saliva, throat and buccal mucosa contain more than 95% of human-aligned reads (Human Microbiome Project Consortium, 2012b; Lloyd-Price et al., 2017). In samples where only a restricted fraction of the DNA represents microbial DNA, a high quantity of sequences are required for realistic coverage of the microbial communities present (Human Microbiome Project Consortium, 2012b; Lloyd-Price et al., 2017). In response to this issue, the implementation of real-time selective sequencing software 'read until', capable of extruding selected host DNA molecules, is gaining popularity amongst nanopore users (Payne et al., 2021; Kovaka et al., 2021). While still in its infancy, the incorporation of selective sequencing in future wound microbiome studies would be extremely beneficial, increasing run efficacy and enriching low abundance genomes (Kovaka et al., 2021). Overall, overcoming host contamination issues is critical for future of long-read sequencing. The adaptation of sequencing platforms to achieve appropriate microbial sequencing depths will guarantee the production of cost-effective clinically useful information, needed to inform the next generation of treatments for poor wound healing (Ciuffreda et al., 2021).

As with other research, a focus of this study was to compare microbial profiles with clinical factors (Gardner et al., 2013; Park et al., 2019; Tipton et al., 2021). Diabetes, a systemic disease directly influencing immune response and cutaneous healing, was the first clinical factor to be specifically investigated (Wilkinson and Hardman, 2020). Minimal variation was identified between the global wound profiles of diabetic and non-diabetic participants (Figure 3.19). However, SparCC correlation identified individual taxa which correlated strongly with

diabetic status. Pathogenic species *Anaerococcus mediterraneensis and Clostridium difficile* were associated with positive diabetic status. Such species indicate an impaired immune response, high bioburden and a pathogenic shift in colonising species (Maden et al., 2012; Gupta et al., 2014).

In contrast, *S. epidermidis, a* recognised commensal resident of the normal skin flora, known to facilitate cutaneous barrier repair, was associated with the non-diabetic wound environment (Leonel et al., 2019). In parallel with the *Staphylococcus* population present on intact skin (Figure 3.11), diabetic skin revealed a considerable increase of *Staphylococcus aureus,* compared to that of both the healthy skin and intact non-diabetic groups, in which the *Staphylococcus* population was dominated by *Staphylococcus epidermidis*. Previous studies have also compared the diabetic/non-diabetic wound microbiome. Jnana et al., 2020 recently profiled 122 wounds (*100 db, 22 ndb*), and highlighted the genus *Methylobacterium* to be associated with positive diabetic status. Despite the contemporaneousness, Jnana and colleagues utilised techniques capable of only genus-level microbial identification. The ability to discern between species of the same genus is of profound clinical relevance, as single genera often encompass various species that have different pathogenicity characteristics, innate virulence factors and treatments (Brown and Horswill, 2020). Relevant to current findings, we revealed differential *Staphylococcus* inner-genus species abundance profiles, each with unique pathogenic capabilities (Otto, 2009; Brown and Horswill, 2020). This information would be missed by the methods employed in Jnana et al., 2020. The superior taxonomic resolution achieved using third generation long-read sequencing technologies, may facilitate clinically useful discoveries at a deeper biological depth; such as those that remain currently unexplored at the genus level (Johnson et al., 2019).

Finally, glycaemic control (HbA1c index) was identified in this study as a significant factor associated with individual wound taxa. Functioning as an important prognostic indicator, lack of glycaemic control has been repeatedly and independently associated with impaired wound healing (Christman et al., 2011). Gardner et al., 2013 were the first group to consider associations between the colonising DFU microbiome and related clinical factors. Able to define only to a genus level, Gardner et al., 2013 associated lack of glycaemic control with

Staphylococcus-rich and *Streptococcus*-rich ulcer clusters. More recently, Park et al., 2019 showed that proportions of *Bacteroidetes, Peptoniphilus*, and *Streptococcus* were higher in the wounds of non-controlled glycaemic patients. Within this current study, glycaemic control was associated strongly with an increase in certain species, both at a global and more in-depth level. *Porphyromonas asaccharolytica* (*p=0.04*) *and Peptoniphilus harei* (*p=0.009*) were the only OTUs determined as significantly different between the conditions, whilst 5 individual species of *Prevotella* (specifically *intermiedia, jejuni, enoeca, dentalis, meaninogenica)* were also non-significantly elevated (Figure 2.25). Whilst studies such as Park et al., 2019 report that *Prevotella*, *Peptoniphilus*, *Porphyromonas* are more abundant in samples taken from wounds of higher severity, all wounds in the current study were determined to be of high severity, yet the presence of these species was almost exclusively in wounds of participants of poor glycaemic control. Further studies are clearly necessary to validate the relationship between diabetic management and the role of diabetic wound microbiota.

Little is known about the effects of antibiotic use on the cutaneous microbiome, and few studies have attempted to characterise how antibiotics influence the wound microbiota (Punjataewakupt et al., 2019; Kaiser et al., 2021). Existing as a biodiverse ecosystem, the wound environment incorporates a vast collection of cohabiting and interacting multi-kingdom microbes (Kaiser et al., 2021). With many of these species capable of altering phenotypes and shifting virulence, it's unsurprising that the effects of antibiotics on this complex environment are difficult to characterise. In agreement with Loesche et al., 2017 no significant changes in community composition were detected in response to antimicrobial therapy of any known mechanism (Figure 3.27). This lack of association may be due to unique interactions between specific treatment regimes and personal microbial communities. In addition, sample sizes within the current study, specifically according to antimicrobial mechanism of action, were limited, hindering intra-group comparison. Regardless, these findings are contrasting to those seen in other locations including the gut where, antimicrobial exposure is strongly associated with decreased microbial community diversity, predisposing the environment to pathogenic invasion and *Clostridium difficile* infection (Dethlefsen and Relman, 2011; Stein et al., 2013).

While the bacterial fraction of the microbiome was considered the focus of this study, shotgun metagenomics simultaneously captured eukaryotic reads. Fungal communities constituted a small fraction (1%) of the combined "biome" compared to bacterial species (Figure 3.28). Lower eukaryotic read abundance may be due to the suboptimal extraction of eukaryotic DNA, as extraction and processing methods were optimised for effective genomic bacterial DNA isolation (Jo et al., 2017; Byrd et al., 2018). Previously studies have identified and highlighted 144 fungal species that remain poorly understood in chronic wound care (Kalan and Grice, 2018; Wu et al., 2020). The importance of these communities is further amplified by the finding that up to 90% of wounds contain fungi, with reports that in multi-kingdom wound biofilms, fungal species provide a scaffold for bacterial attachment and offer additional protection from antimicrobial therapy (Kalan et al., 2016; Kalan and Grice, 2018, Kean et al., 2017). Whilst *Malassezia restricta* was observed as the dominant non-host eukaryotic species present in healthy tissue samples, the necrotrophic fungal species *Boytris cinerea* was identified as the dominant species in all post-amputation samples. This conflicts with previous data, in which *Candida parapsilosis, Candida tropicalis, Trichosporon asahii, Candida albicans,* and *Aspergillus* species are frequently reported as the predominant DFU fungal isolates (Chellan et al., 2010; Dowd et al., 2011; Kalan and Grice, 2018). Whilst none of these species were identified in the current study, this finding certainly highlights the need to encompass all aspects of the microbiota, including multi-kingdom interactions that contribute to poor clinical outcomes (Grice et al., 2021).

Finally, clinical culture and sequenced microbial profiles were directly compared across participant wound samples (Figure 3.30). All participant clinical culture results in the current study were collected from those with a clinically infected wound, in which identification of the causative organisms was essential for effective clinical wound management. As described previously, current clinical 'gold-standard' approach's include culture (which can be slow to obtain results; 48-72 hours), or PCR-based analysis (which fails to detect the entire pathogenic spectrum or antimicrobial resistance. Charalampous et al., 2018, recently used ONT sequencing to identify causative organisms in lower respiratory infections. The research group reported that using nanopore technology, they achieved rapid pathogen identification (300 seconds) and antimicrobial resistance profiling for all bacterial species present within

their metagenomic samples. The use of ONT for real-time in-clinic wound microbiome analysis would enable improved clinical management and rapid strategic antimicrobial administration, whilst simultaneously, providing insight into the emergence and spread of pathogenic species.

Upon direct comparison of the long-read sequencing and culture based methods, approximately 60% of participant samples displayed a corresponding dominant microbe. Within the limited literature, inconsistencies amongst culture and sequencing results are common, with metagenomic methods frequently reporting increased microbial diversity (Gardner et al., 2013; Mudrik-Zohar et al., 2022). Gardner et al., 2013 reported that culture techniques underestimate sample bacterial load by 2.34 logs when compared to quantitative PCR-based estimations. One discrepancy in the current study was due to the clinical culture-based identification of 'anaerobes'. In such circumstances, metagenomic methods frequently characterised a diverse wealth of anaerobic species, each with varying clinical implication. Within donor 20, four separate anaerobic species were detected including; Gram-positive anaerobic cocci (GPAC) species *Anaerococcus mediterraneensis, and* Gram-negative organisms *Prevotella intermedia, Porphyromonas asaccharolytica and Prevotella melanogenic.* Whilst culture data described only the presence of 'anaerobes', such species have varying publication-based prognostic associations. For example, Min et al., 2020 identified that GPAC species specifically, are associated with impaired healing and are a significant predictor of poor clinical outcomes.

Within this GPAC population, Min et al., 2020 further described how the specific presence of *Peptoniphilus* species can act as a biomarker of delayed healing. In three separate donors, *Peptoniphilus harei* was amongst the 'anaerobes' metagenomically identified. In 2021, Wan et al, further reported *Peptoniphilus harei* as a previously underestimated emerging pathogen, commonly undetected by clinical anaerobic cultures. Not limited to a single genus, further studies have also described the prognostic impact of wound anaerobic populations, with Kalan et al., 2019, observing that the presence of specific genera including *Anaerococcus*, *Helcococcus* and *Porphyromonas* were significantly elevated in unhealed DFUs. Alongside current publications, this data suggests that technological advancement to enable rapid

species level diagnostic identification of anaerobes is essential for understanding how specific components of the wound microbiota contribute to the delayed healing phenotype.

Whilst the current study collectively reinforces the clinical and biological importance of utilising nanopore-based long-read sequencing technologies in wound care, high-resolution microbiome research is ultimately still in its infancy. Third-generation sequencing costs have drastically reduced, allowing widespread accessibility to metagenomic techniques, and opening previously unprecedented opportunities to deliver sub-species level characterisation. Research, is however, somewhat hindered by a range of issues, including the inability to discriminate between live and dead microbes (Fu et al., 2018; Emerson et al., 2017). A lack of standardisation in experimental and specifically bioinformatic workflows remains a fundamental challenge, requiring attention, so as to not limit the clinical applicability or comparison of findings between research groups (Wang et al., 2021; Bharti and Grimm, 2021). Other specific issues currently being addressed include sequencing accuracy, with ONT boasting a 5-year increase in sequence accuracy from 65% to 96.5%, Furthermore, the current implementation of $1D^2$ Nanopore sequencing techniques act to further reduce error rates by sequencing both strands of the DNA duplex consecutively (Silvestre-Ryan and Holmes, 2021).

Despite these limitations, this study demonstrates that the chronic wound microbiome can be successfully characterised using novel long-read sequencing approaches. Whilst clear sample heterogeneity was observed, our research has demonstrated that bacterial species-specific differences are associated within clinical parameters. Healthy donors show differential species-level distribution when compared to profiles of both diabetic and non-diabetic participant wounds. Participant glycaemic status was found to have a strong relative influence on the wound microbiome, whilst wound duration, infection status and previous antibiotic therapy had only a weak influence. Nanopore offers clinically useful wide-spectrum rapid pathogen identification and antimicrobial resistance profiling information not considered possible using culture-based approaches. What remains to be determined is if any community features have associated clinical outcomes, and, if microbiome modulation represents a viable option for informing future treatment strategies in poorly healing wounds.

4 The Host-Microbiota Axis

4.1 Introduction

Interactions between the wound microbiota and host immune system play an important role in wound repair, specifically in the activation of the host inflammatory response (Durand et al., 2022). Recent advancements in microbial characterisation techniques have revolutionised our understanding of the microbial world, as reviewed in Zhao et al., 2022. In turn, information gathered using these novel methods has enabled unprecedented insight into host-microbe interactions that occur in chronic wound environments (Miguel and Grice, 2015; Sachdeva et al., 2022).

Upon the formation of a cutaneous wound, a highly coordinated series of cellular events is initiated to re-establish tissue integrity (Wilkinson and Hardman, 2020). This process involves a vast network of signalling molecules, stimulating the recruitment of resident immune cells, and the secretion of innate host defence peptides (Drayton et al., 2021). Acting as a first line of defence, these peptides are essential for preventing bacterial invasion and promoting cutaneous wound repair (Gera et al., 2022). As witnessed in diabetes, derangement in wound-linked cellular defence behaviours often leads to infection, excessive tissue inflammation and chronic wound formation (Wilkinson and Hardman, 2020; Gera et al., 2022). Previous studies have investigated clinical healing phenotypes to assess the role of tissue defence mechanisms in the wound host-microbe interaction (Njeim et al., 2020; Rodríguez-Carlos et al., 2020; Tipton et al., 2020). Within the defence process, antimicrobial peptides (AMPs), which exist as a class of small endogenously produced agents, gain frequent attention for their potent inhibitory effects against bacteria, fungi, parasites and viruses (Figure 4.1; Rončević and Puizina, 2019).

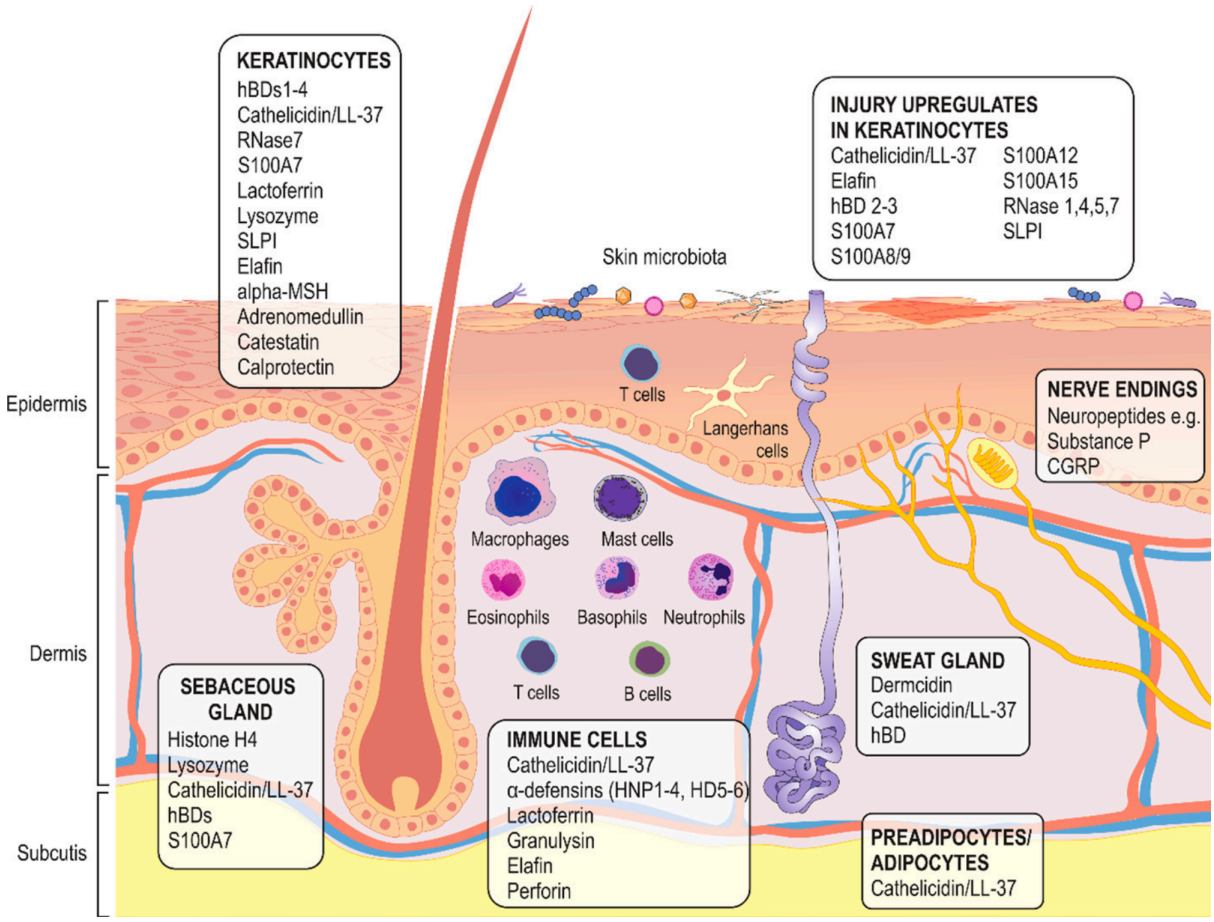

Figure 4.1: Antimicrobial peptide (AMP) distribution within human skin. AMPs are extensively produced in human skin under normal physiological conditions. As key response molecules of the innate immune system, their expression is induced in response to tissue damage or pathological stimuli (Image adapted from Gera et al., 2022).

Recent studies deciphering the role of defence proteins, such as AMPs, in the wound environment have reported a range of findings (Njeim et al., 2020; Rodríguez-Carlos et al., 2020; Tipton et al., 2020) (Table 4.1). Rodríguez-Carlos et al., 2020 observed a metformin-induced depletion of *RNase 7* levels, with associated increased susceptibility to cutaneous infection in the diabetic foot ulcer population. In a murine model, Williams et al., 2017 identified that *Nod2* deficient mice maintained an altered skin microbiome, represented by a significant shift in *Pseudomonas* colonisation, alongside impaired wound healing. Additional studies have focused on how aspects of the immune response may influence microbial modulation (Njeim et al., 2020; Hassanshahi et al., 2022). This includes wound immune cells, such as neutrophils and macrophages, which are commonly described as having a double-

edged role, stimulating pathogenic clearance whilst also maintaining chronic inflammation (Chesko and Wilgus, 2022). Circulating immune cells which are recruited to the wound environment during tissue repair, are significant producers of host defence peptides (Chesko and Wilgus, 2022). In addition, Tipton et al., 2020 investigated the role of patient genetics in the host wound-microbiome interaction. They correlated patient focal adhesion patterns with significant inter-patient variation in the relative abundance of two key wound pathogens, *Pseudomonas aeruginosa* and *Staphylococcus epidermidis*. Many of these studies suggest that aspects of host wound-microbiome crosstalk may act as biomarkers for clinically relevant predictive risk models in the development and persistence of infection (Njeim et al., 2020; Tipton et al., 2020).

Table 4.1: Recent host-wound microbiome interaction profiling studies.

Study Reference	**Sample Type**	**Observations**
Williams et al., 2017	*Nod*2-null murine model	*Nod2* deficient mice had an inherently altered skin microbiome and demonstrated impaired healing
Njeim et al., 2020	Diabetic wounds (Nonspecific wound type)	The excessive presence of tissue neutrophils contributed to the pathogenesis of diabetes and its complications, including impaired wound healing
Rodríguez-Carlos et al., 2020	Wagner's grade 3 diabetic foot ulcers	AMPs including RNase 7 levels were decreased in both diabetic groups when compared with skin from healthy donors.
Tipton et al., 2020	Chronic Wounds (Nonspecific wound type)	Patient genetics were linked to chronic wound microbiome composition.

The majority of recent host defence profiling studies have utilised protein-based or PCR-based gene expression characterisation methods for the detection and quantification of selected peptides (Sabbah et al., 2009; Simanski et al., 2010; Contreras et al., 2020; Takahashi et al. 2021). These studies are limited by such methods, which typically assess a single predetermined protein or gene transcript (Takahashi et al. 2021). By contrast, studies presented in this chapter used transcriptional profiling (RNA-seq) to globally profile the functional transcriptome of complex clinical wound samples. Previous microbial profiling studies have typically addressed the question of "who's there?". By combining long-read sequencing with histological analysis, clinical data and tandem transcriptional profiling (RNA-seq) this chapter starts to address the questions "why are they there?" and "what are they doing?".

4.1.1 Aims

1) To characterise the host transcriptional profile of clinical wound samples, correlating microbial composition to host gene expression.

2) To integrate complex clinical and biological datasets to gain critical insight into functional elements of the host-microbe interaction.

3) To identify novel signalling events associated with wound pathology and microbial profiles.

4.2 Methods

4.2.1 Ethics

All human tissue was collected from theatres at Hull Royal Infirmary (Hull, UK) or Castle Hill Hospital (Cottingham, UK) under full REC approval (REC: 17/SC/0220 & 19/NE/0150). All patients provided written, informed consent. Identifiable information was anonymised.

4.2.2 Tissue Collection

Across the study, and for each microbiome profiling specimen collected, host tissue samples were simultaneously collected from the corresponding participant donor sites. In total, biopsy specimens were harvested from five locations from each donor, each with increasing proximity to the wound, including the upper leg (amputation margin), apical foot, extended wound zone, peri-wound and wound bed (Figure 4.2). Tissue samples were collected using a 6mm biopsy punch (Stiefel, North Carolina, United States) and processed using three independent methods: including snap-freezing in liquid nitrogen and mounting in optimal cutting temperature media (OCT; CellPath, Newtown, Wales), before −80°C storage. Alternatively, histological samples were also collected and placed in uniquely labelled cassettes to maintain sample identity.

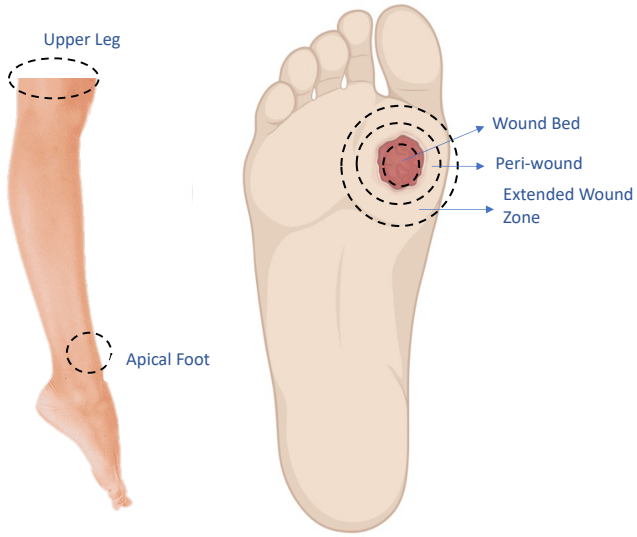

Figure 4.2: Schematic representation of tissue samples collected from lower extremity tissue donors. Participant tissue biopsy specimens were harvested from five locations with increasing proximity to the wound environment, including the upper leg (amputation margin), apical foot skin, extended wound area, peri-wound and wound bed.

4.2.3 *Ex-vivo* Skin Wounding

Following tissue collection, skin strips were used to create human *ex-vivo* skin wound models (Wilkinson et al., 2021). Skin samples were prepared into linear strips (8x3cm) and adipose tissue was removed. Skin samples were then washed twice in Hank's balanced salt solution (HBSS) (Gibco™, Thermo Fisher Scientific, UK) containing 2% antibiotic-antimycotic (Gibco™). A final wash was then performed by placing skin in Dulbecco's phosphate-buffered saline (DPBS) for 5 minutes at room temperature with intermittent shaking. Following this procedure, skin samples were placed dermis side down in a 90mm sterile Petri dish (Thermo Scientific™) and dried with sterile gauze. To create the *ex-vivo* wound, a partial thickness biopsy restricted to the epidermis and upper dermis was created in the centre of the skin using a 2mm biopsy punch (Stiefel). Next, a 6 mm full-thickness biopsy was created to fully excise the skin at an equal margin around the original partial-thickness biopsy. Skin explants were then placed on a nylon filter membrane (Merck-Millipore, Hertfordshire, UK) on a stack of two absorbent pads (Merck-Millipore) in 60mm dishes (Thermo Scientific™) containing 3mL

of standard culture media. Plates were then incubated in standard culture conditions (Section 2.3).

4.2.4 *Ex-vivo* Whole-mount Tissue Staining

Following incubation (48 hours), wound explants were collected in 1.5 mL microcentrifuge tubes containing 500 µL of 10% formalin tissue fixation solution (Appendix 8.8) and incubated at 4 °C for 24 hours. *Ex-vivo* wound biopsies were then washed three separate times in *ex-vivo* staining wash buffer (Appendix 8.8) and left overnight. Post washing, samples were again rinsed three times in *ex-vivo* staining buffer (Appendix 8.8). Samples then underwent blocking by adding 150 µL of *ex-vivo* blocking buffer (Appendix 8.8) to each sample and leaving to incubate at RT for 60 minuets. Following the blocking procedure, samples were again washed three times in *ex-vivo* staining buffer before primary antibody staining. Post-washing, a primary anti-mouse keratin 14 (K14) (Invitrogen, USA) antibody solution was diluted in *ex-vivo* staining blocking buffer (Appendix 8.8) at a concentration of 1:1000. 150 µL of the antibody solution was then added to each sample and left to incubate overnight at 4 °C. The next day, the primary antibody solution was removed, and the samples were washed three times in *ex-vivo* staining buffer to remove all excess primary antibody. The secondary antibody solution was then prepared by diluting a Alexa Fluor™ 488 goat anti-Mouse IgG secondary antibody (Invitrogen) in *ex-vivo* staining wash buffer at a concentration of 1:300. The secondary antibody was added to the *ex-vivo* wound specimens and left to incubate for 90 minutes in the dark at RT. Upon completion, the secondary antibody was removed, and samples were washed three times in *ex-vivo* staining buffer. Finally, the skin explants were counterstained with a 4',6- diamidino-2-phenylindole (DAPI) (Invitrogen) 5 mg/mL stock solution (in dimethyl sulfoxide) at a concentration of 1:1000 in *ex-vivo* staining wash buffer and left to incubate for 15 minutes at RT. Skin explants were then again washed three times and stored in buffer until imaging. For quantification, inverted microscopy images were captured using the Zeiss LSM710 Laser Scanning Confocal Microscope (Carl Zeiss, Germany). Explants were imaged using a 2.5x objective (25x total magnification). Images of the full biopsies were obtained and taken for future analysis. Image J 1.5.2 software (San Diego, CA) was then used to quantify to overall biopsy size and remaining open wound area. These

measurements were then used to determine the percentage of wound closure/re-epithelization.

4.2.5 Tissue Fixation and Processing

For tissue samples collected in section 4.2.2, cassettes containing the tissue biopsy specimens were placed in a 10% formalin tissue fixation solution (Appendix 8.8) for 24 hours. Post fixation, samples were transferred into 70% ethanol: 30% dH_2O for 18 hours. The full protocol of tissue fixation, processing and embedding is summarised in (Table 4.2) Post fixation, samples were processed to replace the internal tissue water content with a solidifying medium for future histological sectioning. Tissue was dehydrated in the following sequence: immersion in 90% ethanol for 30 minutes, 95% ethanol for 30 minutes, and 100% ethanol for 30 minutes, followed by a final emersion in a fresh solution of 100% ethanol for 50 minutes. For clearing, ethanol was then exchanged with xylene (Thermo Fisher Scientific, Loughborough, UK), and samples were immersed for two changes, 30 minutes and then 45 minutes. Xylene was then exchanged with Molten paraffin Lamb wax (Epredia^{TM}, Fisher Scientific). Tissue cassettes were immersed in molten wax (maintained at 58-60^{o}C) for 60 minutes, followed by a second immersion in fresh wax for 60 minutes. Tissue sections were removed from their respective cassettes and embedded in fresh paraffin wax within metal moulds, before being allowed to set on a cold plate (EG1150, Leica Biosystems, Milton Keynes, UK). Representative tissue sections from the formalin-fixed paraffin-embedded (FFPE) blocks were sectioned into ribbons of 5 µm thickness using a microtome (Leica RM2235). Wax tissue ribbons were then stretched and floated on a paraffin section flotation bath (TFB 45, Medite, Burgdorf, Germany) maintained at 45°C, allowing the expansion and manipulation of wax sections onto Vectabond (Vector, Peterborough UK) coated glass slides.

Table 4.2: Stages of human tissue processing

Stage	Time	Temperature
Formalin Fixative	24 hours	RT
70% Ethanol	18 hours	RT
90% Ethanol	30 minutes	RT
95% Ethanol	30 minutes	RT
100% Ethanol	30 minutes	RT
100% Ethanol	50 minutes	RT
Xylene	30 minutes	RT
Xylene (fresh change)	45 minutes	RT
Wax	1 hour	60°C
Wax (fresh change)	1 hour	60°C

RT = room temperature

4.2.6 Haematoxylin and Eosin Staining

Wax sections were deparaffinised in xylene for 20 minutes at room temperature (RT). Tissue samples were then transferred through a series of ethanol changes (of decreasing strength - 100%, 100%, 90%, 70% and 50%) for approximately two minutes in each solution to hydrate the sections. Samples were immersed in dH_2O and rinsed to remove any residual ethanol. Slides were stained in filtered Harris' haematoxylin from Sigma-Aldrich (Poole, UK) for 30 seconds and rinsed in tap water until the effluent ran clear. Sections were then transferred and counterstained with Eosin B (Sigma-Aldrich) for 5 seconds with gentle agitation and rinsed thoroughly in dH_2O. Stained tissue sections were then transferred through an ascending gradient of increasing strength ethanols: 50%, 70%, 90% for 30 seconds, and 100% and 100% for 1 minute each. Tissue was then cleared by immersion in xylene for 10 minutes at RT, before mounting with a coverslip using a Pertex® mounting medium (CellPath, UK). Samples were allowed to dry for 24 hours prior to imaging.

4.2.7 Gram-Twort Staining

Samples embedded in optimal cutting temperature media (OCT, CellPath) were cryosection at 12 µm (CM3050 S; Leica Biosystems) and stored at −80°C until use. Before staining, sectioned slides at −80°C were brought to −20°C and fixed for 10 minuets in methanol (Thermo Fisher Scientific). A modified Gram-Twort stain was carried out by staining with Crystal Violet (Sigma-Aldrich) and Gram's Iodine solutions (Sigma-Aldrich). Samples where then differentiated in 2% acetic-alcohol (Sigma-Aldrich) and counterstained with a 0.2% neutral red (Sigma-Aldrich) and 0.2% fast green (Sigma-Aldrich) (9:1) solution (Sigma-Aldrich). Sections were then dehydrated by immersion for 1 minute in increasing gradients of ethanol (50%, 70%, 90%, 100% and 100%) and mounted with a coverslip using with Pertex® mounting medium (CellPath).

4.2.8 Immunohistochemistry (IHC)

Slides containing FFPE tissue sections were deparaffinised as described in Section 4.2.6. Heat-induced epitope retrieval methods were utilised to disrupt methylene bridges and expose antigenic sites (Magaki et al., 2019). Tissue sections were boiled in antigen retrieval citrate buffer (pH 6) for 3 minutes and allowed cool fully on ice (Appendix 8.8). Sections were then immersed in dH_2O for 5 minutes. A hydrophobic isolator pen was used to draw a wax border around the slide-mounted tissue. Endogenous tissue peroxidases were quenched by incubating each section in a 0.3% hydrogen peroxide solution (Sigma-Aldrich) for 30 minutes at RT. The tissue was then washed in PBS (Sigma-Aldrich) for 15 minutes.

Non-specific antibody binding was mitigated by the process of blocking (Magaki et al., 2019). For tissue undergoing staining with primary rabbit-raised antibodies, 30 µl of 10% goat serum in PBS (v/v) (Vector Laboratories, US) was applied to each tissue section for 20 minutes. Once complete, the blocking solution was then removed, and the primary antibody (prepared in the blocking solution) was added to each tissue section. When staining utilising antibodies raised in mice, tissue blocking was conducted by applying 30 µL of MOM block (M.O.M.® ,Mouse on Mouse Immunodetection Kit, Vector Laboratories) to each tissue section

for 5 minutes (prepared in accordance with manufactures instructions). Excess MOM block was gently removed from the slide, and the primary antibody (prepared in MOM diluent, Mouse on Mouse Immunodetection Kit, Vector Laboratories) was added to the tissue. All primary antibodies used were left to incubate at 4°C overnight. Positive and negative controls (PBS only) were included for each antibody.

Table 4.3: Primary antibodies used for immunohistochemistry

Antibody	**Working concentration**	**Incubation Time**	**Temperature**	**Manufacturer**	**Host Species**
Anti-CD68	1 µg/mL	O/N	4°C	Abcam	Mouse
Anti-Neutrophil Elastase	1.5 µg/mL	O/N	4°C	Abcam	Rabbit

O/N = overnight for 16 hours

Following overnight primary antibody incubation, tissue sections were rinsed through a series of PBS washes. Sections were then incubated with the appropriate peroxidase-linked anti-IgG secondary antibody. Rabbit primary antibody: secondary goat anti-rabbit (BioLegend, San Diego, United States) antibody for 30 minutes at RT. Mouse primary antibody: MOM secondary antibody (Mouse on Mouse Immunodetection Kit, Vector Laboratories): (10 ml of MOM secondary antibody into 2.5 mL of MOM diluent) for 40 minutes at RT. Sections were rinsed in PBS before incubation for 30 minutes with 30 µL per section of ABC reagent (Vectastain® ABC-HRP Peroxidase Kit, Vector Laboratories). ABC reagent contains enzymes including horseradish peroxidase (HRP) and avidin to detect and amplify signals from the HRP-linked secondary antibody. Colourimetric visual tissue staining was performed using Nova Red (NovaRED® Substrate Peroxidase Kit, Vector Laboratories), by applying the solution until a visible colour change could be observed. Slides were then rinsed in dH_2O for approximately 5 minutes. Counterstaining was achieved by immersing slides in Harris' haematoxylin (Sigma) for 2-3 seconds before rinsing under running tap water for approximately 2-3 minutes. The tissue was dehydrated and mounted as described in Section 4.2.6.

4.2.9 Histological Image Analysis

All non-fluorescent tissue staining was visualised using a Nikon Eclipse E400 microscope with SPOT camera software (Image Solutions Ltd.). For epidermal thickness, Haematoxylin & Eosin (H&E) stained tissue was captured at X4 magnification. Five images were collected along the epidermis of each donor. Image J was used to measure epidermal thickness; distance scales were calibrated using graticules and five measurements were taken from each image captured. Prior to analysis, each sample was assigned a unique identification number to blind the researcher analysing the samples from introducing unconscious bias during the analysis. For immune cell profiling (CD68 and neutrophil elastase) images were captured at X20. Five images were captured for each tissue section in three separate regions (Figure 4.3), with increasing tissue depth. CD68 staining was quantified by determining the number of CD68-positive cells in each image per mm^2. Neutrophil elastase was quantified by percentage area positivity using the ImageJ colour deconvolution tool (Colour Deconvolutio2). For OCT embedded samples and Gram-Twort staining, images were captured at x100 with oil. Five images were taken per tissue section. Staining was again quantified by percentage area positivity using the ImageJ colour deconvolution tool (Colour Deconvolutio2).

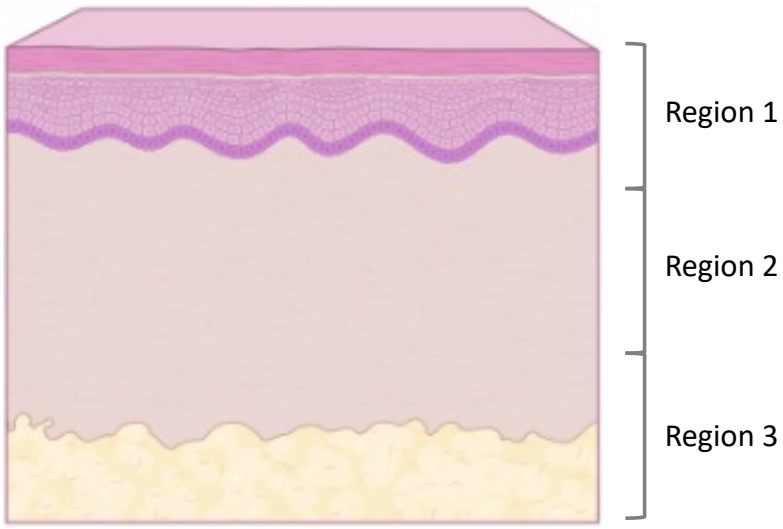

Figure 4.3: Schematic of the three depth-based regions of tissue selected for IHC staining analysis in immune cell profiling.

4.2.10 Bacterial Culture Preparation

All bacterial culture preparations were conducted in a Class II microbiological safety cabinet (Microflow, Bioquell, Hampshire, UK) using aseptic technique. Overnight (O/N) cultures were prepared by inoculating a single bacterial colony in 10 mL Mueller Hinton Broth (MHB; Oxoid, UK) followed by incubation at 37°C for 16 hours at 140 revolutions per minute (rpm) (shaking) (Labnet 211DS shaking incubator, Labnet International, USA). Supernatants of excreted bacterial products were prepared from overnight cultures by pelleting cells and sterile filtering the acellular supernatant using a Millipore 0.2 µm sterilizing PES membrane (Millipore Express®)

4.2.11 Cell Viability Assay

Cell viability assays were conducted to assess the influence of specific treatments, including bacterial supernatant on cell viability and proliferation. Primary human dermal fibroblasts (HDFs) and human keratinocytes (HaCaT) cells were used throughout the study. HDFs were cultured in high glucose, no glutamine, no phenol red, Dulbecco's Modified Eagle Medium (DMEM) (Gibco™) (Appendix 8.8). HDF media was further supplemented with 10% heat-inactivated foetal bovine serum (FBS) (Gibco™), 1% L-glutamine (Gibco™) and 1% Penicillin-

streptomycin (Gibco™). HaCaTs cells were cultured in high glucose, no glutamine, no calcium DMEM (Gibco™) supplemented with 10% heat-inactivated FBS, 1% L-glutamine, 1% Penicillin-streptomycin and 1mM calcium chloride (Sigma) throughout (Appendix 8.8). Mammalian cell populations were maintained in standard culture conditions at 37°C, 5% CO_2 and >95% relative humidity (standard culture conditions).

On reaching 80% total confluency, cells were seeded into a 25-well TC-treated microplate (Corning®, Sigma-Aldrich) at a concentration of $5x10^4$ cells/per well for HDFs and $1x10^5$ cells/per well for HaCaTs, and appropriate treatments were applied. Cells were incubated in standard culture conditions for a period of 24 hours. Plates were then removed from the incubator and washed with DPBS and trypsinised (Gibco™) to facilitate the detachment of cells from the culture vessel. Following incubation and dissociation, standard culture media was used to neutralise the trypsin and the cell suspension was centrifuged at 400 relative centrifugal force (RCF) for 5 minutes. Cellular pellets were resuspended in equal volumes of culture media. 10 µL of cell suspension was removed and combined with an equal volume of 0.4% Trypan blue (Thermo Fisher). The number of viable cells remaining in each suspension was determined using a haemocytometer counting chamber (Scientific Laboratory Supplies (SLS), Germany). Percentage cellular viability and cytotoxicity were calculated using the control culture measurements.

4.2.12 Scratch Closure Assay

Mammalian cell scratch closure assays were conducted to assess the migratory ability of cell populations following exposure to treatment. Cell cultures were maintained as described previously (Section 4.2.11). Upon reaching 80% total confluency, cells were seeded into a 24-well TC-treated microplate (Corning®, Sigma-Aldrich) at a concentration of $4.5x10^4$ cells/per well for HDFs and $1.5x10^5$ cells/per well for HaCaTs. Following cell seeding, plates were left undisturbed for 16-24 hours in standard culture conditions and allowed to reach 80% confluency. Scratches were then performed on confluent wells using a 1 mL pipette tip. The tip was held vertically and pulled downwards through the cell monolayer whilst maintaining an even pressure. Cells were washed with PBS and a control (0hr) well was stained

immediately with 2% (v/v) crystal violet solution (Sigma-Aldrich). Culture media was then replaced, including desired treatments, and FBS serum concentration reduced to 2% (v/v) for the remainder of the assay. Plates were incubated in standard culture conditions for either 16 (HaCaTs) or 24 hours (HDFs). Upon collection, cell culture media was aspirated, wells were washed with DPBS and then stained with 2% crystal violet. All non-fluorescent tissue staining was visualised using a Nikon Eclipse E400 microscope with SPOT camera software (Image Solutions Ltd). For each well, five images were collected and Image J was used to measure the scratch width from each image captured. Percentage closure was calculated using the 0-hour scratch assay control data.

4.2.13 Bacterial Enumeration

For viable bacterial enumeration, swabs were collected from either the wound bed, peri-wound or skin of lower extremity tissue donors. Sterile cotton swabs were pre-moistened in sterile PBS and rotated continuously over the sampling area for 30 seconds. Each swab was then placed into a fresh 0.5 mL Eppendorf tube containing 250 mL PBS, and vortexed for 20 seconds. Samples were then centrifuged to collect any remaining liquid from the swab, and serially diluted in MHB. A dilution series for each sample was then plated directly on Mueller Hinton agar (MHA) and chromogenic *Staphylococcus* selective agar (CHROMagar™, Springfield, United states), by spreading 100 mL of each dilution evenly across the agar plate. Plates were incubated at 37°C O/N and counted the following day to determine colony forming units (CFU) per swab.

4.2.14 Tissue RNA Extraction

Tissue samples were previously snap-frozen (Section 4.2.3) and stored at −80°C storage prior to RNA extraction. During RNA collection, tissue samples were maintained on dry ice to prevent sample thawing. At the point of extraction, tissue samples were removed from dry ice and divided in half, ensuring a representative section containing both epidermal and dermal tissue was harvested. Tissue specimens were separated into small pieces (<1 mm)

using a scalpel blade and incubated in 1 mL of chilled TRIzol (Invitrogen). The tissue then underwent homogenisation (IKA T10 basic homogeniser, Oxford, UK) for exactly 30 seconds and was left to stand at RT for approximately 5 minutes. For each 1 mL TRIzol, 200 µL of chloroform (Fisher Scientific) was also added to each sample, followed by 15 seconds of vigorous shaking. Eppendorf samples containing the TRIzol/tissue were then centrifuged (13000rpm) at 4^{o}C for 15 minutes. At this stage, tissue samples in each tube had separated into three distinct horizontal layers: the top clear aqueous layer, the pink organic bottom phase and the middle white layer/ interphase, containing the precipitated DNA.

The aqueous phase was then carefully removed, leaving approximately 1 mm of sample margin above the middle phase to avoid contamination (Toni et al., 2016). The collected sample was then deposited into a corresponding 1.5 mL Eppendorf containing 500 µL of 70% ethanol (Thermo Fisher). RNA was purified using the PureLink® RNA Mini Kit, (Fisher Scientific). This process included gently inverting the sample and then adding 700 µL of the RNA solution to a silica spin column (Fisher Scientific) followed by centrifugation at 14000rpm (14462 X g) for 15 seconds. Liquid throughflow was discarded and the process was repeated twice with 500 µL of Wash Buffer II (PureLink® RNA Mini Kit, Fisher Scientific). Spin columns and collection tubes were centrifuged again for approximately 1 minute to clear and dry the membrane within the spin column. At this stage, the collection tubes were replaced with recovery tubes. 30 µL of RNase-Free Water (Eurogentec, Belgium) was then added to each spin column and left to stand at RT for 1 minute. Spin columns and attached recovery tubes were then centrifuged for approximately 2 minutes at 14000rpm (14462 xg), to elute the RNA from the spin column membrane. Recovery tubes containing the extracted RNA solution were detached from the spin columns and immediately stored at -80°C.

4.2.15 RNA Quantification

The SimpliNano™ Spectrophotometer (Biochrom, Cambridge, UK) was used to determine the RNA and direct (A280) purity. From each tube, 2 µL of the sample was placed on the built-in

sample port and RNA levels were measured. Samples then underwent preparation for external RNA-sequencing or in-house cDNA synthesis.

4.2.16 RNA sequencing (RNA-seq)

RNA-seq methods were employed for the deep transcriptional profiling of 16 tissue samples from diabetic patients (8 donors in total, intact skin site and peri-wound/wound margin). Tissue RNA was extracted as described in Section 4.2.14. RNA sequencing was outsourced and conducted by Novogene Biotech Co^{Ltd} (Beijing, China). Total eukaryotic mRNA isolated for sequencing included samples over >200 ng in a volume of > 10 µL (concentration 20 ng/ µL) with a purity (NanoDrop) OD260/280 >2.0, OD260/230 >2.0. Following quality testing (Library QC), a 150 bp paired-end sequencing strategy was used to sequence the samples (Figure 4.4). Resultant data also underwent quality control (Data QC). Illumina PE150 technology was employed for sample sequencing. Finally, bioinformatic analyses and data visualisation was conducted using R studio (v.1.3) and DESeq2 (v.1.30.1).

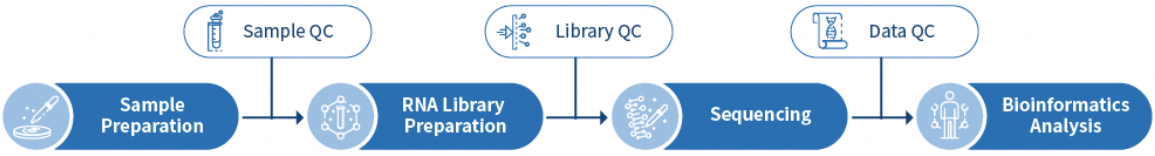

Figure 4.4: RNA-Seq sample workflow.

4.2.17 cDNA Synthesis

Once quantified, RNA samples were adjusted to 1 µg/ µL in RNase-free water for complimentary cDNA synthesis. 2 µL of a solution containing equal amounts of dNTP (Promega, Wisconsin, United States) and random primers (Promega) was added to each sample. Mixed samples were then placed in a Techne TC-412 Thermal Cycler (Techne, Essex,

UK) and denatured at 70°C for 5 minutes. Once cooled to 4°C, a master mix solution was then added to each sample containing 0.5 µL of reverse transcriptase (Eurogentec, Belgium), 1 µL of RNase Out (Eurogentec) and 2.5 µL RNase free water (Eurogentec). Samples were returned to the thermal cycler and allowed to complete an optimised cDNA run. Throughout this run, samples were held at 25°C for 10 minutes, 42°C for 60 minutes, then 85°C for 5 minutes. cDNA samples were stored at 4°C for immediate use, or -20°C for long-term storage.

4.2.18 RT-qPCR Amplification

For the creation of PCR primers, nucleotide sequences were acquired from the NCBI gene database and primers were developed using Primer3Plus Software (Untergasser et al., 2007). Throughout, primers were designed across exon junctions, in order to prevent genomic DNA contamination (Laurell et al., 2012). Primer specificity was checked using NCBI BLAST, and primer products were checked via the assessment of amplification curves (Appendix 8.6). Single product amplification was confirmed by the presence of a single melt curve peak. All primers were initially designed to be between 18-30 nucleotides in length to create an amplicon sequencing product of less than 300 base pairs. Sequence GC content was maintained between 40-60% and repeated sequences of more than four bases were eliminated to prevent secondary structure hairpin loop formation (Laurell et al., 2012).

For qPCR, template cDNA was serially diluted by 10-fold using nuclease-free water (NFW; Eurogentec, Belgium). cDNA samples were then stored on ice during plating. 10 µL of cDNA solution from each sample was added to the corresponding wells within a multiplate 96-well PCR plate (Bio-Rad, USA). Following this, Takyon master mix (Eurogentec, Belgium) was combined with host gene-specific forward and reverse primers (See Appendix 8.5) and NFW, in order to create a final mixture, of which 10 µL was pipetted into each of the 96 wells containing the produced cDNA. Following the addition of this mix (creating a final well volume of 20 µL) samples were ran on a CFX-Connect machine (Bio-Rad, USA). Cycling conditions included an initial 3-minute hold at 95°C, followed by 39 cycles at 95^{o}C for 10 seconds before adjustment to 59.5^{o}C and 70^{o}C for 30 seconds each. Plates were analysed on the CFX

Connect™ platform using CFX manager software (Bio-Rad Laboratories).Gene expression was determined relative to housekeeping genes (GAPDH and YWHAZ). For analysis, relative expression was determined from a sample standard and standard curve produced.

4.3 Results

4.3.1 Histological characterisation of wound samples evaluated for microbiome profiling revealed altered epidermal structure at the wound edge.

Alongside samples for microbiome profiling (Chapter 3), each donor provided tissue samples from a selection of wound related sites for histological and gene expression analysis (Figure 4.2). From these donors, wound microbial community composition signatures were correlated to host tissue transcriptional profiles (RNAseq), structural tissue information, clinical parameters and markers of favourable clinical outcomes. Initially, histological samples from each donor underwent H&E staining to assess broad tissue structure and morphology (Figure 4.5) (Farci and Mahabal, 2022). Across each donor, both the epidermal and dermal layers of the healthy skin and peri-wound skin could be clearly visualised (Figure 4.6). In acute wound healing, keratinocytes, the main cellular component of the epidermis, regenerate over deposited granulation tissue (Takeo et al., 2015). This epidermal layer exists as both a structural and functional antimicrobial shield, restoring tissue integrity whilst secreting a selection of innate immune mediators (Takeo et al., 2015). In chronic wounds, this process becomes dysregulated (Brugués et al, 2014; Nusbaum et al., 2014). In the current study, epidermal thickness was significantly elevated in the peri-wound region compared to that of the intact skin harvested from the amputation margin ($p < 0.001$, *paired t-test*). Average epidermal thickness across intact skin was measured at 93 µM, ranging from 51 µM to 175 µM (Figure 4.5:A, B). However, in the peri-wound, epidermal thickness increased to an average of 425 µM, ranging from 222 µM to 674 µM (Figure 4.5: A, C). A selection of donors, including donors 15, 17, 20 and 22, demonstrated clear hyperkeratosis, as shown by the thickening of the outer stratum corneum (Del Regno et al., 2022; Figure 4.6). This extensive increase in epidermal thickness is a common characteristic of the peri-wound environment and is thought to contribute to the delayed healing phenotype (Pastar et al., 2014).

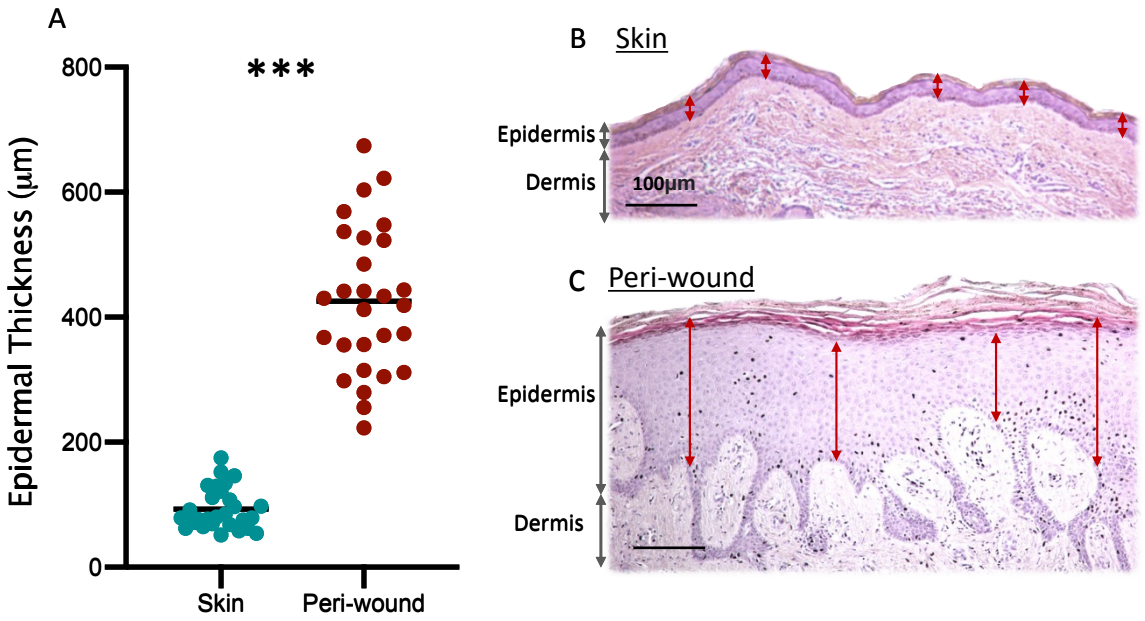

Figure 4.5: Tissue structure and epidermal thickness across skin amputation margin and peri-wound tissue. Formalin-fixed paraffin-embedded (FFPE) tissue subject to H&E staining. Red arrows demonstrate the collection of epidermal thickness measurements. Five individual epidermal thickness measurements were collected from each donor. Data points represent the mean thickness of a single donor sample (A). Black horizontal line represents the mean for each location *[n=32]*. Representative photomicrographs of healthy skin (B) and peri-wound sites (C). Bar = 100µm. ****p < 0.001, paired t-test.*

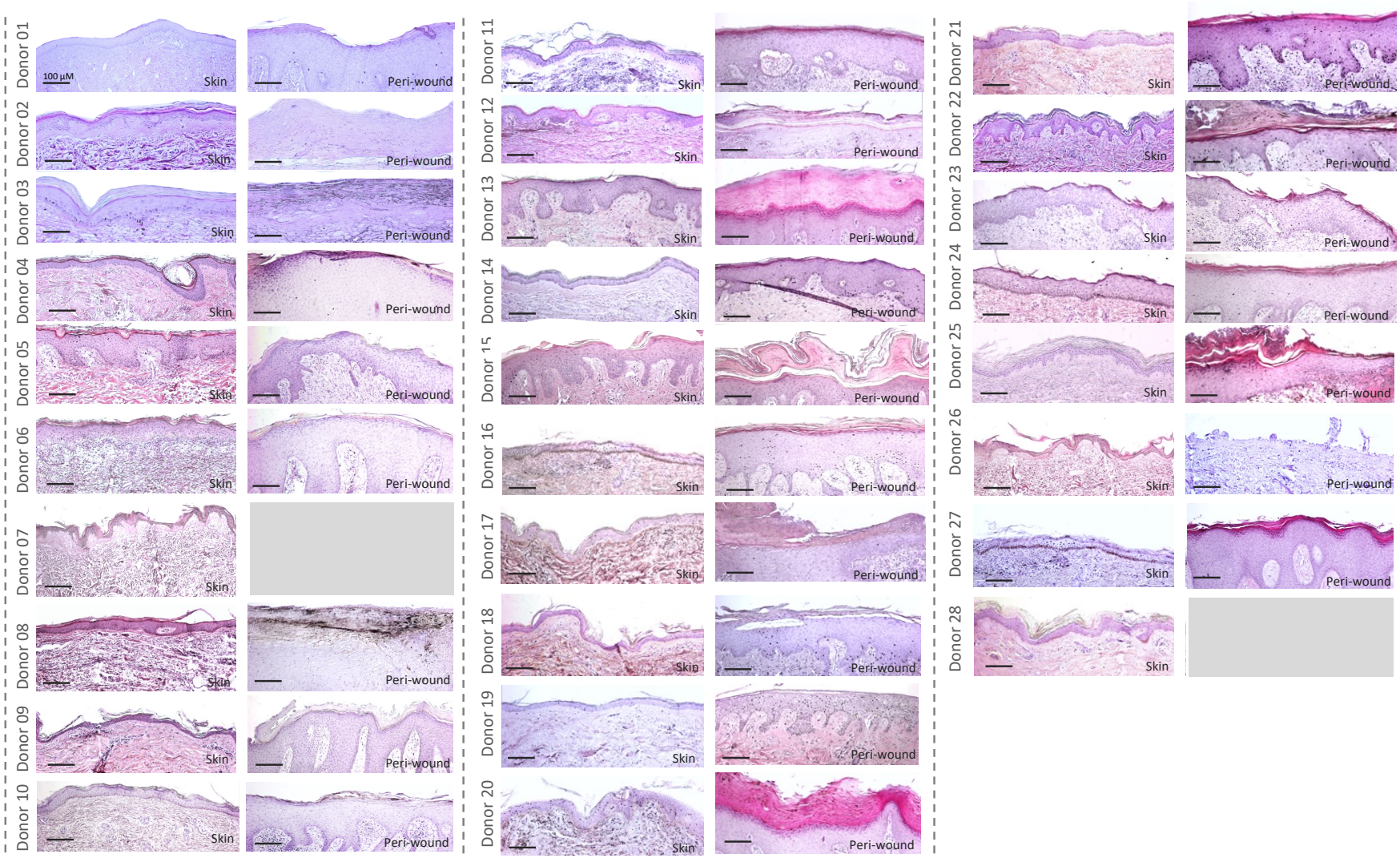

Figure 4.6: Representative appearance of tissue from donors presenting with a non-healing wound. Representative haematoxylin and eosin stain of tissue from healthy and peri-wound regions of each donor *[n=28]*. Scale Bar = 100 µM

4.3.2 Gene expression profiling reveals distinct signatures between the upper leg intact skin and peri-wound regions across study donors.

Following H&E staining analysis, in-depth transcription analysis was conducted in the first eight individual diabetic donors to be recruited into the study. In this donor subset, RNA-seq profiling was performed to gain further insight into the host differences between intra-donor tissue sites with increasing proximity to the wound environment (Figure 4.7). For a subset of diabetic donors, global gene expression profiles were collected from both the peri-wound (wound margin) and the upper leg intact skin of the amputation margin (Schematic: *Figure 4.2*). One of the key benefits of RNA-seq transcriptomic profiling within this study was the ability to assess intra-donor changes in transcript abundance according to sampling site (Wang et al., 2009).

To select relevant information, Gene Ontology (GO) analysis was employed to identify human genes associated with the biological process of wound healing (Gene Ontology Consortium, 2021). Gene ontology provided a collection of approximately 500 genes (Gene list ID: GO 0042060) associated with the series of events that restore integrity to damaged tissue, following an injury. Raw transcript data underwent variance stabilisation transformation (VST) and was then explored using hierarchical clustering (Heatmap: *Figure 4.7*). Differential expression analysis was employed using DESeq2, creating a heatmap to visualise the top 150 most variable wound healing genes across the tissue samples from the two distinct collection sites. Euclidean clustering of samples according to gene expression profiles grouped the tissue samples entirely into by location (intact upper leg skin and peri-wound).

.

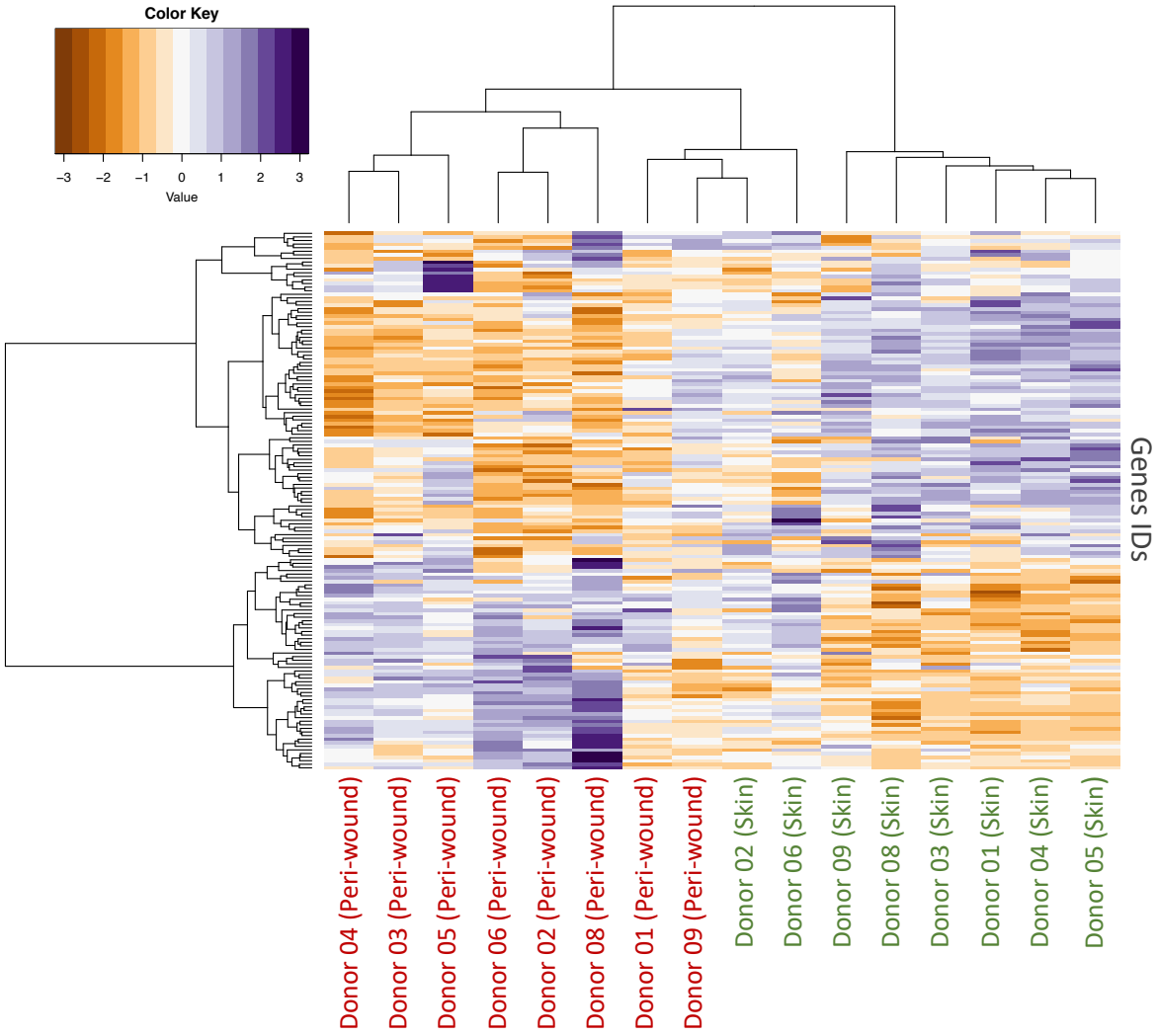

Figure 4.7: Community heatmap analysis of the 150 most variable GO wound healing-associated genes identified in the skin and peri-wound tissue of diabetic participants. Differential expression analysis highlights clustering patterns within the heatmap. Row dendrograms show hierarchical structure based on gene expression profile similarity as a result of Euclidean clustering. Reduced proportions are represented in orange and highly expressed genes are highlighted in purple. Supplementary labelling on the horizontal axis reveals Donor ID and sampling location within the heatmap. *[n=16, from a total of n=8 donors].*

4.3.3 Host defence gene analysis reveals distinct clustering between the profiles of intact skin and peri-wound sites.

Next, a refined list of the most important genes differentially expressed between skin and peri-wound was selected. This list was derived from relevant literature with a focus on host defence. Differential expression analysis was again employed using DESeq2. For visualisation, the top 20 most variable genes across the tissue samples from the 'intact upper leg skin' and 'peri-wound' regions were presented in a heatmap (Figure 4.8). Hierarchical clustering revealed three distinct clusters. Cluster 1 was comprised exclusively of 'intact skin, with increased expression of 'Zone 1' genes. Cluster 3 contained only peri-wound region with elevated expression of genes contained within 'Zone 2'. Genes contained in 'Zone 1' and 'Zone 2' were selected for further downstream investigation.

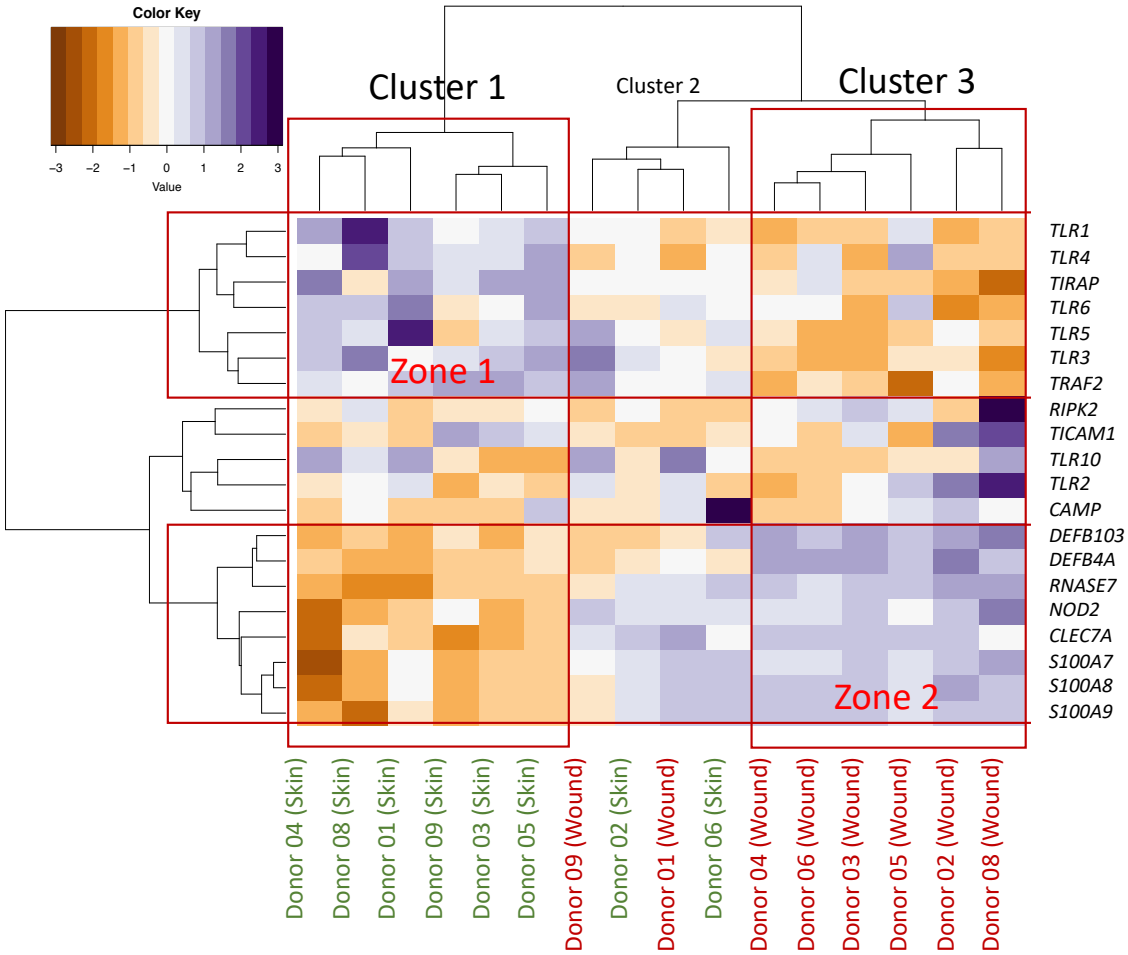

Figure 4.8: The 20 most variable host defence-associated genes identified in skin and peri-wound tissue of diabetic participants. Differential expression analysis highlights clustering patterns within the heatmap. Samples within the heatmap were grouped into either cluster 1, 2 or 3 depending on their gene expression profiles. Genes contained within the highlighted red areas (zone 1, zone 2) were selected, extracted, and processed for further downstream investigation. Supplementary labelling on horizontal axis reveals Donor ID and sampling location within the heatmap. *[n=16, from a total of n=8 donors]*.

4.3.4 'Zone 1' gene subset containing toll-like microbial recognition receptors displayed decreased expression in participant peri-wound samples.

'Zone 1' contained seven host defence-related genes that were downregulated in the participant wound environment. Toll-like receptors (TLRs) accounted for the majority of these genes, including *TLR1, TLR3, TLR4, TLR5*, and *TLR6*; Figure 4.9: A-E). TLRs function as keystone factors in innate immune regulation, endowed with the capacity to respond to microbial signals from the environment (El-Zayat et al., 2019). Multiple studies have shown that the absence of TLRs delays wound healing, perturbating inflammatory cell infiltration and cytokine expression (Munir et al., 2020; Portou et al., 2020).

On average, genes contained within this signature demonstrated a 1.5-1.6-fold decrease in relative expression at the peri-wound region (Figure 4.9). TLR1 showed the greatest decrease at 2.1-fold. Whilst other TLR genes also presented decreased expression (TLR3, TLR4, TLR5 and TLR6), these changes were determined to be none significant (*p > 0.05, paired t-test*). Signalling adaptor/receptor genes TIR domain-containing adaptor protein (TIRAP) and TNF receptor-associated factor 2 (TRAF2) were also contained within this cluster. Whilst both genes were downregulated in peri-wound, only the expression of TIRAP was statistically significant (*p = 0.03*, *paired t-test*).

Generally, TLRs are considered a major component of the dysfunctional inflammatory cascade in the chronic diabetic wound environment (Portou et al., 2020). Whilst *in-vivo*, systemically antagonising TLR receptors have been shown to improve diabetic wound healing, clinical studies of diabetic foot ulcer patients have also found that TLR signalling is often mitigated as a result of epigenetic silencing in diabetic foot ulcers (Singh et al., 2014). As TLRs play a key role in wound inflammation and tissue repair, it is believed that repression or imbalances in the TLR- mediated signalling cascade may inhibit healing and contribute toward the delayed healing phenotype witnessed in diabetic wounds (Davis et al., 2020).

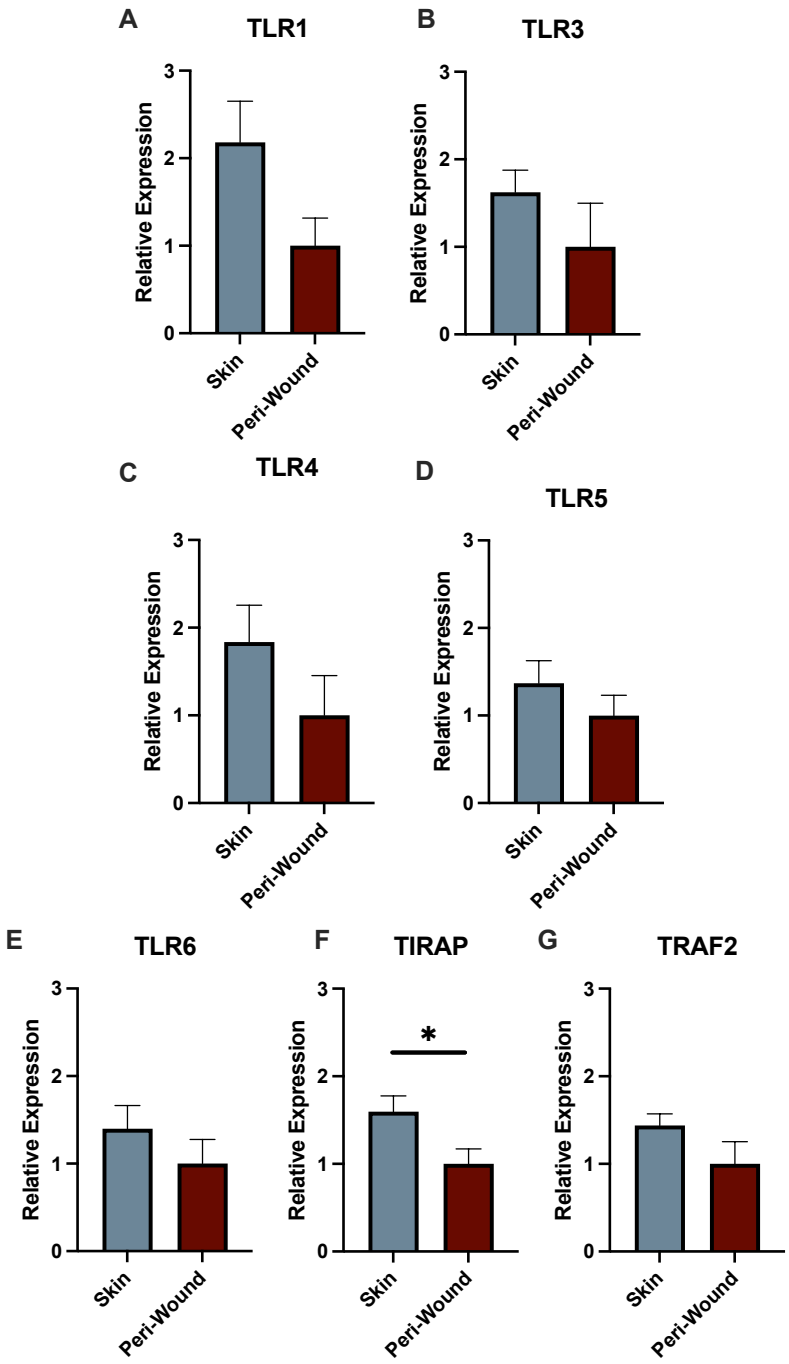

Figure 4.9: Relative expression of signature genes elevated in the contralateral skin of diabetic donors presenting with a non-healing wound. *TLR1* (A), *TLR3* (B), *TLR4* (C), *TLR5* (D), *TLR6* (E), *TIRAP* (F) AND *TRAF2* (G). Mean + SEM *[n=8]*. Significance determined using paired t-test, **p < 0.05*.

4.3.5 'Zone 2' containing a selection of innate antimicrobial peptide genes displayed elevated expression in the peri-wound.

'Zone 2' contained eight individual host defence-related genes with elevated expression in the peri-wound region (Figure 4.10). These included, defensin beta 103A (*DEFB103A*), defensin beta 4A (*DEFB4A*), ribonuclease A family member 7 (*RNASE7*), nucleotide-binding oligomerization domain containing 2 (*NOD2*), C-type lectin domain family 7 member A (*CLEC7A*), S100 calcium-binding protein A7 (*S100A7*), S100 calcium-binding protein A8 (*S100A8*) and S100 calcium-binding protein A9 (*S100A9*; Figure 4.10).

DEFB4A (Beta-defensin 2) and *DEFB103A* (Beta-defensin 3) have established associations with epithelial surface microbial colonisation (Takahashi et al., 2021). Equally, *NOD2* is a PRR that has previously been linked to maintaining the composition of the microbiome (Williams et al., 2017). *RNase 7* is a peptide that exhibits potent broad-spectrum antimicrobial activity and has numerous links with diabetes, chronic wounds, and therapeutic metformin response (Rodríguez-Carlos et al., 2020). Finally, while the S100 genes have limited previous association with wound healing, the expression of mRNA-associated proteins *S100A7* (Psoriasin) and *S100A8/A9* (Calprotectin) are considered markers of inflammation and infection (Lallyett et al., 2018). Contained within this signature, six host defence genes were determined to be significantly elevated, *DEFB4A* ($p = 0.04$), *RNASE7* ($p = 0.01$), *NOD2* ($p = 0.002$), *CLEC7A* ($p < 0.001$), *S100A7* ($p = 0.02$) and *S100A8* ($p = 0.005$), with *DEFB4A* demonstrating an average 158-fold increase in gene expression.

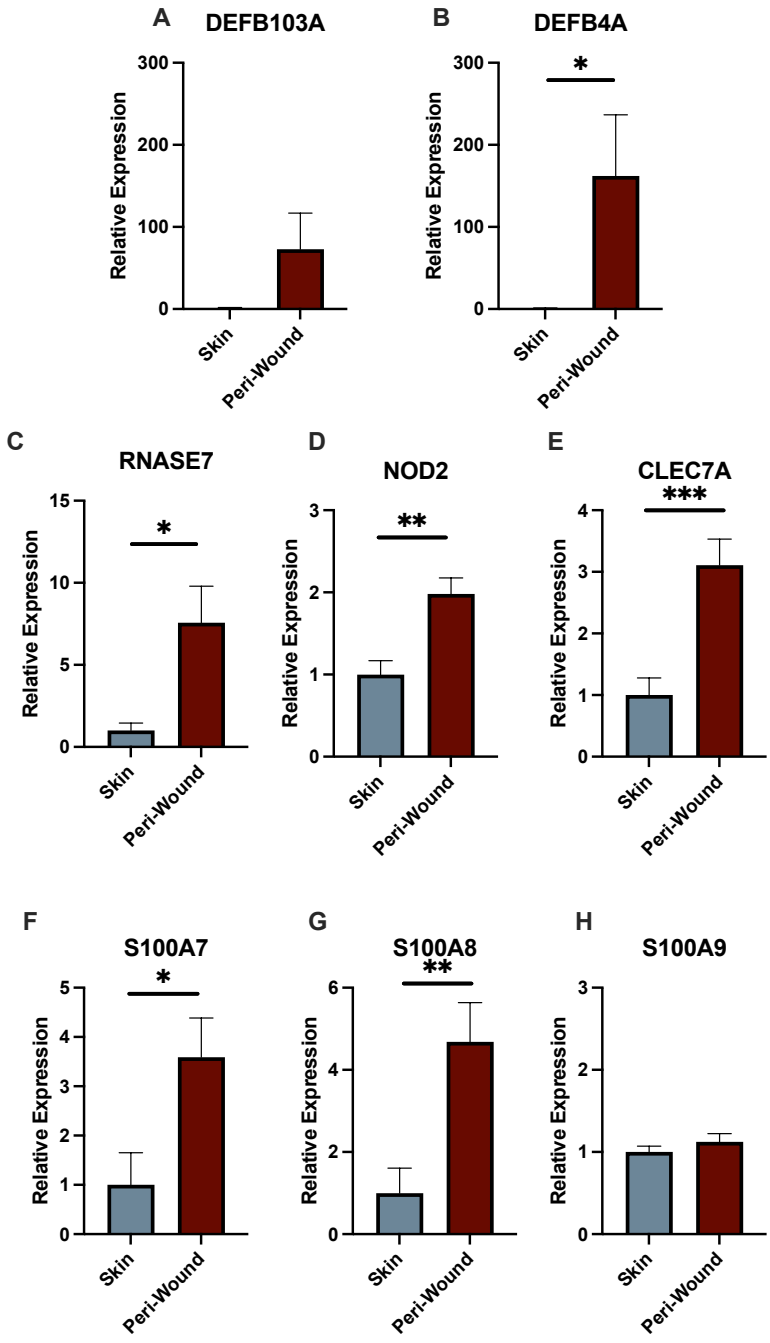

Figure 4.10: Relative expression of signature genes locally elevated in the peri-wound tissue of diabetic donors presenting with a non-healing wound. *DEFB103A* (A), *DEFB4A* (B), *RNASE7* (C), *NOD2* (D), *CLEC7A* (E), *S100A7* (F), *S100A8* (G) and *S100A9* (H). Bars represent mean relative expression, +/- SEM values *[n=8]*. Statistical significance determined using paired t-test. **p < 0.05, **p < 0.01, ***p < 0.001.*

4.3.6 Host defence gene expression profiles are linked to microbial composition.

To further explore the relationship between microbial profiles and host defence genes, differential expression analysis of peri-wound tissue profiles was conducted using DESeq2. The top 25 most variable OTUs across all 8 peri-wound samples were displayed as a heatmap, with hierarchical clustering highlighting profile similarity (Figure 4.11). Donors 02 and 06 showed distinct clustering according to host defence gene expression profiles. In parallel, both donors presented a higher relative abundance of the bacterial phyla '*Proteobacteria*' than any other donors within the study. Donors 08 and 09 also exhibited unique microbial community signatures and gene expression profiles. Of note, donor 08 presented considerably higher relative abundances of *Acinetobacter johnsonii* and *Acinetobacter lwoffi* than other donors. Donor 09 had increased *Streptococcus* and *Prevotella* species, compared to the other participants.

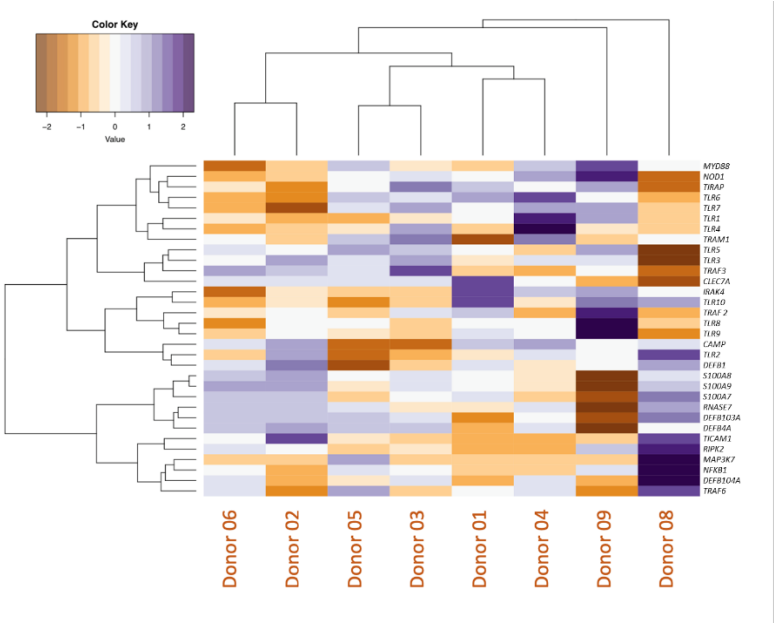

Figure 4.11: Community heatmap of the 30 most variable host defence-associated genes in peri-wound tissues. Row dendrograms show hierarchical gene expression profiles as a result of Euclidean clustering. Horizontal axis shows Donor ID *[n=8]*.

4.3.7 Healing-associated host defence gene expression profiles were altered in donors presenting with a non-healing wound.

To further investigate potential associations between microbiome and host response, gene expression analysis, microbiome profiles, clinical data, histological analysis and tissue immune cell profiling were combined across a wider range of participants (n=32). Nine host defence genes were selected, including: *TLR2, NOD2, RNASE7, MYD88, CLEC7A, HBD1, S100A7, S100A8 and S100A9* (Figure 4.12). Several genes from this list have previously established links with cutaneous healing (Dasu et al., 2019), however, corresponding association with skin/wound bacterial signatures remains to be addressed. The following data compares expression between a larger collection of both diabetic and non-diabetic donors, comparing expression to that of healthy abdominal skin (Figure 4.12).

Across these nine genes, limited significance was identified in gene expression between the two investigated donor sites and healthy skin tissue, *TLR2, NOD2, MYD88, CLEC7A, HBD1, S100A7, S100A8* and *S100A9 ($p > 0.05$, One-way analysis of variance; ANOVA)*. This was potentially attributed to the limited number of healthy control donors present within the study *[n=3]*. *RNASE7* expression, however, was significantly elevated in peri-wound tissue compared to the healthy skin (*$p = 0.03$, One-way ANOVA*). Expression of this host defence gene was consistently low in the healthy skin donors. Relative expression of *RNASE7* in the pathological upper leg intact skin of active wound donors demonstrated a non-significant six-fold rise compared to the healthy control skin (*$p > 0.05$*).

NOD2 expression was 2-fold higher in both the intact pathological upper leg skin and peri-wound of those with an active wound compared to healthy control donors (Figure 4.12: B). Additionally, *CLEC7A* expression was 3.4-fold and 4.2-fold higher in the intact skin and peri-wound region compared to the expression in the healthy control skin. Finally, S100 gene expression was consistently low across all healthy skin samples (Figure 4.12: G, H, I). However, a limited average change in expression was observed between the healthy skin, pathological 'intact' upper leg skin and peri-wound region, with most of the variation being attributed to high expression in a small number of donors.

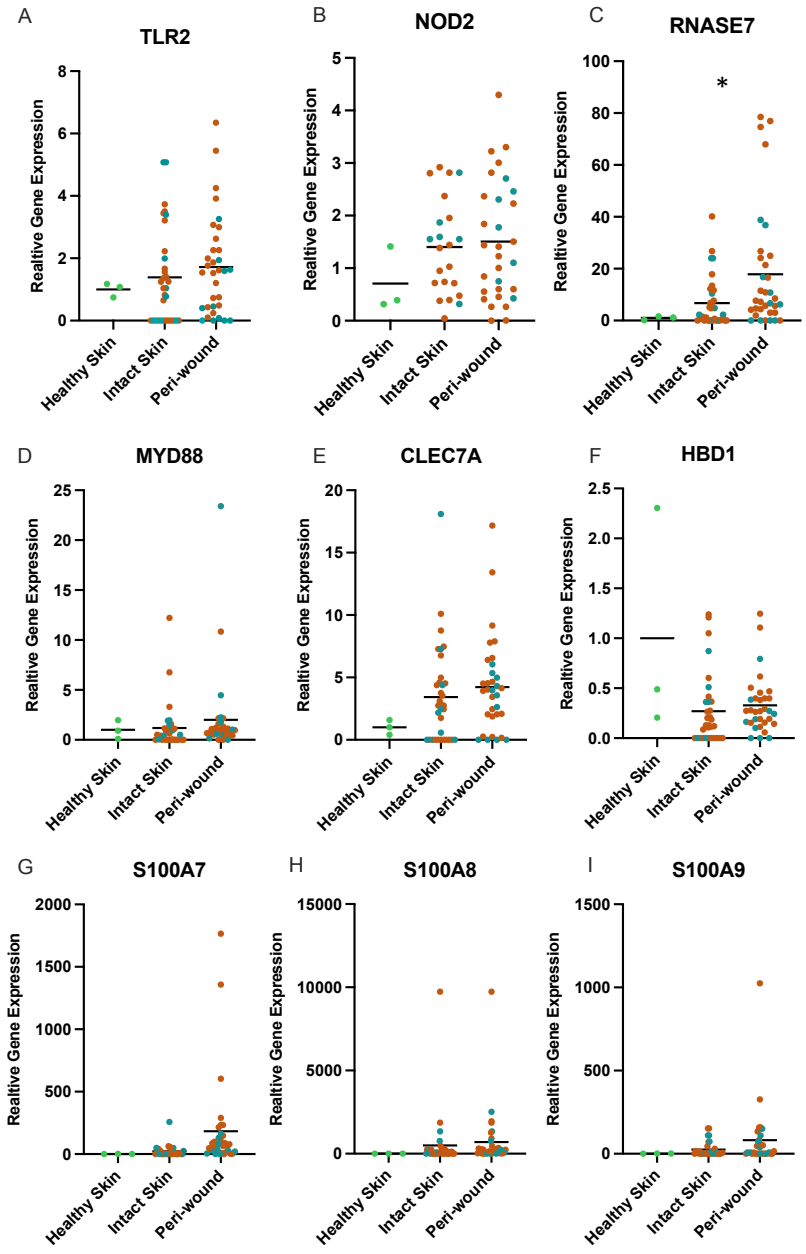

Figure 4.12: Relative host defence gene expression in healthy skin, pathological intact skin and peri-wound tissue of human donors according to qPCR quantification. Genes include *TLR2* (A), *NOD2* (B), *RNASE7* (C), *MYD88* (D), *CLEC7A* (E), *HBD1* (F), *S100A7* (G), *S100A8* (H), and *S100A9* (I). Each dot represents the measurement from of a single donor. Column black lines indicate mean gene expression. Healthy skin *[n=3]*, intact pathological skin *[n=22]* and peri-wound *[n=32]*. Dot coloring represents diabetic status, blue = ndb, orange = db. One-way ANOVA followed by a Tukey post hoc test. *$p < 0.05$, **$p < 0.01$, ***$p < 0.001$.

4.3.8 Tissue donor clinical blood marker profiles.

Clinical information was incorporated in the current study, including blood profiling of each tissue donor: Haemoglobin, Platelets, White Cell Count, Neutrophil Count, Sodium, Potassium, Urea, and Creatinine. Individual participant values and normal clinical ranges are summarised below (Table 4.4, Figure 4.13).

Participant haemoglobin levels were lower than the normal healthy patient range (104 g/L; Table 4.4). By contrast, mean white cell and neutrophil counts were elevated (Table 4.4). Participant blood urea was also higher than 'normal' in a large percentage of donors, although the donor mean fell within the considered 'normal range'.

Table 4.4: Normal and mean participant blood marker values.

Blood Marker	Normal Range	Participant Mean (Range)
Haemoglobin	Female: 120-160 g/L Male: 130-180 g/L	104 g/L (76 – 150 g/L)
Platelets	150-450 PLT per µL	361 PLT per µL (145 – 587 PLT per µL)
White Cell Count	4.5 - 11 WWC per µL	12.2 WWC per µL (4.5 – 24.7 WWC per µL)
Neutrophil Count	1.45 – 7.5 NE per µL	9.5 NE per µL (2.2 – 19.8 NE per µL
Sodium	135 – 145 mEq/L	132 mEq/L (121 – 139 mEq/L)
Potassium	3.6 – 5.2 mmol/L	4.5 mmol/L (3.5 – 5.9 mmol/L)
Urea	2.1 – 8.5 mmol/L	7.5 mmol/L (1.6 – 14.8) mmol/L)
Albumin	34 - 54 g/L	23 g/L (13 – 34 g/L)

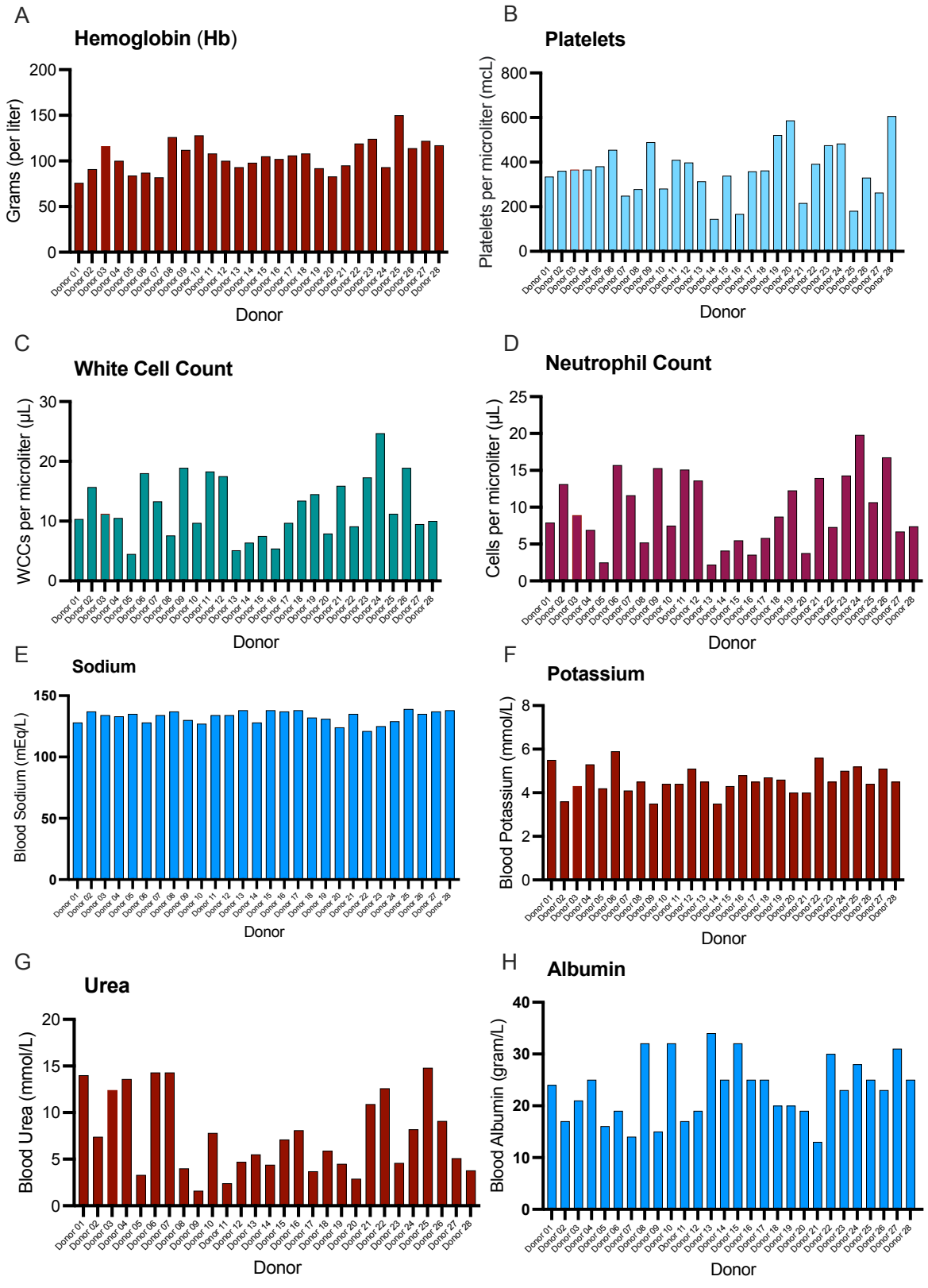

Figure 4.13: Blood screening measurements across all study participants. Panel includes blood*:* Haemoglobin (A), Platelets (B), White Cell Count (C), Neutrophil Count (D), Sodium (E), Potassium (F), Urea (G), Albumin (H). Each bar represents a single donor *[n=28]*.

4.3.9 Gram-Twort staining for bacterial detection in the tissue revealed great inter-donor variation.

The detection of bacteria in histological tissue specimens is key in the field of microbiology (Becerra et al., 2016). In this study, modified Gram-Twort staining was conducted to detect the presence of microorganisms within host tissue (Becerra et al., 2016; Figure 4.14). The mean area of wound tissue containing bacteria, as determined by positive Gram-Twort staining, was 7.97%. However, extensive variation was seen between donors (Figure 4.16). Donor 18 displayed only 1.49% positive tissue Gram-Twort staining while donor 21 presented with 22.09% positive staining.

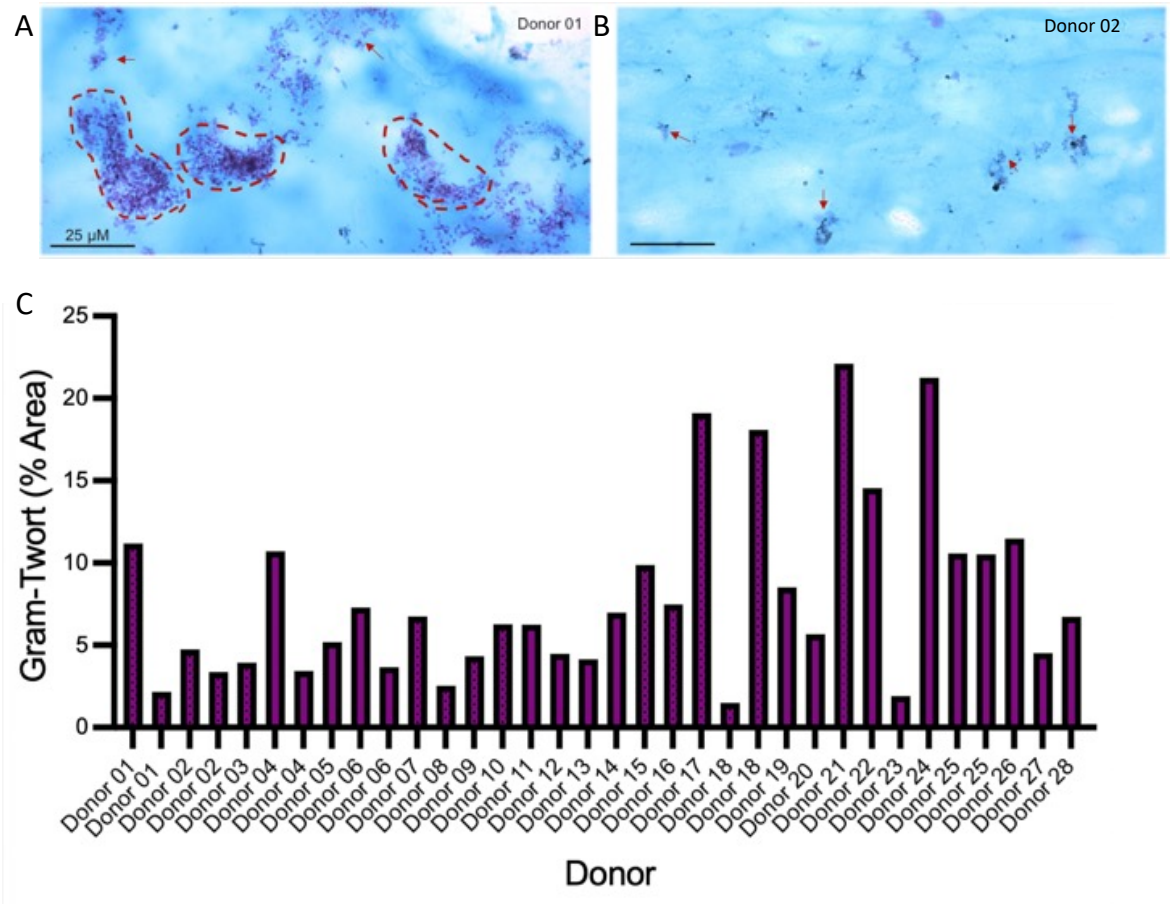

Figure 4.14: Gram-Twort staining identified the presence of bacteria within the wound tissue. Representative photomicrographs (x1000 total magnification) of patient-derived wound tissue containing high (A) and low (B) levels of bacteria. Modified Gram-Twort staining illustrates the presence of both bacterial aggregates (red dashed lines) and individual bacteria (red arrows) within the tissue. Each bar represents the average percentage area positive staining within each donor (C), *[n=34, n=28 unique (total) donors]*. Bar = 25 *µM*

4.3.10 Immune cell profiling of peri-wound tissue reveals high inter-donor and inter-regional dispersion.

Immune cell profiling of peri-wound tissue was conducted, with macrophage (CD68) and neutrophil elastase profiled in all available donors. CD68 is highly expressed by cells in the monocyte lineage, circulating macrophages, and tissue macrophages (Ren et al., 2017). Neutrophil elastase is a serine proteinase with broad substrate specificity, this proteinase is secreted by neutrophils during inflammation, acting to eliminate bacteria and host tissue (Gramegna et al., 2017).

High-variation in resident immune cells was observed across participant peri-wound sites. The mean number of CD68 positive cells in each region per mm^2 was 18.1, ranging from of 1.6 to 40.57 positive cells per mm^2 (Figure 4.15: A). Across the neutrophil elastase staining, the average percentage positive area of tissue staining per region was 10.2%, ranging from 3.4 to 21.2% (Figure 4.15: B) (Figure 4.18). Despite the variation witnessed between donors, a significant correlation was identified between the two immune cell markers (*R = 0.495, p = 0.0015,* Spearman's rank-order correlation coefficient*).*

In addition to variation between donors, significant depth-based inter-regional variation was also identified (Schematic: Figure *4.3*). The average number of CD68 positive cells per mm^2 was 9.9 in region 1, 26 in region 2 and 18.45 in region 3. A significant difference in cells per mm^2 was observed between all three regions, region 1 vs 2 (*p = 0.0001, one-way ANOVA*), and region 1 vs 3 (*p = 0.0027, one-way ANOVA*) and region 2 vs region 3 (*p= 0.0001, one-way ANOVA*). For neutrophil elastase, the average number of percentage area positivity was 11.63% in region 1, 11.34% in region 2 and 7.39% in region 3. A significant difference was observed between only region 1 vs 3 (*p = 0.003, one-way ANOVA*), and region 2 vs 3 (*p = 0.0002, one-way ANOVA*), minimal difference was observed between region 1 vs region 2 (*p = 0.9333, one-way ANOVA*) (Figure 4.17).

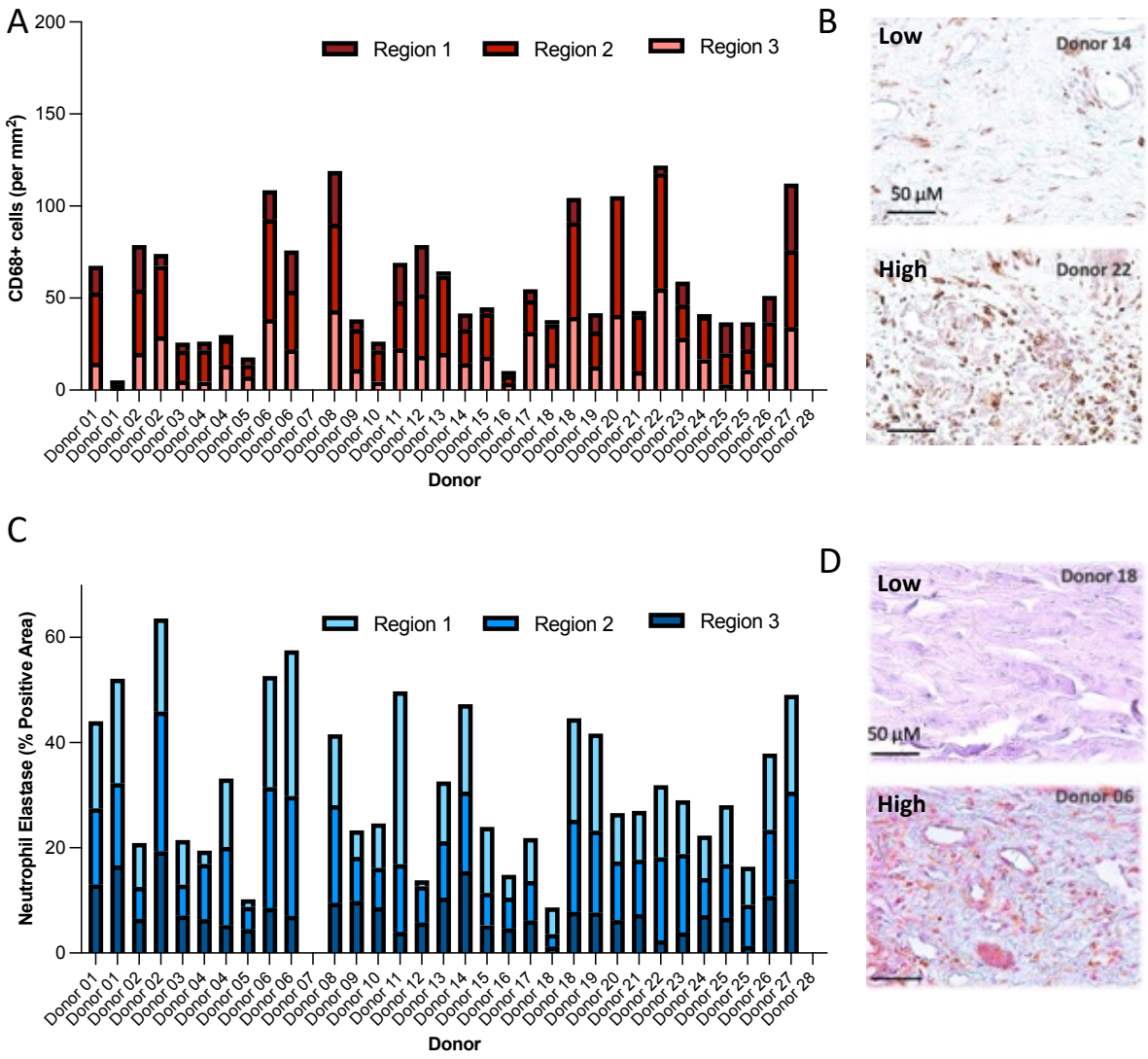

Figure 4.15: Quantification of CD68 positive cells and presence of neutrophil elastase in the peri-wound tissue of human wound donors according to immunohistochemical staining distribution. Each column represents a single donor, presenting CD68 positive (A) and positive neutrophil elastase (C) staining, based on the mixed contribution of regionally stained areas. Mean, statistical significance was determined using a one-way ANOVA followed by a Tukey post hoc test. Representative microscopic appearance of CD68 positive tissue (B) and neutrophil elastase staining (D) in FFPE tissue, X200 total magnification *[n=32, n=28 unique (total) donors]*. Bar = 50 µM.

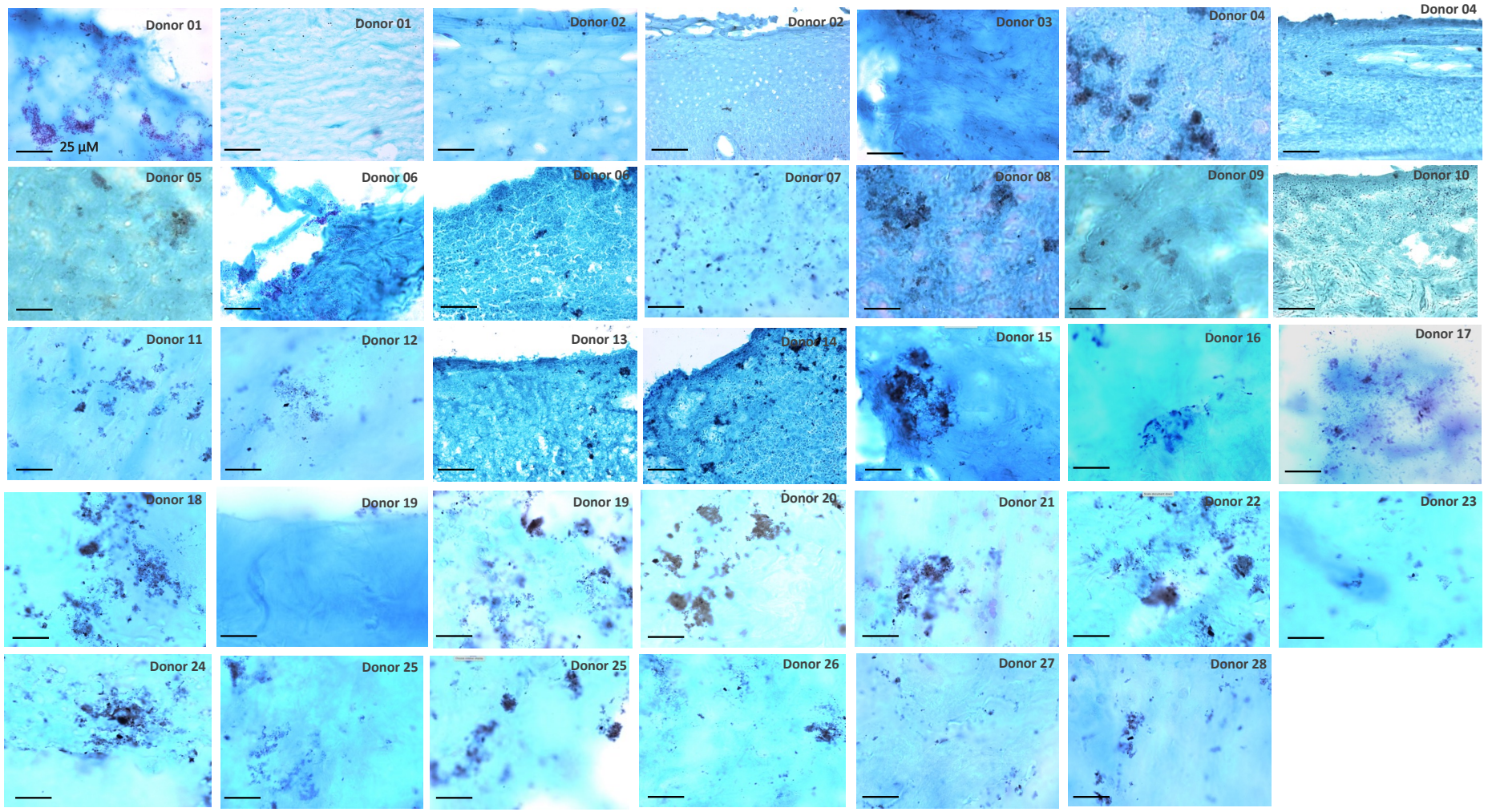

Figure 4.16: Representative microscopic appearance of bacterial load in tissue collected from donors presenting a non-healing wound. Each image represents an individual wound. OCT embedded wound tissue subject to Gram-Twort staining, x1000 total magnification, *[*n=34, n=28 unique (total) donors*]*. Bar = 25 µM.

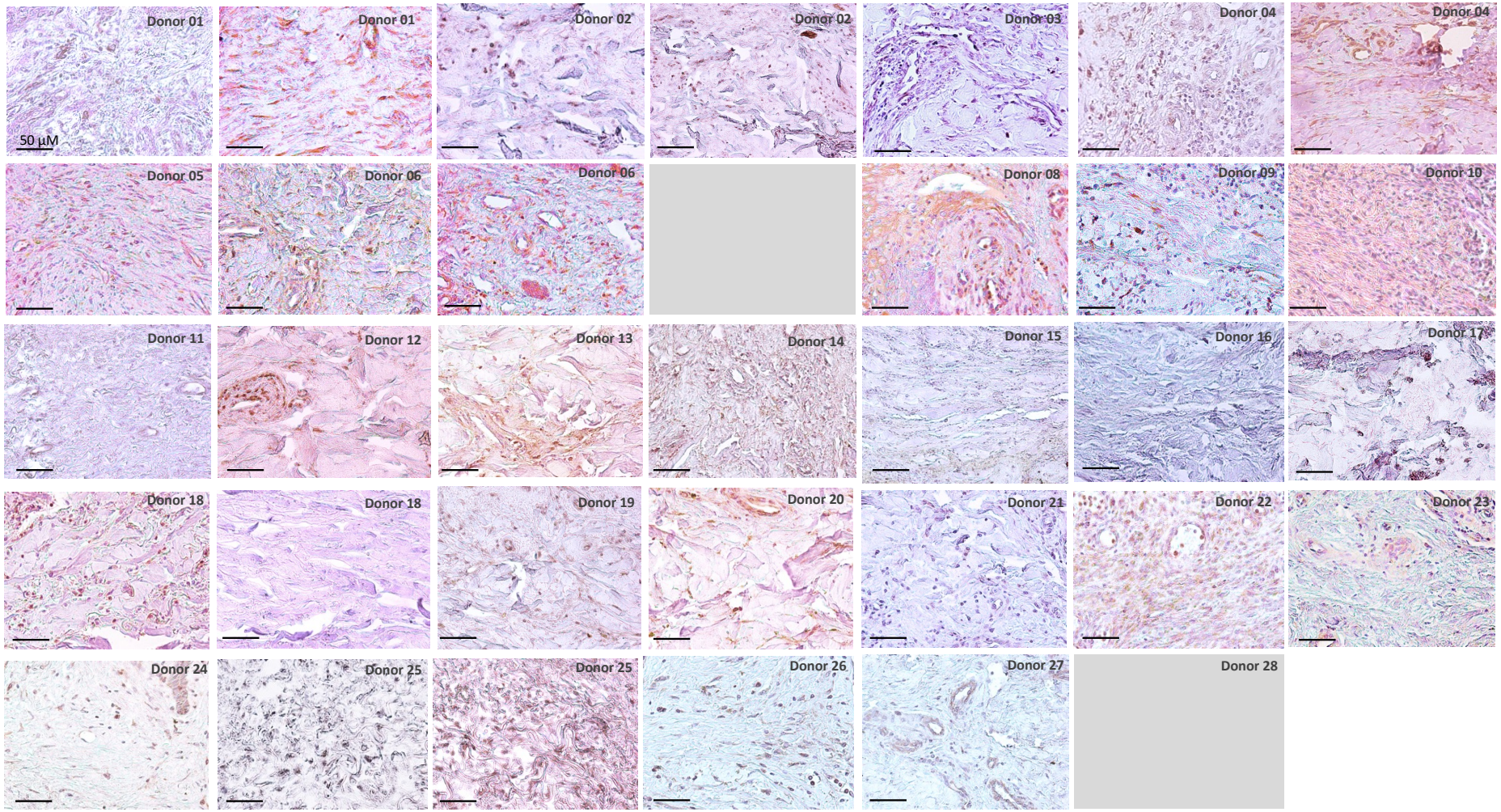

Figure 4.17 Representative microscopic appearance of neutrophil elastase staining in FFPE tissue collected from donors presenting with lower-extremity non-healing wounds. Each image represents an individual donor peri-wound, images captured from tissue region 2, x200 total magnification, *[n=32, n=28 unique (total) donors]*. Bar = 50 µM.

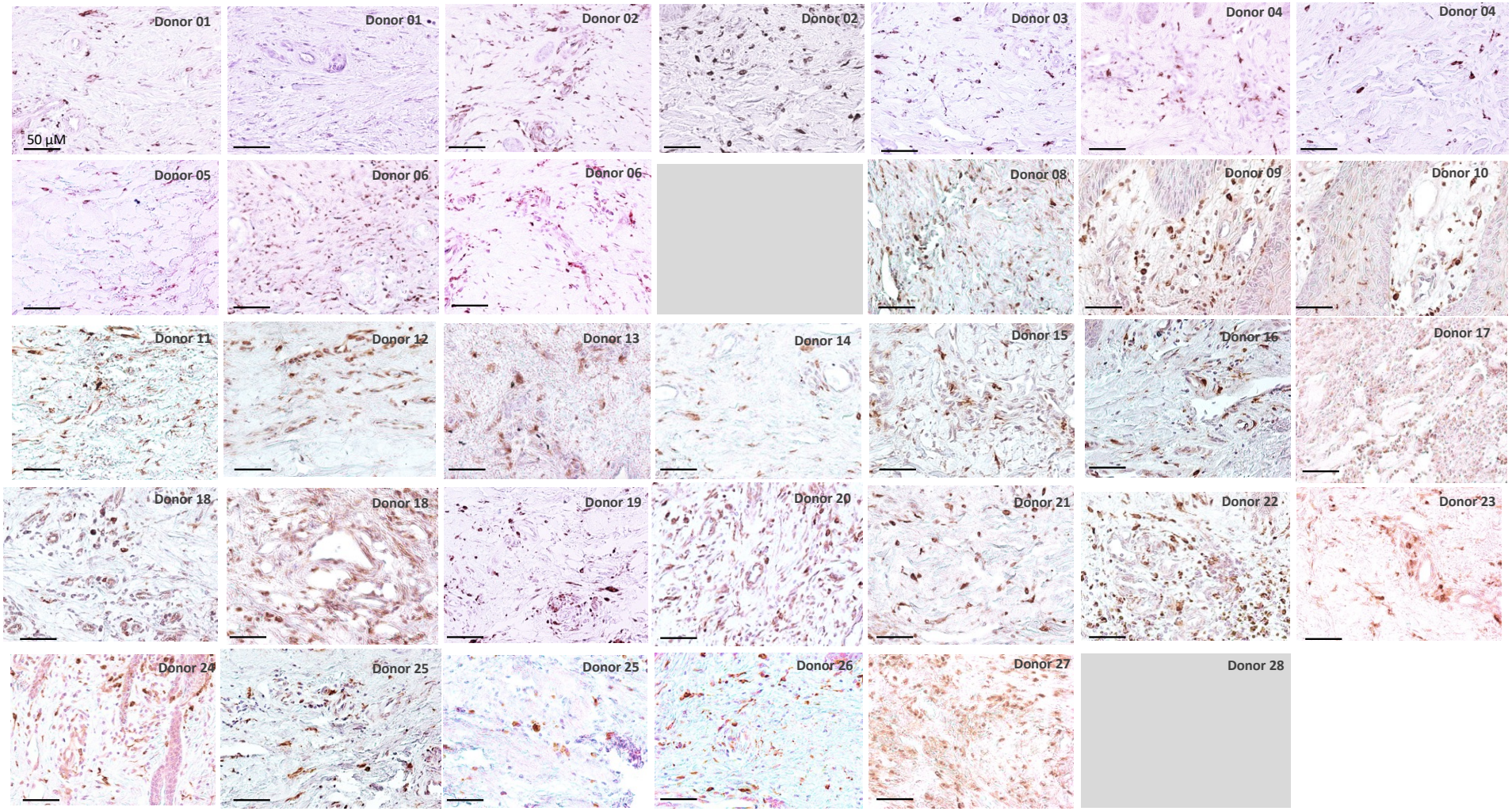

Figure 4.18 Representative microscopic appearance of CD68 staining in FFPE tissue collected from lower-extremity wound donors. Each image represents an individual donor peri-wound, images captured from tissue region 2, x200 total magnification, *[n=32,* n=28 unique (total) donors*]*. Bar = 50 µM.

4.3.11 Combining microbial profiles, gene expression signatures and clinical data reveals a selection of informative correlations.

The microbial profiles of individual peri-wound samples were compared to gene expression profiles, histological features and participant clinical characteristics, including age, wound duration, infection status and blood profiles. Principal component and correlation analysis were implemented to identify correlations within the complex biological and clinical datasets (Figure 4.19). For complex datasets, as within the current study, principal component analysis (PCA) biplots are extremely useful for identifying patterns within data (Jolliffe et al., 2016). The angles between vectors represent correlation strength (Jolliffe et al., 2016), while the length of the line represents the variance of the variable and overall contribution. Typically, a smaller angle between two selected vectors represents a positive correlation. Whilst vectors that diverge to form a larger angle (nearing 180°) are negatively correlated (Akoglu, 2018). If vectors meet each other at 90°, they share no identifiable correlation.

A correlation heatmap, determined using Spearman's rank-order correlation coefficient allows the visualisation of correlation strength between the described variables (Figure 4.20; Mukaka et al., 2012). The relationship (correlation) between the two variables is denoted by the letter r and quantified with a number, which varies between −1 and +1 (Akoglu, 2018). Zero means there is no correlation, whereas a value of 1 indicates perfect correlation. The relationship between two variables is generally considered strong when the r value is >0.4; correlations between 0.2 and 0.4 are moderate, and those below 0.2 are considered weak (Mukaka et al., 2012).

Correlation analysis of the datasets contained within this study highlighted a large number of interesting biological findings. The remainder of this chapter focuses on a selection of key correlations deemed to be of biological and clinical relevance, including factors related to diabetes, hyperglycaemia, and infection (Figure 4.21-26). For example, the average age of donors undergoing a lower-extremity amputation was significantly higher in non-diabetic participants (88.7 years old), reduced to only 63.2 years old in the diabetic population. (p =

0.0014, unpaired t-test). In addition, a number of blood markers were found to be associated with the presence of specific bacterial strains and host defence genes (top right quadrant of PCA biplot; Figure 4.19). Specific observations include: blood creatinine inversely correlated with *NOD2* expression (*p = 0.0061, r = -0.46)*. Haemoglobin levels negatively associated with the presence of infection (*p = 0.001, r = -0.532*). White blood cells and neutrophils were negatively associated with the presence of *Corynebacterium striatum* (*r = -0.59, r = -0.64)*. Interestingly, local and systemic immune markers showed only weak correlation, CD68 cellular positivity and blood white cell count (*r = 0.13*), and tissue neutrophil elastase and blood neutrophil count (*r = 0.17*). Systemic creatinine and urea were negatively correlated with *NOD2* expression (*r = -0.51, r = -0.42*), and weakly correlated with the presence of *S. aureus* (*r = 0.221, r = 0.307*), *P. mirabillis* (*r = 0.187, r = -0.185*) and *E. coli* (*r = 0.218, r = 0.105*). The relative abundance of *E. coli* was also negatively associated with *CLEC7A* and *MYD88* expression (*r = -0.34, r = -0.33*).

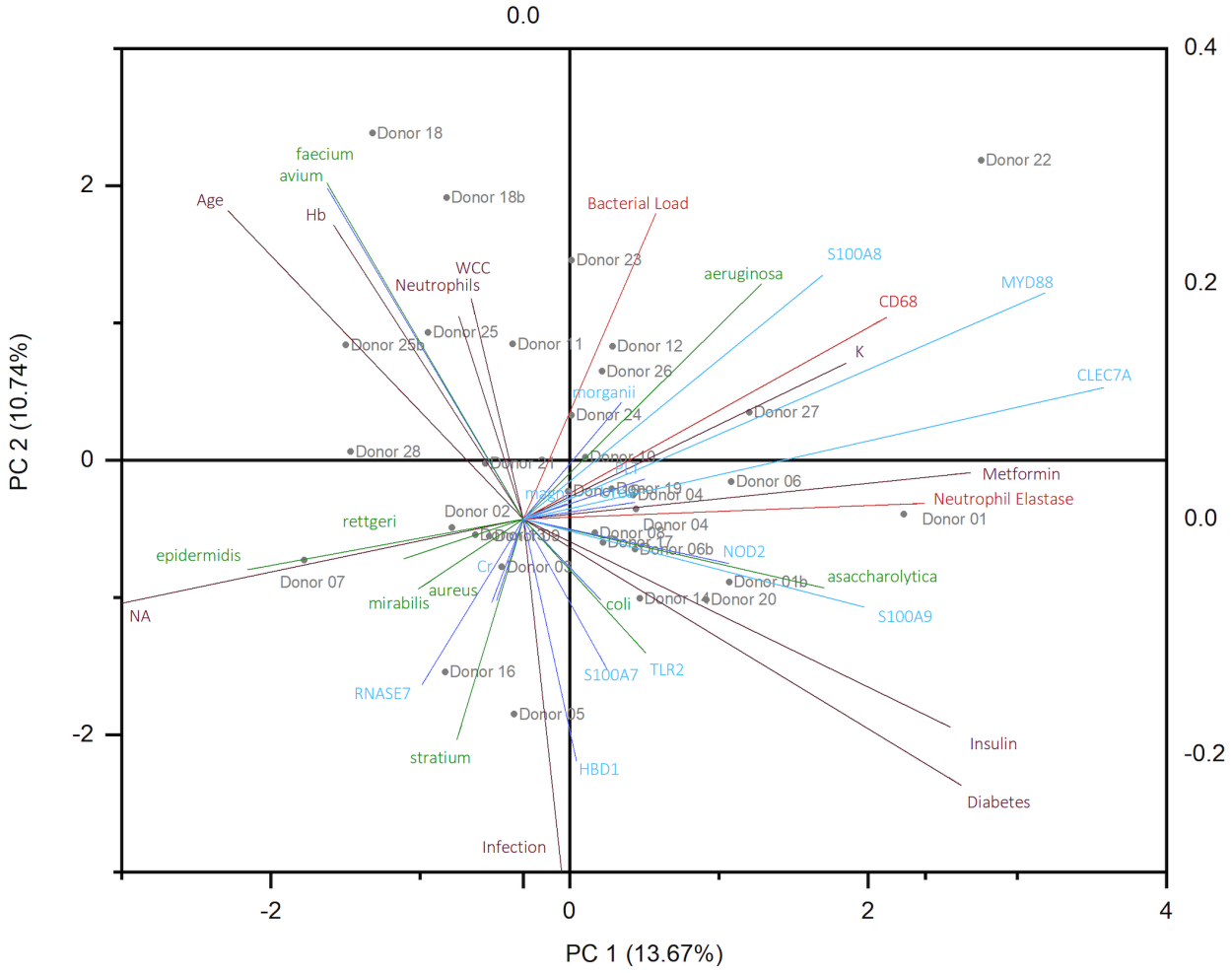

Figure 4.19: PCA biplot across participant samples. Variables investigated include microbial profiles (green), gene expression signatures (light blue), clinical data (purple) and tissue immune cell profiles (red). Samples clustered based on profile similarity. Eigenvalues of the correlation matrix symbolised as vectors representing the traits measured in the study. PC1 = 13.67%, PC2 = 10.74%, [*n=34, n=28 unique (total) donors, all available patient data*]

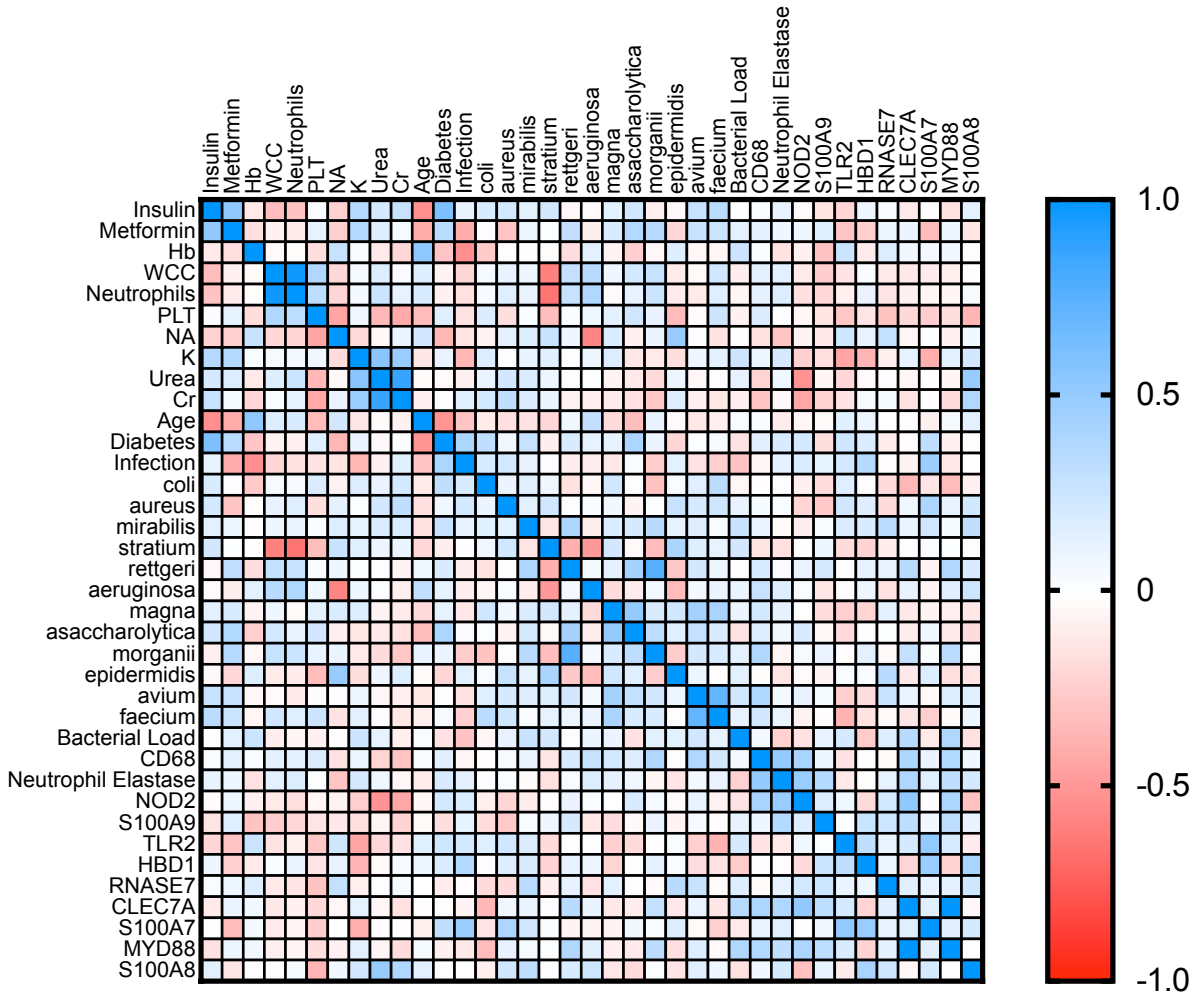

Figure 4.20: Correlation heatmap for participant variables investigated across the study. Heatmap visualising the correlation strength of participant data across all donors, according to Spearman's rank correlation coefficient (rs). Positive correlations are shown in blue, negative correlations are shown in red. [*n=34, n=28 unique (total) donors, all available patient data*].

4.3.12 Wound bacterial load is associated with relative abundance of *Pseudomonas aeruginosa* and impaired cutaneous healing.

PCA biplot analysis of patient microbiology and histological investigation revealed a correlation between the wound tissue bacterial load, identified using modified Gram-Twort staining, and the relative abundance of *P. aeruginosa* in participant microbial profiles (*r = 0.33, p = 0.02*) (Figure 4.21).

To understand the influence of bacterial load in cutaneous wound healing, complementary studies were undertaken (Figure 4.21: C/D). The effect of bacteria and increased bacterial load on mammalian cell viability was investigated using a human keratinocyte cell line model. HaCaT cells were treated with 5% supernatant (v/v) from planktonic *P. aeruginosa* cultures at a density of either 10^3, 10^5 or 10^7 CFU/mL. At 48 hours post-treatment, a significant reduction in cell viability was identified in cultures treated with high-density (10^5/10^7 CFU/mL) supernatant (*p = 0.025, p = 0.025, two-way ANOVA*). This effect was reduced in cells treated with supernatant from lower-density *P. aeruginosa* cultures (10^3), with no significant reduction in HaCaT cell viability observed at this concentration (*p > 0.5, two-way ANOVA*).

In a direct assessment of cutaneous healing in human *ex-vivo* wounds (Wilkinson et al., 2021), a previously validated pre-clinical model of wound repair was treated with supernatant from a planktonic *P. aeruginosa* culture. Following 48-hours of treatment, total *ex-vivo* closure was reduced from an average of 100% (total closure), to 58% percentage closure following treatment planktonic *P. aeruginosa* culture product (*p < 0.01, paired t-test*). Together, this data reinforces the important detrimental effects of pathogenic bacterial species on human wound healing.

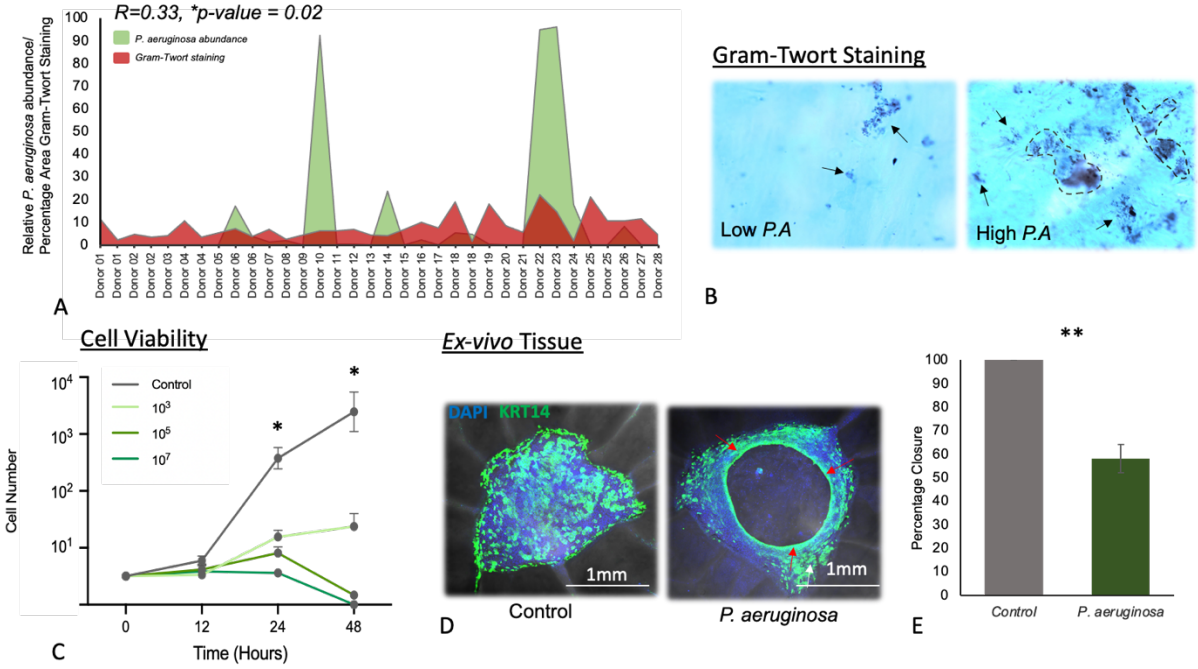

Figure 4.21: Correlation between wound tissue bacterial load, *P. aeruginosa,* and human cutaneous healing. (A) Area plots representing percentage positive Gram-twort tissue staining and relative *P. aeruginosa* abundance across participant *[n=34]* wound samples. Representative photomicrographs (x1000 total magnification) of patient-derived samples from the low and high relative *P. aeruginosa* abundance groups, modified Gram-Twort stain illustrating the presence of both large aggregates (dashed lines) and as individual bacteria (arrows) within the tissue (B). HaCaT cell viability following treatment of cells with 5% supernatant from planktonic *P. aeruginosa* cultures at 10^3, 10^5 and 10^7 CFU/mL. *Two-way ANOVA.* Representative photomicrographs (x25 total magnification) (D) and quantification (E) of human *ex-vivo* healing in wound models following treatment with supernatant from planktonic *P. aeruginosa* cultures. Measurements were collected 48 hours post-wounding [*n=3*]. *Paired t-test. *p < 0.05, **p < 0.01, ***p < 0.001. Bar =1mm.*

4.3.13 Patient infection status correlates with unique host defence, histological and blood marker signatures.

The presence of infection and elevated tissue microbial bioburden is considered a major driver of impaired healing and wound chronicity (Wilkinson and Hardman, 2020). Clinically, it is accepted that acute or chronic wound infection exists when the microbial load is $>10^5$ CFU/gram of viable tissue (Bowler et al., 2001). The current study contains donors with both clinically defined infected and non-infected wounds, affording the opportunity to assess wound bacterial load and compare host defence profiles between these two clinical subsets. Initially, we investigated the correlation of tissue bacterial load, as determined by Gram-twort staining, with the diagnosis of positive clinical infection. Surprisingly, wound tissue bacterial load, as determined by positive Gram-twort staining, was elevated in the non-infected group (Infected: 6.45% vs non-infected: 10.10%, *p = 0.05, unpaired t-test*).

Multiple methods of bacterial detection, including tissue bacterial load, assessment of colony forming units and microbial read sequencing number were directly compared across patient samples, again revealing minimal correlation (Figure 4.22: C). Interestingly, whilst tissue bacterial load was consistent across two wound sites within a single donor (donor 25), bacterial enumeration (CFU values) were very different between the two wound sites. In contrast, donor 26 demonstrated the highest CFU count and tissue bacterial load (Gram-Twort Staining) across the three donors, yet also presented the lowest sequencing read count.

In parallel with tissue bacterial load, the level of blood neutrophils and white cells was also higher in the non-infected group (Figure 4.22: G/H). The average blood white cell count was $10.1x10^3$ cells per µL in the non-infected group and $6.4x10^3$ cells per µL in the infected group. Non-infected wound donors also exhibited a blood neutrophil count of 10.6 ($x10^3$ cells per µL), compared to those with a diagnosed infection, presenting a measurement of only 8.71 ($x10^3$ cells per µL). Interestingly, participant blood white cell and neutrophil levels show very little correlation with the presence of tissue CD68+ cells (*r = 0.109, p > 0.05*) and the presence of neutrophil elastase (*r = 0.174, p > 0.05*). In relation to gene expression profiles, *HBD1*, the gene that encodes human beta-defensin 1 was significantly higher in the infected group,

presenting a 2.3-fold increase in expression (*unpaired t-test, p = 0.03*) (Figure 4.22: E/F). S100A7 was also higher in the infected group, however, this was influenced heavily by a small selection of donors (*unpaired t-test, p > 0.05*)

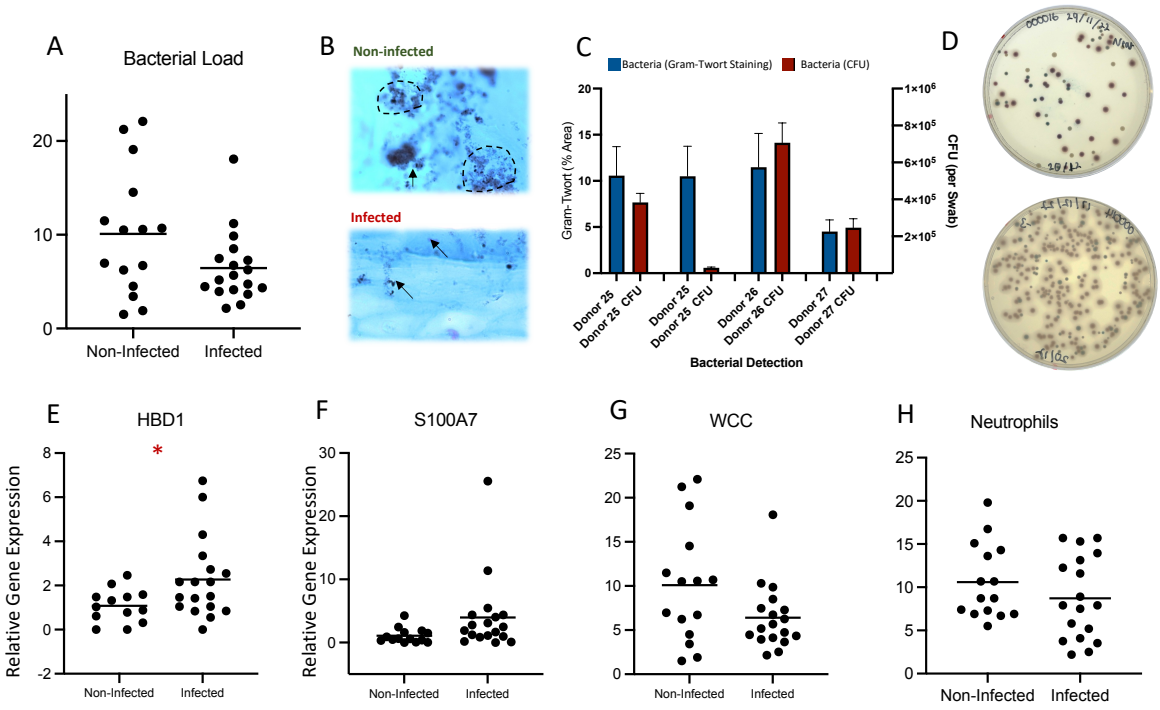

Figure 4.22: Correlation between participant infection status, tissue bacterial load and host defence response. Percentage area positivity (A) and representative microphotograph images (B) (x100 oil) of Gram-Twort staining in the clinically defined infected and non-infected wound donor tissue *[n=34]*. Direct comparison of tissue bacterial load according to CFU tissue swabs and Gram-twort percentage area positivity across four participant wound samples *[n=4]*. Representative agar images of bacterial load images as determined by swab CFU values (D). The relative gene expression of *HBD1* (E) and *S100A7* (F) **according to qPCR quantification** in the tissue of both clinically infected [18] and non-infected [13] participants. Blood marker values: white cell count (G) and neutrophil count (H) in both clinically infected *[n=18]* and non-infected *[n=13]* participants. Each dot represents a single donor. **p < 0.05.*

4.3.14 Patient diabetic status is associated with increased expression of host defence genes and impaired tissue repair.

PCA biplot correlation analysis revealed an assortment of factors with a strong association to participant diabetic status (Figure 4.19). These host factors also correlated with previous findings that positive diabetic status is associated with a pathogenic shift in colonising species of the wound environment (Figure 3.19). It is well established that diabetes is a key risk factor in chronic wound formation (Wilkinson and Hardman, 2020), due to complex underlying pathophysiology, involving vascular, neuropathic, immune, and biochemical components (Grice et al., 2012). Therefore, we aimed to explore microbial and host defence factor interactions that occur in the diabetic wound environment and may contribute toward the delayed healing phenotype.

To confirm the biological importance of the diabetic host defence response, the impairment of wound healing in the presence of diabetes was demonstrated. Scratch closure analysis in HDFs isolated from the tissue of both non-diabetic and diabetic donors revealed a significant reduction in scratch closure (79% vs 62%) in the diabetic group (*p = 0.001, unpaired t-test*) (Figure 4.23: A). Additionally, *ex-vivo* wounding on the skin of both diabetic and non-diabetic donors revealed a significant difference in repair capabilities. Following generation of a partial thickness wound, overall wound repair and closure following 48 hours of incubation was reduced from 78% in the non-diabetic population to 32% in the diabetic population (*p = 0.0042, unpaired t-test*) (Figure 4.23: C).

In parallel with impaired healing, positive patient diabetic status was associated with the increased expression of *TLR2*, *NOD2*, *S100A7* and *S100A9* genes (Figure 4.23: E, F, G, H). Relative to the non-diabetic population, the expression of TLR2 demonstrated a significant 2.5-fold increase in diabetic tissue (*p = 0.02, unpaired t-test*). The remaining host defence genes also demonstrated a relative increase, e.g., 22% in NOD2 expression (*p > 0.05, unpaired t-test*).

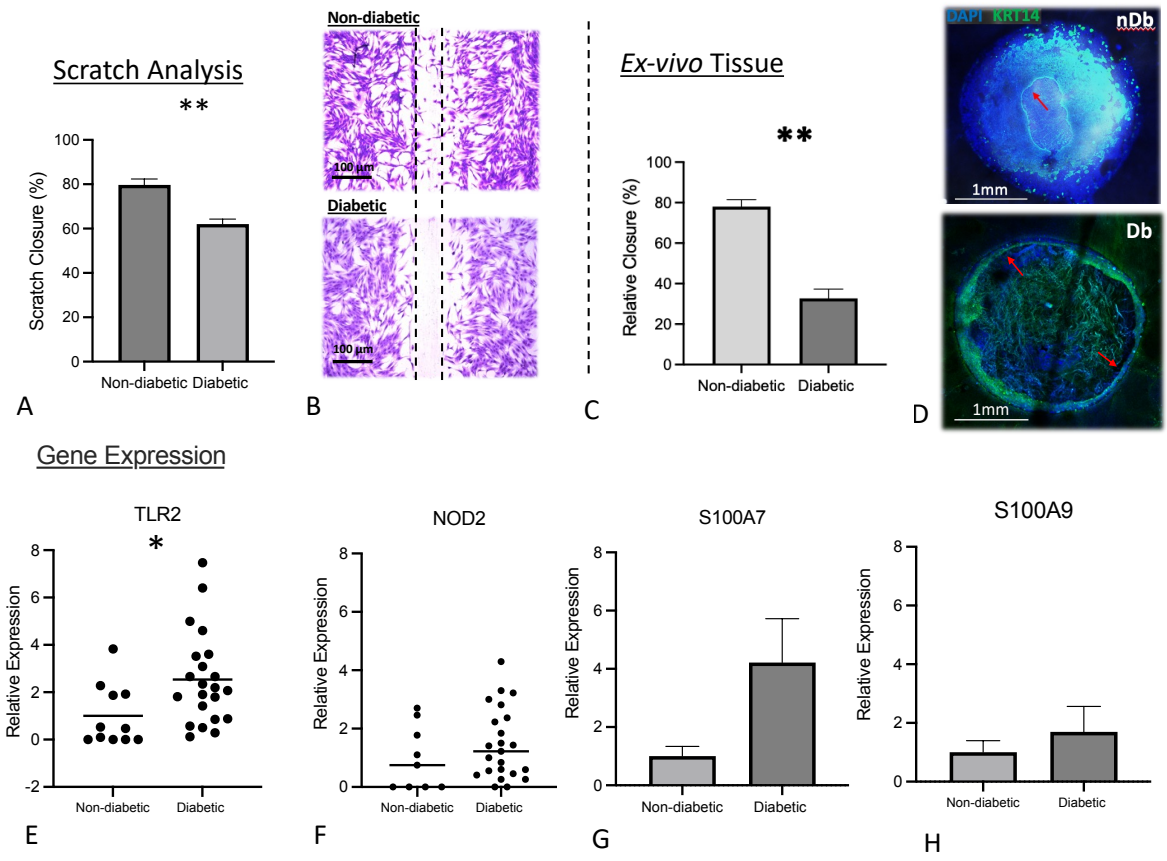

Figure 4.23: Impaired healing and unique host defence gene expression in diabetic tissue donors. Percentage scratch assay closure (A) and representative photomicrographs (B) (x40 total magnification) of both diabetic and non-diabetic primary human dermal fibroblasts *[n=1]*, measurements acquired 24 hours post incubation. Bar = 100 µM Quantification of total healing (F) and representative photomicrographs (x25 total magnification) (G) of human *ex-vivo* wound models in both diabetic and non-diabetic human tissue donors *[n=3]*. The relative expression of TLR2 (E), NOD2 (F), S100A7 (G) and S100A9 (H) in the tissue of both diabetic and non-diabetic participants (*data are derived from QPCR)*, *[Db n=21, nDb=11]*. Each dot represents a single donor *[Db n=21, nDb=11]*. *$p < 0.05$, **$p < 0.01$, ***$p < 0.001$. Bar = 1mm.

.

4.3.15 The inter-genus shifts in *Staphylococcus* species abundance are capable of significantly impairing cutaneous healing.

Through the current study, a reoccurring theme has been the shift in species contribution within the genus *Staphylococcus* from *S. epidermidis* dominance in the non-diabetic population, to the elevated presence of *S. aureus* in the diabetic population (Figure 3.10). Negative diabetic status was also associated with the presence of *S. epidermidis* in the wound bed (Figure 3.19). Therefore, this shift in species, contained within a single bacterial genus, was investigated for potential influence on both mammalian cell viability/scratch closure and overall *ex-vivo* cutaneous healing (Figure 4.24).

Two individual mammalian cell populations including human dermal fibroblasts and HaCaTs were utilised *in-vitro* to assess the impact of these bacterial species on cellular viability, proliferation, and scratch closure. Investigating cell viability, each population was initially assessed following a 12-, 24- and 48-hour incubation with supernatant from either *S. epidermidis* or *S. aureus*. In response, a total reduction in viable cells in both mammalian cell populations was observed following incubation with *S. aureus* product (*Two-way ANOVA, $p < 0.001$*), over the course of 48 hours (Figure 4.24: A, B). In contrast, incubation of cell cultures with commensal supernatant from *S. epidermidis* resulted in only a minimal non-significant decrease of 18% (HDF) and 16% (HaCaT) in mammalian cell number (T*wo-way ANOVA, $p > 0.05$*). This trend was further replicated when assessing mobility, where cellular scratch closure was not detrimentally influenced by the presence of *S. epidermidis* supernatant (Figure 4.24*:* C, D). In response to incubation with *S. aureus* supernatant, however, scratch closure in HDFs and HaCaTs was significantly inhibited, reducing overall closure from 72% to 24% in HDFs and from 70% to 26% in HaCaTs (*$p = 0.003$ and 0.0031, One-way ANOVA, $p < 0.003$*) (Figure 4.24: C, D).

Next, the influence of bacterial supernatant from these species was tested in a pre-validated pre-clinical *ex-vivo* human skin wound model. In parallel with the *in-vitro* studies, the presence of *S. epidermidis* supernatant on *ex-vivo* wounds had no influence on overall closure, with both groups achieving full closure at 48 hours (Figure 4.24: F, G). In contrast, the

presence of *S. aureus* significantly inhibited cutaneous healing, reducing *ex-vivo* wound closure from an average of 86% to 16.6% (*paired t-test, p < 0.002*). Throughout, strong reductions in cell and tissue proliferation, viability, and scratch closure were observed following exposure to *S. aureus* products, but not the following incubation with *S. epidermidis* product, signifying the importance of this shift on clinical wound repair.

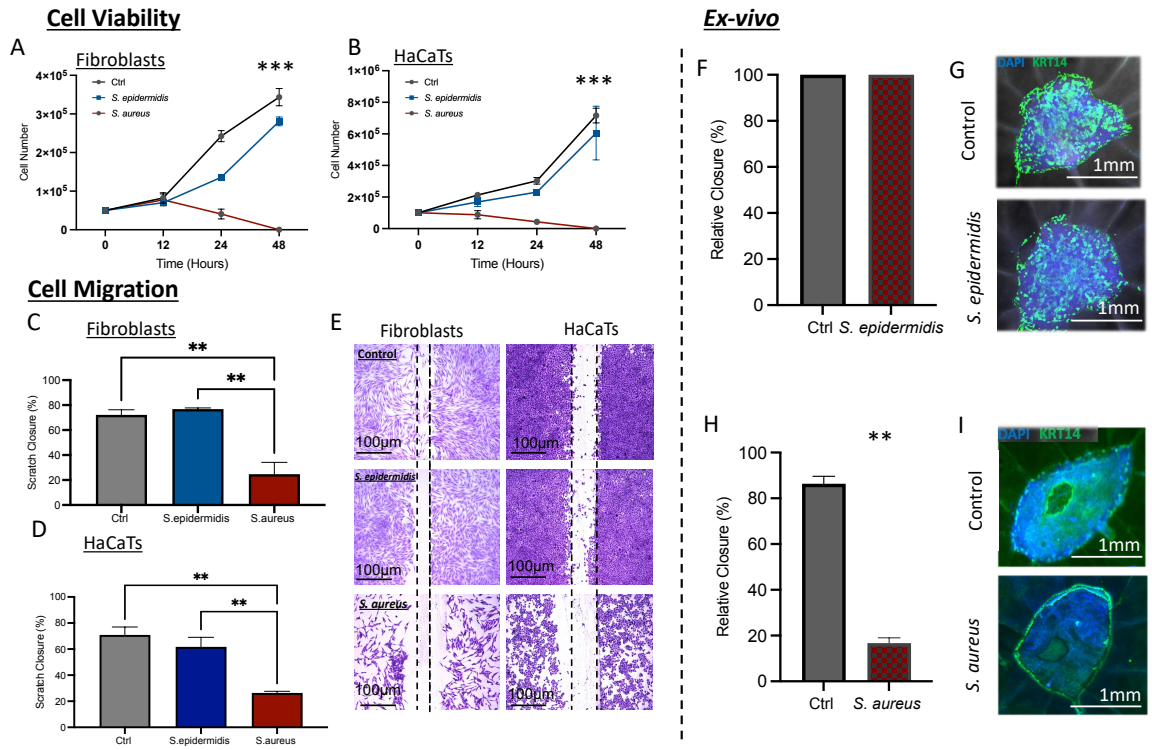

Figure 4.24: The influence of *Staphylococcal* species on mammalian cell viability, proliferation and tissue repair. The average cell number (A, B) and scratch closure assays (C, D) closure of both HDFs and HaCaTs following incubation with bacterial supernatant from both *S. epidermidis* and *S. aureus [n=3]*. Representative photomicrographs of *in-vitro* scratch closure assays (E) (x40 total magnification). *Bar = 100 µM.* Measurements collected following 24 hours of treatment incubation *[n=3]*. Quantification of *ex-vivo* human skin wound healing and representative photomicrographs (x25 total magnification) (G) following incubation with supernatant from both *S. epidermidis* (F, G) and *S. aureus* (H, I). *Ex-vivo* measurements collected following 48 treatment incubation. *[n=3]. *p < 0.05, **p < 0.01, ***p < 0.001. Bar = 1mm.*

4.3.16 Limited correlation of host factors with participant glycaemic status.

In the previous chapter, participant hyperglycaemic status was associated with the increased relative abundance of certain bacterial species, including *Peptoniphilus harei and Prevotellla intermedia*. As long-term glycaemic control and overall diabetes management acts as important prognostic indicators, we investigated this factor further in host data (Campbell et al., 2019).

Limited deviation in relative host defence gene expression was observed in participants according to glycaemic control. A non-significant 8-fold decrease in relative *S100A8* gene expression was observed in control participants compared to the hyperglycaemic group (*p = 0.05, unpaired t-test)*. Across the remaining host defence genes (*HBD1* and *RNASE7*), changes in relative gene expression were also minimal between the hyperglycaemic group compared to the control group (*p > 0.05, unpaired t-test*) (Figure 4.25: B, C).

In the peri-wound margin, mean wound tissue bacterial load (Gram-Twort staining) was marginally elevated in the hyperglycaemic wound tissue (*p > 0.05, unpaired t-test)* (Figure 4.25: D). This trend was further replicated in relation to CD68 positive cells, in which a mean increase from 18.01 to 19.65 cells per mm^2 was observed (*p > 0.05, unpaired t-test*). In contrast, the presence of neutrophil elastase was marginally decreased in the hyperglycaemic group, declining from 10.4% tissue area positivity to 9.45%. Overall, limited clinical and host factors specifically correlated with the subset of donors presenting hyperglycaemia.

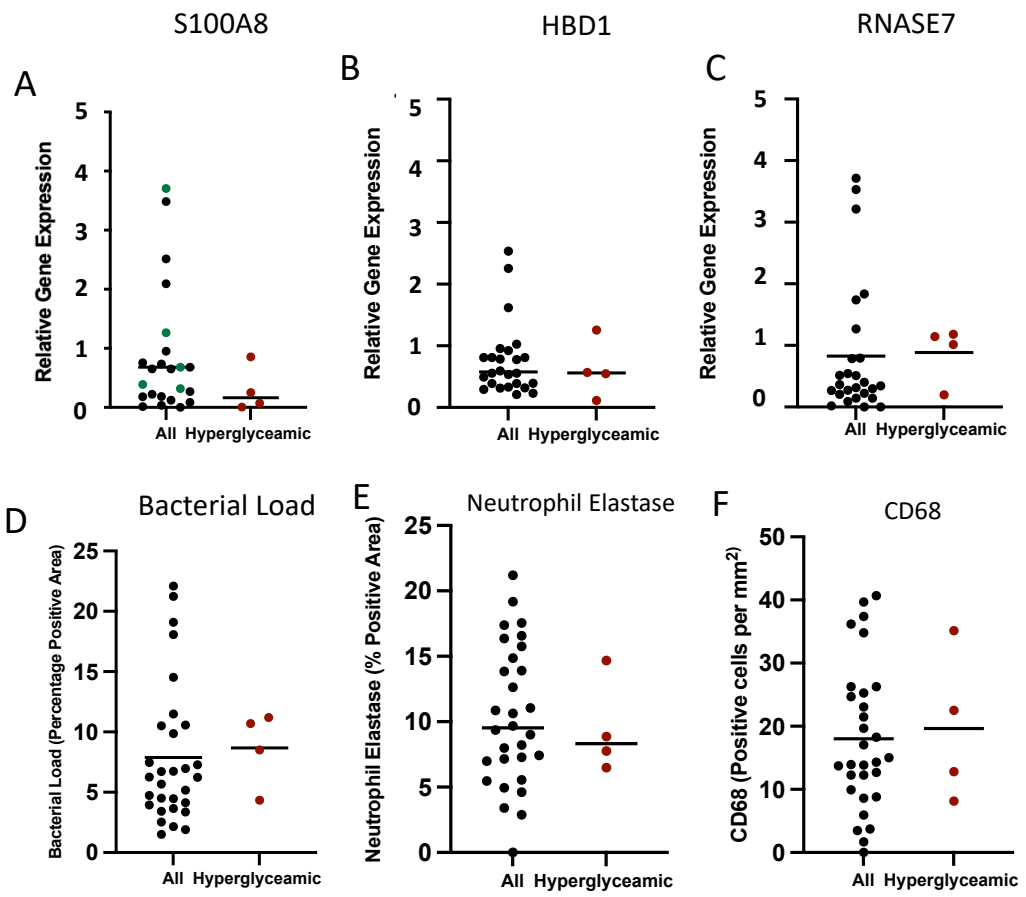

Figure 4.25: Host defence gene expression and tissue profiling of hyperglycaemic donors. Relative gene expression, according to qPCR, of *S100A8* (A), *HBD1* (B) and *RNASE7* (C) in the peri-wound tissue of both hyperglycaemic and control donors *[All n=28, Hyperglycaemic n=4]*. Histological analysis of wound bacterial load, as defined by Gram-Twort percentage area positivity (D), neutrophil elastase percentage area positivity (E) and CD68 positive cells per mm^2 (F).

4.3.17 Strong correlation between tissue immune cells and host defence gene expression.

In a selection of clinical wound samples that had been profiled using a novel species-level taxonomic identification approach, a dominant trend related to the correlation of tissue immune cells with host defence gene expression (Figure 4.19). This trend is particularly evident on the top right-hand side of the PCoA biplot (Figure 4.19), with strong correlations highlighted between tissue immune cells and genes such as *NOD2, CLEC7A, MYD88* and *S100A9*. The positive correlation between AMP expression and host innate immune cells such as monocytes, macrophages, and neutrophils has been described previously, as AMPs induce a variety of responses, including immune cell recruitment (Lai and Gallo, 2009).

Further investigation revealed that the presence of tissue neutrophil elastase was significantly correlated with three specific host defence genes including *NOD2* ($p = 0.024$), *CLEC7A* ($p = 0.0015$) and *S100A9* ($p = 0.004$, simple linear regression analysis) (Figure 4.26: A, B, C). The strongest trend was witnessed between neutrophil elastase levels and *S100A9* gene expression ($r = 0.73$), whilst weaker trends were identified in relation to the expression of *NOD2* ($r = 0.69$) and *CLEC7A* ($r = 0.69$) (Figure 4.26: A, B, C). In parallel, relative *NOD2* expression was also correlated with host tissue CD68 cell positivity ($r = 0.3$), however, this was non-significant ($p = 0.08$). Notably, *MYD88* was significantly associated with the level of tissue CD68 cell positivity ($p = 0.01$), ($r = 0.44$).

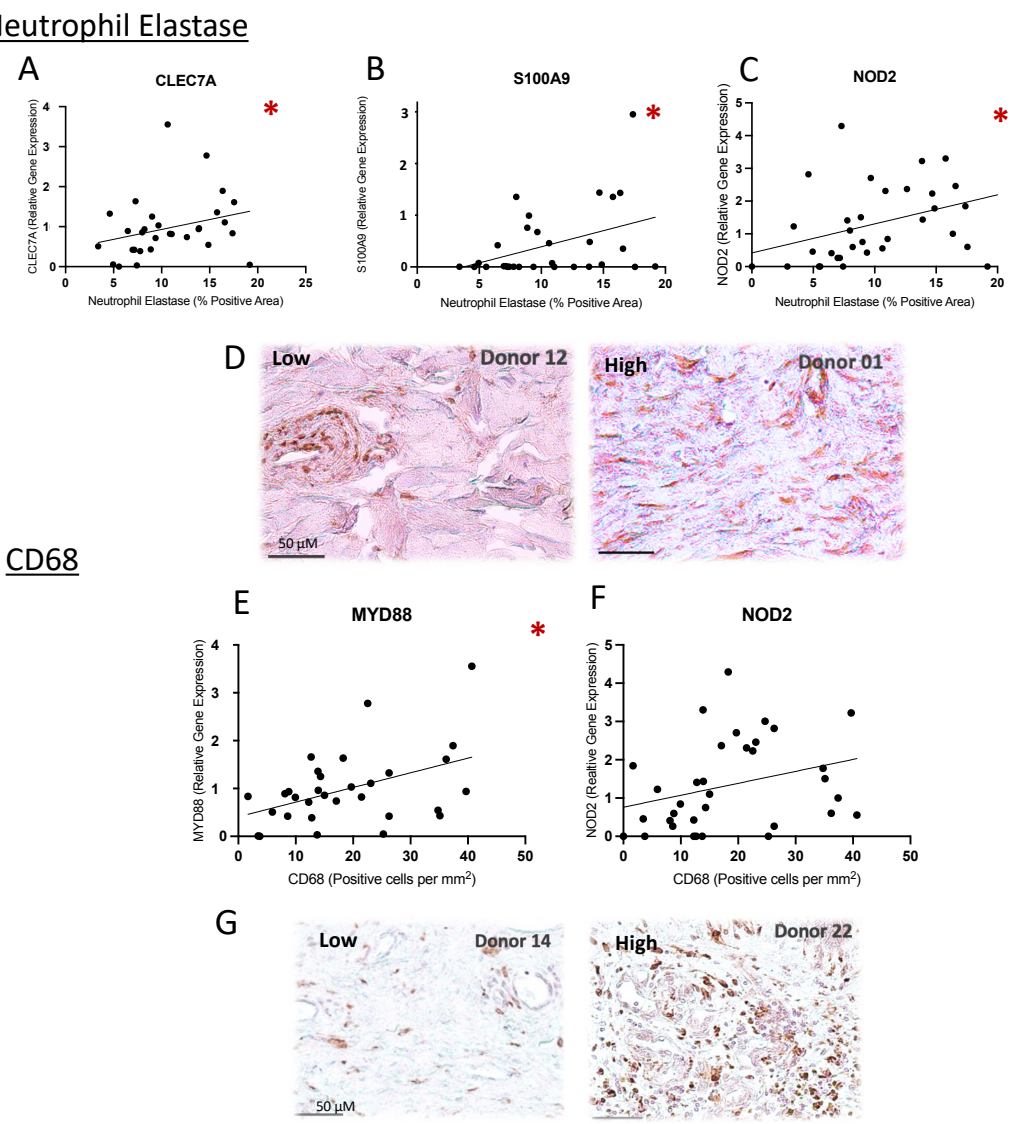

Figure 4.26: Correlation between the presence of tissue immune cells and host defence gene expression in the peri-wound tissue of active wound donors. The number of CD68 positive cells per mm^2 in wound margin tissue in correlation with relative *CLEC7A* (A), *S100A9* (B) and *NOD2* (C) expression. Quantification of percentage area positivity of neutrophil elastase staining on the peri-wound tissue of active wound donors in relation to relative *MYD88* (E) and *NOD2* (F) expression. Representative microphotographs of example low and high (D) neutrophil elastase and CD68 (G) in the peri-wound tissue of wound donors according to immunohistochemical staining distribution *[n=32]*. Each dot represents a single donor. Simple linear regression analysis. Black line represents linear regression trend line. Red asterisks represent significance. **p < 0.05, **p < 0.01, ***p < 0.001. Bar = 50* µM.

4.4 Discussion

Non-healing wounds, including diabetic foot ulcers, represent a momentous healthcare problem (Guest et al, 2020; Wilkinson and Hardman, 2020). The skin microbiota is known to be intimately coupled with cutaneous health, with the host repair system and wound microbiota interacting to promote barrier restoration (Byrd et al., 2019). In chronic wounds, however, the host-wound microbiome dialogue becomes dysregulated, contributing to inflammatory stage arrest (Trøstrup et al., 2020). In this novel study, species-level taxonomic sequencing data was combined with clinical, histological and deep transcriptome profiling to gain previously unprecedented insight into the complex host-microbe interactions within the wound environment.

The purpose of this study was to gain deep insight into drivers of chronicity and functional elements of the host wound response. The first step of this involved conducting RNA-seq transcriptional profiling on both peri-wound and upper leg skin from a selection of diabetic donors. Between these sampling locations, major differences were identified in key wound healing-associated pathways, including host defence genes that were related to bacterial signatures. We identified that TLRs were generally downregulated in proximity to the wound, whilst human defensins, *NOD2, CLEC7A* and the *S100* genes were significantly upregulated at the wound edge. Unfortunately, with limited donor numbers (*n = 8*), we struggled to identify strong correlations with microbial profiles.

Instead, we selected a panel of host defence markers, including *TLR2, NOD2, CLEC7A, RNAse7, MYD88, HBD-1 and S100A7, S100A8 and S100A9* for characterisation across multiple sites, including the wound margin, upper leg pathological skin and healthy donor skin controls. This data was then combined with bacterial signatures, histological markers, tissue immune cell presence and overall tissue structure. In comparison to the healthy skin donors, *NOD2, RNASE7 and CLEC7A*, were upregulated in those donors presenting with an active wound, specifically in the wound margin. This expression profile was related to the enrichment of

commensal *Staphylococcus* species in healthy skin, in contrast to the high contribution of pathogenic species in the skin of active wound donors. These findings are consistent with previous literature, such as Sabaté Brescó et al., 2017, who reported that *S. epidermidis* seems to trigger lower levels of the innate pro-inflammatory response in comparison to pathogenic species, such as *S. aureus*. Overall host defence expression profiles in the wound edge related strongly to bacterial load and the presence of wound edge neutrophils and macrophages. Diabetes and infection were associated with elevated *HBD1* and *TLR2* expression, potentially related to their microbial profiles, such as the increased presence of *Anaerococcus mediterraneensis and Clostridium difficile.* In correlation to previous literature, Hevari et al., 2020 identified that in the diabetic wound environment, *Anaerococcus mediterraneensis* is one of the most transcriptionally active pathogens and is known to rapidly induce the innate immune response (Grice and Segre, 2011).

Following the global transcriptional profiling (RNA-seq) of the original eight diabetic donors, numerous identified genes were associated with proximity to the wound bed. A selection of individual host defence-related genes displayed elevated expression, exclusive to the healthy skin environment. From this collection, TLRs accounted for a major number of genes comprising the signature. TLRs are essential in the innate immune response, demonstrating a strong capacity to respond to environmental microbial signals (El-Zayat et al., 2019). Despite the absence of studies focusing on TLRs in keratinocytes, these receptors are considered keystone modulators of wound epithelialisation (Munir et al., 2020). Within the current study, TLR1, 3,4,5 and 6 were notably downregulated in the peri-wound skin, compared to that of the intact upper leg diabetic tissue. Whilst previous studies comparing TLR expression in clinical DFU skin and wound specimens' samples are limited, Dasu et al., 2014 reported a significant increase of TLR expression in the wounds of diabetic patients compared with non-diabetic participants (Dasu et al., 2014). However, previous studies have failed to compare PRR/TLR expression to bacterial signatures as conducted in this study, as for example, the wound edge skin typically contained higher levels of pathogenic bacteria, which is known to strongly induce TLR signalling (Askarian et al., 2018). Whilst the downregulation of TLRs in the peri-wound tissue may be considered unexpected, one factor to consider in the reduction of TLR signalling expression at the wound edge is that these key peptides, such as TLR4, are

primarily upregulated 6 hours to 3-days post injury (Chen and DiPietro, 2017). In the current study, over half of the wounds had been present over 6 months before surgical intervention and sample collection, therefore limiting the application of these results to previous TLR expression characterisation studies (Dasu et al., 2014).

In the wound environment, it's widely considered that TLRs function as a double-edged sword, requiring tight regulation to allow early immune response, without the induction of prolonged local inflammation (Davis et al., 2020; Mills et al., 2022). Numerous studies have identified how the absence of TLRs (specifically *TLR2, 3, 4, and 9*) delay wound healing via the perturbation of inflammatory cell infiltration and cytokine expression (Davis et al., 2020; Munir et al., 2020). In contrast, other studies report how TLR signalling inhibition may improve healing (Chen and DiPietro, 2017). In agreement with the current study, Dasu et al., 2012 reported that diabetic chronic wound tissue contained higher levels of *TLR1, 2, 4, 6, MyD88, IRAK-1, NF-κB, IL-1β*, and *TNF-α* expression, than the wound tissue of healthy subjects. Across the experiments carried out in this thesis, qPCR validation identified that tissue proximity to the wound bed did not significantly influence TLR expression. Yet, positive diabetic status was significantly associated with elevated *TLR2* expression. While it is not well-known if *TLR2* contributes to the immune dysregulation and uncontrolled inflammation witnessed in diabetes, positive diabetic status was associated with the presence of specific bacterial species, including *Clostridium difficile* and *Anaerococcus mediterraneensis*. These species are known to colonise the wound bed in times of host immune impairment and dysregulated immune response (Heravi et al., 2020), which we can hypothesise may be linked to disrupted TLR signalling.

Parallel to the skin, the wound margin tissue showed strong expression of specific host defence genes. *NOD2* expression was upregulated in the peri-wound tissue compared to that of the intact skin. Previous studies from our research group have demonstrated NOD2 as an important microbial regulator and pattern recognition receptor in skin wound repair (Williams et al., 2018). Williams et al., 2017 reported that *Nod2*-deficient (Nod2-/-) mice had an inherently altered skin microbiome compared with wild-type controls. Furthermore, the study found that a *Nod2*-/- skin microbiome caused impaired healing and microbial

composition shifts, especially an increase in pathogenic wound species (Sidiq et al., 2016). However, limited new progress has been made since the publication of these papers. Whilst the expression of *NOD2* was elevated in the pathological skin/wound margin groups compared to the healthy skin, it appears that a balance of *NOD2* activity is essential for wound repair and keratinocyte function.

S100 genes, *S100A7* (Psoriasin) and *S100A8/A9* (Calprotectin), were found to be elevated specifically in the wound margin of the diabetic and infected groups. *S100A7* and *S100A8/A9* are considered markers of inflammation and infection, with Calprotectin recently being used as a biomarker to detect mild infection in early onset diabetic foot ulcers (Ingram et al., 2018). This calcium-responsive signalling protein is known for characteristic overexpression in inflammatory skin conditions, such as psoriasis, whilst being downregulated in cases of invasive carcinoma, suggesting a key role in keratinocyte function. Additionally, Su et al., 2022 identified that certain S100 genes are able to significantly promote adipose-derived stem cell (ADCS) proliferation and differentiation. In rat models, the treatment of wounds with S100A8-overexpressing ADSCs was shown to significantly improve wound healing and granulation tissue neovascularisation compared to the control group. However, in chronic inflammation, we see the mis-regulation of S100 protein expression and function. In the gut, the presence of species *C. difficile, S. aureus and E. coli* restrict the bioavailability of nutrient metals such as iron, zinc and manganese which in turn alters the function of S100 proteins (Zackular et al., 2016; Murdoch and Skaar, 2022). Whilst the S100 genes have received limited attention in human wound healing, it is important to understand both the beneficial and detrimental role of these peptides, including how members of the wound microbiome may interact to alter their beneficial functions.

Another gene receiving limited attention in human wound healing is *CLEC7A*, encoding the protein Dectin-1. This gene was elevated in the pathological skin and wound margin compared to the skin of healthy donors. In the GI tract, *CLEC7A* proteins function as an essential component of both CD4+ T-cell activation, and the protective immune response to numerous fungal pathogens (Goyal et al., 2018; Mata-Martínez et al., 2022), with Dectin-1 knockout (*CLEC7a*-/-) mice being highly susceptible to fungal infection (Drummond et al.,

2015). As within this study, the fungal composition of healthy donor skin was determined to be vastly different from the collectively similar wound-related samples, this association highlights an interesting correlation. Generally, fungal species are considered silent wound pathogens. Therefore, exploring the role of *CLEC7A* signalling pathways could provide further insight into the host-mycobiome interaction, and the impact of dysregulated pathogenic fungal communities on human skin repair (Goyal et al., 2018; Mata-Martínez et al., 2022).

The majority of published studies exploring host defence peptides in wound healing have investigated only in *in-vitro* cellular or *in-vivo* animal models (Yang et al., 2020, Grönberg et al., 2015 and Wang et al., 2022). Studies that have used human participants have frequently used wound exudate samples (Tan et al., 2022) or treated participants with exogenously produced synthetic peptides (Mahlapuu et al., 2021), providing no additional insight into how these peptides function and interact in the wound environment. To our understanding, we are the first group to combine the investigation of bacterial species with AMP gene expression, across multiple wound locations and compare these to the skin profiles of healthy donors. This was possible as participants in the current study underwent surgical intervention at the time of recruitment. Whilst this experimental design provides data from only a narrow clinical phenotype, the inclusion of such participants afforded the opportunity to conduct detailed host histological and tissue transcript-based analysis alongside microbial profiling. Such techniques are not often possible when studying lower extremity ulcers, due to the medical and ethical concerns regarding the determinantal effects of tissue collection on patient healing.

Initially, host gene expression profiling in the current study was conducted using RNA-sequencing (RNA-seq), a sensitive method for gene expression analysis (Peymani et al., 2022). This global transcriptional profiling method enhanced discovery power to detect novel gene associations, allowing the entire transcriptome to be profiled, without requiring knowledge on specific gene targets or sequencing information (Peymani et al., 2022). While advantageous, this method profiles the total expression level of an entire piece of tissue, failing to distinguish unique signals from individual cell populations (Jovic et al., 2022). AMPs are produced by multiple cell types, including cutaneous immune cells and keratinocytes

(Gera et al., 2022). As each of these cells contribute differently towards the wound repair process, it is important to gain insight into the functional activity of each population (Gera et al., 2022). For example, Jovic et al., 2022 identified that defence proteins *RNase7* and Psoriasin are often elevated in only specific layers of the epidermis, highlighting the need to differentiate between the functional differences of individual cell populations (Jovic et al., 2022). A future option would be to use single-cell RNA sequencing (Jovic et al., 2022) to, for example, assess gene expression information from wound keratinocytes, identifying signatures previously hidden within the analyses of bulk cell tissue populations (AlJanahi et al., 2018).

In addition to gene expression profiling, histological analysis of the tissue was conducted. Histological quantification of wound tissue bacterial load was conducted using Gram-Twort staining, a method frequently used to assess the efficacy of anti-microbial compounds (Wilkinson et al., 2018). Surprisingly, across the entire study, the burden of bacterial load inversely correlated with the presence of clinical infection. A lack of correlation was also witnessed between bacterial load, clinical infection and microbial read number. Clinical infection was diagnosed based on visual examination and microbial bioburden (critical colonisation bioburden level of $>10^5$ bacteria per gram of tissue threshold) (Bowler, 2003). One key difference between these methods is that microbiome profiling focuses predominantly on swabbing the tissue surface, whilst Gram-twort staining accounts for bacterial load within the tissue (Wilkinson et al., 2018). Whilst previous studies have demonstrated that the assessment of infection does not significantly differ regardless of the detection method, (Haalboom et al., 2019) this subject is widely debated (Bowler et al., 2001). Commonly used methods which focus on the quantification of CFU and other bacterial enumeration methods fail to consider complex bacterial factors. For example, multiple species, including *P. aeruginosa*, can maintain a viable but not culturable (VBNC) state, where they may still contribute to biofilm formation and community virulence (Zhang et al., 2015).

Overall, these discrepancies highlight the complex issues that need to be considered when assessing bacterial load in wound samples. Misleading results in relation to the diagnosis of infection often result in the misuse of antibiotics, increasing treatment costs, and hospital

stays, in turn contributing to antibiotic resistance (Gori et al., 2014). Despite the discrepancies in clinically diagnosed infection and bacterial load, one clear trend was that human β-defensin-1 gene expression was found be significantly elevated in infected tissue samples. Not surprisingly, the human β-defensins genes were repeatedly highlighted as genes of interest throughout the study, with human beta-defensin 2 (*DEFB4*) and human beta-defensin 3 (*DEFB103A*) expression being elevated in the wound margin tissue compared to corresponding donor upper leg tissue. Whilst studies have explored the option of using defensins as therapeutic antimicrobials, defensins function as complex modulators of inflammation and immune response (Zhu et al., 2021; Sabbatini et al., 2021; Njeim et al., 2020). Defensins are able to stimulate immune cell migration, pro-inflammatory cytokine release and activate the Th1-immune response, effectively linking innate and adaptive immunity (Sabbatini et al., 2021). Therefore, the therapeutic use of this proteins for clinical benefit is a process which will need to be carefully controlled.

While studies boast the beneficial pro-inflammatory influence of these defensin molecules, such as the ability to remove pathogens via the stimulation of neutrophil extracellular trap (NET) release (Njeim et al., 2020; Sabbatini et al., 2021), the true benefit of using defensins to stimulate healing remains unclear. Zhu et al., 2021 recently found that prolonged NET formation and associated toxic component secretion, directly impaired wound healing. In relation to the work outlined in this chapter, existing studies suggest that NETs, as stimulated by HBD-1 expression in infection, exert mainly negative effects on wound healing (Njeim et al., 2020).

However, most of the studies investigating NET formation have focused on diabetic wounds, which demonstrate fundamentally impaired healing. During the healing process in normoglycemic conditions, neutrophils produce very few, if any, NETs (Njeim et al., 2020). Despite this, across the current study, no correlation was observed between diabetic status and the presence of wound margin neutrophil elastase (NE), a key component of extracellular traps (Okeke et al., 2020). Going forward, it is clear more studies are needed to fully characterise the protective antimicrobial balance of NETs versus their destructive capabilities (Honda and Kubes, 2018), specifically in intricate multifactorial wound healing scenarios.

Further investigation of wound neutrophils and macrophages in the peri-wound tissue revealed that immune cell presence was significantly correlated with the expression of *NOD2* and *MYD88*. Mar et al., 2003 identified that macrophages derived from the bone marrow of *MYD88*-deficient mice (*MYD88*$^{-/-}$) demonstrated impaired phagocytosis and intracellular killing of *C. albicans* compared to wild-type (*MyD88*$^{+/+}$) macrophages. It is known that in the wound environment, TLRs mediate the macrophage-based recognition of microbial ligands, ultimately inducing the expression of microbicidal molecules and cytokines via the adapter protein *MYD88*. The differential role of MYD88 may represent one mechanism by which macrophages are able to regulate innate responses to different pathogenic fungi. *In vivo*, *Nod2*$^{-/-}$ mice demonstrate a higher fungal burden in the gut than wild-type mice. Again, in chitin-exposed bone marrow-derived macrophages, a *NOD2*$^{-/-}$ phenotype results in a decreased frequency of mesenteric lymph node–derived type 3 ILCs (ILC3s) and IL-17 mechanism, allowing the overgrowth of opportunistic fungi (McAndrew, et al., 2022).

However, almost all these studies have been conducted in mice (McAndrew, et al., 2022; Mar et al., 2003). A recent study by our group aimed to establish a clinically relevant model of the human skin, and wound microbiome, revealing stark differences in the cutaneous microbiome of humans and mice. However, the study established that humans and pigs have more closely related microbiomes, suggesting pigs could be a more clinically relevant model for wound microbiome studies (Paper under review).

Overall, wound healing is a multifaceted process, further complicated by underlying host pathology and systemic disease (Wilkinson and Hardman, 2020). The microbial composition of the chronic wound unquestionably plays a key and interactive role in contributing toward the delayed healing phenotype, particularly in augmenting and propagating aspects of the inflammatory innate immune response. Use of comprehensive host tissue characterisation methods combined with novel third-generation sequencing technology allows unparalleled insight into wound microbe-host interactions. Whilst this study demonstrates the power of integrating clinical and biological datasets, the current findings are limited by the relatively

low number of donors contained with this pilot study. Furthermore, understanding and dissecting the molecular mechanisms that modulate host-microbe interactions will also likely require a range of further extensive *in-vitro*, *ex-vivo* and *in-vivo* studies. These study approaches may involve microbial manipulation, through the selective inhibition of pathogenic bacteria or the promotion of diverse symbiotic communities, providing a cost-effective technique for chronic wound management. With relation to host contribution, host defence and innate inflammatory factors may also provide a valuable target, modulating the microbiome, and inhibiting pathogenic populations while limiting the deleterious and persistent cycle of inflammatory arrest. Future larger studies focused on untangling the mechanisms of this relationship are desperately needed and will undoubtedly be accompanied by a selection of unexpected challenges. However, the knowledge generated will provide a valuable foundation for clinical translation into improved future therapeutic interventions for poor wound healing.

5 The Influence of Extracorporeal Shockwave Therapy on Human Wound Repair

5.1 Introduction

There is an urgent need for novel, clinically usable efficacious wound-healing therapies (Xiao et al., 2023). Studies outlined in this chapter investigated the role of an emerging technology, extracorporeal shockwave therapy (ESWT), and its specific effects on distinct aspects of the human wound repair process.

Implemented clinically over 30 years ago in the field of orthopaedic repair, extracorporeal shockwave therapy was highlighted as an effective, yet minimally invasive therapeutic technique (Auersperg and Trieb, 2020). Since its original application, studies investigating ESWT have described effective osteogenic stimulating potential, specifically reporting enhanced osteoblast activation and subsequent increases in total bone density (Haupt, 1997; Rompe et al, 2002; Wang, 2003). Interestingly, over the course of these studies, it was observed that participants treated with shockwave therapy displayed simultaneously enhanced orthopaedic and soft tissue repair. Encouraged by such promising data, clinical studies investigating shockwave therapy for human wound healing were commenced (Schaden et al., 2007). While a small number of clinical studies have been generated promising outcomes (Table 5.1), the biomolecular mechanisms by which ESWT is able to influence wound repair remain poorly understood (Auersperg and Trieb, 2020).

Briefly, shockwave therapy delivers targeted transient interim acoustic pulses, which rapidly propagate to deliver high peak pressure to selected areas of host tissue (Simplicio et al., 2020). Though the biological influences of these acoustic pulses remain elusive, studies investigating ESWT have reported a selection of beneficial effects, including increased ECM production, upregulated proliferation, reduced apoptosis, and anti-microbial activity (Yan et al., 2009 and Meirer et al., 2007). One proposed mechanism of shockwave therapy is the local improvement of vascular tissue perfusion, with multiple *in-vitro* studies demonstrating post-treatment perfusion enhancement. In *in-vivo* rat models of ischemic skin flaps, both Yan et

al., 2009 and Meirer et al., 2007 reported significantly reduced skin flap necrosis following shockwave therapy, with enhanced local perfusion, vasodilation and elevated tissue VEGF and NOS gene expression.

Pilot studies on the potential clinical benefits of shockwave therapy have also been conducted (Table 5.1). Moretti et al., 2009 demonstrated a total healing status increase in plantar DFUs, from 33% within the control group to 53% in the group receiving ESWT. In addition, Wang et al., 2009 also reported improved DFU complete healing (22% in control vs 31% with ESWT) and 50% wound surface area reduction (72% in control group versus 89% in the ESWT group).

Table 5.1: Summary of shockwave-based wound-healing clinical studies

Study	Wound type	Number	Therapy	Generator	Findings
Schaden et al., 2007	Various aetiologies	N=208	EFD = 0.1mJ/mm2 N = 100 pulses/cm2 Freq = 5 pulses/sec	Electrohydraulic (dermagold, TRT)	75% of participants fully reepithelised. No control group.
Saggini et al., 2008	Venous, Diabetic and, post traumatic ulcer	N=32	EFD = 0.034mJ/mm2 N = 100 pulses/cm2 Freq = 4 pulse/sec	Electrohydraulic (evotron, HMT)	Reduced pain and increased healing in the treatment group
Moretti et al., 2009	Diabetic plantar ulcers	N=30	EFD=0.03mJ/mm2 N = 100 pulses/cm2 Freq = not specified	Electromagnetic (minilith SL1, Storz Medical)	Increased healing in the ESWT group compared to the control
Wang et al., 2009	Recurrent diabetic foot ulcer	N=36	EFD=0.11mJ/mm2 N = (300+) 100 pulses/cm2 Freq = not specified.	Electrohydraulic (orthowave 180, MTS)	ESWT appears to be more effective than HBO in chronic diabetic foot ulcers.

Current techniques for the management of chronic wounds remain inadequate, often requiring prolonged, costly, and ineffective clinical approaches (Ongarora, 2022). New, effective techniques are desperately required to alleviate both patient morbidity and the current chronic wound-related economic burden (Xiao et al., 2023). In addition to its potential clinical efficacy, the advantages of ESWT include ease of use, cost-effectiveness, non-invasiveness, and rarity of side effects (Simplicio et al., 2020). However, existing evidence on the clinical benefits of shockwave therapy remains weak (Hitchman et al., 2023) and the cellular and antimicrobial mechanistic basis of shockwave therapy remain poorly understood (Simplicio et al., 2020). Furthermore, in a clinical setting limited study standardisation and comparability between devices and patient groups hinders the development of optimal therapeutic indices for clinical ESWT application (Moretti et al., 2009; Wang et al., 2009).

This chapter will explore the current clinical evidence and underlying biological mechanisms of shockwave treatment. Initially, the influence of shockwave therapy on wound-related cell populations and chronic wound-derived host tissues will be examined. The impact of therapy on microbial communities will then be examined; both on common wound isolates *in-vitro,* and as part of a novel pilot clinical trial assessing the role of shockwave treatment on the clinical diabetic foot ulcer microbiome.

5.1.1 Aims

1) To determine the effect of ESWT on proliferation, viability, and cytotoxicity in both human dermal fibroblasts and human immortalised keratinocytes.

2) To determine the influence of ESWT on cutaneous wound closure, and histological markers of healing (eg. proliferation, angiogenesis) in a human *ex vivo* wound model.

3) To investigate the antimicrobial efficacy of ESWT on clinical wound bacterial isolates.

4) To undertake a clinical pilot study to assess the longitudinal influence of ESWT on cutaneous healing and associated changes in the diabetic foot ulcer microbiome.

5.2 Methods

For all studies in this chapter, shockwave treatment was applied to mammalian cells, human *ex-vivo* wound models, bacterial isolates and clinical DFUs using the PiezoWave2 multi-use 40 (linear FBL10x5 G2 adaptor; Richard Wolf GmbH, Pforzheimer Straße, Germany). Treatment was applied at an energy flux density of 0.018, 0.041, 0.069 or 0.106 mJ/mm^2, 5 shocks per second for a total of 0, 100, 500, 1000 or 2000 shocks (Figure 5.1).

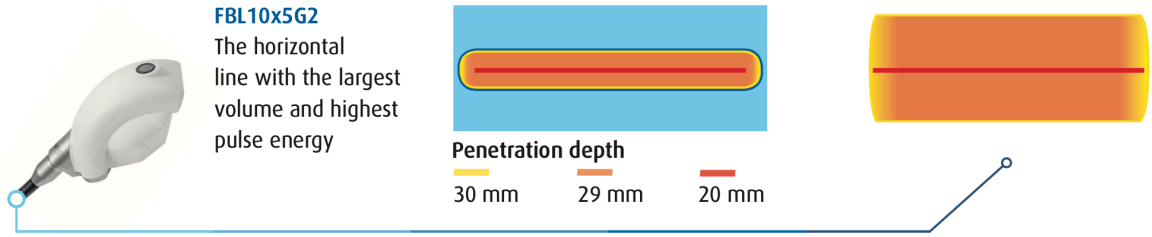

Figure 5.1: PiezoWave2 multi-use 40 linear FBL10x5 G2 adaptor schematic. Focal size, therapeutic impact zone, -6dB zone, 5 megapascals (MPa) zone, central penetration depth, maximum/distal penetration depth of shockwaves produced by the FBL10x5 G2 adaptor schematic used within the current study.

5.2.1 MTS Tetrazolium Assay

Cell viability and proliferation assays were performed using the colourimetric CellTiter 96® AQueous One Solution Cell Proliferation Assay (Promega, Southampton, UK). The assay is based on the conversion of tetrazolium to formazan by the reduced cell-permeable intermediate electron acceptor reagent, phenazine ethosulphate, which is reduced in only viable cells (Ghasemi et al., 2021). Human cells cultured in standard culture conditions (Section 2.4) were passaged and resuspended as described previously (Section 2.4). Cultures were adjusted to 5x10^4 (HDF) or 1x10^5 (HaCaT) cells per mL, and 1 mL of cell suspension placed into each universal treatment tube. Shockwave therapy was applied directly to the side of each tube using the FBL 10x5G2 adaptor (Richard Wolf GmbH). Cell suspensions were seeded into 96-well plates at 100 µL per well (5x10^3 HDFs or 1x10^4 HaCaT cells per well). Plates were returned to standard culture conditions (Section 2.4) and left for 24 hours. Following

incubation, cells were removed from the incubator and 20 µL of CellTiter 96® aqueous one solution was added to each well, and plates were then left in standard incubation conditions (Section 2.4) for four hours. Following incubation, plates were removed and assessed to detect colourimetric changes, using a plate reader (492 nm) (ThermoScan, Thermo Fisher Scientific). The number of viable cells present in each treatment well was determined using cellular calibration curves, seeded post-incubation prior to the addition of CellTiter 96® aqueous one solution.

5.2.2 Scratch Closure Assay

Human cell populations were cultured, and scratch closure assays were prepared and conducted as described previously (Section 4.2.12). For assays that underwent incubation with bacterial supernatant prior to scratching, supernatant treatments were prepared as described in section (Section 4.2.1). Supernatants were diluted in standard cell culture media at 5% (v/v) and applied to the cells four hours prior to scratch formation. For the application of shockwave therapy to scratch closure assays, shockwave treatments were applied post-scratching via the direct application of the FBL 10x5G2 adaptor to the underside of the culture plate. Plates were then incubated in standard incubation conditions for 24 hours (Section 2.4). Following incubation, plates were washed, stained, imaged, and analysed as previously described (Section 4.2.9).

5.2.3 *Ex-vivo* Wounding and Tissue collection

Following the acquisition of human wound tissue (Section 4.2.3), skin samples were prepared into linear strips (8x3cm) and adipose tissue was removed. Skin samples were then washed twice in Hank's Balanced Salt Solution (HBSS) (Gibco, Thermo Fisher Scientific, UK) containing 2% anti-anti solution (Gibco). Following adequate washing, skin samples were placed dermis side down in a 90mm sterile Petri dish and dried with sterile gauze. Skin samples then underwent shockwave treatment using the PiezoWave^2 multi-use 40 linear FBL10x5 G2 adaptor (Richard Wolf). Shockwave therapy was applied directly to the top (epidermis) of the skin samples (Figure 5.2). Experimental groups were generated by altering only one experimental parameter, the number of shockwave impulses (total shocks= 0, 100, 500, 1000

and 2000). Shockwave therapy was applied to the skin at an energy flux density of 0.106 mJ/mm2, 5 shocks per second, and 0mm penetration depth.

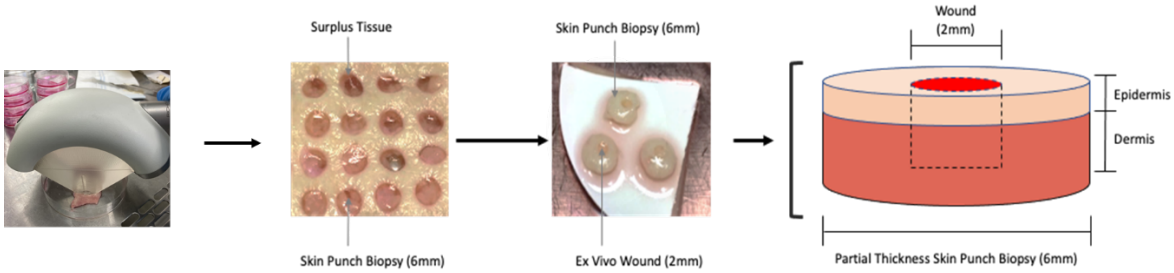

Figure 5.2: Shockwave treatment human *ex-vivo* wound model workflow. Excised *ex-vivo* skin samples underwent shockwave treatment using the PiezoWave^2 multi-use 40 (linear FBL10x5 G2 adaptor). Shockwave-treated tissue was then wounded to create human *ex-vivo* human skin wound models and later collected to assess ex-vivo wound repair. See the above schematic depicting partial thickness (complete epidermis and partial dermis) *ex-vivo* wound biopsies.

Following ESWT treatment, skin strips were used to create human *ex-vivo* skin wound models (Section 4.2.3). Post-incubation in standard culture conditions (Section 2.4), samples for future RNA isolation and downstream differential gene analysis were collected at 6 hours, snap-frozen and stored at -80^{o}C (Figure 5.3). The remaining *ex-vivo* samples for whole mount staining and histological analysis were collected at 48 hours post-wounding. *Ex-vivo* whole-mount samples were collected, stained, imaged, and analysed as described in section (Section 4.2.4).

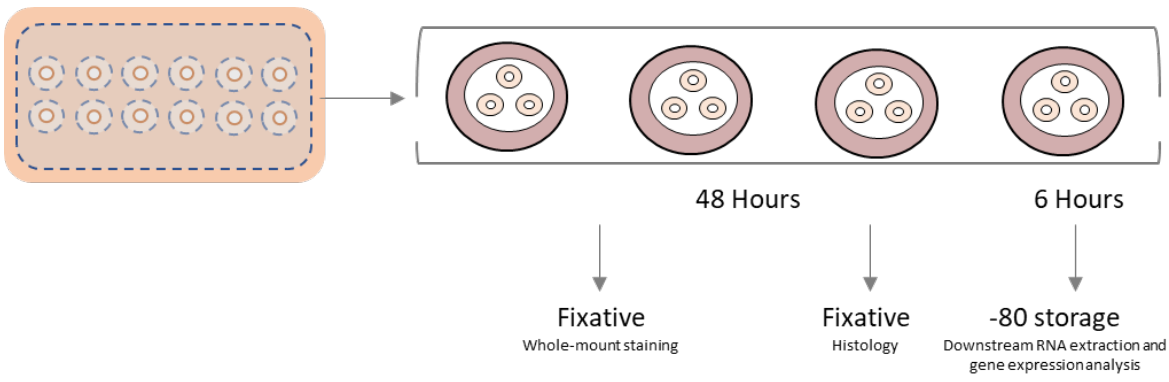

Figure 5.3: *Ex-vivo* tissue collection schematic for shockwave-treated human tissue. *Ex-vivo* wounded tissue was collected following treatment with shockwave therapy at an energy flux density of 0.106 mJ/mm2, 5 shocks per second, 0mm penetration depth (total shocks= 0, 100, 500, 1000 and 2000).

5.2.4 Immunohistochemistry

Following the collection of *ex-vivo* wound biopsies for histology and wax embedding, tissue process and sectioning were conducted as described previously (Section 4.2.5). Tissue samples then underwent IHC staining as described previously (Section 4.2.8), using the antibodies described below (Table 5.2)

Table 5.2: Antibody Titration, Reactivity and Optimal Dilution Information.

Antibody	Host Species and Species Reactivity	Optimal IHC Concentration	Manufacturer
Anti-human Keratin 6	Rabbit Anti-human	1:1000	Biolegend, San Diego, United States
Anti-human Keratin 1	Rabbit Anti-human	1:1000	Biolegend, San Diego, United States
Anti-human Ki-67	Mouse Anti-human	1:100	Novocastra, Milton Keynes, UK

5.2.5 Histological Image Analysis

All non-fluorescent tissue staining was visualised using a Nikon Eclipse E400 microscope with SPOT camera software (Image Solutions Ltd.). For Ki-67 basal cell positivity, images were captured at X20. Images were taken across the entire neo-epidermal edge. Both total and positive basal cell numbers were calculated to determine relative basal cell staining positivity. For markers of new epidermal formation (K6 and K1) images were captured at X20. Five images were captured for each epidermal edge and tissue sections were either scored blinded (K1) for relative staining intensity, or the length of positive (K6) epidermal staining was directly measured. For K6 image analysis, an X20 graticule image was used to set an accurate

scale using the 'set scale' tool of Image J 1.5.2 software. Following this, the overall length and area measurement of both the right and left re-epithelised area surrounding the wound was measured. See appendix 8.9 for neo-epidermal length quantification.

5.2.6 RNA Isolation and RT-qPCR Amplification

Tissue RNA isolation, cDNA synthesis and RT-qPCR amplification techniques were conducted as described in section (Section 4.2.18). *Ex-vivo* tissue was treated with shockwave therapy and assessed specifically for the relative tissue gene expression of angiogenic markers VEGFa and CD31 (Appendix 8.5).

5.2.7 Planktonic Culture Preparation and Enumeration

Overnight (O/N) cultures were created by inoculating 10mL Mueller Hinton Broth (MHB; Oxoid, UK) with a single colony followed by incubation at 37°C for 16 hours with 140rpm shaking (Labnet 211DS shaking incubator, Labnet International, USA). The following day, bacterial cultures were diluted and adjusted to a bacterial cell density of either 10^3, 10^5 or 10^7 CFU/mL. Culture densities were calculated using bacterial growth curves specific to each species used within the study. Supernatants of excreted bacterial products were prepared as described in Section 4.2.10. Once adjusted, ESWT was applied to the cultures using the FBL 10x5G2 adaptor on the outside of the treatment tube. Treatment was then applied through the adaptor at an energy flux density of 0.106 mJ/mm^2, 5 shocks per second for a total of 2000 shocks.

Surviving bacterial culture counts were confirmed using spot-plating techniques, as described by Chen et al. (2003). The resulting control and shockwave-treated bacterial planktonic cultures were then kept neat and serially diluted 1:10, for 6 total dilutions. Serial dilutions of the adjusted cultures were plated onto MHA in a series of 10 µL spots. Plates were left to dry for 15 minutes and incubated inverted at 37°C for 16-18 hours. The following day, the present bacterial colonies were counted and used to calculate the total CFU/mL per culture. Bacterial

culture start densities were confirmed using corresponding techniques. Results are presented as surviving CFU per mL.

$$CFU/mL = \frac{number\ of\ colonies \times dilution\ factor}{volume\ of\ culture\ plated}$$

5.2.8 Colony Biofilm Preparation and Enumeration

Overnight cultures were diluted and adjusted to a bacterial cell density of 10^7 CFU/mL, confirmed by spot plating techniques (Section 4.2.13). As described by Merritt et al. (2005), biofilms were prepared by inoculating sterile filter membranes (0.22µm, GE Healthcare, USA) on MHA with 20 µL of adjusted inoculum. Plates were left to dry for 15 minutes and incubated inverted at 37°C for 24hrs. Membranes containing the bacteria were then removed from the agar surface using sterile forceps and placed inside an empty petri dish. Shockwave therapy was applied to the biofilm's direct application of the FBL 10x5G2 adaptor to the outside of the Petri dish at the corresponding surface of the biofilm membrane. Treatment was applied at an energy flux density of 0.106 mJ/mm^2, 5 shocks per second for a total of 2000 shocks. Once complete, colony biofilms were resuspended by vortexing for 30s in universal tubes containing 2.5mL sterile borosilicate glass beads (Sigma-Aldrich) and 1mL MHB. The resulting resuspension cultures were then kept neat and serially diluted 1:10, for 6 total dilutions. Serial dilutions of the adjusted cultures were plated onto MHA in a series of 10 µL spots. Plates were left to dry for 15 minutes and incubated inverted at 37°C for 16-18 hours. The following day, the present bacterial colonies were counted and used to calculate the total CFU/mL per culture. Bacterial culture start densities were confirmed using corresponding techniques. Results are presented as surviving CFU per mL.

5.2.9 Minimum Inhibitory Concentration (MIC) Testing

The standard broth minimum inhibitory concentration (MIC) testing microdilution method (Andrews et al., 2001) was used to investigate the combined inhibitory effects of both alone antimicrobial efficacy and in combination with shockwave therapy. Serial two-fold dilutions

in sterile MH broth in flat 96-well plates were prepared for each antimicrobial agent used within the study. Cultures of common wound isolates used within the study were adjusted to give a standard bacterial concentration (1-5x10^5 CFU/mL). Shockwave therapy was applied to bacterial culture tubes using the FBL 10x5G2 adaptor at an energy flux density of 0.106 mJ/mm^2, 5 shocks per second for a total of 0 (control) or 2000 total shocks. Following treatment, 50 µL of bacterial culture was added to each well to determine the MIC in a total volume of 100 µL MH broth. All plates were statically incubated at 37°C for 24hrs. To determine the MIC breakpoint and presence of cell viability, 96-well plates were stained with 10 µL of 0.02% resazurin sodium salt (Sigma-Aldrich, Germany) (Appendix 8.8). Plates were then incubated at 37°C for 30mins. Resazurin sodium salt (Sigma-Aldrich, Germany) was used as a colourimetric marker for cell viability (Elshikh et al., 2016). A redox indicator, resazurin (blue/purple, non-fluorescent) is irreversibly converted into resorufin (pink, fluorescent) when present in a reducing environment including metabolically active cells (Elshikh et al., 2016). Following incubation, all plates were imaged, and absorbance was measured at 570nm. The relative breakpoint was defined as the concentration at which antimicrobial testing was able to inhibit growth.

5.2.10 Minimum Bactericidal Concentration (MBC) procedure

For each species, minimum bactericidal compound concentration breakpoints were estimated from MIC curves. Overnight cultures were set up as described above for all bacterial strains. The following day overnight cultures were adjusted to the McFarland standard (0.08-0.12) and diluted (1:150) to provide a cell density of 5x10^5 cells per mL). Shockwave therapy was applied to bacterial culture tubes using the FBL 10x5G2 adaptor at an energy flux density of 0.106 mJ/mm^2, 5 shocks per second for a total of 0 (control) or 2000 total shocks. Following treatment, 50 µL of bacterial culture was added to each well in a total volume of 100 µL MH broth. All plates were statically incubated at 37°C for 24hrs. The following day, bacteria cultures were removed from the plates and then kept neat and serially diluted 1:10, for 6 total dilutions. Serial dilutions of the adjusted cultures were plated onto MHA in a series of 10 µL spots. Plates were left to dry for 15 minutes and incubated inverted at 37°C for 16-18 hours. The following day, the present bacterial colonies were counted and used to calculate the total

CFU/mL per culture. Bacterial culture start densities were confirmed using corresponding techniques. Results are presented as surviving CFU per mL.

5.2.11 Pilot study: Participant Enrolment and ESWT

Within the pilot study, six individual donors presenting clinically with a non-infected diabetic foot ulcer consented for trial enrolment (IRAS: 311664, R&D R2743). From the total six donors, three were assigned to the group receiving ESWT, whilst three donors remained in the control 'sham' treatment group. ESWT was administered at an EFD of 0.1mJ/mm2, 5 pulses/second at a penetration depth of 5mm, the total number of shocks per donor was calculated by multiplying the ulcer surface area (mm^2) by 500. Each intervention was delivered across three 30-minute sessions over 7 days+/-9 at three separate intervals within the first week of trial enrolment. Throughout the study, participants were randomised on a 1:1 allocation ratio to sham shockwave therapy or ESWT. Randomisation was be performed by an online randomisation service provided by York Trials Unit's (YTU) secure, web-based randomisation service, therefore ensuring allocation concealment and immediate unbiased allocation (Cook et al., 2020). Participants were stratified by ulcer size (<1cm2 and >1cm2) and presence of ischaemia (neuroischaemic and neuropathic). The pilot stratified patients by these two parameters because ulcer size and ischaemic status are known to affect healing.

5.2.12 Microbial DNA Extraction and ONT Microbiome Profiling

For each participant, wound swabs were collected, and genomic DNA was extracted for microbiome sequencing at four individual time points: baseline, 1 week, 6 weeks and 12 weeks post-trial enrollment treatment. Throughout the study, DNA extraction, library preparation, and nanopore sequencing were conducted as described previously (Section 3.2.3 – 3.2.5). Participant clinical wound samples were sequenced on the GridION using FLO-MIN106D Flow cells and the minnow-core-gridiron:4.1.2 software (Oxford Nanopore Technologies). Wound samples were sequenced using a standard 72-h run script with and without adaptive sampling (depletion). For 'human depletion experiments', the human

reference genome GCA_000001405.28_GRCh38.p13 was selected and used to define depletion targets.

5.2.13 Bioinformatic Analysis

Bioinformatic-based methods analysis was performed using enhanced terminal MobaXterm (v.20.1) connected remotely to the University of Hull VIPER High Performance Computing (HPC) sever (as described in Section 3.2.6) Profiling data was then further transformed and assembled into feature table format using Quantitative Insights Into Microbial Ecology version 2 (QIIME2) software (Caporaso et al., 2010). For profiling community analysis data visualisation, MicrobiomeAnalystR (Chong et al., 2020; et al., 2017) and in RStudio (v.1.3) were used.

5.3 Results

5.3.1 Mammalian cell cytotoxicity and scratch closure screening following treatment with increasing doses of shockwave therapy.

Initially, cellular effects of shockwave were evaluated by screening a range of energy flux densities and total dosages. Screening was conducted to determine both the maximum tolerance and potential positive effects of ESWT on mammalian cells at specific doses. A goal was to identify dosing strategies for further investigation across *in-vitro, ex-vivo* and bacterial growth inhibition studies. Cell viability was determined (MTS assay) in HDF and HaCaT cells following shockwave treatment (Figure 5.4: B, C). Across both the HDF and HaCaT cells, a increasing EDF led to a decrease in cell viability and scratch closure. At the highest treatment EDF (0.106 mJ/mm^2), cell number was significantly reduced in both cell populations (*$p<0.05$, one-way ANOVA*; Figure 5.4: B, C). In HaCaTs, exposure to shockwave at the higher energies (0.069 and 0.106 mJ/mm^2) let to substantial loss of adherent cells.

While similar effects of shockwave treatment were observed across both cell types, primary HDFs appeared to be slightly more resistant to the detrimental treatment effects (Figure 5.4: D). By contrast, positive effects on scratch assay closure were evident in response to treatment at an EDF of 0.018 mJ/mm^2. In HaCaTs, a significant increase in scratch closure was observed at an EDF of 0.018 mJ/mm^2, 5 shocks per second. While a positive effect was observed across all total shock dosages, significant was observed only at 2000 total shocks *($p=0.009$, One-way ANOVA;* Figure 5.4*: E)*. Throughout the study, the only positive effects on mammalian cell viability and scratch closure were observed following shockwave treatment at the lowest energy flux density of 0.018mJ/mm^2.

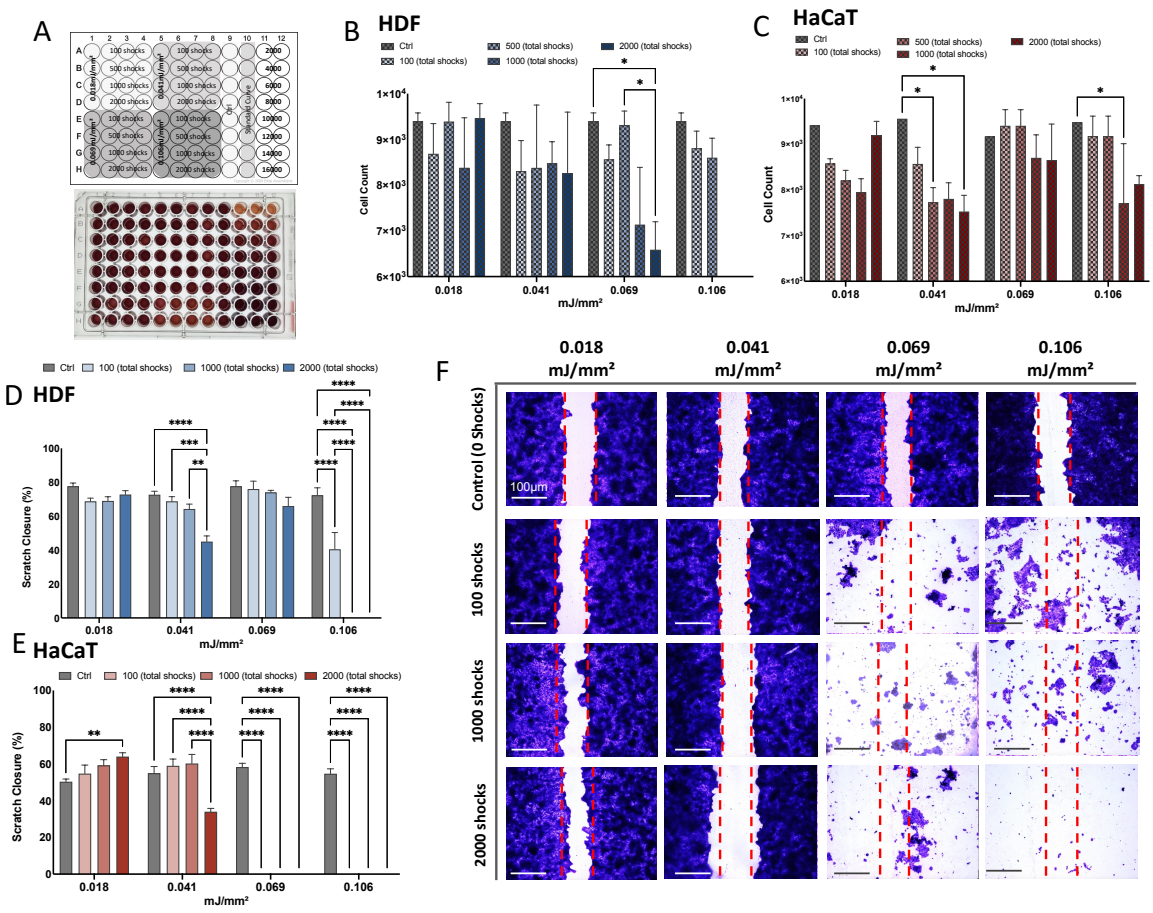

Figure 5.4: Mammalian cell viability and scratch closure following treatment with shockwave therapy. Average HDF (B, (D) and HaCaT (C, E) cell viability (B, B) and total scratch assay analysis closure (D, E) following shockwave treatment at an energy flux density of 0.018, 0.041, 0.069 and 0.106 mJ/mm^2, 5 shocks per second for a total of 0, 100, 1000 or 2000 shocks. Representative photomicrographs (x40 total magnification) of *in-vitro* scratch closure analysis assays following shockwave treatment. MTS viability measurements were acquired 24 hours post-treatment, whilst scratch closure assay measurements/images were captured 18 (HaCaT) or 24 hours (HDF) post-treatment exposure [n=3 technical repeats]. Bars represent treatment, mean + SEM. Statistical significance *was* determined using a two-way analysis of variance (ANOVA) followed by a Tukey multiple-comparison post hoc test, **p < 0.05, **p < 0.01, ***p < 0.001, ****p < 0.001.*

5.3.2 Shockwave therapy shows a trend of consistently increased scratch assay closure in the presence of inhibitory pathogenic stimuli.

Following cell scratch closure and viability screening, shockwave therapy at an energy flux density of 0.018mJ/mm^2 was applied to three biological replicates of primary human dermal fibroblasts and HaCaT cells (Figure 5.5). In addition to treatment with shockwave therapy alone, cells were also pre-treated with supernatant from *Pseudomonas aeruginosa* cultures, at a concentration known to inhibit cell mobility.

In human dermal fibroblasts, scratch closure analysis revealed a trend towards scratch closure following ESWT treatment, with the highest percentage closure increase being observed following the application of 1000 total shocks (Control: 67% vs 1000 total shocks: 82 %, *p>0.05, one-way ANOVA*) (Figure 5.5: A, B). This trend was further replicated following the treatment of primary cells with *Pseudomonas aeruginosa* culture supernatant (5% v/v). While the total closure of the *Pseudomonas aeruginosa* control group was lower than that of the standard culture control group (59%) (Figure 5.5: C), total closure was improved following ESWR, specifically in cells treated with 100 total shocks (73% relative closure, *p>0.05, one-way ANOVA*).

In HaCaT cultures, treatment with shockwave therapy was again shown to non-significantly increase scratch closure, from 56% total closure in the control group to 67% in cells receiving 2000 total shocks *(p>0.05, one-way ANOVA)*. In cultures treated with *Pseudomonas aeruginosa* culture supernatant (5% v/v), total relative scratch closure was reduced to only 33%. However, following ESWT, an overall increase in closure was observed following the applicate shockwave treatment at all doses. In this population, HaCaT cells receiving 2000 total shocks demonstrated an increase in relative closure from 33% to 45% (Figure 5.5: G) *(p>0.05, one-way ANOVA)*. Collectively, these results demonstrate that ESWT is able to consistently increase a trend towards enhanced cellular scratch closure in human wound-related cell populations, specifically in the presence of inhibitory pathogenic stimuli.

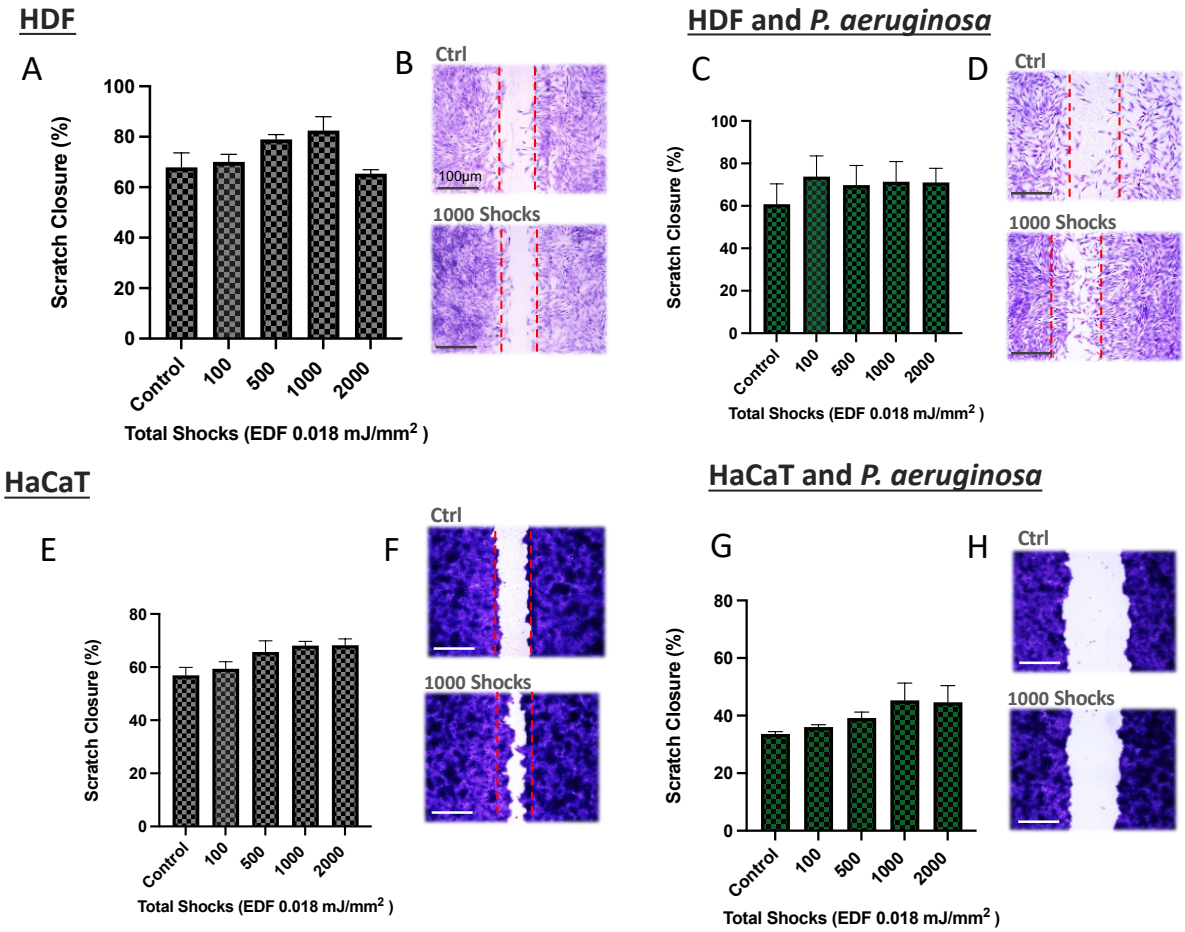

Figure 5.5: Mammalian scratch closure following treatment with shockwave therapy and exposure to pathogenic stimuli. Average total scratch migration assay in HDF (A) HaCaT (E), in both standard culture conditions and following exposure to *Pseudomonas aeruginosa* culture supernatant (5% v/v) (C, G). Shockwave therapy was applied at an energy flux density of 0.018, mJ/mm^2, 5 shocks per second for a total of 0, 100, 500, 1000 or 2000 shocks. Representative photomicrographs (x40 total magnification) (B, D, F, H) and measurements of *in-vitro* scratch closure analysis assays were captured 18 (HaCaT) or 24 hours (HDF) post-treatment exposure [n=3 biological repeats]. Bars represent treatment, mean +/- SEM. Statistical significance *was* determined using a one-way analysis of variance (ANOVA) followed by a Tukey multiple-comparison post hoc test. Scale bar = 100 µm)

5.3.3 Shockwave therapy significantly improves wound closure in a pre-clinical *ex-vivo* model of cutaneous repair.

Next, shockwave therapy was evaluated in a previously validated (Wilkinson et al., 2019), clinically relevant *ex-vivo* human tissue wound model. Human *ex-vivo* wounds were assessed after 48 hours of incubation following shockwave treatment at an energy flux density of 0.106 mJ/mm2, 5 shocks per second for a total of 0, 100, 500, 1000 or 2000 shocks.

Throughout the study, treatment at all doses led to an increase in *ex-vivo* wound closure (Figure 5.6). The greatest increase in percentage wound closure was observed in wounds treated with 1000 shocks, which were fully closed versus a mean 63.4% closure in the control group (*One-way ANOVA, p<0.001*). *Ex-vivo* wound biopsies receiving a total of 100 or 2000 shocks also demonstrated increased closure (*One-way ANOVA, p<0.0001*).

5.3.4 Histological analysis revealed a shockwave-mediated increase in markers of proliferation and neo-epidermal formation.

In parallel to overall *ex-vivo* wound closure (Figure 5.6), histological markers of cutaneous wound repair were also assessed in the shockwave-treated *ex-vivo* wound tissue (Figure 5.7). Investigated markers including Ki-67, Keratin 1, and Keratin 6 were used to assess shockwave-mediated influence on tissue cellular proliferation and neo-epidermal formation. During wound repair, proliferation is essential for the formation of granulation tissue, restoration of the vascular network and wound re-epithelization (Leydon et al., 2014).

The Ki-67 protein is a cellular marker for proliferation (Leydon et al., 2014). An increase in Ki67-positive keratinocytes was observed in the basal and suprabasal epidermal layers of shockwave treated samples (Figure 5.8:A), suggesting that ESWT is linked with cell proliferation. Whilst a broad overall trend of increasing proliferation was observed in response to all treatment regimes, the highest increase in Ki-67 positive basal cells was observed following ESWT at 500 total shocks. In this group, Ki-67 cellular positivity was non-

significantly elevated from 12.9% in the control group, to 22% in the basal and suprabasal layers epidermal of ESWT-treated *ex-vivo* wounds (*One-way ANOVA*, *p=0.72*).

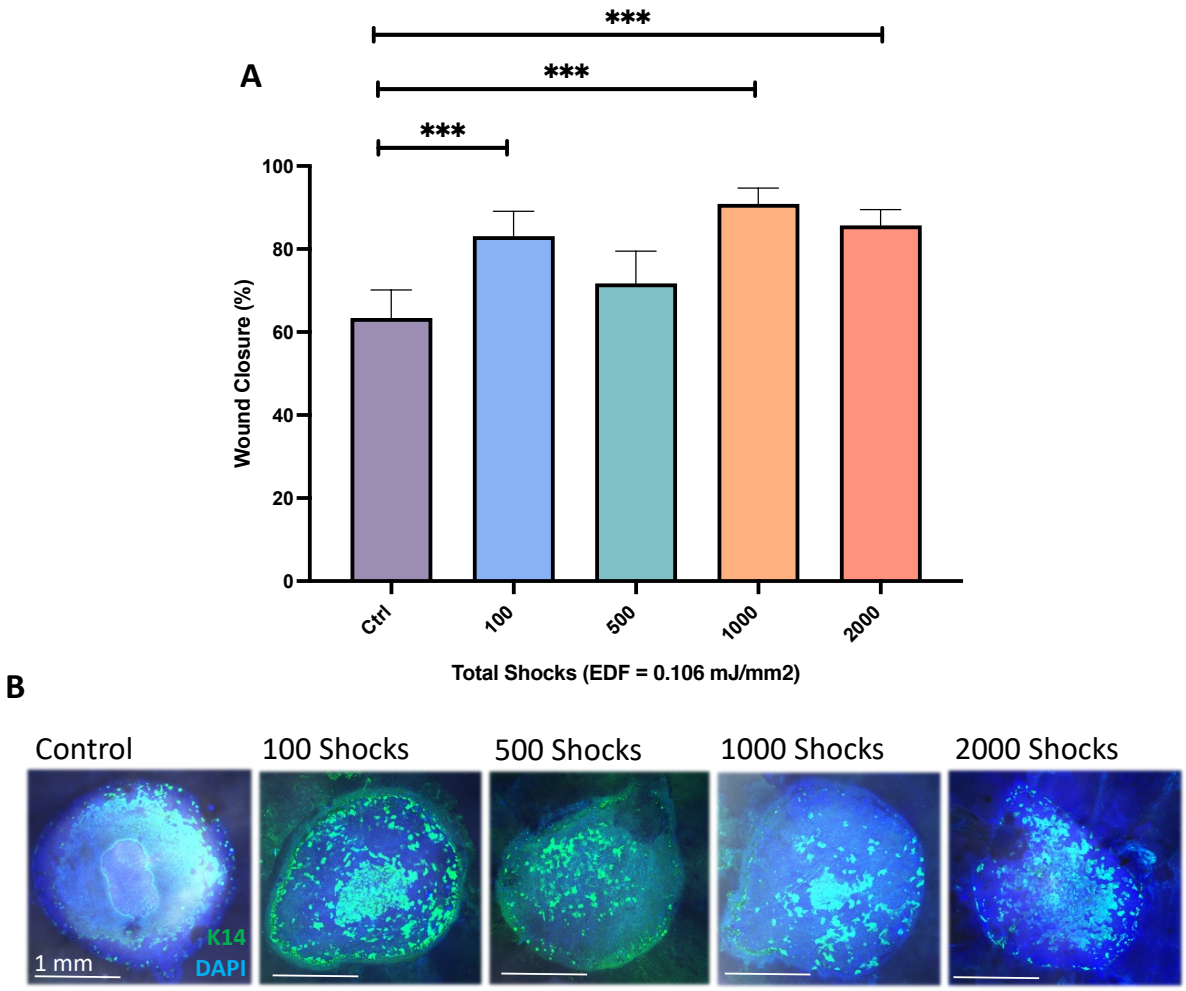

Figure 5.6: Percentage closure of human ex-vivo wound models following treatment with shockwave therapy. Average total closure of human partial thickness *ex-vivo* wound models (A), following shockwave treatment at an energy flux density of 0.106 mJ/mm2, 5 shocks per second for a total of 0, 100, 500, 1000 or 2000 shocks. Representative photomicrographs (x25 total magnification) of human *ex-vivo* wound models in human tissue donors following shockwave treatment. All images were captured 48 hours post-shockwave treatment exposure [n=3]. Bars represent the average across all donors, mean +/- SEM. Statistical significance *was* determined using a one-way analysis of variance (ANOVA) followed by a Tukey post hoc test, **p < 0.05, **p < 0.01, ***p < 0.001.*

Next, expression of migration and neo-epidermal regeneration-associated tissue markers was investigated (Figure 5.7:B/C). While initially high levels of K14 and K5 are expressed by mitotically active basal layer cells, the terminal differentiation of local keratinocytes induces the expression of alternative keratins, such as K1 and K10 (Konop et al., 2021). Within the shockwave-treated samples, a non-significant increase in relative keratin 1 expression was demonstrated in the treatment groups receiving 500, 1000 and 2000 total shocks (*One-way ANOVA*, *p>0.05*) (Figure 5.7:B). This observation suggests that shockwave-treated wounds *ex-vivo* achieve re-epithelialization, differentiation and wound maturation at an enhanced rate. Following the formation of a cutaneous wound, a coordinated repair response functions to begin the process of skin barrier restoration (Hobbs et al., 2015). The dynamic switch in keratin gene expression at the wound edge is an essential part of this process (Hobbs et al., 2015). The expression of Keratin 6 (K6) by wound edge keratinocytes is strongly associated tissue injury with neo-epidermal formation (Kommine et al., 2001). Within *ex-vivo* tissue, the length of K6 positivity in the recently regenerated neo-epidermis demonstrated an overall increase in length following ESWT treatment (Figure 5.7: C). In comparison to the control group, cutaneous wounds treated with 500, 1000 or 2000 total shocks demonstrated an increase in K6 positive neo-epidermal length (Figure 5.8:C). Overall, while trends could be observed in the presence of K6-positive neo-epidermis following ESWT, no statistical significance was detected (*p>0.05, One-way ANOVA*).

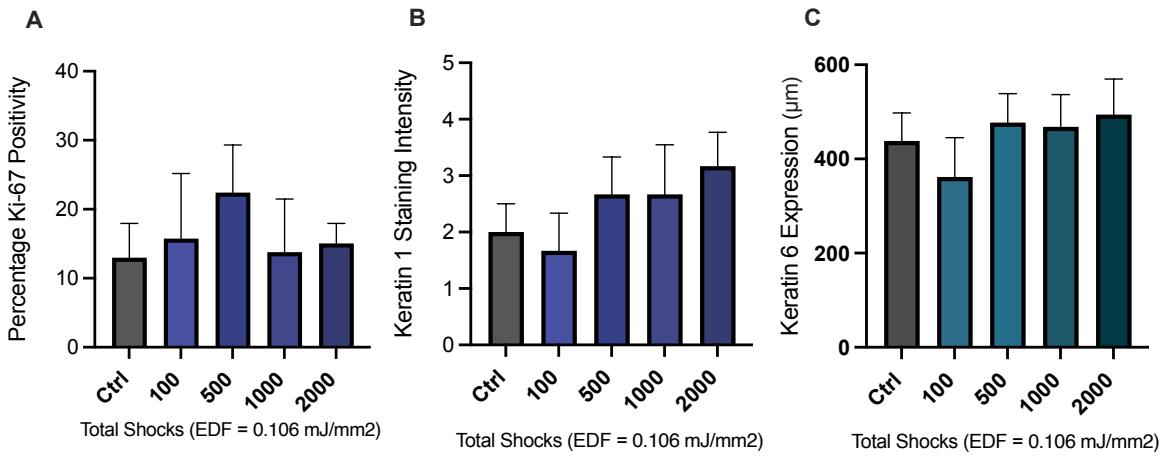

Figure 5.7: Quantification of histological tissue regeneration markers in human *ex-vivo* wounds following shockwave therapy. Percentage cellular Ki-67 positivity (A), Keratin 1 staining intensity (B) and Keratin 6 expression (C) in human *ex-vivo* partial thickness biopsy wounds following treatment with shockwave therapy at an energy flux density of 0.106 mJ/mm^2, 5 shocks per second for a total of 0, 100, 500, 1000 or 2000 shocks [n=3]. All measurements were taken 48 hours post-shockwave treatment exposure. Bars represent the average across all donors, mean +/- SEM. Statistical significance *was* determined using a one-way analysis of variance (ANOVA) followed by a Tukey post hoc test (*p>0.05*).

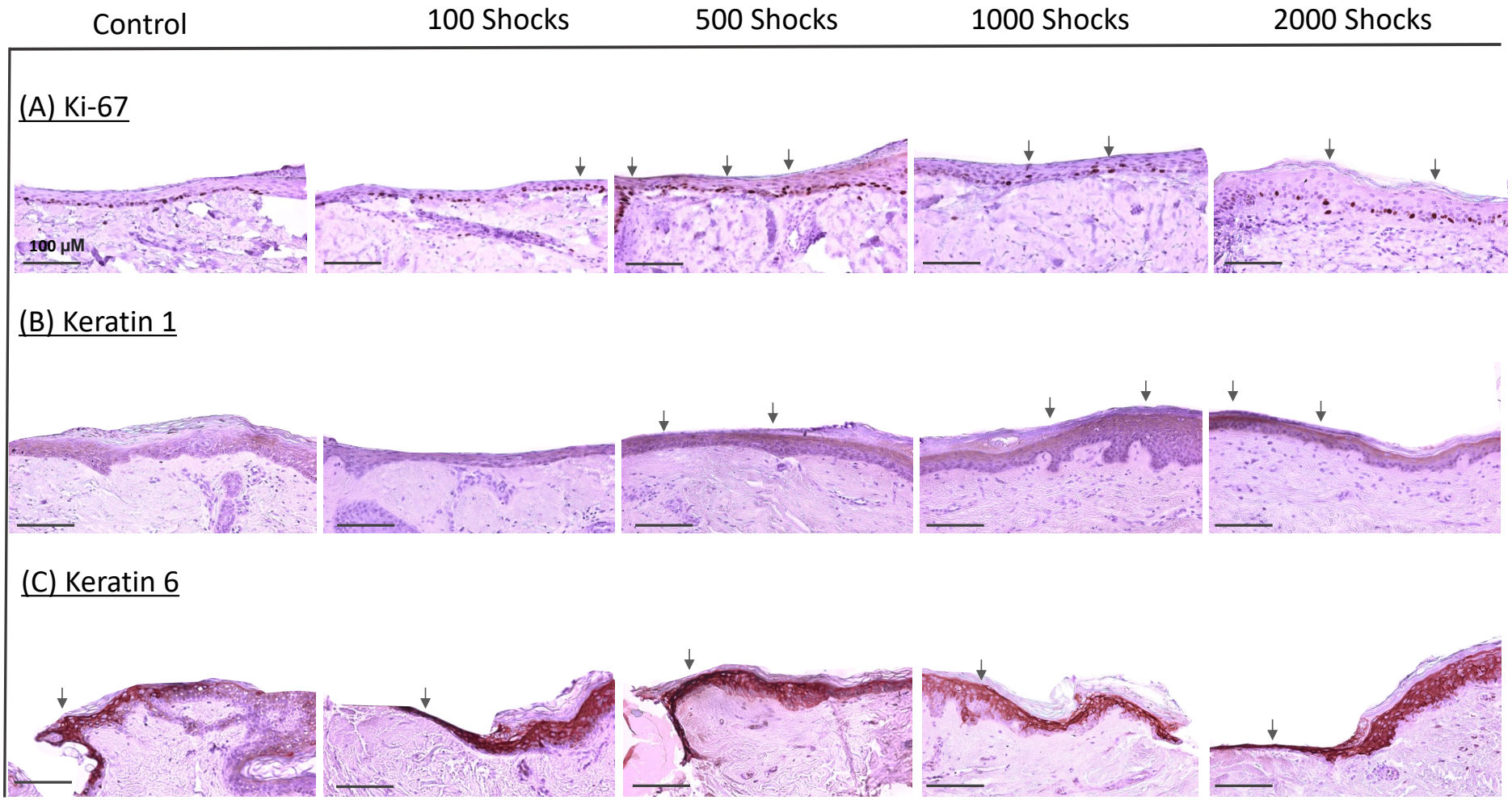

Figure 5.8: Markers of tissue proliferation and neo-epidermal formation in the epidermis of ex-vivo wound tissue following ESWT treatment. Representative microphotographs (x200 total magnification) of FFPE following staining for the presence of the (A) Ki-67 antigen, (B) Keratin 1 and (C) Keratin 6 in *ex-vivo* wound biopsy tissue sections following treatment with shockwave therapy, [n=3]. Black arrows represent positive IHC staining in tissue basal cells (A) and neo-epidermis (B, C).

5.3.5 ESWT increases the expression of angiogenic tissue markers.

Angiogenesis, the growth of novel blood vessels from pre-existing vasculature, is essential to provide the oxygen and nutrients required to support tissue repair (Veith et al., 2021). Platelet endothelial cell adhesion molecule (CD31) exists as a comprehensive marker to identify highly angiogenic and vasculogenic cells in human tissue (Chacko et al., 2015). In comparison, vascular endothelial growth factor (VEGF) is one of the most potent proangiogenic growth factors in human tissue, with the expression levels of VEGF present being known to significantly influence wound repair (Li et al., 2018). Therefore, the combined expression profiles of these two markers were assessed in this study to gain insight into the angiogenic stimulating capabilities of ESWT (Figure 5.9).

Relative angiogenic gene expression (qPCR) in human *ex-vivo* wound tissue was assessed following shockwave treatment at an energy flux density of 0.106 mJ/mm2, 5 shocks per second for a total of 0, 100, 500, 1000 or 2000 shocks (Figure 5.9). Overall, gene expression profiling analysis revealed a non-significant increase in angiogenic markers in the tissue of shockwave-treated human wound *ex-vivo* explants. Independently, CD31 transcripts presented a dose-dependent increase in expression following shockwave treatment (Figure 5.9: A). Increases in CD31 gene expression were witnessed following all ESWT treatment doses, however, the topmost increase in relative gene expression was witnessed in the higher treatment groups, presenting a non-significant average 1.34-fold (1000 total shocks) and 1.61-fold (2000 total shocks) increase (*One-way ANOVA, p=0.76, p=0.3*).

In parallel, *ex-vivo* wound tissue also demonstrated an ESWT-mediated increase in relative VEGF gene expression (Figure 5.9:B). While ESWT-treated samples did not exhibit a consistent dose-dependent increase as witnessed in relation to CD31 expression, all ESWT-treated *ex-vivo* wound samples did exhibit elevated VEGF expression. The highest increases in expression were witnessed at 100 and 1000 total shocks, showing a 1.57 and 2.2-fold increase in gene expression (*One-way ANOVA, p=0.9, p=0.57*). In combination, the increased expression of

these angiogenic markers demonstrates that shockwave therapy has the potential to enhance angiogenic capabilities in the human wound environment.

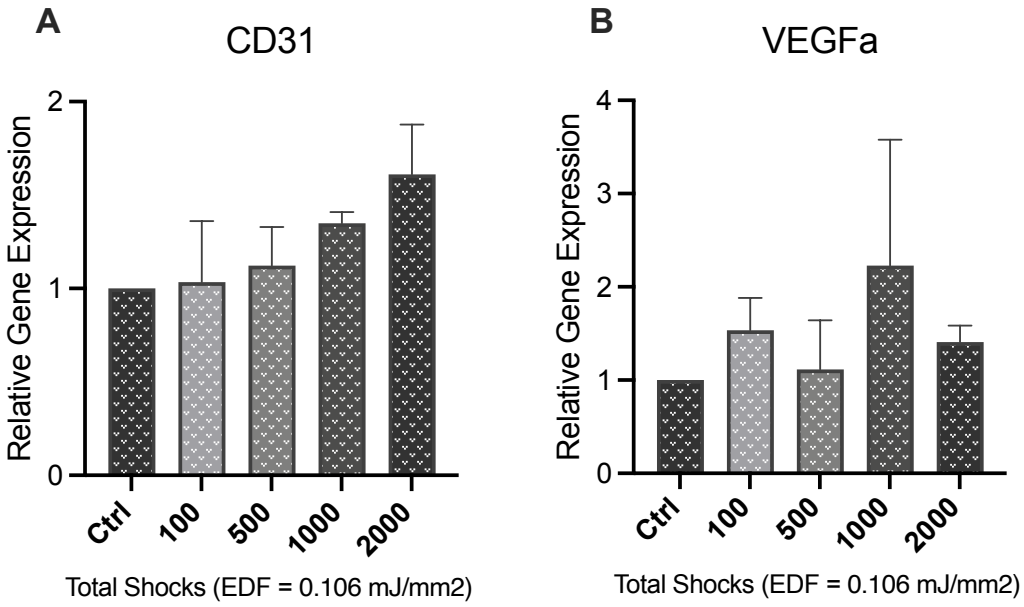

Figure 5.9: Relative gene expression tissue angiogenic markers following treatment with shockwave therapy. Gene expression profiling of (A) CD31 and (B) VEGFa (B), following shockwave treatment at an energy flux density of 0.106 mJ/mm2, 5 shocks per second for a total of 0, 100, 500, 1000 or 2000 shocks. Expression was assessed 6 hours post wounding/ESWT, according to qPCR quantification. Data (bars) represents the mean ± SEM of all tissue donors [n=3]. Mean, and statistical significance *was* determined using a one-way analysis of variance (ANOVA) followed by a Tukey post hoc test (*p>0.05*)

5.3.6 The effect of shockwave therapy on common wound bacterial isolates.

Previously published studies mostly focused on the effects of ESWT on mammalian cells and human tissue (Table 5.1). Fewer studies have explored the effect of shockwave therapy on microbial viability and antimicrobial sensitivity in common wound isolates. Based on known relevance to cutaneous healing and wound infection, four clinically isolated bacterial strains (Table 5.3) were selected for treatment with ESWT.

Investigated microbial strains included *Pseudomonas aeruginosa (PS1)*, multiple strains of *Staphylococcus aureus (*MRSA: MR1 and MSSA: MS4*)*, *Staphylococcus epidermidis (CN7)* and *Candida albicans (C.A; Table 5.3)*. Standardised cultures, both planktonic and biofilm derived, of all five microbial populations were assessed for viability prior to and following shockwave therapy at an energy flux density of 0.106 mJ/mm2, 5 shocks per second for a total of 2000 shocks using the PiezoWave2 multi-use 40.

Table 5.3: ID code, species identification and clinical origin of microbial strains selected for shockwave treatment using the PiezoWave2 multi-use 40 (linear FBL10x5 G2 adaptor).

ID Code	Species	Clinical origin
PS1	*Pseudomonas aeruginosa*	Leg Swab
MR1	*Methicillin-Resistant Staphylococcus aureus*	Leg Ulcer
MS4	*Methicillin Sensitive Staphylococcus aureus*	Leg Ulcer
CN7	*Staphylococcus epidermidis*	Leg Swab
C.A	*Candida albicans*	N/A

5.3.7 Shockwave treatment had no effect on the planktonic microbial culture viability of common wound isolates.

To assess the influence of shockwave therapy on common clinical wound isolates, ESWT was applied to planktonic cultures of clinically isolated strains of both *S. aureus* and *P. aeruginosa* at a density of 10^3, 10^5 and 10^7 colony-forming units per ml (CFU/ml; Figure 5.10). For each culture, ESWT treatment was applied at an energy flux density of 0.106 mJ/mm2, 5 shocks per second, for a total of 2000 shocks. In response to ESWT, no detectable impact on bacterial viability was observed for either bacterial species, regardless of initial culture density (*$p > 0.05$, paired t-test*).

Following this result shockwave therapy was tested on a wider range of clinical wound isolates, including methicillin suspectable *S. aureus* (MS4), commensal S. *epidermis* (CN7), and a commonly isolated fungal strain, *Candida albicans (*Figure 5.11*).* Specifically, planktonic microbial cultures were exposed to shockwave therapy at 10^5 colony-forming units per ml (CFU/ml). Again, exposure to ESWT at an EDF of 0.106 mJ/mm2, 2000 total shocks exhibited no detectable effect on microbial viability (*$p > 0.05$, paired t-test*).

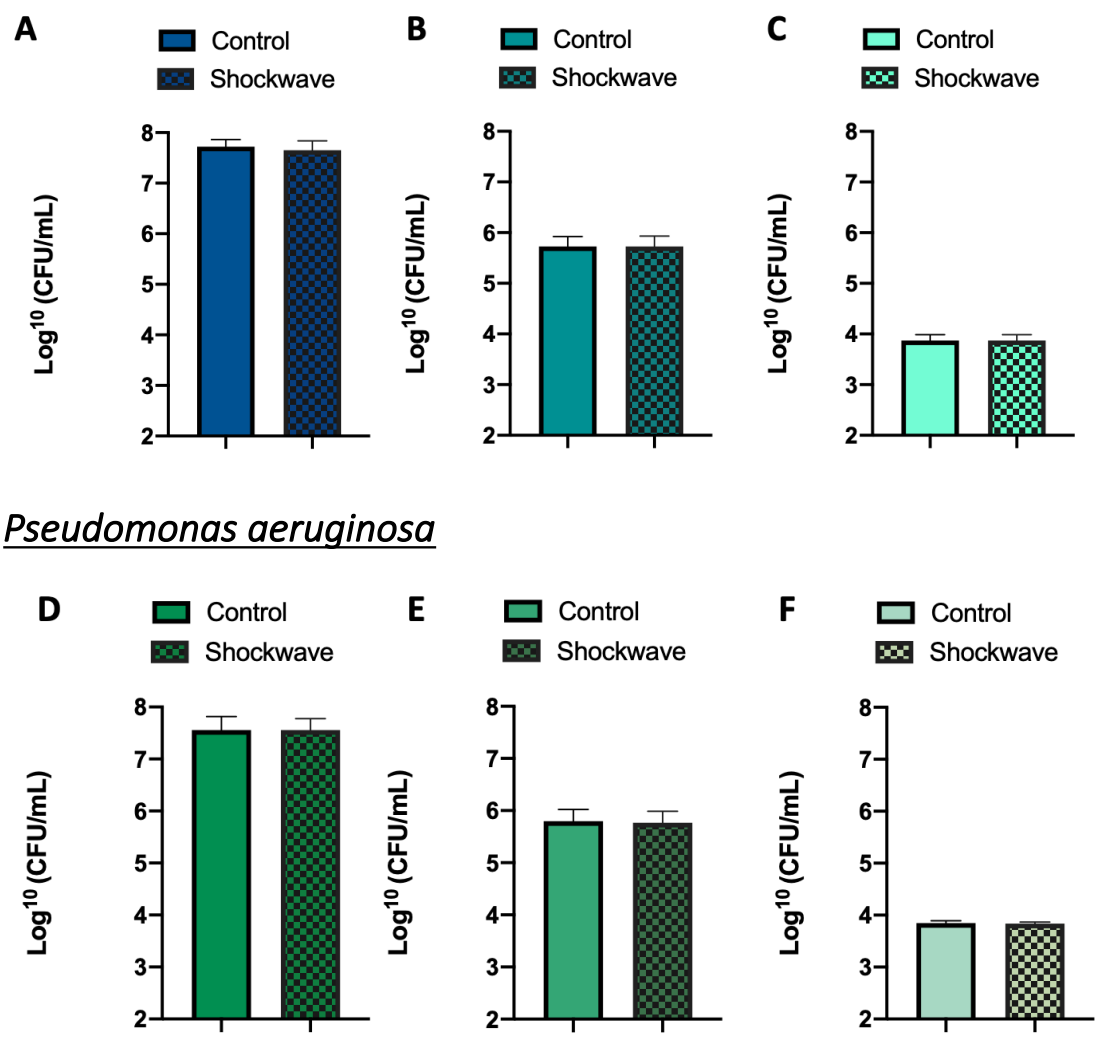

Figure 5.10: The influence of shockwave therapy on the viability of planktonic cultures at multiple densities. Number (Log^{10} CFU/ml) of viable planktonic *S. aureus* (MR1) (A, B, C) and *P. aeruginosa* (PS1) (D, E, F) following shockwave treatment at an EDF of 0.106 mJ/mm2, 5 shocks per second for a total of 2000 shocks. Adjusted bacterial starting concentrations varied from between, 1-5 x 10^3, 1-5 × 10^5 and 1-5 × 10^7 colony-forming units per ml (CFU/ml). Data represents the mean ± SEM, *p > 0.05, paired t-test*. Data were obtained from four independent experiments (*n* = 4 per treatment). LoD = 10^2 CFU/mL.

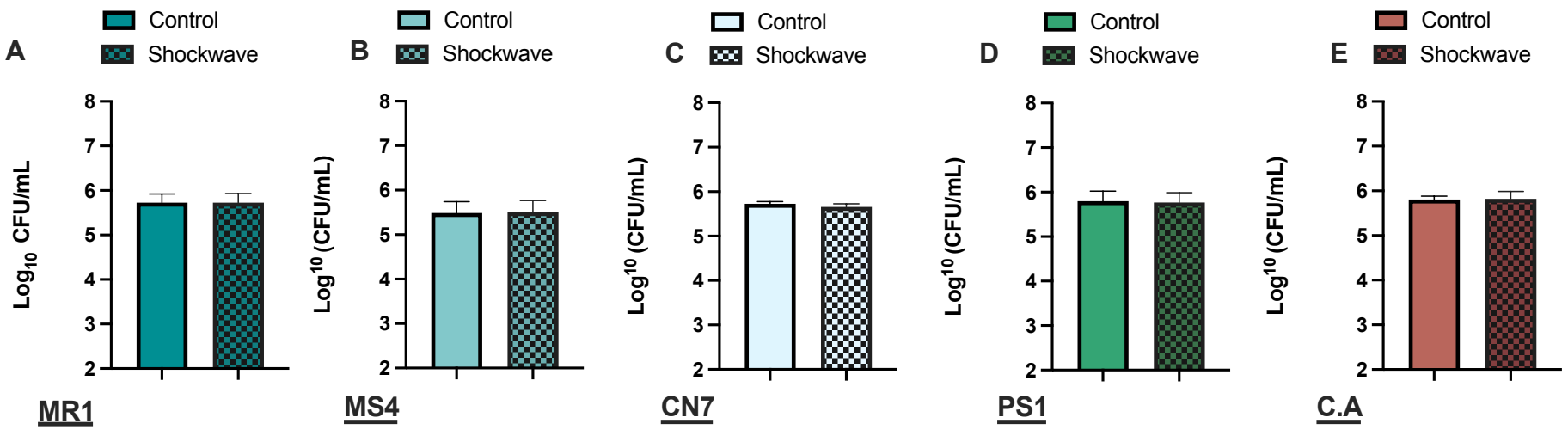

Figure 5.11: The influence of shockwave therapy on the planktonic culture viability of frequent wound isolates. Number (Log^{10} CFU/ml) of viable planktonic MR1 (A), MS4 (B), CN7 (C), PS1 (D) and C.A (E) following shockwave treatment at an energy flux density of 0.106 mJ/mm2, 5 shocks per second for a total of 2000 shocks. Adjusted bacterial started concentrations were between 5×10^5 and 1×10^6 colony-forming units per ml (CFU/ml). Data shows the mean ± SEM. $p > 0.05$, paired t-test. Data were obtained from four independent experiments ($n = 4$ per treatment). LoD = 10^2 CFU/mL.

5.3.8 ESWT does not affect the viability of bacterial biofilms from common wound pathogens.

In the chronic wound environment, common pathogens, including *S. aureus* and *P. aeruginosa* often aggregate to form biofilm structures (Wilkinson and Hardman, 2020). Bacteria present within these biofilms become encapsulated in a matrix of extracellular polymeric substances (Wilkinson and Hardman, 2020). Biofilms protect microbes from environmental threats, while hampering the host immune response (Omar et al., 2017). Shockwave treatment was applied to bacterial biofilms at an energy flux density of 0.106 mJ/mm2, 5 shocks per second for a total of 2000 shocks. Bacterial enumeration was used to determine the number of viable bacterial present before and after treatment. Treatment was initially applied to the bacterial biofilms of both *S. aureus* and *P. aeruginosa*, following 24 hours of growth post-seeding (*Figure 5.12*). As in planktonic cultures, exposure to ESWT had no detectable impact on bacterial biofilm viability in either of the tested wound isolates (*p > 0.05, paired t-test*).

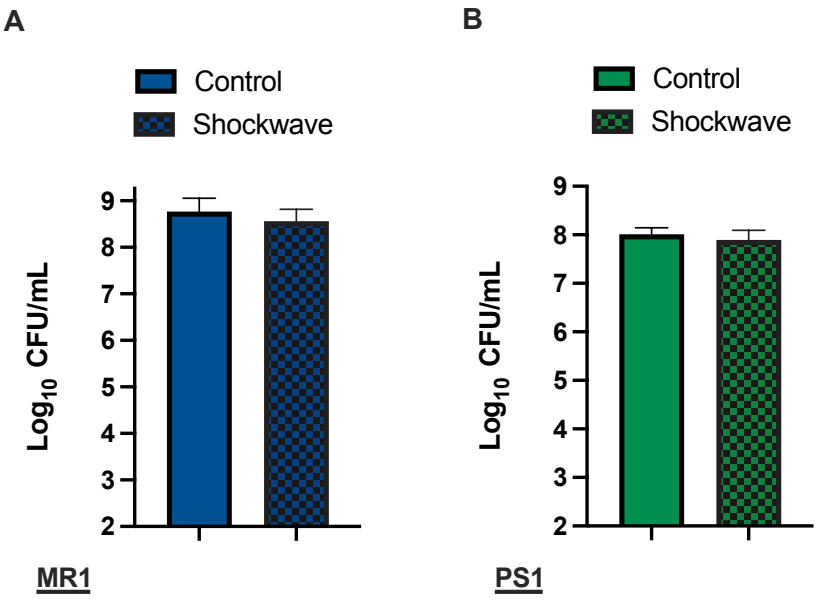

Figure 5.12: The influence of shockwave therapy on the bacterial biofilms of frequent wound pathogens. Number (Log^{10} CFU/ml) of viable biofilm-derived (A) MR1 and (A) PS1 following the treatment of 24-hour incubated colony biofilms with shockwave therapy at an energy flux density of 0.106 mJ/mm2, 5 shocks per second for a total of 2000 shocks. Data show the mean ± SEM. *P > 0.05, paired t-test*. Data were obtained from three individual experiments. LoD = 10^2 CFU/mL.

5.3.9 Treatment with shockwave therapy increases antimicrobial sensitivity in common wound isolates.

Following the ESWT treatment of planktonic and biofilm-derived bacterial cultures, with no observed effect of microbial viability, selected bacterial strains were subject to treatment with ESWT in combination with antimicrobial therapy. Four antibiotic agents commonly prescribed for diabetic foot ulcer infection were selected (Table 5.4). Microbial breaking points were identified by minimum inhibitory and bactericidal concentration testing. Bacterial species were incubated with/without prior exposure to shockwave therapy at the break point. Multiple species exhibited a significant increase in antimicrobial susceptibility when treated with a combination of antimicrobial and shockwave therapy (Figure 5.13 – 5.16).

Table 5.4 Antimicrobial agents selected for co-treatment of common wound pathogens with shockwave therapy.

Antimicrobial	Class	Mechanism of Action
Ciprofloxacin	Fluoroquinolone	Inhibition DNA separation and cell division via inhibiting a type II topoisomerase (DNA gyrase) and topoisomerase IV (Xu et al., 2021).
Gentamicin	Aminoglycoside	Inhibition of the bacteria 30S ribosomal, inhibiting protein synthesis (*Garneau-Tsodikova et al., 2016)*.
Flucloxacillin	Penicillin	Inhibition of bacterial cell wall synthesis by peptidoglycan polymer chain cross-linkage (Munita et al., 2016)
Amoxicillin	Penicillin	Inhibition of bacterial cell wall synthesis by peptidoglycan polymer chain cross-linkage (Munita et al., 2016)

When comparing ciprofloxacin/ESWT and ciprofloxacin treatment alone, *Pseudomonas aeruginosa* exhibited a significant 4-log reduction in culture viability, below the limit of detection (2 x $\log^{10}$ CFU/mL) (*p<0.001,* paired t-test) (Figure 5.13: A). A significant multi-log

viability reduction was also identified in MRI and CN7 isolates following treatment with combined ciprofloxacin/ESWT compared to ciprofloxacin treatment alone, with a retrospective 3-log and 2-log viability reduction (*p=0.001, p=0.0006,* paired t-test). No effect on bacterial growth or viability was identified in the MS4 isolate following combined shockwave and ciprofloxacin treatment *(p=0.75,* paired t-test*).* Again, in the gentamicin group, multiple isolates presented a significant reduction in bacterial viability with combined ESWT therapy, with MS4 demonstrating the greatest (5-log) viability reduction (*p<0.001, paired t-test*). Relative to treatment with gentamicin alone, both PS1 and MR1 also demonstrated a significant log reduction in viability following combined ESWT (*p<0.05, paired t-test*).

Following this, simultaneous experiments on the Gram-positive clinical isolates (MR1, MS4 and CN7), were carried out using flucloxacillin/ amoxicillin in combination with ESWT (Figure 5.14) In response, it was observed that combined flucloxacillin/ESWT had a significant 1-log (MR1), and 2-log reduction (MS4) on bacterial viability compared to antimicrobial therapy alone (*p=0.0139, p=0.0009*, *paired t-test*). No reduction of CN7 viability was observed in response to antimicrobial therapy or combined shockwave therapy (*p>0.05, paired t-test*) (Figure 5.14: A, B). Within the isolates treated with amoxicillin, no observable differences were identified in bacterial viability following treatment with antimicrobial alone or in combination with ESWT. Collectively, these findings indicate that ESWT may facilitate increased antimicrobial sensitivity in common wound isolates.

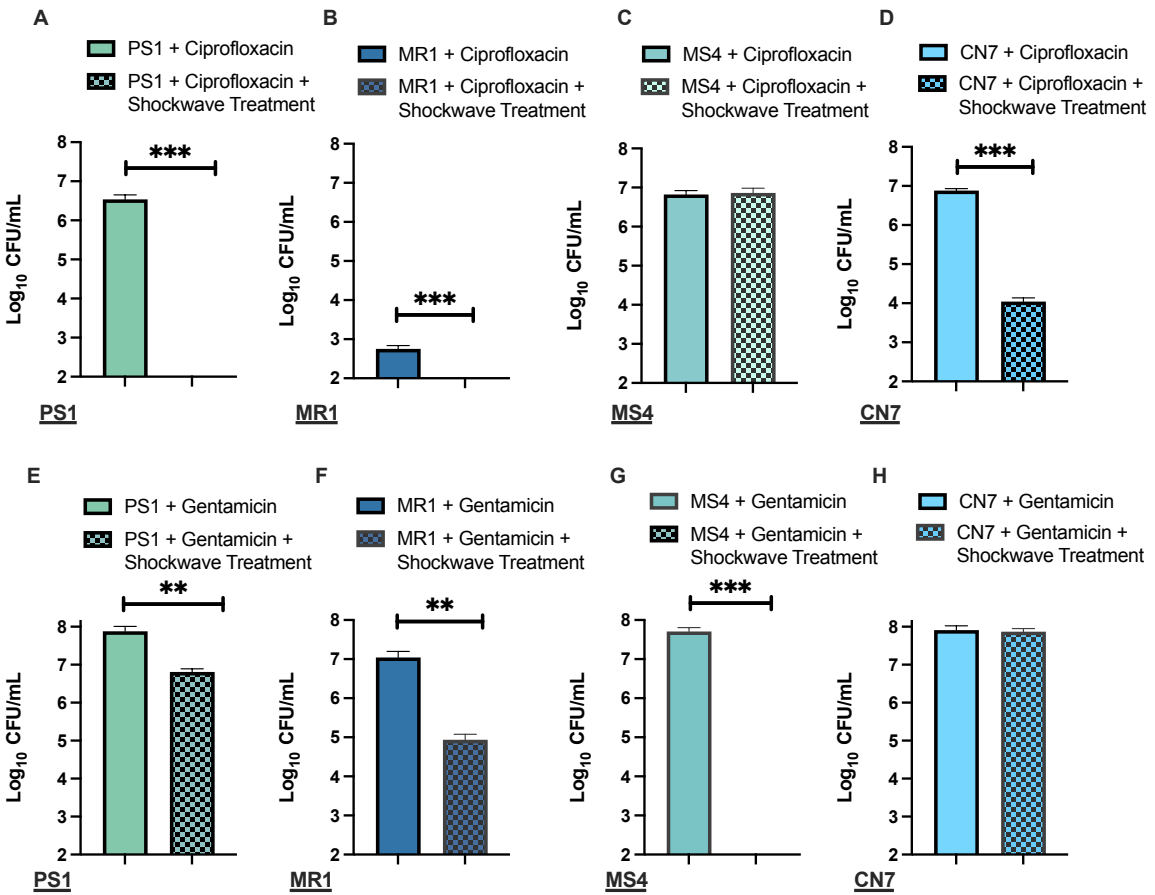

Figure 5.13: Bacterial viability following treatment with antimicrobial and combined shockwave therapy. Number (Log^{10} CFU/ml) of viable planktonic PS1 (A, E), MR1 (B, F), MS4 (C, G) and CN7 (D, H) following a 24-hour incubation with either Ciprofloxacin (A, B, C, D), or Gentamicin (E, F, G, H) alone or in combination with shockwave treatment at an energy flux density of 0.106 mJ/mm^2, 5 total shocks per second for a total of 2000 shocks. Bacterial starting concentration ranged 5×10^5 and 1×10^6 colony forming units per ml (CFU/ml). Data show the mean ± SEM. $P > 0.05$, paired t-test, *$p < 0.05$, **$p < 0.01$, ***$p < 0.001$, [n=4]. LoD = 10^2 CFU/mL.

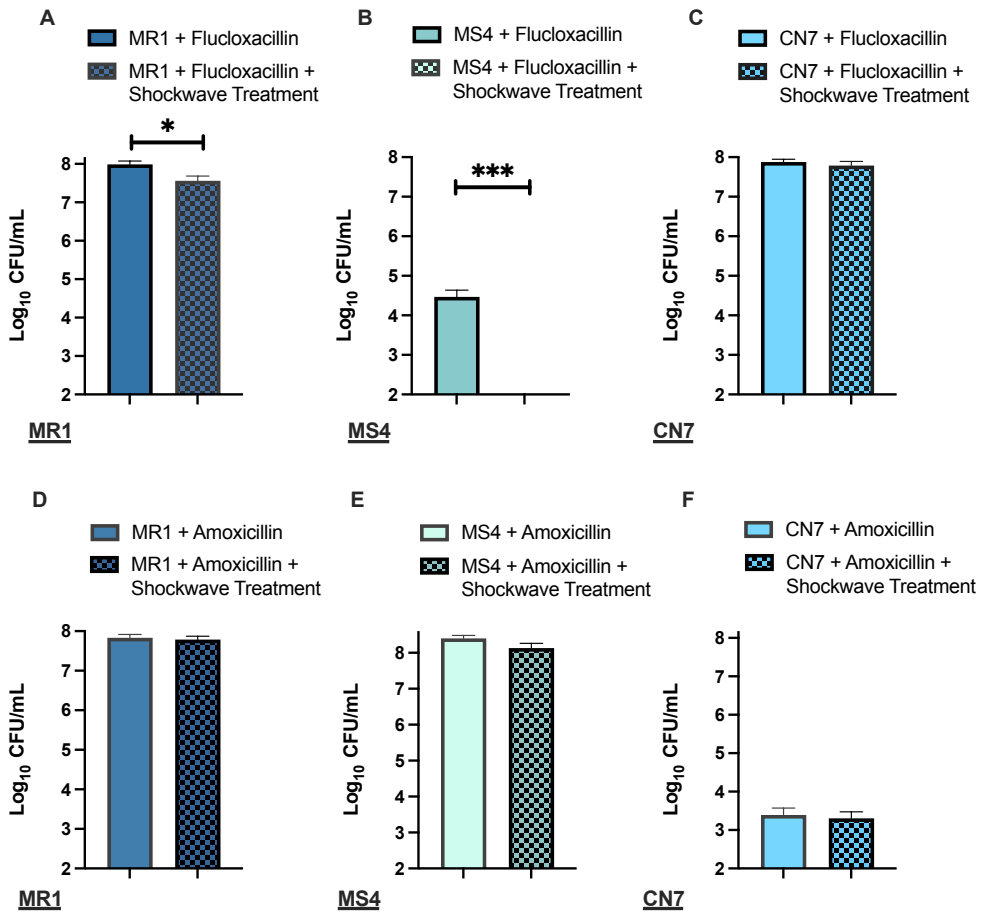

Figure 5.14: Bacterial viability following treatment with antimicrobial and combined shockwave therapy. Number (Log^{10} CFU/ml) of viable planktonic MR1 (A, C), MS4 (B, E) and CN7 (C, F) following a 24-hour incubation with either Flucloxacillin (A, B, C), or Amoxicillin (D, E, F) alone or in combination with shockwave treatment at an energy flux density of 0.106 mJ/mm^2, 5 total shocks per second for a total of 2000 shocks. Bacterial starting concentration ranged from 5×10^5 and 1×10^6 colony forming units per ml (CFU/ml). Data show the mean ± SEM. P > 0.05, paired t-test, **p < 0.05, **p < 0.01, ***p < 0.001, [n=4]*. LoD = 10^2 CFU/mL.

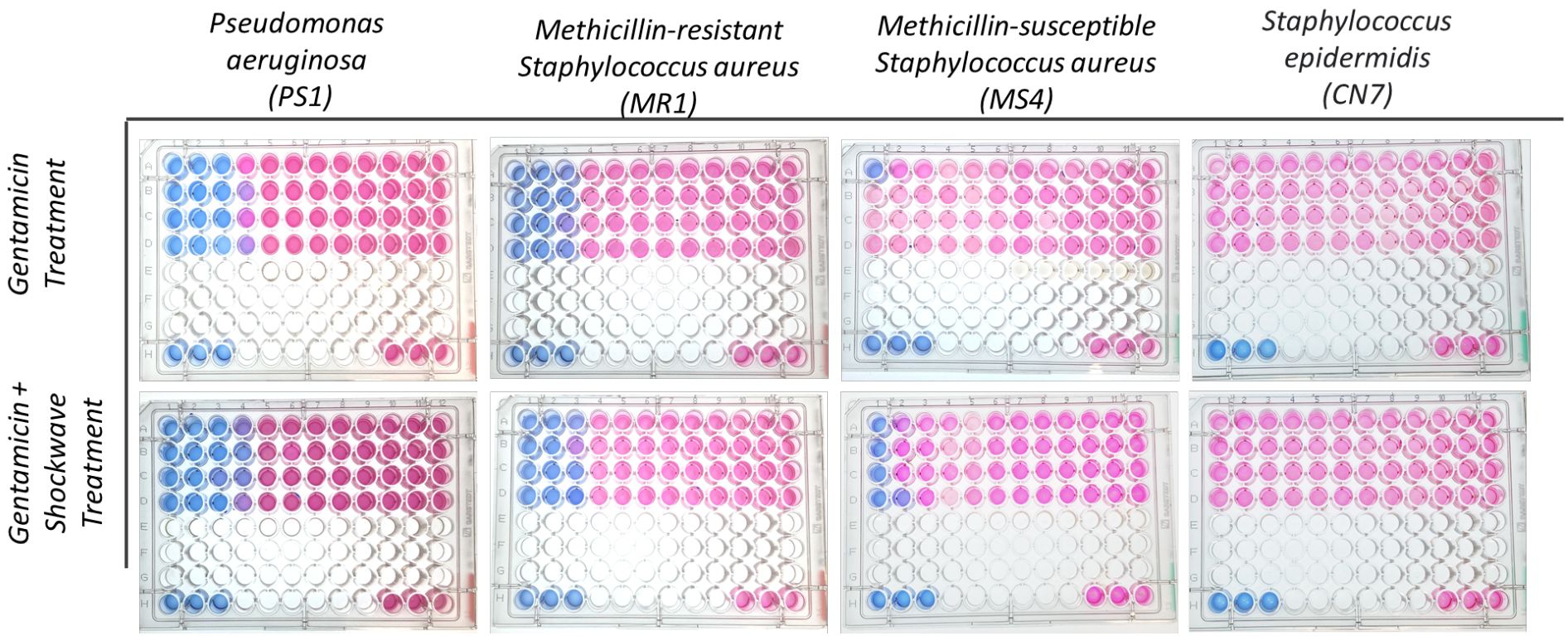

Figure 5.15: Bacterial viability following treatment with antimicrobial and combined shockwave therapy. Representative images of bacterial viability following a 24-hour incubation with either Ciprofloxacin alone or in combination with shockwave treatment at an energy flux density of 0.106 mJ/mm^2, 5 total shocks per second for a total of 2000 shocks. This conversion of blue-due into pink resorufin is indicative of the presence of viable cells.

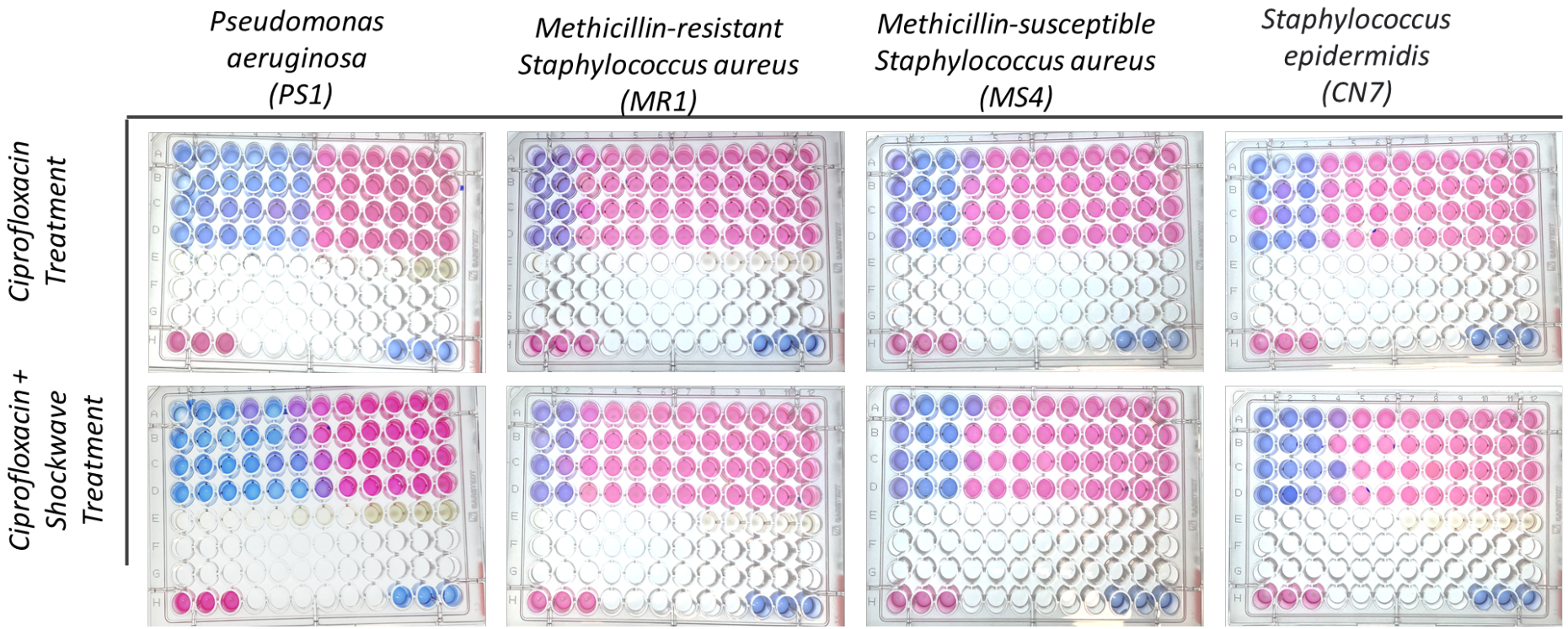

Figure 5.16: Bacterial viability following treatment with antimicrobial and combined shockwave therapy. Representative images of bacterial viability following a 24-hour incubation with either Ciprofloxacin alone or in combination with shockwave treatment at an energy flux density of 0.106 mJ/mm^2, 5 total shocks per second for a total of 2000 shocks. This conversion of blue-due into pink resorufin is indicative of the presence of viable cells.

5.3.10 A longitudinal pilot study assessing the role of extracorporeal shockwave therapy on the clinical diabetic foot ulcer microbiome: an introduction of adaptive sequencing.

This thesis section focuses on a pilot study assessing the longitudinal influence of ESWT on the diabetic foot ulcer microbiome.

5.3.11 Nanopore adaptive sampling for host DNA depletion significantly improves bacteria prokaryotic sequencing depth.

As demonstrated within previous chapters, long-read nanopore metagenomic sequencing provides a promising technique for microbial profiling. It may be particularly beneficial for clinical studies exploring how microbial composition may influence patient wound outcomes (Bharti and Grimm, 2021; Kwa et al., 2023). However, thus far, clinical wound sequencing profiles have commonly exhibited high relative abundances of contaminating host DNA (> 90%), decreasing overall microbial resolution (Chapter 3). The recent introduction of ONT's integrated adaptive sampling methodology offers selective DNA depletion, directly rejecting DNA molecules during real-time sequencing without the need for specialized sample preparation (Marquet et al., 2022). Therefore, host DNA depletion methods were optimised to increase total microbial sequencing depth and provide higher taxonomic profiling sensitivity. Twelve wound swab DNA samples were sequenced using both standard and adaptive sequencing methods, and profiles directly compared. Depletion experiments were performed using a human genome reference (GDF_000001495.39).

Read-length histogram summaries were compared for sequencing runs conducted using both standard (Figure 5.17:A) and integrated adaptive techniques (Figure 5.17:B). For the standard run, the average N50 completed read base length was 3.3 kb, with the overall run containing very few reads below 1.5kb. In contrast, the run conducted using integrated host DNA depletive adaptive sequencing contained a high number of short-read sequences (450-1000bp), representing target-aligned reads expelled from the sequencing pore (Figure 5.17:B). Therefore, whilst both runs contained between 16.1 and 18 estimated gigabases (Gb) of sequence, the adaptive sequencing run total read count was 12.19 M, whilst the standard

sequencing run contained only 5.83 M reads. The average base length for adaptive sampling voltage reversal was 506 bps, whilst the N50 completed read base length remained at 3.35 kb. The rejection of target sequence aligned reads, resulted in this initial peak of short adaptive sampling voltage reversed reads. For depletion, the minimum number of bases required for ejection is ~450, but up to 4000 bases can be read before a strand is ejected. The selection of 'rejected reads' contained within this initial peak were then filtered and removed for the remaining data analysis.

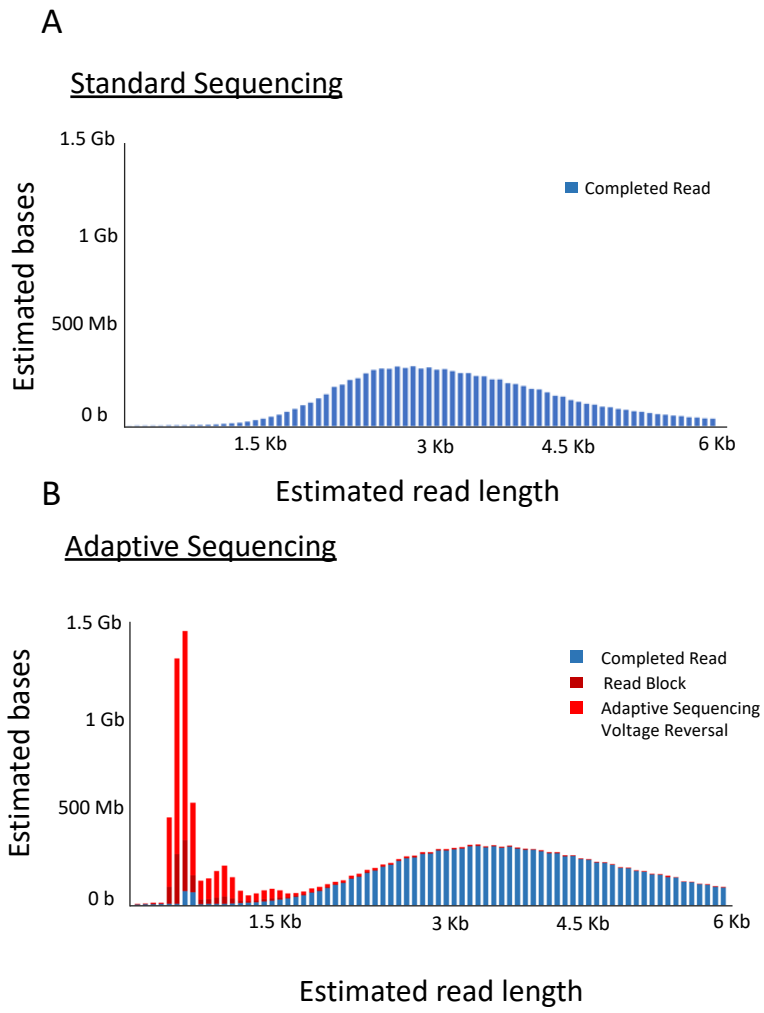

Figure 5.17: Representative read-length histogram summaries for nanopore sequencing runs. Histograms represent sequencing runs conducted using both standard (A) and adaptive sequencing techniques (B). Completed reads are represented in blue, while reads subject to pore blockage or adaptive sequencing voltage reversal are visualised in red, [*standard n=12, adaptive n=12*].

5.3.12 Adaptive sampling significantly reduces host DNA contamination without altering microbial composition profile.

To evaluate the suitability of host depletion for clinical wound metagenomic sequencing, samples subject to adaptive sampling were directly compared to a non-adaptive standard sequencing control run. Amongst these two experimental groups, the relative prevalence of host contamination and microbial sequences were examined. Overall, standard experiments contained 78% human-aligned reads, with bacterial reads accounting for only 21% of the total read population (Figure 5.18: A, B). In the run subject to adaptive sampling, this host contribution was dramatically reduced, with only 8% of the total completed filtered reads being classified as human, and bacterial reads contributing over 91% of the total read population. Overall, in the adaptive run, the 'rejected' read fraction contained approximately 90% of all human-aligned reads, indicating successful and highly selective depletion.

In addition to the total bacterial contribution, microbial community composition, including total and relative genus and species contributions were assessed to identify potential bias introduced as a result of adaptive sampling. Moreover, the run subject to host depletion exhibited extremely similar relative contribution of the top 10 bacterial genera and species. Using both standard and adaptive sequencing techniques, *Anaerococcus (18.7% v 18.6%), Staphylococcus (12.5% v 12.3%)* and *Enterococcus* (10.8% v 10.7%) were identified as the three most abundant genera across both sequencing runs (Figure 5.18: C). Both standard and adaptive sequencing methods also simultaneously identified *Staphylococcus aureus (11.5% v 11.4%), Enterococcus faecalis (10.5% v 10.4%), Finegoldia* magna *(9.9% v 9.9%)* as the top three species across all wound samples (Figure 5.18: D).

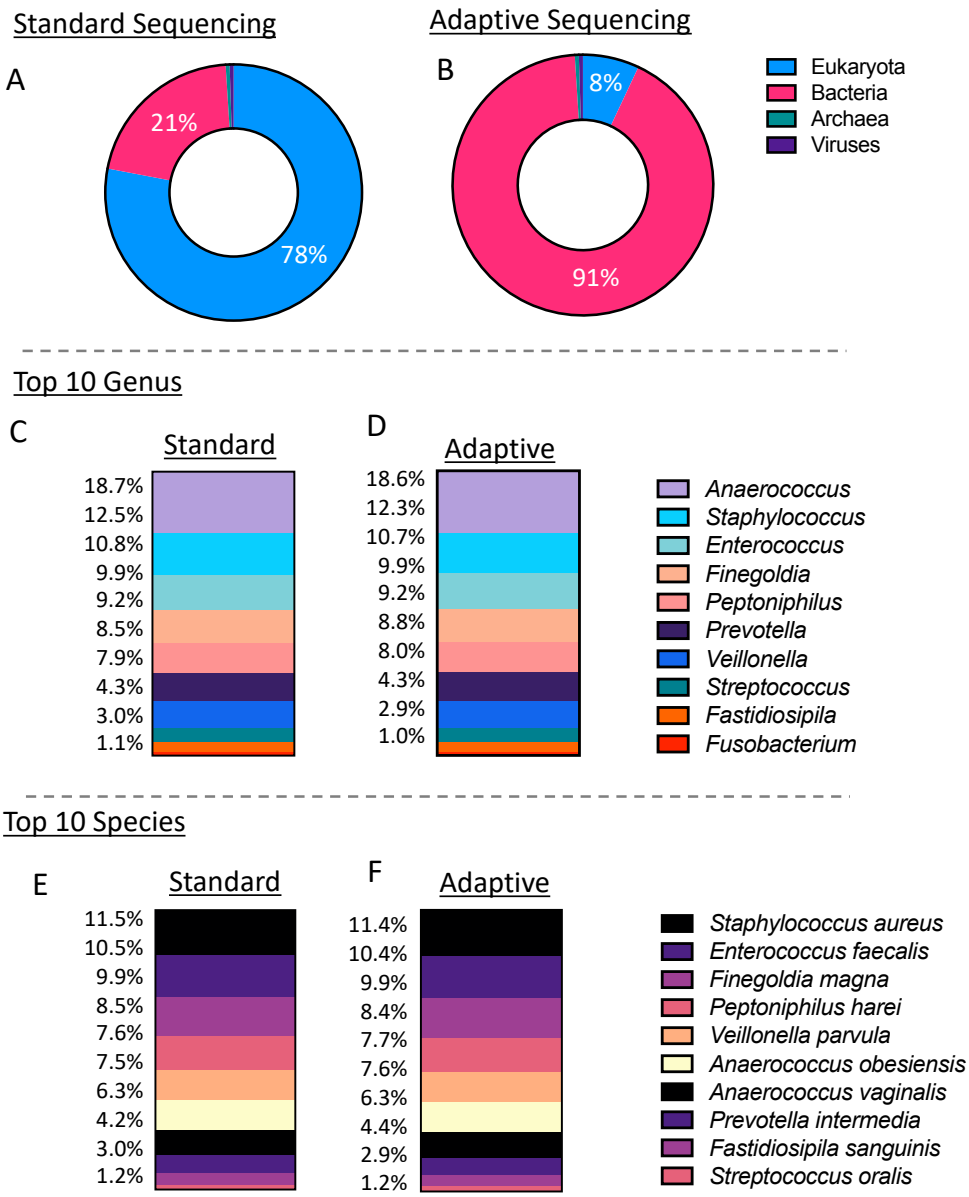

Figure 5.18: The relative contribution of the super kingdoms and bacterial genera and species to the overall sequencing-derived wound community population. The relative proportions of eukaryotes, bacteria, archaea, and viruses to overall wound community structures using both standard (A) and adaptive (B) techniques. The relative microbial proportions of the top 10 bacterial genera and species across runs were sequenced using both standard (C, E) and adaptive (D, F) techniques. [*standard n=12, adaptive n=12*].

5.3.13 Adaptive sampling drastically increases microbial sequencing depth and diversity, allowing enhanced OTU identification.

Following the assessment of relative microbial genera and species contribution, total microbial abundance was investigated to assess the power of adaptive sequencing to enhance microbial sequencing yield and depth. When directly compared to the control sequencing group, adaptive sequencing techniques presented an overall 2.26-fold increase in bacterial reads (
*Figure **5.19***:A/B). Upon direct comparison to standard control samples, the run subject to host depletion displayed a highly consistent increase in sequencing reads across all bacterial genera and species (
*Figure **5.19***:A, B). Within the top 10 genera alone, a 2.3, 2.2 and 2.2-fold increase in *Anaerococcus, Staphylococcus* and *Enterococcus* reads were observed. In parallel, across the top 10 species, a 2.2, 2.3 and 2.2-fold increase in *Staphylococcus aureus*, *Enterococcus faecalis* and *Finegoldia magna* reads were identified. In relation to alpha diversity, an average 1.3-fold increase in sample alpha diversity according to both ACE and Chao1 diversity metrics was observed. However, neither of these increases in diversity proved to be significant ($p>0.05$, Mann-Whitney test) (
*Figure **5.19***:C).

This increase in sample diversity was further correlated with an increase in identified unique bacterial OTUs (*Figure 5.20*). When assessing runs based on the read filter of >1000 reads per individual OTU present, adaptive sequencing techniques observed the presence of a total 57 unique bacterial OTUs across all samples, a number that was reduced to only 37 in the parallel standard sequencing run.

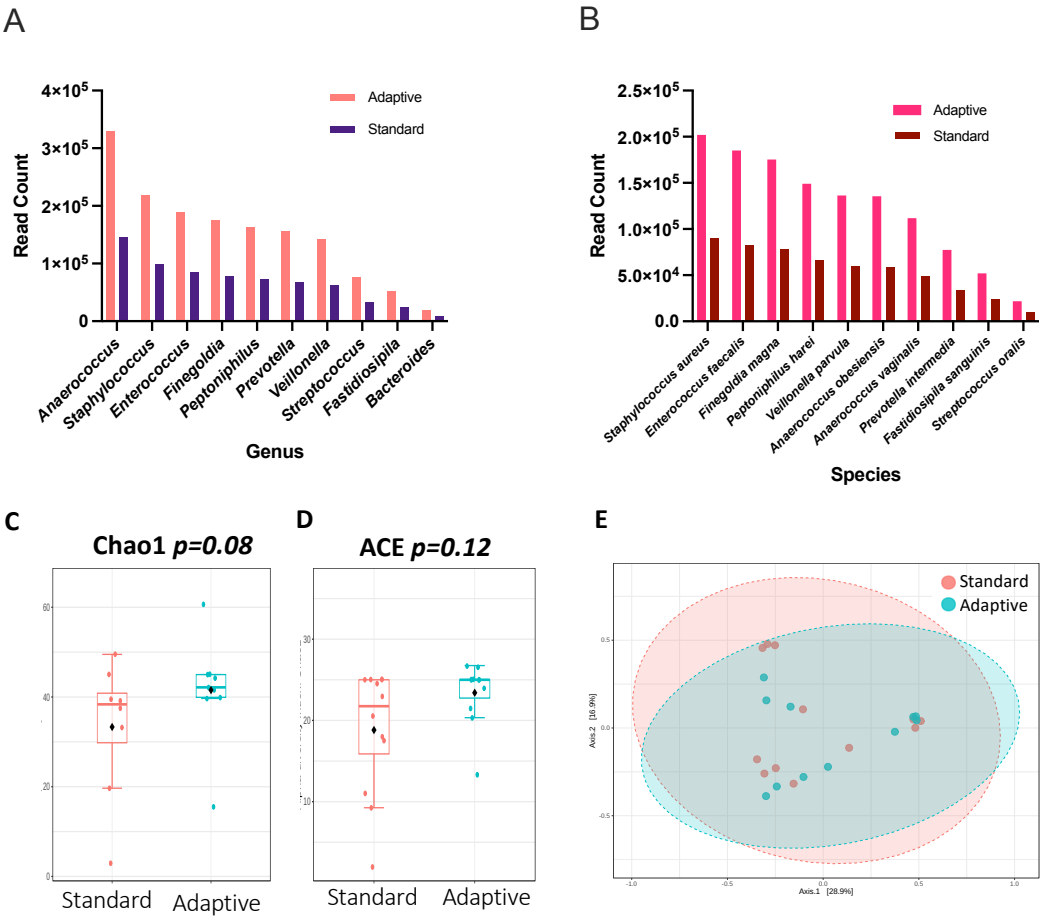

Figure 5.19: Community analysis using total abundance and alpha/ beta diversity of the sequenced wound microbiome with and without the integration of adaptive sequencing. Total read count and sequencing depth of the top 10 bacteria genera (A) and species (B) across runs profiled using both standard and adaptive sequencing techniques. Alpha diversity of standard and adaptive sequencing runs measured using Chao1 (C) and ACE (D) metrics (Mann-Whitney: *p = 0.08, 0.12*). Outer regions on each box plot represent 25/75th percentiles, the diversity median is visualised by a solid line and the group mean by a black diamond. Whiskers extend to the furthest points up to 1.5x interquartile range (IQR). Beta diversity measured via the Bray-Curtis index (E) and presented in a PCoA plot (PERMANOVA: p = 0.9). [*standard n=12, adaptive n=12*].

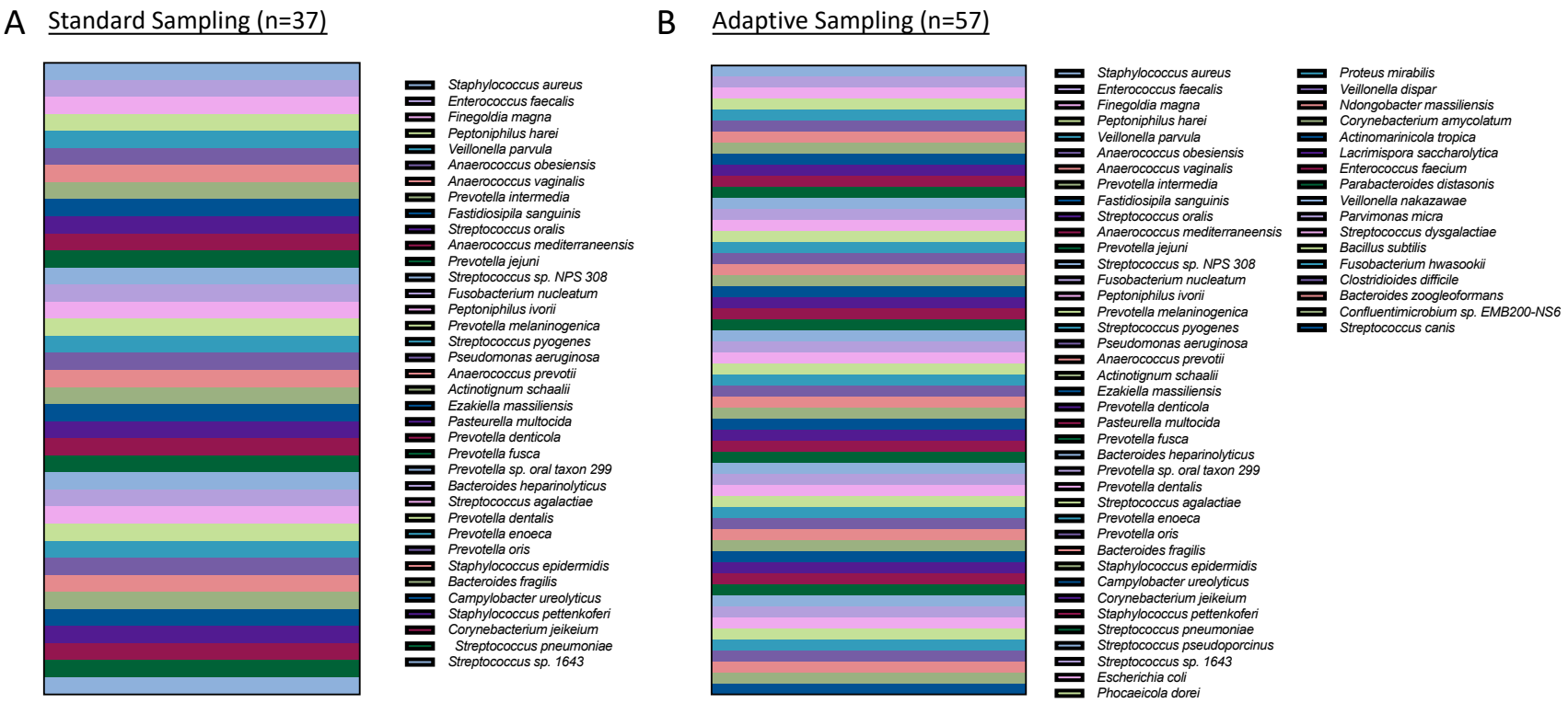

Figure 5.20: Unique OTUs identified across wound profiling sequencing runs. The number of unique OTUs (>1000 total reads per individual OTU) identified across sampling runs conducted using both standard (A) and host depletion adaptive sequencing (B) techniques, [*standard n=12, adaptive n=12*].

5.3.14 A longitudinal pilot study assessing the role of extracorporeal shockwave therapy on the clinical diabetic foot ulcer microbiome.

Following the optimisation of adaptive sequencing techniques, a longitudinal pilot study assessing the role of extracorporeal shockwave therapy on the clinical diabetic foot ulcer microbiome was conducted. At the time of trial enrollment, all participants presented clinically with a non-infected diabetic foot ulcer (Table 5.1). Within this pilot study, 24 wound swabs from a total of 6 patients were collected over a series of four individual time points: baseline, 1 week, 6 weeks and 12 weeks post-trial enrollment and treatment (Figure 5.21). Three participants were assigned to the group receiving ESWT, whilst three were assigned to the control 'sham' treatment group. ESWT was administered at an EFD of 0.106mJ/mm2, 5 pulses/second at a penetration depth of 5mm, the total number of shocks per donor was calculated by multiplying the ulcer surface area (mm^2) by 500. Each intervention was delivered across three 30-minute sessions over 7 days+/-9 at three separate intervals within the first week of trial enrolment. At each visit, wound swabs were collected, and genomic DNA extracted for microbiome sequencing. The samples within this study generated a combined 1,914,489 microbial reads spanning 6562 operational taxonomic units (OTU), from three distinct domains: bacteria (99%) eukaryotes (1%) and archaea (1%). The mean read number observed per sample was 79,770 reads.

Table 5.5: Participant Characteristics for ESWT Pilot Study

Donor Number	Age	Sex	Diabetic Status	Wound Status
Donor 01	58	Male	Positive	Non-infected
Donor 02	80	Male	Positive	Non-infected
Donor 03	58	Male	Positive	Non-infected
Donor 04	33	Male	Positive	Non-infected
Donor 05	68	Male	Positive	Non-infected
Donor 06	64	Male	Positive	Non-infected

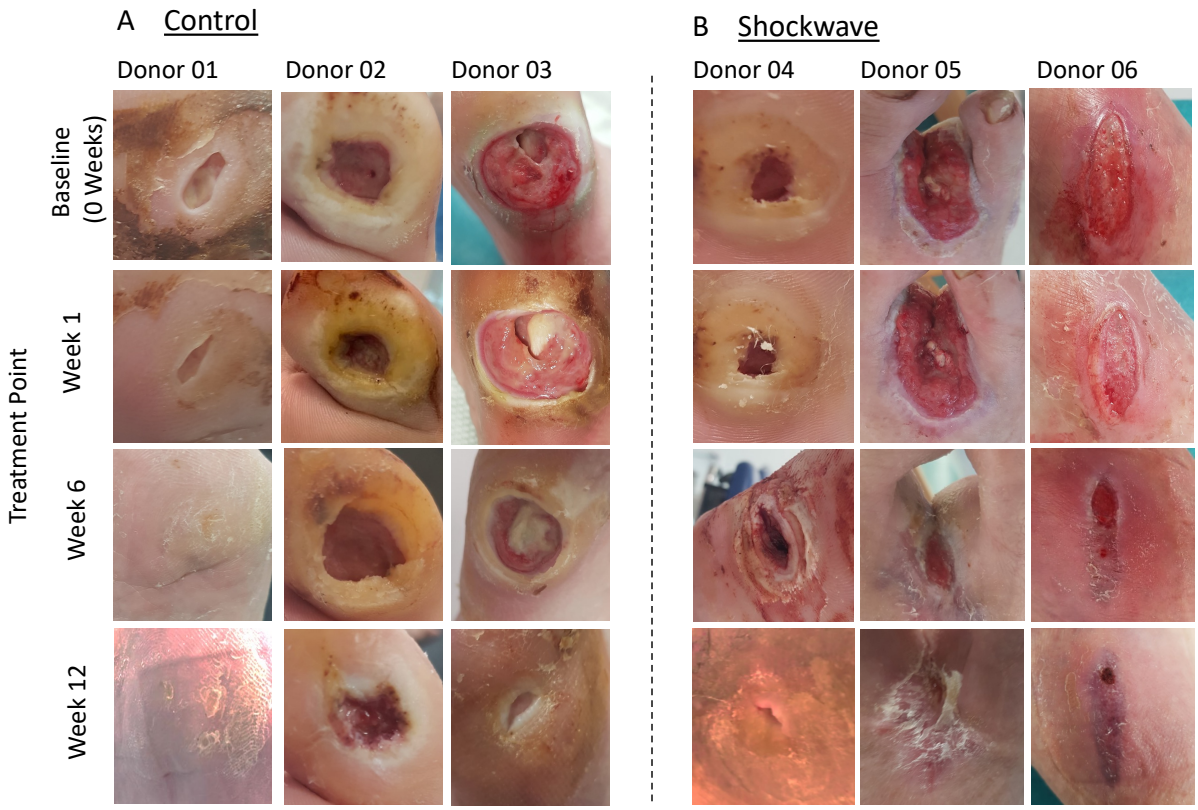

Figure 5.21: Representative images of participant wounds enrolled within the current study. Participants were stratified in either the control 'sham' (A) or the shockwave-treated group (B). Swabs of the wound bed were collected longitudinally using the Levine swabbing technique at baseline, one, six- and 12 weeks post-trial enrolment/treatment.

5.3.15 Microbial community profiles showed a strong association with individual donors.

Initially, microbial community composition was investigated across all participant wound samples. Participants were classified according to their treatment status (control/shockwave), and data was subsetted according to treatment phase. Following this, taxonomic visualisation was performed to assess the relative contribution of the top 50 most dominant species (Figure 5.22).

Across all participant wound profiles*, Staphylococcus aureus, Pseudomonas aeruginosa, Enterococcus faecalis, Citrobacter koseri, Finegoldia magna and Peptoniphilus harei* were determined to be the most abundant overall taxa. As the topmost dominant species*, Staphylococcus aureus* accounted for an average 15% of total reads across all collected samples. However, substantial variation in this relative contribution was observed, with some samples presenting 100% *Staphylococcus aureus* assigned reads (Figure 5.22:A, Donor 01: Baseline), whilst other specimens frequently exhibited non-detectable levels of *Staphylococcus aureus (*Figure 5.22*:B,* Donor 06: Baseline*/* week one). Similarly*, Pseudomonas aeruginosa,* which presented as the second most dominant taxa, accounted for an average of 12.3% of reads across all collected samples. However, this contribution was donor-specific, for example, Donor 02 presented an overall average 33.7% relative *Pseudomonas aeruginosa* abundance across all time points, whilst Donor 04, presented a 0.1% relative *Pseudomonas aeruginosa* read contribution.

This trend of donor-specific taxa profiling was evident throughout the pilot study, where microbial profiles segregated strongly according to donors, rather than treatment status or time point. For example, for Donor 01 and Donor 06, both participant profiles were heavily defined by their relative contribution of *Staphylococcus aureus. For Donor 02,* the profile centred strongly around the altering contribution of three dominant species, including *Pasteurella multocida, Proteus mirabilis and Streptococcus agalactiae. In contrast for Donor 05,* profiles centred strongly according to the varying contribution of *Enterococcus faecalis, Citrobacter koseri and Finegoldia magna.* Overall, each donor exhibited a collection of dynamic timepoint-based profiles. Whilst the profiles of those treated with ESWT appeared

to transition more as time progressed, globally, no consistent specific shockwave-dependent alterations in microbial profiles could be identified.

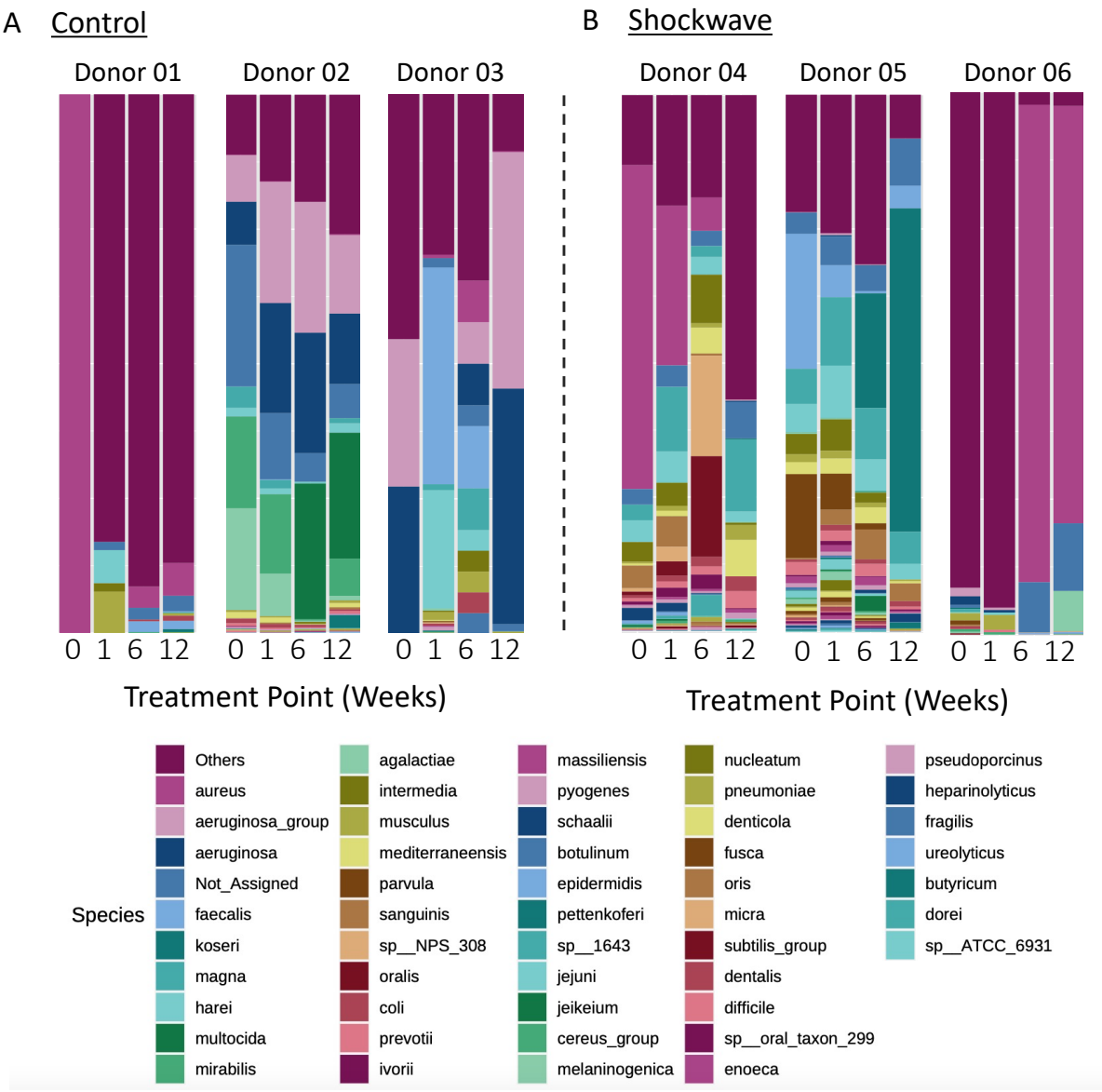

Figure 5.22: Topmost abundant bacterial species isolated from clinical diabetic foot ulcer specimens. Wound bed profiles (top 50 taxa) of 6 individual donors, from both the control (A) and shockwave-treated foot ulcer groups (B). Swabs were collected longitudinally at baseline, one, six- and 12 weeks post-trial enrolment/treatment. Each bar represents an individual specimen, visualising the total relative bacterial abundance [*n=3 for each treatment group*].

5.3.16 Microbial community diversity shows great donor-donor variation.

Following the assessment of relative taxa contribution to wound microbial profiles, overall community diversity was assessed. Profile diversity was calculated using Simpson alpha diversity metrics, accounting for the number of species present, as well as the relative abundance of each species (Nikolova et al., 2021). Patients within each treatment arm exhibited highly heterogenous fluctuations in profile alpha diversity at both baseline and across the remaining time points (Figure 5.23). Donor 03 of the control group displayed the lowest overall baseline diversity (0.1, Simpson diversity value), which increased gradually across post-treatment profiles (Figure 5.23:A). In the ESWT group, donor 06 presented the lowest overall baseline diversity, which fluctuated marginally across the remaining time points (Figure 5.23:B). Overall, no consistent time-point or shockwave-dependent observations in community diversity could be identified.

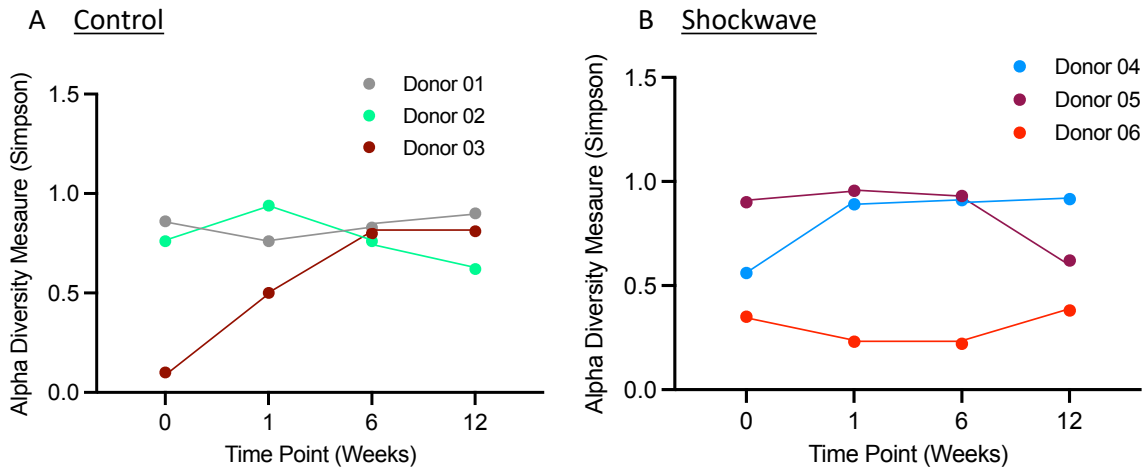

Figure 5.23: Longitudinal community diversity profiles of clinical diabetic foot ulcer specimens. Wound bed alpha diversity profiles (calculated using Simpson diversity metrics) from a total of 6 individual donors, from both the control (A) and shockwave-treated foot ulcer group (B). Swabs were taken longitudinally from baseline, one, six- and 12 weeks post-trial enrolment/treatment. Each data point represents an individual swab [*n=3 for each treatment group*].

5.3.17 Microbial community composition differed significantly following treatment with ESWT.

Following the assessment of dominant taxa and wound profile diversity, overall bacterial community composition was assessed using principal coordinate analysis (PCoA; Figure 5.24). At baseline, high dispersion in donor wound profile composition was observed, suggesting that no pre-existing community bias was present prior to treatment group allocation (Figure 5.24:A, PERMANOVA, p>0.05). In contrast, at post-treatment time points, a significant difference in microbial community profiles was observed between the control 'sham' and the shockwave-treated group (Figure 5.24:B, *PERMANOVA, p=0.08*). Overall, the post-treatment control group demonstrated greater community dispersion than the shockwave-treated group, which was primarily observed along the first axis (Figure 5.24:B). In contrast, ESWT-treated samples exhibited greater clustering on the first axis with greater dispersion along axis 2. Collectively, this analysis suggests participant wound bed profiles exhibited significant ESWT-mediated alterations in microbial community composition.

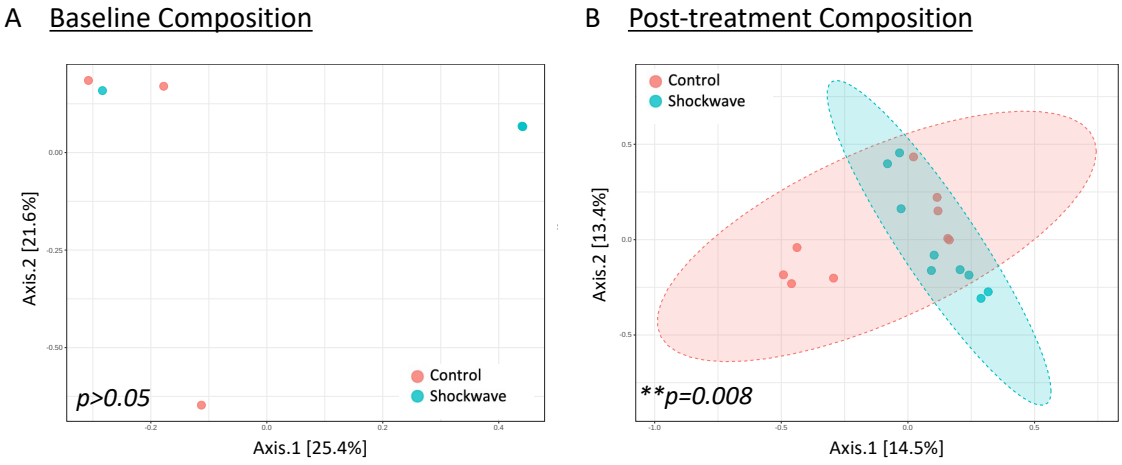

Figure 5.24: Microbial community composition of diabetic foot ulcer specimens. Wound profile beta diversity from a total of 6 individual donors, from both baseline (A) combined post-treatment measurements (B) Swabs were taken longitudinally from baseline, one, six- and 12 weeks post-trial enrolment/treatment. Beta diversity was measured via *the* Bray-Curtis index and presented in a PCoA plot. Each data point represents an individual swab [n=3 for each treatment group].

5.3.18 Correlation analysis revealed specific bacterial genera and species with reduced presence in the ESWT treatment group.

Following the assessment of microbial community composition, bacterial genera and species-based profile differences between control and ESWT groups were investigated using SparCC correlation analysis. SparCC analysis infers correlations in genomic data sets, accounting for a large number of present OTUs and the presence of a sparse correlation network (Cosma-Grigorov et al., 2021). Using these analysis techniques, multiple bacterial genera and species were correlated with a decreased presence within the shockwave-treated wound profiles (

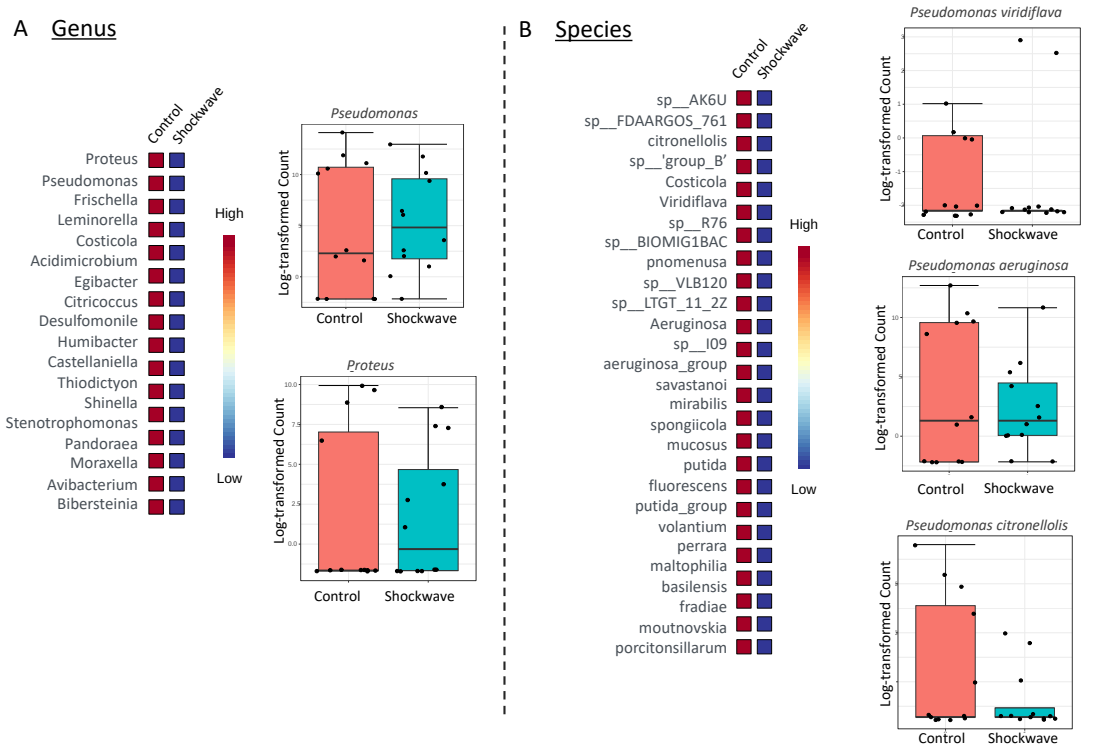

Figure 5.25: Unique microbial taxa with decreased presence in the ESWT group. Individual genera (A) and species (B) were identified using SparCC analysis coefficients, which were associated with the elevated presence in the control group (*p>0.05*). Named genera include *Pseudomonas* and *Proteus*, with named species including *Pseudomonas viridiflava*, *Pseudomonas aeruginosa* and *Pseudomonas citronellolis*. Heat map represents abundance profiles of species genera and species within each group [red= high abundance, blue = low

abundance]. Each data point represents an individual wound profile. [n=3 for donors at each treatment group, with 4 individual data points per donor.

5.3.19 Correlation analysis revealed bacterial genera and species associated with the ESWT treatment group.

Following the assessment of bacterial taxa reduced post-ESWT, the presence of elevated bacterial taxa associated with ESWT was examined again using SparCC correlation network (Figure 5.26). Multiple genera exhibit significant elevation in the ESWT group, including *Bacillus*, *Planococcous*, and *Akkermansia* (Figure 5.26:A, SparCC corelation analysis, p<0.05). In relation to species-level distribution, *Bacillus cereus, Staphylococcus argenteus and Bacillus thuringienis* demonstrated very low abundance control group and were significantly elevated in the ESWT-treated group (*SparCC correlation analysis, p=0.04*)

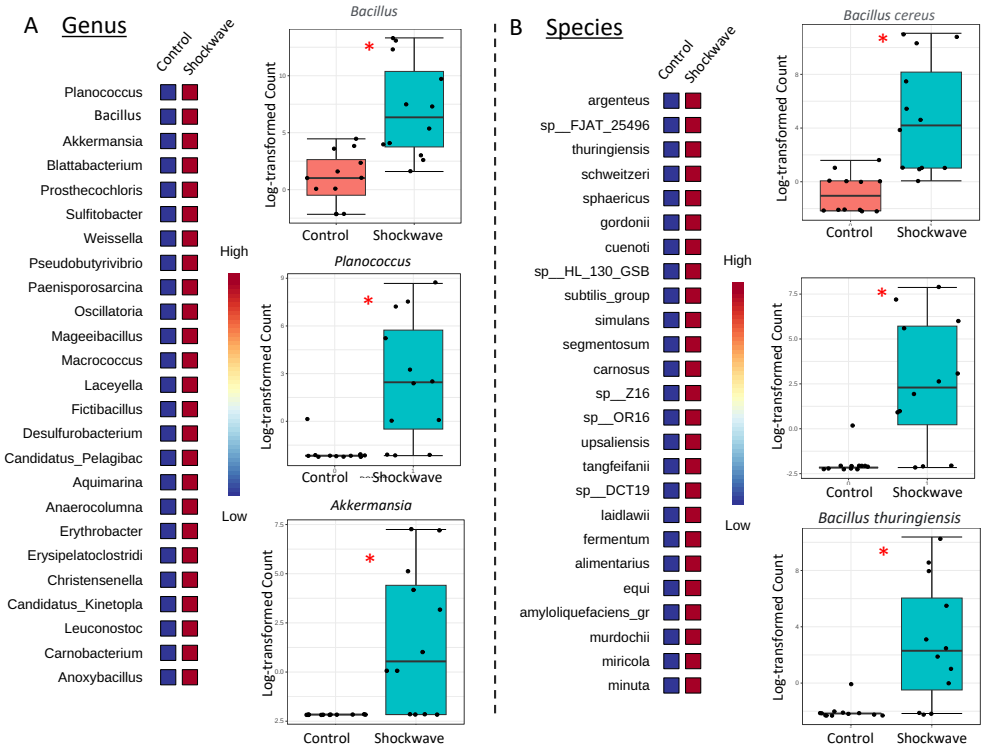

Figure 5.26: Unique microbial taxa with significantly elevated presence in the ESWT group. Individual genera (A) and species (B) were identified using SparCC analysis coefficients, that were associated with the presence in the control group. Names genera include *Bacillus and Planococcus and Akkermansia* with named species including *Bacillus cereus, Staphylococcus argenteus and Bacillus thuringienis.* Each data point represents an individual wound profile. [n=3 for donors at each treatment group, with 4 individual data points per donor correlation with treatment time points].

5.3.20 Longitudinal shockwave-mediated changes in bacterial wound community profiles according to metabolic oxygen requirements and overall taxa abundance.

Following the observation of specific taxa that were significantly elevated in the ESWT group, the presence of taxa with varying oxygen requirements were observed to assess the influence of ESWT therapy on microbes of these varying metabolic classifications. This was led by findings of previous research groups, such as Verbanic et al., 2020 who, in a report on microbial predictors of healing, observed that aerobes and especially facultative anaerobes were significantly associated with the delayed healing phenotype.

Relative contributions of the top bacterial taxa were classified into aerobes, anaerobes, or facultative anaerobes. The classification of bacteria as anaerobic, aerobic, or facultative is based on the nature of reactions they employ to generate energy for growth and metabolism (Angrup et al., 2022). Broadly, aerobes require molecular oxygen as a terminal electron acceptor and are unable to grow without its presence. In contrast, anaerobes are unable to replicate in the presence of oxygen. Their metabolism is generally fermentative, based on the reduction of alternative compounds to various metabolic end products, including organic acids and alcohols (Huang et al., 2022). Facultative organisms, preferentially utilize oxygen as a terminal electron acceptor, in the absence of oxygen however, they can reduce other compounds as usable energy (Huang et al., 2022).

At baseline, the relative contribution of aerobic bacteria was higher in the control group than in the shockwave-treated group (56% vs 35%) (Figure 5.27:A/B). Following an initial average decrease in contribution across both treatment groups, the mean aerobic contribution was 68.2% and 67.1% at 6 and 12 weeks post 'sham treatment', a figure that was notably lower in the ESWT group at 52.5% and 35.4% at 6- and 12-weeks post-treatment (Figure 5.27:B). In parallel, the relative contribution of anaerobic and facultative anaerobic bacteria decreased gradually from 10.5% and 12.5% at baseline to approximately 0.2% and 1.7% at 12 weeks post

'sham' treatment in the control group (Figure 5.27:A). In the ESWT-treated group, a gradual increase in facultative anaerobic bacterial contribution from 9.9% at baseline to 26% at 12 weeks post-treatment was observed.

Next, the longitudinal abundance variation of the most dominant taxa across both the control 'sham' and ESWT treated group was investigated. While the comparability of described taxa was low at baseline between the two groups, longitudinal abundance patterns could be observed. For both *Staphylococcus aureus and Pseudomonas aeruginosa,* baseline levels were higher in the ESWT groups (Figure 5.27:C/F). This contribution exhibited a gradual decline following ESWT, while a contrasting increase was observed in the control groups. *For* the remaining *Staphylococcal* species, including *Staphylococcus epidermidis and Staphylococcus hominis,* low average baseline levels of these species were observed at baseline and one week post 'sham' treatment, with an average increase at both 6- and 12-weeks post-treatment (Figure 5.27:D/E). In the ESWT group, an overall decline in the contribution of *Staphylococcus epidermidis and Staphylococcus hominis* was observed across the course of the trial. Overall, it should be acknowledged that many of these taxa abundance profiles exhibited high donor-donor variability, with no statistical significance being identified.

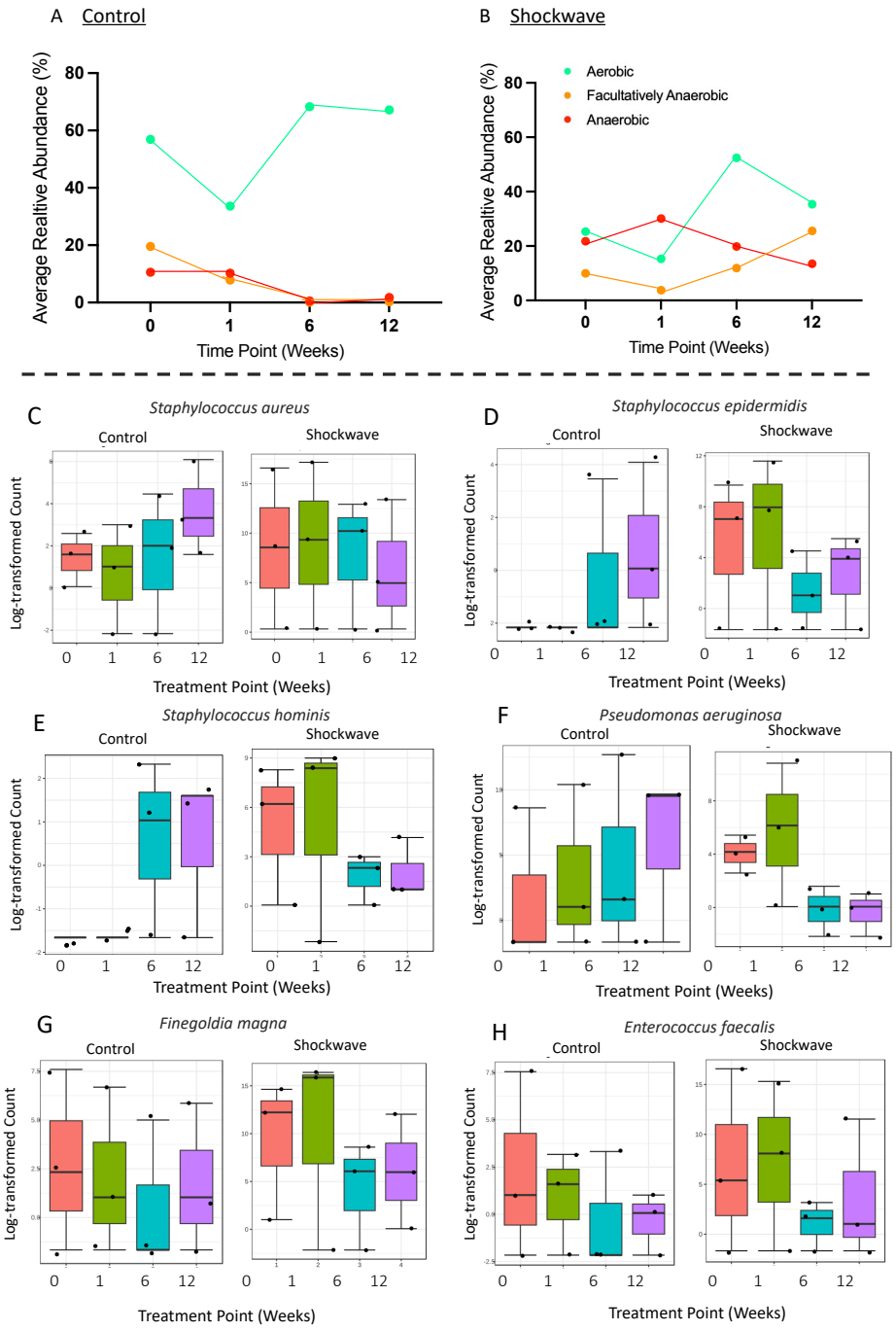

Figure 5.27: Longitudinal microbial profiles of diabetic foot ulcer samples. Longitudinal control (A) and shockwave-mediated (B) changes in bacterial wound community profiles according to metabolic oxygen requirements. Longitudinal control and ESWT-treated abundance (Log-transformed Count) of *Staphylococcus* aureus (C), *Staphylococcus* epidermidis (D), *Staphylococcus* hominis (E), *Pseudomonas aeruginosa* (F)*, Finegoldia magna (G) and Enterococcus faecalis (F).* Swabs were taken longitudinally from baseline, one, six- and 12 weeks post-trial enrolment/treatment. Each data point represents an average of the three donors present within each treatment group.

5.4 Discussion

While previous chapters aimed to improve our basic understanding of the cellular and microbial mechanisms of delayed healing phenotypes, there is currently an urgent need for new clinically efficacious wound-healing therapies (Kolimi et al., 2022). Therefore, in this current chapter, the novel wound healing technique, extracorporeal shockwave therapy (ESWT) was investigated for its potential role in multiple aspects of human wound repair. Initially, the underlying biological mechanisms of shockwave treatment on wound-related cell populations, such as keratinocytes and primary human dermal fibroblasts were examined *in-vitro*. In this setting, shockwave therapy presented a beneficial effect on cellular proliferation and scratch closure, even in the presence of pathogenic bacterial stimuli. In a pre-clinical *ex-vivo* model of chronic wound repair, shockwave therapy significantly increased relative wound closure. Simultaneously, histological analysis of *ex-vivo* wound shockwave-treated tissue revealed an ESWT-mediated increase in markers of proliferation, neo-epidermal formation and angiogenic marker expression. In relation to wound bacteria, shockwave alone had little effect on the viability of common clinical wound isolates. In contrast, however, shockwave did significantly increase bacterial sensitivity to antimicrobial agents.

In the latter half of the chapter, the impact of shockwave therapy was assessed as part of a novel pilot clinical trial. This aspect of the study aimed to assess the role of shockwave treatment on clinical diabetic foot repair in combination with integrated longitudinal adapted microbiome profiling. The integration of adaptive sequencing dramatically decreased host DNA contribution, whilst also increasing bacterial reads, and the number of overall identified OTUs, without introducing bias into the microbial community composition. Once optimised, long-read adaptive-based sequencing techniques were used to longitudinally assess the impact of ESWT on the clinical diabetic foot ulcer microbiome as part of a novel pilot clinical trial. Here, the wound profiles of ESWT-treated ulcers displayed a significantly altered microbial composition to those in the control ‘sham’ group. Overall, while strong baseline microbial heterogeneity made the identification of individual responsible taxa challenging, ESWT-treated wounds did display a significant alteration in species-level abundance across multiple genera, including *Bacillus, Staphylococcus and Pseudomonas* species.

Initially, shockwave therapy was found to have stimulatory effects on mammalian wound-related cell proliferation and scratch assay closure. This positive influence was observed in both keratinocyte and fibroblast populations and occurred both in standard *in-vitro* conditions and in the presence of inhibitory pathogenic stimuli. In agreement with these current findings, other recent studies have also investigated the influence of shockwave therapy on *in-vitro* mammalian cell populations. For example, Salcedo-Jiménez et al., 2020 reported that treatment with shockwave increased mesenchymal stromal cells (MSCs) proliferation, migration and metabolic activity. In a wound-relevant model, Basoli et al., 2020 reported that ESWT treatment (EFD = 0.19 mJ/mm2) increased fibroblast cell proliferation and inflammatory cytokine production. Aschermann et al., 2017 also reported shockwave-mediated morphological changes, increased cell migration and increased secretion of pro-angiogenic cytokines in human keratinocytes.

However, combined findings across the literature remain conflicting. Cui et al., 2018 reported that in human dermal fibroblasts, shockwave therapy does not influence cell viability and has a negative influence on cell migration. Interestingly, this study reports that adherent cells treated with shockwave therapy at a clinically relevant energy flux density of 0.1-0.3 mJ/mm^2 resulted in significant cell detachment from the culture vessel. Initial dosage screening in the current study revealed comparable results (Figure 5.4), with the beneficial effects of shockwave therapy not being observed until reaching the lower treatment doses (EDF= 0.018 mJ/mm2). While treatment at an energy flux of 0.1-0.3 mJ/mm2 appears comparable to clinically deliverable doses, it is common that *in-vitro* single-cell monolayers are less able to withstand significantly lower treatments than the complex human wound environment (Harris et al., 2012).

In addition to differences in the intensity of published ESWT treatment regimes, further limitations include the incomplete publishing reporting of a fully characterised medical therapy description (Cui et al., 2018; Aschermann et al., 2017; Jiménez et al., 2020). To report a completed method, all parameters of the treatment procedure, including therapeutic machine, delivery penetration level, pulse regularity, frequency duration and overall energy flux density are required, with almost all published studies lacking at least one segment of

this complete description (Holsapple et al., 2021). This may account for why studies previously focused on identical clinical indications frequently report opposing clinical findings, as the incomplete reporting of therapy parameters obstructs data comparability between research groups, whilst also hindering the development of optimal therapeutic indices. Furthermore, this issue is also complicated by the wide availability of commercial shockwave devices. For example, this current study used the PiezoWave^2 multi-use 40 (linear FBL10x5 G2 adaptor), whilst Cui et al., 2018 used a Duolith SD-1® device (StorzMedical, Tägerwilen, Switzerland). Aschermann et al., 2017 utilised an electro-hydraulic machine (CellSonic® Medical machine, Kenyo), whilst Salcedo-Jiménez et al., 2020 used the electrohydraulic shock wave generator (VersaTron, Pulse Veterinary Technologies, Alpharetta GA, USA). Finally, in Basoli et al., 2020 the shockwave device used was Ortho-Gold100 (Tissue Regeneration Technologies, LLC, manufactured by MTS Europe GmbH). In the future, it may be necessary to further standardise clinical treatment regimes, in relation to both manufacturer and therapy parameters, in order to fully understand the clinical potential of shockwave therapy in the field of regenerative wound care.

Throughout this current pilot study, access to patient skin samples afforded the ability to assess to impact of shockwave therapy on a previously validated pre-clinical model of *ex-vivo* wound repair (Wilkinson et al., 2019). Unlike *in-vitro* cell models, this approach allows the application of treatment in an environment that replicates the dynamic multifaceted process of wound repair, including the range of cellular populations, countless channels of post-injury communication and a general tissue environment that is commonly involved in the repair process (Wilkinson et al., 2019). Parallel to previous clinical research (Cheng et al., 2022), shockwave therapy significantly increased *ex-vivo* wound closure (Figure 5.6). Simultaneous histological analysis of *ex-vivo* wound tissue also revealed a shockwave-mediated increase in markers of epidermal basal cell proliferation (ki-67) and neo-epidermal formation, migration and maturation (Keratin 1 and Keratin 6). Collectively, these findings suggest that shockwave therapy is capable of enhancing re-epithelisation, wound closure and cutaneous barrier restoration (Mansy et al., 2020; Évora et al., 2021). In contrast, parallel results are often reported *in-vivo*, with Weihs et al., 2014 observing that shockwave-treated mice showed no

increase in post-wounding epidermal proliferation and ki-67 basal cell positivity (Weihs et al., 2014).

Alongside other studies (Moortgat et al., 2020), shockwave therapy was also found to increase the expression of angiogenic markers (including VEGFa and CD31) post-wounding (Figure 5.9). The establishment of new vasculature via angiogenesis is considered a critical aspect of repair (Shaabani et al., 2022), a process which is commonly complicated and impaired in the chronic wound environment (Veith et al., 2019). Therefore, the increase of angiogenic gene expression in tissue isolated from the chronic wound environment ultimately highlights a role for shockwave therapy in supporting microvascular network regeneration in chronic wound repair. These results are further confirmed by previous studies, such as Sundaram et al., 2018 who reported that in human endothelial cells, shockwave therapy was able to increase angiogenic marker via the PI3K mediated induction of VEGFA expression. Additionally, in a clinical group of diabetic foot ulcers, Wang et al., 2011 also reported a significant increase in angiogenic markers vWF, VEGF, eNOS, PCNA and EGF) after ESWT compared to the control group.

While the discussed findings focus heavily on the effects of extracorporeal shock-wave therapy (ESWT) in eukaryotic tissues, minimal data is available concerning its influence on prokaryotic populations. The assessment of shockwave antimicrobial activity was a priority throughout this chapter, as chronic wound infections are considered one of the leading causes of delayed wound healing (Wangoye et al., 2022). Therefore, shockwave therapy was tested on a selection of common wound isolates including both planktonic and biofilm-derived cultures *Pseudomonas aeruginosa*, *Staphylococcus aureus*, *Staphylococcus epidermidis* and *Candida albicans*. Overall, across all the tested isolates, shockwave treatment had little effect on microbial viability. Surprisingly, this contrasted with the limited number of previous studies published on microbial viability. For example, Gerdesmeyer et al., 2005 identified that ESWT is able to exert significant antibacterial effects on standardised planktonic *Staphylococcus aureus* (ATCC 25923) suspensions (Gerdesmeyer et al., 2005). Furthermore, Datey et al., 2019 also identified that shockwave treatment is effective in clearing a multispecies biofilm in a humanised rat model of chronic periodontitis.

While interesting, it is unknown why current results deviated so heavily from previously reported data (Gerdesmeyer et al., 2005; Datey et al., 2019). This discrepancy in findings may also be due to microbial strain or growth phase variation. Whilst the current study utilised bacterial isolates from the clinical wound environment, these often exhibit increased durability and resistance (Hailemariam et al., 2021: Gerdesmeyer et al., 2005; Datey et al., 2019). Additionally, the colony biofilm approach utilised through this study involves biofilms maintained at the air-agar interface, with underlying nutrient availability. Whilst this was deemed to be most translatable to an infected wound site, other models of biofilm may have more closely replicated the delivery of shockwave treatment in the clinical wound environment. Multiple models of *in-vitro* biofilms exist including, static minimal biofilm eradication concentration (MBEC) assay®, microtiter plate systems and more dynamic microfluidic co-culture models may be considered moving forward (Lebeaux et al., 2013).

Perhaps one of the most interesting and clinically useful study findings was the shockwave-mediated increase in the sensitivity of bacteria to antimicrobial agents. Currently, the development of antibacterial resistance is considered one of the leading and most serious public health concerns (León-Buitimea et al., 2020). In response, the development of novel antimicrobial therapies, including those that increase sensitivity to current antimicrobials, is considered imperative (León-Buitimea et al., 2020). Across multiple wound isolates, shockwave therapy significantly increased the sensitivity of specific wound isolates to ciprofloxacin and gentamicin (Figure 5.13). This trend has been previously reported, with Yao et al., 2020 observing that shockwave therapy enhances the sensitivity of *S. epidermidis* biofilms topical gentamicin treatment *in-vitro*. Gnanadhas et al., 2015 also reported that both *Pseudomonas* and *Staphylococcus* biofilms demonstrated enhanced suitability to ciprofloxacin treatment following shockwave application. Whilst previous studies did not speculate on the mechanisms of increased antimicrobial activity, Horn et al., 2009 postulated that shockwave therapy may temporarily disrupt the cell wall, increasing cellular permeability therefore susceptibility to internally acting ciprofloxacin and gentamicin (Salvetti et al., 2021). This theory further correlated with additional findings, that shockwave therapy failed to increase bacterial susceptibility to amoxicillin and flucloxacillin, which both act to externally inhibit DNA wall synthesis (Munita et al., 2016). In contrast, Tsikopoulos et al., 2020 reported

that shockwave therapy does not influence bacterial cell wall permeability, highlighting that these mechanisms of increased antimicrobial sensitivity require further investigation.

Finally, in the latter half of the chapter, the impact of shockwave therapy was assessed as part of a novel pilot trial in clinical diabetic ulcer healing. Throughout this pilot study, multiple aspects of clinical wound repair were investigated in combination with integrated adapted species-level microbiome profiling. Longitudinal profiling techniques were employed to evaluate the temporal dynamics of the microbiota colonizing in diabetic foot ulcers. This has recently proved to be essential as, one foundational paper in the field of microbiome research, Loesch et al., 2017 reported that longitudinal microbiota community instability was associated with faster healing and improved outcomes.

This portion of the study also introduced the concept of adaptive sequencing. Throughout this pilot trial, host depletion techniques were optimised to increase the economical use of nanopores, whilst simultaneously increasing microbial sequencing depth to increase coverage for enhanced functional metagenomic profiling (Martin et al., 2022; Weilguny et al., 2023). As demonstrated, adaptive sampling dramatically reduced the relative prevalence of contaminating host reads from 78% in the control experiment to 8% in the adaptive run. In parallel, an average 1.3-fold increase in alpha diversity and a species-consistent 2.26-fold increase in total bacterial reads were observed, whilst no distortion was observed on microbial community composition. In parallel, Marquet et al., 2022 also used Oxford Nanopore's adaptive sequencing for host DNA depletion in human vaginal samples, reporting a relative host read contribution decrease from 87.93% to 34.73%. Furthermore, the current study observed that adaptive sampling also enables enhanced taxonomic profiling, providing enhanced sequencing data, and identifying a higher number of unique OTUs. In our initial experiment alone, these additional OTUs included the taxa *Escherichia coli and Proteus Mirabilis*, both of which have known associations with the delayed healing phenotype (Osumi et al., 2017; Oliveira et al., 2022).

In addition, while quantitative long-read analysis is sufficient to assess the information about the composition and diversity of specified communities, to uncover in-depth information regarding functional annotation and AMR profiling, metagenomic assembly is needed to analyse the extended genomic regions (Rooney et al., 2022). It is currently guided that >20X coverage genome coverage is required for complete species AMR profiling and >30X coverage genome coverage for complete metagenomic assembly (Raphenya et al., 2022). For rare less minor community members, insufficient sequencing data often results in partial genome coverage and suboptimal assemblies (Rooney et al., 2022). Effective host depletion and enhanced bacterial sequencing strategies, such as adaptive sequencing, act to maximise the sequencing outputs for rare species and help to address this weakness and biodiversity blind spot (Lapidus and Korobeynikov, 2021). In addition, from an economical perspective, increased sequencing depth via adaptive sampling will allow more samples to be barcoded and sequenced simultaneously, reducing the total cost per sample (Lapidus and Korobeynikov, 2021).

One overall limitation of the study is that human DNA could not be completely removed. It is possible that adapting the provided reference genome(s) may improve the depletion performance. Additionally, sequencing-based depletion methods may be coupled with wet lab host DNA depletion techniques via, e.g., saponin or the "MolYsis Complete5" (Charalampous et al., 2019; Yap et al., 2020). In an attempt to further reduced host contamination, previous studies such as Marquet et al., 2022 and Martin et al., 2022 utilised enrichment-based adaptive sampling techniques to enrich taxa of interest by depleting off-target regions. Marquet et al., 2022 reported that adaptive sampling with bacterial enrichment strongly reduced the proportion of sequenced human reads from 87.93% in the control to only 8.29% post-enrichment, while also increasing the microbial sequencing yield of all 15 target species. Whilst both studies described the enhanced removal of host reads with enrichment compared to depletion methods, it was also observed that the enrichment-based technique changed the overall identified bacterial composition by depleting certain microbial sequences (Marquet et al., 2022). Collectively, this illustrates that the enrichment method may be poorly suited for global non-targeted microbiome studies (Rooney et al., 2022). Therefore, it is likely that such enrichment methods may be better suited when only

'selectable' known target species are of interest. Despite these improvements, is still likely that raw sequencing data will contain some portion of human sequences, which poses a potential ethical problem (Marquet et al., 2022).

Following the optimisation of host depletion methods, long-read adaptive-based sequencing techniques were used to longitudinally assess the impact of ESWT on the clinical diabetic foot ulcer microbiome as part of a novel pilot study. In the literature, multiple studies report the effects of shockwave therapy on biofilm clearance in murine/ rat models (Datey et al., 2019, Wuerfel et al., 2022). However, no current studies exist assessing the role of ESWT on complex microbial communities or on aspects of the human wound microbiome. In the current pilot study, six donors presenting clinically with a non-infected diabetic foot ulcer were assigned to control 'sham' or ESWT treatment groups. For the active therapy group, ESWT was administered at an EFD of 0.1mJ/mm2, 5 pulses/second at a penetration depth of 5mm, three times within the first week of trials enrolment, swabs were then collected at baseline, 1 week, 6 weeks and 12 weeks post-trial enrollment treatment (Figure 5.21). Across these donors, the impact of ESWT on the wound microbiota, including how treatment may longitudinally alter the proportions and distribution of wound taxa was investigated.

Initially, community analysis revealed that ESWT-treated ulcers exhibited a significantly altered microbial composition to those in the control 'sham' group. The distribution of the top-most dominant wound taxa was directly compared to examine the treatment-specific significant differences identified by PCoA analysis. In parallel to other wound microbiome studies, *Staphylococcal* species, including *S. aureus* was identified as the most abundant wound taxa (Price et al., 2011; Han et al., 2011; Gardner et al., 2013; Loesche et al., 2017; Park et al., 2019; Min et al., 2020; Kalan et al., 2019). However, upon a direct comparison of the treatment groups, despite the presence of similar healing outcomes, strong donor-donor baseline microbial variability made the identification of ESWT-mediated alterations in individual taxa very challenging.

Following on, correlation analysis revealed significant alterations in genus and species-level abundance between the two treatment groups, including *Bacillus, Staphylococcus* and *Pseudomonas* species. Notably, the baseline abundance of *Staphylococcus aureus* and *Pseudomonas aeruginosa* were higher in the ESWT than in the control group. However, while an average longitudinal increase in abundance was observed across the control groups, post-ESWT, the contribution of these two species exhibited an average gradual decline (Figure 5.27). In a clinical setting*, Staphylococcus aureus and Pseudomonas aeruginosa* are often regarded as the dominant cause of wound infections, with studies establishing that both species are able to impair granulation tissue formation (Ruffin and Brochiero, 2019; Roy et al., 2022). While the current study failed to observe an inhibitory influence of ESWT on bacteria *in-vitro*, the selective depletion of pathogenic species in this pilot study offers promise for shockwave therapy as a positive microbiome mediator for the future. Additionally, whilst the investigation of infected wounds was beyond the scope of the pilot trial, this study showed that shockwave did significantly increase bacterial sensitivity to antimicrobial agents. In the diabetic wound environment, infections caused by multi-drug resistant pathogenic isolates are considered a leading cause of lower limb amputations. Therefore, the discovery of potential treatments to enhance the antimicrobial susceptibility of common wound pathogens are critical for the future of wound care (Ruffin and Brochiero, 2019; Roy et al., 2022).

Following the assessment of individual taxa, microbial community diversity was assessed across healing time points to further investigate possible composition changes associated with ESWT. Recently, microbial community diversity has been shown to influence the cutaneous repair process, with Loesche et al., 2019 reporting that microbiota community diversity and instability are associated with faster healing and improved wound outcomes. Despite conducting a similar analysis, the study was not able to identify any strong associations between ESWT and community diversity, with each donor exhibiting a unique pattern of community diversity and stability across their healing trajectories (Figure 5.23). In addition to diversity, Loesche et al., 2019 also classified foot ulcer microbiota profiles into four distinct community types, each of which experienced non-random transitions throughout the study that correlated with total healing time. Whilst the low number of

participants in the current pilot study severely limited the ability to categorise wound profiles into unique community types, it is possible that further studies with larger participant samples would allow such complex analysis.

Overall, future studies will likely require far higher participant numbers to identify correlations of significance between treatment profiles and microbial signatures. For the classification of community types, Loesche et al., 2019 conducted profiling of over 100 wound samples. In addition, further microbial heterogeneity will be introduced by the broad types of wounds and participant clinical phenotypes included within our study. Pathophysiologically distinct wounds are likely coupled with different host/wound environments, ultimately confounding the identification of microbial populations associated with the administration of ESWT (Kalan and Grice, 2018; Wu et al., 2020). However, regardless of the included wounds, variation will likely continue to remain a problem, with Gardner et al., 2013, reporting wound microbiomes to be extremely heterogeneous, even in the presence of a highly homogenous study population.

In conclusion, current chronic wound management techniques remain largely inadequate, often requiring prolonged, costly, and ineffective clinical approaches (Ongarora, 2022). In a time where more effective techniques are desperately required, shockwave treatment identifies as a useful tool in the field of chronic wound management. While the advantages of ESWT include high clinical efficacy, ease of use, cost-effectiveness and non-invasiveness, existing evidence on the mechanisms and likely clinical benefits remains weak (Hitchman et al., 2023). Throughout this study, it was identified that extracorporeal shockwave therapy (ESWT) is able to positively influence multiple aspects of human wound repair. *In-vitro*, shockwave therapy presented beneficial effects on mammalian cell proliferation and scratch assay closure. In *ex-vivo* models, ESWT significantly enhanced wound closure, simultaneously increasing markers of proliferation, neo-epidermal formation, and angiogenesis. Interestingly, in prokaryotic communities, a shockwave-mediated increase in antimicrobial sensitivity was observed. As the development of novel antimicrobial therapies, including those that increase sensitivity to current antimicrobials, is considered imperative (León-Buitimea et al., 2020),

this finding offers promise for the future of wound care. For the latter half of the chapter, the influence of ESWT was assessed on the clinical diabetic foot ulcer microbiome as part of a novel pilot clinical trial. As observed within this trial, the integration of novel adaptive sequencing in microbiome profiling is exceptionally useful, specifically when profiling samples containing high host DNA contributions. In response to shockwave therapy, PCoA analysis revealed that ESWT-treated wounds did display a significant alteration in species-level microbial composition, however strong baseline microbial heterogeneity made the identification of individual responsible taxa challenging. Moving forward, the influence of wound healing therapies, such as ESWT, on the complex wound microbiome will likely be important for biomarkers of treatment response and the likelihood of future infection-related complications. However, to fully understand the role of the wound-related microbiome, and how novel therapies may influence the wound microbial composition, larger more comprehensive studies are urgently needed.

6 General Discussion

The overarching research hypothesis of this thesis, centres around the theory that in combination with host factors, species-level alterations in the human wound microbiome contribute towards delayed healing. To address this hypothesis, human wound microbiome swabs were profiled using an optimised long-read nanopore sequencing approach that delivers quantitative species-level taxonomic identification (Chapter 3). In parallel, microbial composition was compared to host tissue transcriptional profiles (RNA-seq), histological and clinical parameters (Chapter 4). Finally, the longitudinal impact of an emerging wound therapy (ESWT) on human wound healing was assessed, *in-vitro*, *ex-vivo* and compared to adaptive microbiome profiling (Chapter 5). Collectively, these studies deliver new insight into the complexity and variability of the human wound microbiome, suggesting clear microbiome-mediated effects on healing.

Previously published studies attempting to profile the human wound microbiome have observed heterogeneous findings, in part reflecting the different technologies employed. Thus, the full extent to which host-microbiome interactions may influence healing pathology remain poorly understood (Price et al., 2011; Han et al., 2011; Gardner et al., 2013; Loesche et al., 2017; Park et al., 2019; Min et al., 2020; Kalan et al., 2019). In response, the aim of Chapter 3 was to undertake one of the first third-generation long-read sequencing-based profiling studies of clinical wound samples. This cutting-edge sequencing technology revealed substantial differences between the skin microbiome of healthy volunteers and the intact skin of individuals presenting with a chronic wound (Figure 3.9). Deeper analysis revealed significant species-specific alterations in microbial composition related to patient diabetic status and overall glycaemic control (Figure 3:18). While the functional implications of these compositional shifts in wound community profiles remain to be explored, it is clear that species-level wide-spectrum rapid pathogen identification provided by these novel sequencing approaches holds major potential for future clinical wound management.

Moving forward, the aim of Chapter 4 was to gain insight into interactions between the host response, microbiome and related drivers of wound chronicity. Whilst previous studies have reported a selection of genes that are frequently upregulated in the wound environment (Murir et al., 2020; Dasu et al., 2020), very few studies have explored global expression signatures in relation to their corresponding microbial signatures. Here, global transcriptional profiling of peri-wound skin and pathological skin from a selection of diabetic donors revealed distinct gene expression signatures in key wound healing-associated pathways liked to bacterial profiles. Overall, host defence expression profiles in the wound edge related strongly to bacterial load, and the presence of resident immune cell populations. Diabetes and infection were associated with elevated pattern recognition and host defence peptide expression, potentially in response to associated shifts in pathogenic species distribution. Collectively, this research acts as one of the first studies to combine long-read sequencing technology with clinical and host transcriptome data, providing unprecedented insight into the complexity of wound host-microbe interactions.

Finally, the effects of an innovative chronic wound treatment, ESWT, were examined in relation to *in-vitro/ex-vivo* processes and wound microbiome. While ESWT has shown previous clinical promise, the mode of action remains unclear (Simplicio et al., 2020). In parallel with a selection of previous studies, *in-vitro* shockwave therapy had beneficial effects on mammalian cell proliferation and migration (Aschermann et al., 2017; Basoli et al., 2020). In a previously unexplored *ex-vivo* wound model, shockwave therapy demonstrated a range of beneficial effects on cutaneous human repair, increasing markers of tissue angiogenesis, proliferation and neo-epidermal formation. The impact of ESWT on the clinical diabetic foot ulcer microbiome was also assessed in a pilot clinical trial. While previous studies have reported conflicting results on the tissue repair-based and antimicrobial influence of ESWT (Mansy et al., 2020; Évora et al., 2021), this unique study assessed healing outcomes alongside changes to wound microbial compositions. Here, novel sequencing techniques revealed that the wound profiles of ESWT-treated ulcers displayed a significantly altered microbial composition to those in the control 'sham' group. ESWT-treated wounds displayed significant alterations in species-level abundance across multiple commensal pathogenic genera, including *Bacillus, Staphylococcus and Pseudomonas*. By way of potential mechanism, ESWT

was shown to significantly increase bacterial sensitivity to antibiotics in wound isolate organisms. Collectively, the findings presented in this study begin to shed light on the mechanistic effects of shockwave therapy. Moving forward, a more detailed evaluation is now needed to support this emerging therapy for chronic wound management.

6.1 Study Limitations

The work outlined in this thesis yielded a variety of unique challenges. The first obstacle involved the integration of a novel DNA sequencing technique in a laboratory with limited experience of internal sequencing. This required extensive methodological optimisation and development. In addition, as reported by previous wound microbiome profiling studies, low sample biomass presented a major challenge throughout the study, severely limiting the choice of both DNA isolation techniques and nanopore sequencing protocols (Selway et al., 2020; Verbanic et al., 2019). Overall, the donors contained within the study presented wounds of a heterogenous nature, potentially limiting the applicability of the findings. Future studies using a higher specimen number in wounds of a single homogenous phenotype may aid in the discovery of clinically important microbial signatures. In addition, the late implementation of adaptive sequencing, due to the novelty of the sequencing platform may have hindered results, as an early application of this technique may have allowed the improved characterisation of wound microbial profiles during the initial study (Chapter 3). The most time-consuming challenge was the development and integration of a robust downstream bioinformatic processing pipeline for long-read sequencing data. In addition to this, the recruitment of sufficient participants was challenging throughout, particularly during the COVID-19 pandemic. The author was responsible for being clinically present, identifying patients suitable for study participation, gaining study ethical approval, achieving participant consent and tissue specimen collection and transportation. While this process was particularly time-consuming, the integration of participant engagement certainly reinforced the clinical need, research motives and translational nature of the research. The onset of the Covid-19 pandemic severely perturbated participant recruitment for the latter half of the study. During this period, IRAS studies were paused, and restrictions were placed on elective surgeries and overall clinical research studies. Finally, the shockwave-based portion of the

study was limited by the availability of clinical ESWT machines. The pilot clinical trial was limited to a low number (n=6) of study participants presenting with wounds of heterogenous clinical phenotype.

6.2 Future Action

It is clear from the data presented in this thesis that obtaining definitive conclusions from wound microbiome studies will require large sample numbers. Future experimental designs should be adapted to in cooperate increased participant numbers, whilst also focusing on a restricted clinical wound phenotype. Stricter inclusion criteria would reduce the heterogeneity observed between wound profiles within this study, increasing the power to detect microbiome community changes that are associated with healing outcomes. Obviously, the likely trade-off will be reduced generalisability. A significant future goal, unfortunately beyond the scope of this current PhD, will be to include microbial genome assembly with functional annotation alongside taxonomic characterisation. As long-read approaches typically contain a higher information content within each sequence, functional analysis would provide a greater understanding of microbial community virulence, metabolic potentials, and antimicrobial resistance profiles. Future studies could combine this greater microbial characterisation with cutting-edge host tissue transcriptional profiling methods, such as single-cell RNA-seq. While costly, this approach would provide unparalleled insight into the host-microbe interaction during wound healing.

Overall, the integration of these extensive clinical and biological datasets advances will allow us to advance our understanding from “Who's there?” to “Why are they there?” and “What are they doing?”. Moving forward, future studies will require extensive *in-vitro*, *ex-vivo* and *in-vivo* studies to further understand the molecular mechanisms that modulate host-microbe interactions. This will allow exploration studies directly exploring functional host-microbe interactions using common wound-derived isolates. Previous research groups have conducted a limited number of relevant studies, such as Kalan et al., 2019 where isolated wound species were tested for their functional abilities and ability to impact *in-vivo* tissue

repair. Eventually, these studies may eventually allow for the development of microbial manipulation strategies, including the selective inhibition of pathogenic bacteria or the expansion of diverse symbiotic communities to aid tissue repair.

In the field of culture-independent microbiome profiling, one common criticism is the inability of DNA-based methods to reliably discern between live, dead, or extracellular DNA (Nelson et al., 2019). Future studies should consider integrated PMA and PCR-based molecular viability methods that allow differentiation between nucleic acids associated with viable and inactivated cells. In addition to DNA isolated from non-viable bacteria, the sequencing of non-bacterial contaminating human DNA remains a fundamental problem in the field of metagenomic profiling (Ciuffreda et al., 2021). At present, reads which align to the human genome undergo bioinformatic removal prior to data visualisation, however, due to the costly implications of long-read sequencing approaches, this is both a wasted use of sequencing channels and a factor that acts to reduce microbial sequencing depth. Initial attempts to deplete host DNA have been reported, predominantly using saponin-based approaches (Charalampous et al., 2019; Street et al., 2020). Charalampous et al., 2019 optimised a saponin-based metagenomic protocol, boasting a 99.99% reduction in host nucleic acids. While the low biomass of samples acquired in the current study failed to allow for successful saponin-based depletion protocols, alternative methods of depletion such as adaptive sampling were investigated (Kovaka et al., 2021; Payne et al., 2021). Throughout the final pilot trial of this thesis, adaptive sequencing methods were optimised to successfully decrease host DNA contribution, whilst enhancing microbial sequencing depth for improved functional metagenomic profiling.

6.3 Concluding Remarks

The findings described throughout this thesis have heightened our understanding of the wound microbiome and highlighted the future capabilities of long-read Nanopore sequencing. Microbiome profiling studies span diverse research areas, rich in unexplored biological depth, where considerable potential remains. Ultimately, the integration of novel

species-level microbial profiling with functional host tissue characterisation methods will revolutionise our understanding of the wound repair process. Whilst this current study demonstrates the impressive power of integrating clinical and biological datasets, considerably more research is needed to fully dissect the molecular mechanisms of host-microbe interactions. Looking to the future, shockwave therapy holds significant promise for the development of future healthcare technologies. In the clinic, ESWT has the potential to act at multiple levels; improving cutaneous healing, increasing antimicrobial efficacy and potentially promoting the restoration of a healthy wound microbiome.

7 References

Ahmad-Mansour, N., Loubet, P., Pouget, C., Dunyach-Remy, C., Sotto, A., Lavigne, J.-P., & Molle, V. (2021) Staphylococcus aureus toxins: An update on their pathogenic properties and potential treatments. *Toxins*, 13(10), 677.

Akbarian, M., Bertassoni, L. E., & Tayebi, L. (2022) Biological aspects in controlling angiogenesis: current progress. *Cellular and Molecular Life Sciences : CMLS*, 79(7), 349.

Akira, S., & Takeda, K. (2004) Toll-like receptor signalling. *Immunology*, 4(7), 499–511.

Alexiadou, K., & Doupis, J. (2012) Management of diabetic foot ulcers. *Diabetes therapy: research, treatment and education of diabetes and related disorders*, *3*(1), 4-9.

AlJanahi, A. A., Danielsen, M., & Dunbar, C. E. (2018) An Introduction to the Analysis of Single-Cell RNA-Sequencing Data. Molecular therapy. *Methods & clinical development*, 10, 189–196.

Allison, D. L., Willems, H., Jayatilake, J., Bruno, V. M., Peters, B. M., & Shirtliff, M. E. (2016) Candida-Bacteria Interactions: Their Impact on Human Disease. *Microbiology spectrum*, *4*(3), 7-8.

Aluri, J., Cooper, M. A., & Schuettpelz, L. G. (2021) Toll-Like Receptor Signaling in the Establishment and Function of the Immune System. *Cells*, 10(6), 1374.

American Diabetes Association. (2010) Standards of medical care in diabetes. *Diabetes care*, 33(1), 11–61.

American Diabetes Association. (2021) Glycemic Targets: Standards of Medical Care in Diabetes. *Diabetes care*, 44(1), 73–84.

Andrews, J. M. (2001) Determination of minimum inhibitory concentrations. *The Journal of antimicrobial chemotherapy*, 48(1), 5–16.

Angrup, A., Sood, A., Ray, P., & Bala, K. (2022) Clinical anaerobic infections in an Indian tertiary care hospital: A two-year retrospective study. *Anaerobe*, 73(1), 102482.

Aschermann, I., Noor, S., Venturelli, S., Sinnberg, T., Mnich, C. D., & Busch, C. (2017) Extracorporal Shock Waves Activate Migration, Proliferation and Inflammatory Pathways in Fibroblasts and Keratinocytes, and Improve Wound Healing in an Open-Label, Single-Arm Study in Patients with Therapy-Refractory Chronic Leg Ulcers. *Cellular physiology and biochemistry : international journal of experimental cellular physiology, biochemistry, and pharmacology*, 41(3), 890–906.

Askarian, F., Lapek, J. D., Jr, Dongre, M., Tsai, C. M., Kumaraswamy, M., Kousha, A., Valderrama, J. A., Ludviksen, J. A., Cavanagh, J. P., Uchiyama, S., Mollnes, T. E., Gonzalez, D. J., Wai, S. N., Nizet, V., & Johannessen, M. (2018) Staphylococcus aureus Membrane-Derived Vesicles Promote Bacterial Virulence and Confer Protective Immunity in Murine Infection Models. *Frontiers in microbiology*, 9(1), 200-262.

Atkinson, M. A. (2012) The pathogenesis and natural history of type 1 diabetes. *Cold Spring Harbor perspectives in medicine*, 2(11), a007641.

Auersperg, V., & Trieb, K. (2020) Extracorporeal shock wave therapy: an update. *EFORT open reviews*, 5(10), 584–592.

Balta, S. (2021) Endothelial Dysfunction and Inflammatory Markers of Vascular Disease. *Current vascular pharmacology*, 19(3), 243–249.

Bandurska, K., Berdowska, A., Barczyńska-Felusiak, R., & Krupa, P. (2015) Unique features of human cathelicidin LL-37. *BioFactors*, 41(5), 289–300.

Bandyk, D. F. (2018) The diabetic foot: Pathophysiology, evaluation, and treatment. *Seminars in vascular surgery*, 31(2-4), 43–48.

Beckert, S., Pietsch, A. M., Küper, M., Wicke, C., Witte, M., Königsrainer, A., & Coerper, S. (2009) M.A.I.D.: a prognostic score estimating probability of healing in chronic lower extremity wounds. *Annals of surgery*, *249*(4), 677–681.

Bharti, R., & Grimm, D. G. (2021) Current challenges and best-practice protocols for microbiome analysis. *Briefings in bioinformatics,* 22(1), 178–193.

Bin Hafeez, A., Jiang, X., Bergen, P. J., & Zhu, Y. (2021) Antimicrobial Peptides: An Update on Classifications and Databases. *International journal of molecular sciences*, 22(21), 11691.

Boer, M., Duchnik, E., Maleszka, R. & Marchlewicz, M. (2016) Structural and biophysical characteristics of human skin in maintaining proper epidermal barrier function. *Advances in Dermatology and Allergology*, 33(1), 1-5.

Bolatchiev, A. (2020) Antibacterial activity of human defensins against Staphylococcus aureus and Escherichia coli. *PeerJ*, 8, e10455.

Bolatchiev, A., Baturin, V., Bazikov, I., Maltsev, A., & Kunitsina, E. (2020) Effect of antimicrobial peptides HNP-1 and hBD-1 on Staphylococcus aureus strains in vitro and in vivo. *Fundamental & clinical pharmacology*, 34(1), 102–108.

Bonnet, M., Lagier, J. C., Raoult, D., & Khelaifia, S. (2019) Bacterial culture through selective and non-selective conditions: the evolution of culture media in clinical microbiology. *New microbes and new infections,* 34(1), 100-622.

Bowden, R., Davies, R. W., Heger, A., Pagnamenta, A. T., de Cesare, M., Oikkonen, L. E., Parkes, D., Freeman, C., Dhalla, F., Patel, S. Y., Popitsch, N., Ip, C., Roberts, H. E., Salatino, S., Lockstone, H., Lunter, G., Taylor, J. C., Buck, D., Simpson, M. A. & Donnelly, P. (2019) Sequencing of human genomes with nanopore technology. *Nature communications*, 10(1), 1869.

Bowers, S., & Franco, E. (2020) Chronic Wounds: Evaluation and Management. *American family physician*, 101(3), 159–166.

Bowler, P. G., Duerden, B. I., & Armstrong, D. G. (2001) Wound microbiology and associated approaches to wound management. *Clinical microbiology reviews*, *14*(2), 244–269.

Bowler, P. G. (2003) The 10(5) bacterial growth guideline: reassessing its clinical relevance in wound healing. *Ostomy/wound management*, 49(1), 44–53.

Brown, M. M., & Horswill, A. R. (2020) Staphylococcus epidermidis-Skin friend or foe?. *PLoS pathogens*, 16(11), e1009026.

Brown, P. J. B., Kysela, D. T. & Brun, Y. V. (2012) Polarity and the diversity of growth mechanisms in bacteria. *Seminary in Cell and Developmental Biology*, 22(8), 790-798.

Bruggeman, M., Ijakipour, H., & Stamboulis, A. (2019) Defensin-Like Peptides and Their Antimicrobial Activity in Free-Form and Immobilized on Material Surfaces*. IntechOpen*.

Brugués, A., Anon, E., Conte, V., Veldhuis, J. H., Gupta, M., Colombelli, J., Muñoz, J. J., Brodland, G. W., Ladoux, B., & Trepat, X. (2014) Forces driving epithelial wound healing. *Nature physics*, 10(9), 683–690.

Brunner, A., Medvecz, M. & Makra, N. (2021) Human beta defensin levels and vaginal microbiome composition in post-menopausal women diagnosed with lichen sclerosus*. Sci Rep,* 11(1), 15999.

Bucekova, M., Sojka, M., Valachova, I., Martinotti, S., Ranzato, E., Szep, Z., Majtan, V., Klaudiny, J., & Majtan, J. (2017) Bee-derived antibacterial peptide, defensin-1, promotes wound re-epithelialisation in vitro and in vivo. *Scientific reports*, 7(1), 7340.

Byrd, A. L., Belkaid, Y., & Segre, J. A. (2018) The human skin microbiome. *Nature reviews. Microbiology*, 16(3), 143–155.

Campbell, L., Pepper, T., & Shipman, K. (2019) HbA1c: a review of non-glycaemic variables. *Journal of clinical pathology*, 72(1), 12–19.

Cangkrama, M., Wietecha, M., & Werner, S. (2020) Wound Repair, Scar Formation, and Cancer: Converging on Activin. *Trends in molecular medicine*, 26(12), 1107–1117.

Cao, X., Ding, L., & Mersha, T. B. (2022) Development and validation of an RNA-seq-based transcriptomic risk score for asthma. *Scientific reports*, 12(1), 8643.

Cascini, S., Agabiti, N., Davoli, M., Uccioli, L., Meloni, M., Giurato, L., Marino, C., & Bargagli, A. M. (2020) Survival and factors predicting mortality after major and minor lower-extremity amputations among patients with diabetes: a population-based study using health information systems. *BMJ open diabetes research & care*, 8(1), e001355.

Caudill, M. T., & Brayton, K. A. (2022) The Use and Limitations of the 16S rRNA Sequence for Species Classification of Anaplasma Samples. *Microorganisms*, 10(3), 605.

Celli, A., Sanchez, S., Behne, M., Hazlett, T., Gratton, E., & Mauro, T. (2010) The epidermal Ca(2+) gradient: Measurement using the phasor representation of fluorescent lifetime imaging. *Biophysical journ*al, 98(5), 911–921.

Chacko, A. M., Han, J., Greineder, C. F., Zern, B. J., Mikitsh, J. L., Nayak, M., Menon, D., Johnston, I. H., Poncz, M., Eckmann, D. M., Davies, P. F., & Muzykantov, V. R. (2015) Collaborative Enhancement of Endothelial Targeting of Nanocarriers by Modulating Platelet-Endothelial Cell Adhesion Molecule-1/CD31 Epitope Engagement. *ACS nano*, *9*(7), 6785–6793.

Chapman, R., D'Angelo, A., & Bagby, S. (2022) Nanopore-based metagenomic sequencing: a diagnostic tool in respiratory tract infection. *ERJ open research*, 8(4), 00461-2022.

Charalampous, T., Kay, G. L., Richardson, H., Aydin, A., Baldan, R., Jeanes, C., Rae, D., Grundy, S., Turner, D. J., Wain, J., Leggett, R. M., Livermore, D. M., & O'Grady, J. (2019) Nanopore metagenomics enables rapid clinical diagnosis of bacterial lower respiratory infection. *Nature biotechnology*, 37(7), 783–792.

Chattaway, M. A., Schaefer, U., Tewolde, R., Dallman, T. J. & Jenkins, C. (2017) Identification of Escherichia coli and Shigella Species from Whole-Genome Sequences. *Journal of Clinical Microbiology*, 55(2), 616-623.

Chellan, G., Shivaprakash, S., Karimassery Ramaiyar, S., Varma, A. K., Varma, N., Thekkeparambil Sukumaran, M., Rohinivilasam Vasukutty, J., Bal, A., & Kumar, H. (2010) Spectrum and prevalence of fungi infecting deep tissues of lower-limb wounds in patients with type 2 diabetes. *Journal of clinical microbiology*, 48(6), 2097–2102.

Chen, C., Krishnan, V., Macon, K., Manne, K., Narayana, S. V. & Schneewind, O. (2013) Secreted proteases control autolysin-mediated biofilm growth of Staphylococcus aureus. *The Journal of Biological Chemistry*, 288(41), 29440-29452.

Chen, L., & DiPietro, L. A. (2017) Toll-Like Receptor Function in Acute Wounds. *Advances in wound care*, 6(10), 344–355.

Chen, Y. E., Fischbach, M. A. & Belkaid, Y. (2018) Skin microbiota–host interactions. *Nature*, 553(7689), 427-436.

Cheng, X., Zhang, Y., Li, Y., Wu, Q., Wu, J., Park, S. K., Guo, C., & Lu, J. (2022) Meta-analysis of 16S rRNA microbial data identified alterations of the gut microbiota in COVID-19 patients during the acute and recovery phases. *BMC microbiology*, 22(1), 274

Cheng, Y. H., Tsai, N. C., Chen, Y. J., Weng, P. L., Chang, Y. C., Cheng, J. H. & Ko, J. Y. (2022). Extracorporeal Shock Wave Therapy Combined with Platelet-Rich Plasma during Preventive and Therapeutic Stages of Intrauterine Adhesion in a Rat Model. *Biomedicines*, 10(2), 476.

Chesko, D. M., & Wilgus, T. A. (2022) Immune Cells in Cutaneous Wound Healing: A Review of Functional Data from Animal Models. *International journal of molecular sciences*, 23(5), 2444.

Childs, D. R., & Murthy, A. S. (2017) Overview of Wound Healing and Management. *The Surgical clinics of North America*, 97(1), 189–207.

Cho, I. & Blaser, M. J. (2012) The human microbiome: at the interface of health and disease. *Nat Rev Genet*, 13(4), 260-270.

Chong, J., Liu, P., Zhou, G. & Xia, J. (2020) Using Microbiome Analyst for comprehensive statistical, functional, and meta-analysis of microbiome data. *Nat Protoc*, 15(3), 799-821.

Christman, A. L., Selvin, E., Margolis, D. J., Lazarus, G. S., & Garza, L. A. (2011) Hemoglobin A1c predicts healing rate in diabetic wounds. *The Journal of investigative dermatology*, 131(10), 2121–2127.

Ciuffreda, L., Rodríguez-Pérez, H. & Flores, C. (2021) Nanopore sequencing and its application to the study of microbial communities. *Comput Struct Biotechnol J*, 19 (1), 1497-1511.

Chuan, F., Tang, K., Jiang, P., Zhou, B., & He, X. (2015) Reliability and validity of the perfusion, extent, depth, infection and sensation (PEDIS) classification system and score in patients with diabetic foot ulcer. *PloS one*, *10*(4), e0124739.

Ciuffreda, L., Rodríguez-Pérez, H. & Flores, C. (2021) Nanopore sequencing and its application to the study of microbial communities. *Computational and Structural Biotechnology Journal*, 19(6), 1497-1511.

Clinton, A. & Carter, T. (2015) Chronic Wound Biofilms: Pathogenesis and Potential Therapies. *Laboratory Medicine*, 46(4), 277-284.

Clotman, K., & Twickler, M. B. (2020) Diabetes or endocrinopathy admitted in the COVID-19 ward. *European journal of clinical investigation*, 50(7), e13262.

Coates, M., Blanchard, S. & MacLeod, A. S. (2018) Innate antimicrobial immunity in the skin: A protective barrier against bacteria, viruses, and fungi. *PLOS*, 14(12), 100-153

Cohen, E., Johnson, C., Redmond, C. J., Nair, R. R., & Coulombe, P. A. (2022) Revisiting the significance of keratin expression in complex epithelia. *Journal of cell science*, 135(20), 1-10.

Contreras, G., Shirdel, I., Braun, M. S., & Wink, M. (2020) Defensins: Transcriptional regulation and function beyond antimicrobial activity. *Developmental and comparative immunology*, 104(1), 103556.

Cook, E., Booth, A., Coleman, E., Scantlebury, A., McDaid, C., Hewitt, C., Corbacho, B., Rangan, A., Adamson, J., Ranganathan, A., Khan, A., Ahuja, S., Turner, E., May, P., Hilton, C., & Torgerson, D. J. (2020) Pragmatic randomised evaluation of stable thoracolumbar fracture treatment outcomes (PRESTO): study protocol for a randomised controlled feasibility trial combined with a qualitative study and survey. *Pilot and feasibility studies*, 6(1), 38.

Cosma-Grigorov, A., Meixner, H., Mrochen, A., Wirtz, S., Winkler, J., & Marxreiter, F. (2020) Changes in Gastrointestinal Microbiome Composition in PD: A Pivotal Role of Covariates. *Frontiers in neurology*, 11(1), 1041.

Cui, H. S., Hong, A. R., Kim, J. B., Yu, J. H., Cho, Y. S., Joo, S. Y., & Seo, C. H. (2018) Extracorporeal Shock Wave Therapy Alters the Expression of Fibrosis-Related Molecules in Fibroblast Derived from Human Hypertrophic Scar. *International journal of molecular sciences*, 19(1), 124.

Daltrey, D. C., Rhodes, B. & Chattwoood, J. G. (1981) Investigation into the microbial flora of healing and non-healing decubitus ulcers. *Journal of Clinical Oathology*, 34(7), 701-705.

Datey, A., Thaha, C. S. A., Patil, S. R., Gopalan, J., & Chakravortty, D. (2019) Shockwave Therapy Efficiently Cures Multispecies Chronic Periodontitis in a Humanized Rat Model. *Frontiers in bioengineering and biotechnology*, 7(1), 382.

Dasu, M. R., Thangappan, R. K., Bourgette, A., DiPietro, L. A., Isseroff, R., & Jialal, I. (2010) TLR2 expression and signaling-dependent inflammation impair wound healing in diabetic mice. *Laboratory investigation; a journal of technical methods and pathology*, 90(11), 1628–1636.

Davis, T. A., Stojadinovic, A., Anam, K., Amare, M., Naik, S., Peoples, G. E., Tadaki, D., & Elster, E. A. (2009) Extracorporeal shock wave therapy suppresses the early proinflammatory immune response to a severe cutaneous burn injury. *International wound journal*, 6(1), 11–21.

Del Regno, L., Catapano, S., Di Stefani, A., Cappilli, S., & Peris, K. (2022) A Review of Existing Therapies for Actinic Keratosis: Current Status and Future Directions. *American journal of clinical dermatology*, 23(3), 339–352.

Demidova-Rice, T. N., Hamblin, M. R. & Herman, I. M. (2012) Acute and impaired wound healing: pathophysiology and current methods for drug delivery, part 1: normal and chronic wounds: biology, causes, and approaches to care. *Advances in skin & wound care*, 25 (7), 304-305.

Deng, X., Gould, M., & Ali, M. A. (2022) A review of current advancements for wound healing: Biomaterial applications and medical devices. Journal of biomedical materials research. Part B, *Applied biomaterials*, 110(11), 2542–2573.

Dethlefsen, L., & Relman, D. A. (2011) Incomplete recovery and individualized responses of the human distal gut microbiota to repeated antibiotic perturbation. *Proceedings of the National Academy of Sciences of the United States of America*, 108(1), 4554–4561.

Dowd, S. E., Wolcott, R. D,. Sun, Y., McKeehan, T., Smith, E., & Rhoads. (2008) Polymicrobial nature of chronic diabetic foot ulcer biofilm infections determined using bacterial tag encoded FLX amplicon pyrosequencing (bTEFAP). *PLoS One*, 3(1)**,** e3326

Dowd, S. E., Sun, Y., Secor, P. R., Rhoads, D. D., Wolcott, B. M., James, G. A., & Wolcott, R. D. (2008) Survey of bacterial diversity in chronic wounds using pyrosequencing, DGGE, and full ribosome shotgun sequencing. *BMC microbiology*, *8(1)*, 43.

Dowd, S. E., Delton Hanson, J., Rees, E., Wolcott, R. D., Zischau, A. M., Sun, Y., White, J., Smith, D. M., Kennedy, J., & Jones, C. E. (2011) Survey of fungi and yeast in polymicrobial infections in chronic wounds. *Journal of wound care*, 20(1), 40–47.

Dowd, S. E., Hanson, J. D., Rees, E., Wolcott, R. D., Zischau, A. M., Sun, Y., White, J., Smith, D. M., Kennedt, J. & Jones, C. E. (2011) Survey of fungi and yeast in polymicrobial infections in chronic wounds. *Journal of Wound Care*, 20(1), 40-47.

Dowden, R. A., McGuinness, L. R., Wisniewski, P. J., Campbell, S. C., Guers, J. J., Oydanich, M., Vatner, S. F., Häggblom, M. M., & Kerkhof, L. J. (2020) Host genotype and exercise exhibit species-level selection for members of the gut bacterial communities in the mouse digestive system. *Scientific reports*, 10(1), 8984.

Drayton, M., Deisinger, J. P., Ludwig, K. C., Raheem, N., Müller, A., Schneider, T., & Straus, S. K. (2021) Host Defense Peptides: Dual Antimicrobial and Immunomodulatory Action. *International journal of molecular sciences*, 22(20), 11172.

Drummond, R., Dambuza, I., Vautier, S. (2016) CD4+ T-cell survival in the GI tract requires dectin-1 during fungal infection. *Mucosal Immunol*, 9(1), 492–502.

Duan, T., Du, Y., Xing, C., Wang, H. Y., & Wang, R. F. (2022) Toll-Like Receptor Signalling and Its Role in Cell-Mediated Immunity. *Frontiers in immunology*, 13(1), 812774.

Durand, B. A. R. N., Pouget, C., Magnan, C., Molle, V., Lavigne, J. P., & Dunyach-Remy, C. (2022) Bacterial Interactions in the Context of Chronic Wound Biofilm: A Review. *Microorganisms*, 10(8), 1500.

El-Zayat, S.R., Sibaii, H. & Mannaa, F.A. (2019) Toll-like receptors activation, signaling, and targeting: an overview. *Bull Natl Res Cent*, 43(2), 187.

Emerson, J. B., Adams, R. I., Román, C., Brooks, B., Coil, D. A., Dahlhausen, K., Ganz, H. H., Hartmann, E. M., Hsu, T., Justice, N. B., Paulino-Lima, I. G., Luongo, J. C., Lymperopoulou, D. S., Gomez-Silvan, C., Rothschild-Mancinelli, B., Balk, M., Huttenhower, C., Nocker, A., Vaishampayan, P., & Rothschild, L. J. (2017) Schrödinger's microbes: Tools for distinguishing the living from the dead in microbial ecosystems. *Microbiome*, *5*(1), 86-101.

Eming, S. A., Martin, P., & Tomic-Canic, M. (2014) Wound repair and regeneration: mechanisms, signaling, and translation. *Science translational medicine*, 6(265), 265-256.

Everett, E., & Mathioudakis, N. (2018) Update on management of diabetic foot ulcers. *Annals of the New York Academy of Sciences*, 1411(1), 153–165.

Évora, A. S., Adams, M. J., Johnson, S. A., & Zhang, Z. (2021) Corneocytes: Relationship between Structural and Biomechanical Properties. *Skin pharmacology and physiology*, 34(3), 146–161.

Fabisiak, A., Murawska, N., & Fichna, J. (2016) LL-37: Cathelicidin-related antimicrobial peptide with pleiotropic activity. *Pharmacological reports*, 68(4), 802–808.

Fadrosh, E. A. E & Rasko, D. (2013) The Human Microbiome: From Symbiosis to Pathogenesis. *Annual Review of Medicine*, 64(3), 145-163.

Falconer, A., Ikram, M., Bissett, C. E., Cerio, R. & Quinn, A, G. (2001) Expression of the Peptide Antibiotics Human β Defensin-1 and Human β Defensin-2 in Normal Human Skin. *Journal of Investigative Dermatology*, 117 (1), 106-111.

Farhan, N., & Jeffery, S. (2021) Diagnosing Burn Wounds Infection: The Practice Gap & Advances with MolecuLight Bacterial Imaging. *Diagnostics*, 11(2), 268.

Feldman, E. L., Callaghan, B. C., Pop-Busui, R., Zochodne, D. W., Wright, D. E., Bennett, D. L., Bril, V., Russell, J. W., & Viswanathan, V. (2019) Diabetic neuropathy. *Nature reviews. Disease primers*, 5(1), 41.

Felipe, R. R., & Plata-Que, M. T. (2021) Predictors of Outcomes of Foot Ulcers among Individuals with Type 2 Diabetes Mellitus in an Outpatient Foot Clinic. *Journal of the ASEAN Federation of Endocrine Societies*, 36(2), 189–195.

Fore, J. (2006) A review of skin and the effects of aging on skin structure and function. *Ostomy/wound management*, 52(9), 24–37.

Fritz, P., Beck-Jendroschek, V., & Brasch, J. (2012) Inhibition of dermatophytes by the antimicrobial peptides human β-defensin-2, ribonuclease 7 and psoriasin. *Medical mycology*, 50(6), 579–584.

Fu, Y., Ho, B. T., & Mekalanos, J. J. (2018) Tracking Vibrio cholerae Cell-Cell Interactions during Infection Reveals Bacterial Population Dynamics within Intestinal Microenvironments. *Cell host & microbe*, 23(2), 274–281.

Gallo, R. L. (2017) Human Skin Is the Largest Epithelial Surface for Interaction with Microbes. *The Journal of investigative dermatology*, 137(6), 1213–1214.

Galtier, F. (2010) Definition, epidemiology, risk factors. *Diabetes & metabolism*, 36(2), 628–651.

Game, F. (2015) Classification of diabetic foot ulcers. *Diabetes Metabolisms Research and Reviews*, 32(1), 186-194.

Ganz, T. (2003) Defensins: antimicrobial peptides of innate immunity. *Nature Reviews Immunology*, 3 (1), 710–720.

Gardner, S. E., Frantz, R. A. & Doebbeling, B. N. (2001) The validity of the clinical signs and symptoms used to identify localized chronic wound infection. *Wound Repair Regeneration*, 9(1)**,** 178-188.

Gardner, S. E., Frantz, R. A., Saltzman, C. L., Hillis, S. L., Park, H. & Scherubel, M. (2006) Diagnostic validity of three swab techniques for identifying chronic wound infection. *Wound Repair Regeneration*, 14(1)**,** 548.

Gardner, S. E. & Frantz, R. A. (2008) Wound Bioburden and Infection-Realted Complications in Diabetic Foot Ulcers. *Biological Research for Nursing*, 10(1), 44-53.

Gardner, S. E., Hillis, S. L., Heilmann, K., Segre, J. A., & Grice, E. A. (2013) The neuropathic diabetic foot ulcer microbiome is associated with clinical factors. *Diabetes*, *62*(3), 923–930.

Garrido-Cardenas, J. A., Garcia-Maroto, F., Alvarez-Bermejo, J. A., & Manzano-Agugliaro, F. (2017) DNA Sequencing Sensors: An Overview. *Sensors*, *17*(3), 588.

Gautam, S. S., Koc, R., Leong, K. W., Mac Aogáin, M., & O'Toole, R. F. (2019) A step-by-step beginner's protocol for whole genome sequencing of human bacterial pathogens. *Journal of Biological Methods*, *6*(1), 110-120.

Gene Ontology Consortium. (2021) The Gene Ontology resource: enriching a GOld mine. *Nucleic acids research*, 49(1), 325–334.

Gera, S., Kankuri, E., & Kogermann, K. (2022) Antimicrobial peptides - Unleashing their therapeutic potential using nanotechnology. *Pharmacology & therapeutics*, 232, 107990.

Gerdesmeyer, L., von Eiff, C., Horn, C., Henne, M., Roessner, M., Diehl, P., & Gollwitzer, H. (2005) Antibacterial effects of extracorporeal shock waves. *Ultrasound in medicine & biology*, 31(1), 115–119.

Ghasemi, M., Turnbull, T., Sebastian, S., & Kempson, I. (2021) The MTT Assay: Utility, Limitations, Pitfalls, and Interpretation in Bulk and Single-Cell Analysis. *International journal of molecular sciences*, 22(23), 12827.

Gläser, R., Harder, J., Lange, H., Bartels, J., Christophers, E., & Schröder, J. M. (2005) Antimicrobial psoriasin (S100A7) protects human skin from Escherichia coli infection. *Nature immunology*, 6(1), 57–64.

Goodwin, S., Gurtowski, J., Ethe-Sayers, S., Deshpande, P., Schatz, M. C., & McCombie, W. R. (2015) Oxford Nanopore sequencing, hybrid error correction, and de novo assembly of a eukaryotic genome. *Genome research*, 25(11), 1750–1756.

Good, I. J. (1953) Species and the Estimation of The Population Frequencies of Population Parameters. *Biometrika*, 40(3-4), 237-264.

Gori, E., Callea, E., Alberani, F., & Orlando, L. (2014) Microbial monitoring and methods of sample collection: a GITMO survey. *Ecancer medical science*, 8(1), 421.

Goyal, S., Castrillón-Betancur, J. C., Klaile, E. & Slevogt, H (2018) The Interaction of Human Pathogenic Fungi With C-Type Lectin Receptors. *Frontiers in Immunology*, 9(1), 261.

Green, E. M., Mansfield, J. C., Bell, J. S., & Winlove, C. P. (2014) The structure and micromechanics of elastic tissue. *Interface focus*, *4*(2), 20130058.

Grice, E. A. (2014) The skin microbiome: potential for novel diagnostic and therapeutic approaches to cutaneous disease. *Semin Cutan Med Surg*, 33(2), 98-103.

Grice, E. A. & Segre, J. A. (2011) The skin microbiome. *Nat Rev Microbiol*, 9(4), 244-253.

Grice, E. A., & Segre, J. A. (2012) Interaction of the microbiome with the innate immune response in chronic wounds. *Advances in experimental medicine and biology*, 946 (1), 55–68.

Grice, E. A., Kong, H. H., Conlan, S., Deming, C. B., Davis, J., Young, A. C., Bouffard, G. G., Blakesley, R. W., Murray, P. R., Green, E. D., Turner, M. L., Segre, J. A., & Program, N. C. S. (2009) Topographical and temporal diversity of the human skin microbiome. *Science,* 324(5931), 1190-1192.

Grönberg, A., Mahlapuu, M., Ståhle, M., Whately-Smith, C., & Rollman, O. (2014) Treatment with LL-37 is safe and effective in enhancing healing of hard-to-heal venous leg ulcers: a randomized, placebo-controlled clinical trial. *Wound repair and regeneration*, 22(5), 613–621.

Gu, W., Miller, S., & Chiu, C. Y. (2019) Clinical Metagenomic Next-Generation Sequencing for Pathogen Detection. *Annual review of pathology*, *14*, 319–338.

Guest, J. F., Ayoub, N., McIlwraith, T., Uchegbu, I., Gerrish, A., Weidlich, D., Vowden, K. & Vowden, P. (2015) Health economic burden that wounds impose on the National Health Service in the UK. *BMJ Open*, 5(12), e009283.

Guest, J. F., Fuller, G. W. & Vowden, P. (2020) Cohort study evaluating the burden of wounds to the UK's National Health Service in 2017/2018: update from 2012/2013. *BMJ Open*, 10(12), e045253.

Gupta, A., Patel, R., Baddour, L. M., Pardi, D. S., & Khanna, S. (2014) Extraintestinal Clostridium difficile infections: a single-center experience. *Mayo Clinic proceedings*, 89(11), 1525–1536.

Gurevich, D. B., Severn, C. E., Twomey, C., Greenhough, A., Cash, J., Toye, A. M., Mellor, H., & Martin, P. (2018) Live imaging of wound angiogenesis reveals macrophage orchestrated vessel sprouting and regression*. The EMBO journal*, 37(13), 77-86.

Gutowska-Owsiak, D., Podobas, E. I., Eggeling, C., Ogg, G. S., & Bernardino de la Serna, J. (2020) Addressing Differentiation in Live Human Keratinocytes by Assessment of Membrane Packing Order. *Frontiers in cell and developmental biology*, 8(1), 573230.

Haalboom, M. (2018) Chronic Wounds: Innovations in Diagnostics and Therapeutics. *Current medicinal chemistry*, 25(41), 5772–5781.

Han, A., Zenilman, J. M., Melendez, J. H., Shirtliff, M. E., Agostinho, A., James, G., Stewart, P. S., Mongodin, E. F., Rao, D., Rickard, A. H., & Lazarus, G. S. (2011) The importance of a multifaceted approach to characterizing the microbial flora of chronic wounds. *Wound repair and regeneration*, *19*(5), 532–541.

Harder, J., & Schroder, J. M. (2002) RNase 7, a novel innate immune defense antimicrobial protein of healthy human skin. *The Journal of biological chemistry*, 277(48), 46779–46784.

Harris, A. R., Peter, L., Bellis, J., Baum, B., Kabla, A. J., & Charras, G. T. (2012) Characterizing the mechanics of cultured cell monolayers. *Proceedings of the National Academy of Sciences of the United States of America*, 109(41), 16449–16454

Haupt, G. (1997) Use of extracorporeal shock waves in the treatment of pseudarthrosis, tendinopathy and other orthopedic diseases. *The Journal of urology*, 158(1), 4–11.

Haupt, G., & Chvapil, M. (1990) Effect of shock waves on the healing of partial-thickness wounds in piglets. *The Journal of surgical research*, 49(1), 45–48.

Hassanshahi, A., Moradzad, M., Ghalamkari, S., Fadaei, M., Cowin, A. J., & Hassanshahi, M. (2022) Macrophage-Mediated Inflammation in Skin Wound Healing. *Cells*, 11(19), 2953.

Hayflick, L., & Moorhead, P. S. (1961) The serial cultivation of human diploid cell strains. *Experimental cell research*, 25(1), 585–621.

Heravi, F. S., Zakrzewski, M., Vickery, K., Malone, M., & Hu, H. (2020) Metatranscriptomic Analysis Reveals Active Bacterial Communities in Diabetic Foot Infections. *Frontiers in microbiology*, 11(1), 1688.

Heravi, A., Henn, A., Deuster, S., McLennan, S., Gloy, V., Mitter, V. R. & Briel, M. (2022) Investigational medicinal products, related costs and hospital pharmacy services for investigator-initiated trials: A mixed-methods study. *PloS one*, 17(3), e0264427.

Hitchman, L. H., Totty, J. P., Cai, P., Smith, G. E., Carradice, D., & Chetter, I. C. (2023) Extracorporeal shockwave therapy for diabetic foot ulcers: a feasibility study. *Journal of wound care*, *32*(3), 182–192.

Ho, C.-H., Liao, P.-W., Fan, C.-K., Liu, S.-P., & Cheng, P.-C. (2022) RNase 7 Inhibits Uropathogenic Escherichia coli-Induced Inflammation in Bladder Cells under a High-Glucose Environment by Regulating the JAK/STAT Signaling Pathway. *International Journal of Molecular Sciences*, 23(9), 5156.

Holsapple, J. S., Cooper, B., Berry, S. H., Staniszewska, A., Dickson, B. M., Taylor, J. A., Bachoo, P., & Wilson, H. M. (2021) Low Intensity Shockwave Treatment Modulates Macrophage Functions Beneficial to Healing Chronic Wounds. *International journal of molecular sciences*, 22(15), 7844.

Honda, M., & Kubes, P. (2018) Neutrophils and neutrophil extracellular traps in the liver and gastrointestinal system. Nature reviews. Gastroenterology & hepatology, 15(4), 206–221.

Horn, C., Mengele, K., Gerdesmeyer, L., Gradinger, R., & Gollwitzer, H. (2009) The effect of antibacterial acting extracorporeal shockwaves on bacterial cell integrity. *Medical science monitor : international medical journal of experimental and clinical research*, 15(12), BR364–BR369.

Huang, Y. E., Shen, X., Yin, D., Lan, S., Lu, Y., Zhou, P., Ma, L., Zhang, Y., Sheng, Y., Zhang, Y., Li, M., Hu, F., Chen, J., Li, P., El-Omar, E. M., & Zheng, H. (2022) Disrupted establishment of anaerobe and facultative anaerobe balance in preterm infants with extrauterine growth restriction. *Frontiers in pediatrics*, *10*, 935458.

Ince, P., Abbas, Z. G., Lutale, J. K., Basit, A., Ali, S. M., Chohan, F., Morbach, S., Möllenberg, J., Game, F. L., & Jeffcoate, W. J. (2008) Use of the SINBAD classification system and score in comparing outcome of foot ulcer management on three continents. *Diabetes care*, *31*(5), 964–967.

Ingram, J. R., Cawley, S., Coulman, E., Gregory, C., Thomas-Jones, E., Pickles, T., Cannings-John, R., Francis, N. A., Harding, K., Hood, K., & Piguet, V. (2018) Levels of wound calprotectin and

other inflammatory biomarkers aid in deciding which patients with a diabetic foot ulcer need antibiotic therapy (INDUCE study). *Diabetic medicine: a journal of the British Diabetic Association*, 35(2), 255–261.

Jalilian, M., Ahmadi Sarbarzeh, P., & Oubari, S. (2020) Factors Related to Severity of Diabetic Foot Ulcer: A Systematic Review. *Diabetes, metabolic syndrome and obesity: targets and therapy*, 13, 1835–1842.

Javeed, N., & Matveyenko, A. V. (2018) Circadian Etiology of Type 2 Diabetes Mellitus. *Physiology*, 33(2), 138–150.

Jeffocoate, W. J., Bus, S. A., Game, F. L., Hinchliffe, R. J., Price, P. E. & Schaper, N. C. (2016) Reporting standards of studies and papers on the preventiona and managment of foot ulcers in diabetes: required details and markers of good qua. *The Lancet*, 4(9), 781-788.

Jnana, A., Muthuraman, V., Varghese, V. K., Chakrabarty, S., Murali, T. S., Ramachandra, L., Shenoy, K. R., Rodrigues, G. S., Prasad, S. S., Dendukuri, D., Morschhauser, A., Nestler, J., Peter, H., Bier, F. F., & Satyamoorthy, K. (2020) Microbial Community Distribution and Core Microbiome in Successive Wound Grades of Individuals with Diabetic Foot Ulcers. *Applied and environmental microbiology*, 86(6), e02608-19.

Johnson, T. R., Gomez, B. I., McIntyre, M. K., Dubick, M. A., Christy, R. J., Nicholson, S. E. & Burmeister, D. M. (2018) The Cutaneous Microbiome and Wounds: New Molecular Targets to Promote Wound Healing. *International Journal of Molecular Sciences*, 19(9), 2699-2722.

Jones, R. E., Foster, D. S., & Longaker, M. T. (2018) Management of Chronic Wounds. *JAMA*, 320(14), 1481–1482.

Jovic, D., Liang, X., Zeng, H., Lin, L., Xu, F., & Luo, Y. (2022) Single-cell RNA sequencing technologies and applications: A brief overview. *Clinical and translational medicine*, 12(3), e694.

Juster-Switlyk, K., & Smith, A. G. (2016) Updates in diabetic peripheral neuropathy. *Research*, 5(1), 738-742.

Kaiser, P., Wächter, J., & Windbergs, M. (2021) Therapy of infected wounds: overcoming clinical challenges by advanced drug delivery systems. *Drug delivery and translational research*, 11(4), 1545–1567.

Kalan, L., & Grice, E. A. (2018) Fungi in the Wound Microbiome. *Advances in wound care*, *7*(7), 247–255.

Kalan, L., Loesche, M., Hodkinson, B. P., Heilmann, K., Ruthel, G., Gardner, S. E., & Grice, E. A. (2016) Redefining the Chronic-Wound Microbiome: Fungal Communities Are Prevalent, Dynamic, and Associated with Delayed Healing. *mBio*, 7(5), e01058-16.

Kalan, L., Loesche, M., Hodkinson, B. P., Heilmann, K., Ruthel, G., Gardner, S. E. & Grice, E. A. (2018) Redefining the Chronic-Wound Microbiome: Fungal Communities Are Prevalent, Dynamic, and Associated with Delayed Healing. *American Society of Microbiology*, 10(11), 16-58.

Kean, R., Rajendran, R., Haggarty, J., Townsend, E. M., Short, B., Burgess, K. E., Lang, S., Millington, O., Mackay, W. G., Williams, C., & Ramage, G. (2017) Candida albicans Mycofilms Support Staphylococcus aureus Colonization and Enhances Miconazole Resistance in Dual-Species Interactions. *Frontiers in microbiology*, 8(1), 258.

Kelmansky, D. M., Martínez, E. J., & Leiva, V. (2013) A new variance stabilizing transformation for gene expression data analysis. *Statistical applications in genetics and molecular biology*, 12(6), 653–666.

Kerkhof, L. J. (2021) Is Oxford Nanopore sequencing ready for analyzing complex microbiomes?. *FEMS microbiology ecology*, 97(3), 001-9.

Kharroubi, A. T., & Darwish, H. M. (2015) Diabetes mellitus: The epidemic of the century. *World journal of diabetes*, 6(6), 850–867.

Khosravi, H., Hou, A., Colgtove, R. C. & Behlau, I. (2018) Group C streptococcal cellulitis, looking deeper than the skin. *JAAD Case Reports*, 4(8), 818-812.

Kiefer, J., & Mazzeffi, M. (2022) Complications of Vascular Disease. *Anesthesiology clinics*, 40(4), 587–604.

Kim, Y. G., Park, J. H., Shaw, M. H., Franchi, L., Inohara, N., & Núñez, G. (2008) The cytosolic sensors Nod1 and Nod2 are critical for bacterial recognition and host defense after exposure to Toll-like receptor ligands. *Immunity*, 28(2), 246–257.

Kim, D., Song, L., Breitwieser, F. P., & Salzberg, S. L. (2016) Centrifuge: rapid and sensitive classification of metagenomic sequences. *Genome research*, 26(12), 1721–1729.

Ko, K. K. K., Chng, K. R., & Nagarajan, N. (2022) Metagenomics-enabled microbial surveillance. *Nature microbiology*, 7(4), 486–496.

Kolimi, P., Narala, S., Nyavanandi, D., Youssef, A. A. A., & Dudhipala, N. (2022) Innovative Treatment Strategies to Accelerate Wound Healing: Trajectory and Recent Advancements. *Cells*, 11(15), 2439.

Konop, M., Rybka, M., & Drapała, A. (2021) Keratin Biomaterials in Skin Wound Healing, an Old Player in Modern Medicine: A Mini Review. *Pharmaceutics,* 13(12), 2029.

Koster, M. I. (2009) Making an epidermis. *Annals of the New York Academy of Sciences*, 1170, 7–10.

Köten, B., Simanski, M., Gläser, R., Podschun, R., Schröder, J. M., & Harder, J. (2009) RNase 7 contributes to the cutaneous defense against Enterococcus faecium. *PloS one*, 4(7), e6424.

Kovaka, S., Fan, Y., Ni, B., Timp, W., & Schatz, M. C. (2021) Targeted nanopore sequencing by real-time mapping of the raw electrical signal with UNCALLED. *Nature Biotechnology*, 39(4), 431–441.

Krizek, T. J. & Robson, M. C. (1975) Evolution of quantitative bacteriology in wound management. *The American Journal of Surgery*, 130(5), 579-584.

Kuo, Y. R., Wang, C. T., Wang, F. S., Yang, K. D., Chiang, Y. C., & Wang, C. J. (2009) Extracorporeal shock wave treatment modulates skin fibroblast recruitment and leukocyte infiltration for enhancing extended skin-flap survival. *Wound repair and regeneration*, 17(1), 80–87.

Kwa, W. T., Sundarajoo, S., Toh, K. Y., & Lee, J. (2023) Application of emerging technologies for gut microbiome research. *Singapore medical journal*, *64*(1), 45–52.

Lallyett, C., Yeung, C. C., Nielson, R. H., Zeef, L., Chapman-Jones, D., Kjaer, M., & Kadler, K. E. (2018) Changes in S100 Proteins Identified in Healthy Skin following Electrical Stimulation: Relevance for Wound Healing. *Advances in skin & wound care*, 31(7), 322–327.

Lapidus, A. L., & Korobeynikov, A. I. (2021) Metagenomic Data Assembly - The Way of Decoding Unknown Microorganisms. *Frontiers in microbiology*, *12*, 613791.

Lavery, L.A., Armstrong, D.G & Harkless, L.B. (1996) Classification of diabetic foot wounds. *Journal of Foot and Ankle Surgery*, 35(1), 528–531.

Lazarus, G. S., Cooper, D. M., Knighton, D. R., Margolis, D. J., Pecoraro, R. E., Rodeheaver, G., & Robson, M. C. (1994) Definitions and guidelines for assessment of wounds and evaluation of healing. *Archives of dermatology*, 130(4), 489–493.

Leaper, D., & Ousey, K. (2015) Evidence update on prevention of surgical site infection. *Current opinion in infectious diseases*, 28(2), 158–163.

Lebeaux, D., Chauhan, A., Rendueles, O. & Beloin, C. (2013) From *in vitro* to *in vivo* Models of Bacterial Biofilm-Related Infections. *Pathogens*, 2(2), 288-356.

Lee, D. Y., Yamasaki, K., Rudsil, J., Zouboulis, C. C., Park, G. T., Yang, J. M. & Gallo, R. L. (2008) Sebocytes express functional cathelicidin antimicrobial peptides and can act to kill propionibacterium acnes. *Journal of Investigative Dermatology*, 128(7), 1863-1866.

Lee, J. Y., Hwang, E. H., Kim, D. J., Oh, S. M., Lee, K. B., Shin, S. J., & Park, J. H. (2016) The role of nucleotide-binding oligomerization domain 1 during cytokine production by macrophages in response to Mycobacterium tuberculosis infection. *Immunobiology*, 221(1), 70–75.

Lei, J., Sun, L., Huang, S., Zhu, C., Li, P., He, J., Mackey, V., Coy, D. H., & He, Q. (2019) The antimicrobial peptides and their potential clinical applications. *American journal of translational research*, 11(7), 3919–3931.

Leon, B. M., & Maddox, T. M. (2015) Diabetes and cardiovascular disease: Epidemiology, biological mechanisms, treatment recommendations and future research. *World journal of diabetes*, 6(13), 1246–1258.

Leonel, C., Sena, I., Silva, W. N., Prazeres, P., Fernandes, G. R., Mancha Agresti, P., Martins Drumond, M., Mintz, A., Azevedo, V., & Birbrair, A. (2019) Staphylococcus epidermidis role in the skin microenvironment. *Journal of cellular and molecular medicine*, 23(9), 5949–5955.

León-Buitimea, A., Garza-Cárdenas, C. R., Garza-Cervantes, J. A., Lerma-Escalera, J. A., & Morones-Ramírez, J. R. (2020) The Demand for New Antibiotics: Antimicrobial Peptides, Nanoparticles, and Combinatorial Therapies as Future Strategies in Antibacterial Agent Design. *Frontiers in microbiology*, 11(1), 1669.

Lepäntalo, M., Apelqvist, J., Setacci, C., Ricco, J. B., de Donato, G., Becker, F., Robert-Ebadi, H., Cao, P., Eckstein, H. H., De Rango, P., Diehm, N., Schmidli, J., Teraa, M., Moll, F. L., Dick, F., & Davies, A. H. (2011) Chapter V: Diabetic foot. *European journal of vascular and endovascular surgery: the official journal of the European Society for Vascular Surgery*, 42(2), 60–S74.

Li, X., Lu, Y., & Wei, P. (2018) Association between VEGF genetic variants and diabetic foot ulcer in Chinese Han population: A case-control study. *Medicine*, *97*(20), 10672.

Levine, N. S., Lindberg, R. B., Mason, A. D. & Pruitt, B. A. (1976) The quantitative swab culture and smear: a quick, simple method for determining the number of viable aerobic bacteria on open wounds. *Journal of Trauma*, 16(1)**,** 89-90.

Lin, X., Xu, Y., Pan, X., Xu, J., Ding, Y., Sun, X., Song, X., Ren, Y., & Shan, P. F. (2020) Global, regional, and national burden and trend of diabetes in 195 countries and territories: an analysis from 1990 to 2025. *Scientific reports*, 10(1), 14790.

Lloyd-Price, J., Mahurkar, A., Rahnavard, G. (2017) Strains, functions and dynamics in the expanded Human Microbiome Project. *Nature* 550, 61–66

Loesche, M., Gardner, S. E., Kalan, L., Horwinski, J., Zheng, Q., Hodkinson, B. P., Tyldsley, A. S., Franciscus, C. L., Hillis, S. L., Mehta, S., Margolis, D. J., & Grice, E. A. (2017) Temporal Stability in Chronic Wound Microbiota Is Associated With Poor Healing. *The Journal of investigative dermatology*, *137*(1), 237–244.

Lu, H., Giordano, F., & Ning, Z. (2016) Oxford Nanopore MinION Sequencing and Genome Assembly. *Genomics, proteomics & bioinformatics*, *14*(5), 265–279.

Madden, G. R., German Mesner, I., Cox, H. L., Mathers, A. J., Lyman, J. A., Sifri, C. D., & Enfield, K. B. (2018) Reduced Clostridium difficile Tests and Laboratory-Identified Events With a Computerized Clinical Decision Support Tool and Financial Incentive. *Infection control and hospital epidemiology*, 39(6), 737–740.

Mahlapuu, M., Sidorowicz, A., Mikosinski, J., Krzyżanowski, M., Orleanski, J., Twardowska-Saucha, K., Nykaza, A., Dyaczynski, M., Belz-Lagoda, B., Dziwiszek, G., Kujawiak, M., Karczewski, M., Sjöberg, F., Grzela, T., Wegrzynowski, A., Thunarf, F., Björk, J., Ekblom, J., Jawien, A., & Apelqvist, J. (2021) Evaluation of LL-37 in healing of hard-to-heal venous leg ulcers: A multicentric prospective randomized placebo-controlled clinical trial. *Wound repair and regeneration,* 29(6), 938–950.

Malla, M. A., Dubey, A., Kumar, A., Yadav, S., Hashem, A. & Abd-Allah, E. F. (2019) Exploring the Human Microbiome: The Potential Future Role of Next-Generation Sequencing in Disease Diagnosis and Treatment. *Frontiers in Immunolog*y, 10(22), 68-89.

Mallick, H., Rahnavard, A., McIver, L. J., Ma, S., Zhang, Y., Nguyen, L. H., Tickle, T. L., Weingart, G., Ren, B., Schwager, E. H., Chatterjee, S., Thompson, K. N., Wilkinson, J. E., Subramanian, A., Lu, Y., Waldron, L., Paulson, J. N., Franzosa, E. A., Bravo, H. C., & Huttenhower, C. (2021) Multivariable association discovery in population-scale meta-omics studies. *PLoS computational biology*, 17(11), e1009442.

Mansy, M., Soliman, M., Mubarak, R., & Shamel, M. (2020) The role of exogenous epidermal growth factor on Ki-67 proliferation marker expression in the submandibular salivary gland of albino rats receiving doxorubicin. *F1000 Research*, 9(10), 1393.

Marcelino, V. R., Clausen, P. T. L. C., Buchmann, J. P., Wille, M., Iredell, J. R., Meyer, W., Lund, O., Sorrell, T. C., & Holmes, E. C. (2020) CCMetagen: comprehensive and accurate identification of eukaryotes and prokaryotes in metagenomic data. *Genome biology*, 21(1), 103.

Marquet, M., Zöllkau, J., Pastuschek, J., Viehweger, A., Schleußner, E., Makarewicz, O., Pletz, M. W., Ehricht, R., & Brandt, C. (2022) Evaluation of microbiome enrichment and host DNA depletion in human vaginal samples using Oxford Nanopore's adaptive sequencing. *Scientific reports*, 12(1), 4000.

Martin, S., Heavens, D., & Lan, Y. (2022) Nanopore adaptive sampling: a tool for enrichment of low abundance species in metagenomic samples. *Genome Biol,* 23(1), 11.

Masago, K., Fujita, S., Oya, Y., Takahashi, Y., Matsushita, H., Sasaki, E., & Kuroda, H. (2021). Comparison between Fluorimetry (Qubit) and Spectrophotometry (NanoDrop) in the Quantification of DNA and RNA Extracted from Frozen and FFPE Tissues from Lung Cancer Patients: A Real-World Use of Genomic Tests. *Medicina*, 57(12), 1375-1386.

Mata-Martínez, P., Bergón-Gutiérrez. M., & del Fresno., C. (2022) Dectin-1 Signaling Update: New Perspectives for Trained Immunity. *Front. Immunol*. 13(1), 81-2148

McMurdie, P. J., & Holmes, S. (2014) Waste Not, Want Not: Why Rarefying Microbiome Data Is Inadmissible. *PLOS Computational Biology*, 10(4), e1003531.

McNaughton, A.L., Roberts, H.E., & Bonsall, L. (2019) Illumina and Nanopore methods for whole genome sequencing of hepatitis B virus (HBV). *Scientific Reports,* 9(4), 70-81.

Mehra, B. K., Singh, A. K., Gupta, D., Narang, R., & Patil, R. A (2017) A clinicomicrobiological study on the incidence of mycotic infections in diabetic foot ulcers. *INJSS*, 4(50), 51–54.

Meirer, R., Brunner, A., Deibl, M., Oehlbauer, M., Piza-Katzer, H., & Kamelger, F. S. (2007) Shock wave therapy reduces necrotic flap zones and induces VEGF expression in animal epigastric skin flap model. *Journal of reconstructive microsurgery*, 23(4), 231–236.

Menon, G. K., Cleary, G. W., & Lane, M. E. (2012) The structure and function of the stratum corneum. *International journal of pharmaceutics*, 435(1), 3-9.

Mikheyev, A. S., & Tin, M. M. (2014) A first look at the Oxford Nanopore MinION sequencer. *Molecular Ecological Resources*, 14(6), 1097-1102.

Min, K. R., Galvis, A., Baquerizo-Nole, K. L., Sinha, R., Clarke, J., Kirsner, R. S., & Ajdic, D. (2020) Association between baseline abundance of Peptoniphilus, a Gram-positive anaerobic coccus, and wound healing outcomes of DFUs. *PLOS ONE*, 10(13), 99-110.

Misic, A. M., Gardner, S. E., & Grice, E. A. (2014) The Wound Microbiome: Modern Approaches to Examining the Role of Microorganisms in Impaired Chronic Wound Healing. *Advances in wound care*, *3*(7), 502–510.

Mittermayr, R., Antonic, V., Hartinger, J., Kaufmann, H., Redl, H., Téot, L., Stojadinovic, A., & Schaden, W. (2012) Extracorporeal shock wave therapy (ESWT) for wound healing: technology, mechanisms, and clinical efficacy. *Wound repair and Regeneration*, 20(4), 456–465.

Modin, O., Liébana, R., Saheb-Alam, S., Wilén, B. M., Suarez, C., Hermansson, M., & Persson, F. (2020) Hill-based dissimilarity indices and null models for analysis of microbial community assembly. *Microbiome*, 8(1), 132.

Moortgat, P., Anthonissen, M., Van Daele, U., Meirte, J., Vanhullebusch, T., & Maertens, K. (2020) Shock Wave Therapy for Wound Healing and Scar Treatment. *Springer,* 10(1), 55.

Moretti, B., Notarnicola, A., Maggio, G., Moretti, L., Pascone, M., Tafuri, S., & Patella, V. (2009) The management of neuropathic ulcers of the foot in diabetes by shock wave therapy. *BMC musculoskeletal disorders*, 10(1), 54.

Munir, S., Basu, A., Maity, P., Krug, L., Haas, P., Jiang, D., Strauss, G., Wlaschek, M., Geiger, H., Singh, K., & Scharffetter-Kochanek, K. (2020) TLR4-dependent shaping of the wound site by MSCs accelerates wound healing. *EMBO reports*, 21(5), e48777.

Murdoch, C. C., & Skaar, E. P. (2022) Nutritional immunity: the battle for nutrient metals at the host-pathogen interface. *Microbiology*, 20(11), 657–670.

Nasseri, S. & Sharifi, M. (2022) Therapeutic Potential of Antimicrobial Peptides for Wound Healing. *International Journal of Peptide Research and Therapeutics*, 28(38), 588-600.

Negut, I., Grumezescu, V., & Grumezescu, A. M. (2018) Treatment Stratergies for Infected Wounds. *Molecules,* 23(9), 2392-2395.

Nelson, M. T., Pope, C. E., Marsh, R. L., Wolter, D. J., Weiss, E. J., Hager, K. R., Vo, A. T., Brittnacher, M. J., Radey, M. C., Hayden, H. S., Eng, A., Miller, S. I., Borenstein, E., & Hoffman, L. R. (2019) Human and Extracellular DNA Depletion for Metagenomic Analysis of Complex Clinical Infection Samples Yields Optimized Viable Microbiome Profiles. *Cell Rep*, 26(8), 2227-2240.

Nicholls, S. M., Quick, J. C., Tang, S., & Loman, N. J. (2019) Ultra-deep, long-read nanopore sequencing of mock microbial community standards. *GigaScience*, 8(5), 043.

Nikolova, V. L., Smith, M. R. B., Hall, L. J., Cleare, A. J., Stone, J. M., & Young, A. H. (2021) Perturbations in Gut Microbiota Composition in Psychiatric Disorders: A Review and Meta-analysis*. JAMA psychiatry*, 78(12), 1343–1354.

Njeim, R., Azar, W. S., Fares, A. H., Azar, S. T., Kfoury Kassouf, H., & Eid, A. A. (2020) NETosis contributes to the pathogenesis of diabetes and its complications. *Journal of molecular endocrinology*, 65(4), 65–76.

Nusbaum, A. G., Sawaya, A., Patel, S. B., Khalid, L., Isseroff, R. R., & Tomic-Canic, M. (2014) Epithelialization in Wound Healing: A Comprehensive Review. *Advances in wound care*, 3(7), 445–464.

Oi, K., Fukumoto, Y., Ito, K., Uwatoku, T., Abe, K., Hizume, T., & Shimokawa, H. (2008) Extracorporeal shock wave therapy ameliorates hindlimb ischemia in rabbits. *The Tohoku journal of experimental medicine*, 214(2), 151–158.

Ojeh, N., Pastar, I., Tomic-Canic, M., & Stojadinovic, O. (2015) Stem Cells in Skin Regeneration, Wound Healing, and Their Clinical Applications. *International journal of molecular sciences*, 16(10), 25476–25501.

Okeke, E. B., Louttit, C., Fry, C., Najafabadi, A. H., Han, K., Nemzek, J., & Moon, J. J. (2020) Inhibition of neutrophil elastase prevents neutrophil extracellular trap formation and rescues mice from endotoxic shock. *Biomaterials*, 238 (1), 119836.

Oliveira, D., Borges, A., & Simoes, M. (2018) *Staphylococcus aureus* Toxins and Their Molecular Activity in Infectious Diseases. *Toxins*, 10(6), 252-253.

Oliveira de Araujo, J. F., Lopes da Silva, A. L., Acioly de Omena, I. C., Alvino, V., Todaro, A. R., & Bastos, M. L. A. (2022) *Proteus mirabilis* resistant to carbapenems isolated from a patient with a venous leg ulcer: a case report. *Journal of wound care*, *31*(5), 460–464.

Olsen, M. E., & Horswill, A. R. (2013) *Staphylococcus aureus* Osteomyelitis: Bad to the Bone. *Cell Host and Microbe*, 13(6), 629-631.

Olsson, M., Järbrink, K., Divakar, U., Bajpai, R., Upton, Z., Schmidtchen, A., & Car, J. (2019) The humanistic and economic burden of chronic wounds: A systematic review. *Wound repair and regeneration*, 27(1), 114–125.

Omar, A., Wright, J. B., Schultz, G., Burrell, R., & Nadworny, P. (2017) Microbial Biofilms and Chronic Wounds. *Microorganisms,* 5(1), 9-10.

Ongarora B. G. (2022) Recent technological advances in the management of chronic wounds: A literature review. *Health science reports*, *5*(3), 641.

Osumi, K., Matsuda, S., Fujimura, N., Matsubara, K., Kitago, M., Itano, O., Ogino, C., Shimizu, N., Obara, H., & Kitagawa, Y. (2017) Acceleration of wound healing by ultrasound activation of TiO2 in Escherichia coli-infected wounds in mice. *Journal of biomedical materials research*, 105(8), 2344–2351.

Oxford Nanopore Technologies (2020) Product information/comparison. Available online: https://nanoporetech.com/products/comparison [Accessed 27/4/2023] .

Oyibo, S. O., Jude, E. B., Tarawneh, I., Nguyen, H. C., Harkless, L. B., & Boulton, A. J. (2001) The effects of ulcer size and site, patient's age, sex and type and duration of diabetes on the outcomes of diabetic foot ulcers. *Diabetes Mellitus*, 10(1), 133- 138.

Pac Bio Sciences (2020) Products and Services. Available online: https://www.pacb.com/products-and-services/ [Accessed 27/4/2020] .

Panuncialman, J., Hammerman, S., Carson, P., & Falanga, V. (2010) Wound edge biopsy sites in chronic wounds heal rapidly and do not result in delayed overall healing of the wounds. *Wound repair and regeneration*, *18*(1), 21–25.

Papatheodorou, K., Papanas, N., Banach, M., Papazoglou, D., & Edmonds, M. (2016) Complications of Diabetes. *Journal of diabetes research*, 20(1), 6989453.

Park, J. U., Oh, B., Lee, J. P., Choi, M. H., Lee, M. J., & Kim, B. S. (2019) Influence of Microbiota on Diabetic Foot Wound in Comparison with Adjacent Normal Skin Based on the Clinical Features. *BioMed research international*, 20(4), 745-923.

Pastar, I., Stojadinovic, O., Yin, N. C., Ramirez, H., Nusbaum, A. G., Sawaya, A., Patel, S. B., Khalid, L., Isseroff, R. R., & Tomic-Canic, M. (2014) Epithelialization in Wound Healing: A Comprehensive Review. *Advances in wound care*, 3(7), 445–464.

Patel, P., & Abate, N. (2013) Body fat distribution and insulin resistance. *Nutrients*, 5(6), 2019–2027.

Pathare, N. A,, Bal, A., Talvalkar, G. V., & Antani, D. U. (1998) Diabetic foot infections: a study of microorganisms associated with the different Wagner grades. *Indian Journal of Pathology and Microbiology*, 41(1), 437–441.

Payne, A., Holmes, N., Clarke, T., Munro, R., Debebe, B. J., & Loose, M. (2021) Readfish enables targeted nanopore sequencing of gigabase-sized genomes. *Nature Biotechnology*, 39(4), 442–450.

Pendsey S. P. (2010) Understanding diabetic foot. *International journal of diabetes in developing countries*, *30*(2), 75–79.

Pereira-Marques, J., Hout, A., Ferreira, R.M., Weber, M., Pinto-Ribeiro, I., van Doorn, L-J., Knetsch, C. M., & Figueiredo, C. (2019) Impact of Host DNA and Sequencing Depth on the Taxonomic Resolution of Whole Metagenome Sequencing for Microbiome Analysis*. Frontiers in Microbiology*, 10(1), 1277-1278.

Pererira, S. G., Moura, J., Carvalho, E., & Empadinhad, N. (2017) Microbiota of Chronic Diabetic Wounds: Ecology, Impact, and Potential for Innovative Treatment Strategies. *Frontiers in Microbiology*, 8(1), 17-91.

Perez-Favila, A., Martinez-Fierro, M. L., Rodriguez-Lazalde, J. G., Cid-Baez, M. A., Zamudio-Osuna, M. J., Martinez-Blanco, M., Mollinedo-Montaño, F. E., Rodriguez-Sanchez, I. P., Castañeda-Miranda, R., & Garza-Veloz, I. (2019) Current Therapeutic Strategies in Diabetic Foot Ulcers. *Medicinia,* 55(11), 714 – 715.

Pervez, M. T., Hasnain, M. J. U., Abbas, S. H., Moustafa, M. F., Aslam, N., & Shah, S. S. M. (2022) A Comprehensive Review of Performance of Next-Generation Sequencing Platforms. *BioMed research international*, 20(1), 3457806.

Petkovic, M., Mouritzen, M. V., Mojsoska, B., & Jenssen, H. (2021) Immunomodulatory Properties of Host Defence Peptides in Skin Wound Healing. *Biomolecules*, 11(7), 952.

Peymani, F., Farzeen, A., & Prokisch, H. (2022) RNA sequencing role and application in clinical diagnostic. *Pediatric investigation*, 6(1), 29-35.

Piipponen, M., Li, D., & Landén, N. X. (2020) The Immune Functions of Keratinocytes in Skin Wound Healing. *International journal of molecular sciences*, 21(22), 8790.

Pitocco, D., Spanu, T., Di Leo, M., Vitiello, R., Rizzi, A., Tartaglione, L., Fiori, B., Caputo, S., Tinelli, G., Zaccardi, F., Flex, A., Galli, M., Pontecorvi, A., & Sanguinetti, M. (2019) Diabetic foot infections: a comprehensive overview. *European review for medical and pharmacological sciences*, 23(2), 26–37.

Pölzl, L., Nägele, F., Hirsch, J., Graber, M., Lobenwein, D., Kirchmair, E., Huber, R., Dorfmüller, C., Lechner, S., Schäfer, G., Hermann, M., Fritsch, H., Tancevski, I., Grimm, M., Holfeld, J., & Gollmann-Tepeköylü, C. (2021) Defining a therapeutic range for regeneration of ischemic myocardium via shock waves. *Scientific reports*, 11(1), 409.

Pondaven-Letourmy, S., Alvin, F., Boumghit, Y., & Simon, F. (2020) How to perform a nasopharyngeal swab in adults and children in the COVID-19 era. *European annals of otorhinolaryngology, head and neck diseases*, 137(4), 325–327.

Porst, H. (2021) Review of the Current Status of Low Intensity Extracorporeal Shockwave Therapy (Li-ESWT) in Erectile Dysfunction (ED), Peyronie's Disease (PD), and Sexual Rehabilitation After Radical Prostatectomy With Special Focus on Technical Aspects of the Different Marketed ESWT Devices Including Personal Experiences in 350 Patients. *Sexual medicine reviews*, 9(1), 93–122.

Pouget, C., Dunyach-Remy, C., Pantel, A., Boutet-Dubois, A., Schuldiner, S., Sotto, A., Lavigne, J. P., & Loubet, P. (2021) Alternative Approaches for the Management of Diabetic Foot Ulcers. *Frontiers in microbiology*, 12(1), 747618.

Prescott, S. L., Larcombe, D. L., Logam, A. C., West, C., Burks, W., Caraballo, L., Levin, M., Etten, E. V., Horwitz, H., Kozyrskyj, A., & Campbell, D. E. (2017) The skin microbiome: impact of modern environments on skin ecology, barrier integrity, and systemic immune programming. *World Allergy Organization Journal*, 10(1), 29-30.

Price, L. B., Liu, C. M., Frankel, Y. M., Melendez, J. H., Aziz, M., Buchhagen, J., Contente-Cuomo, T., Engelthaler, D. M., Keim, P. S., Ravel, J., Lazarus, G. S., & Zenilman, J. M. (2011) Macroscale spatial variation in chronic wound microbiota: a cross-sectional study. *Wound repair and regeneration, 19*(1), 80–88.

Punjataewakupt, A., Napavichayanun, S., & Aramwit, P. (2019) The downside of antimicrobial agents for wound healing. *European journal of clinical microbiology & infectious diseases*, 38(1), 39–54.

Rademacher, F., Simanski, M., & Harder, J. (2016) RNase 7 in Cutaneous Defense. *International journal of molecular sciences*, 17(4), 560.

Radic, M., & Muller, S. (2022) LL-37, a Multi-Faceted Amphipathic Peptide Involved in NETosis. *Cells*, 11(15), 2463.

Ramachandran A. (2014) Know the signs and symptoms of diabetes. *The Indian journal of medical research*, 140(5), 579–581.

Rangaraj, A., Ye, L., Sanders, A. J., Price, P. E., Harding, K. G., & Jiang, W. G. (2017) Molecular and cellular impact of Psoriasin (S100A7) on the healing of human wounds. *Experimental and therapeutic medicine*, 13(5), 2151–2160.

Raphenya, A. R., Robertson, J., Jamin, C., de Oliveira Martins, L., Maguire, F., McArthur, A. G., & Hays, J. P. (2022) Datasets for benchmarking antimicrobial resistance genes in bacterial metagenomic and whole genome sequencing. *Scientific data*, *9*(1), 341.

Raziyeva, K., Kim, Y., Zharkinbekov, Z., Kassymbek, K., Jimi, S., & Saparov, A. (2021) Immunology of Acute and Chronic Wound Healing. *Biomolecules*, 11(5), 1-5.

Reardon, R., Simring, D., Kim, B., Mortensen, J., Williams, D., & Leslie, A. (2020) The diabetic foot ulcer. *Australian journal of general practice*, 49(5), 250–255.

Reinke, J. M., & Sorg, H. (2012) Wound Repair and Regeneration. European Surgical *of America*, 51(6), 12902-12910.

Relman, D. A. & Lipsitch, M. (2018) Microbiomes a tool and target in the effort to address antimicrobial resistance. *Processings of the National academy of Sciences of the United States of America*, 51(6), 12902-12910.

Rodríguez-Carlos, A., Trujillo, V., Gonzalez-Curiel, I., Marin-Luevano, S., Torres-Juarez, F., Santos-Mena, A., Rivas-Santiago, C., Enciso-Moreno, J. A., Zaga-Clavellina, V., & Rivas-Santiago, B. (2020) Host Defense Peptide RNase 7 Is Down-regulated in the Skin of Diabetic Patients with or without Chronic Ulcers, and its Expression is Altered with Metformin. *Archives of medical research*, 51(4), 327–335.

Røikjer, J., Mørch, C. D., & Ejskjaer, N. (2021) Diabetic Peripheral Neuropathy: Diagnosis and Treatment. *Current drug safety*, 16(1), 2–16.

Rompe, J. D., Buch, M., Gerdesmeyer, L., Haake, M., Loew, M., Maier, M., & Heine, J. (2002) Musculoskeletal shock wave therapy--current database of clinical research. *Zeitschrift fur Orthopadie und ihre Grenzgebiete*, 140(3), 267–274.

Rončević, T., Puizina, J., & Tossi, A. (2019) Antimicrobial Peptides as Anti-Infective Agents in Pre-Post-Antibiotic Era?. *International journal of molecular sciences*, 20(22), 5713.

Rooney, A. M., Raphenya, A. R., Melano, R. G., Seah, C., Yee, N. R., MacFadden, D. R., McArthur, A. G., Schneeberger, P. H. H., & Coburn, B. (2022) Performance Characteristics of Next-Generation Sequencing for the Detection of Antimicrobial Resistance Determinants in Escherichia coli Genomes and Metagenomes. *mSystems,* 7(3), e0002222.

Roy, S., Santra, S., Das, A., Dixith, S., Sinha, M., Ghatak, S., Ghosh, N., Banerjee, P., Khanna, S., Mathew-Steiner, S., Ghatak, P. D., Blackstone, B. N., Powell, H. M., Bergdall, V. K., Wozniak, D. J., & Sen, C. K. (2020) Staphylococcus aureus Biofilm Infection Compromises Wound Healing by Causing Deficiencies in Granulation Tissue Collagen. *Annals of surgery*, 271(6), 1174–1185.

Ruffin, M., & Brochiero, E. (2019) Repair Process Impairment by *Pseudomonas aeruginosa* in Epithelial Tissues: Major Features and Potential Therapeutic Avenues. *Frontiers in cellular and infection microbiology*, 9(1), 182.

Sabaté Brescó, M., Harris, L. G., Thompson, K., Stanic, B., Morgenstern, M., O'Mahony, L., Richards, R. G., & Moriarty, T. F. (2017) Pathogenic Mechanisms and Host Interactions in Staphylococcus epidermidis Device-Related Infection. *Frontiers in microbiology*, 8(1), 1401.

Sabbah, A., Chang, T. H., Harnack, R., Frohlich, V., Tominaga, K., Dube, P. H., Xiang, Y., & Bose, S. (2009) Activation of innate immune antiviral responses by Nod2. *Nature immunology*, 10(10), 1073–1080.

Sabbatini, M., Magnelli. V., & Renò, F. (2021) NETosis in wound healing: when enough is enough. *Cells,* 10(1), 494-500.

Saggini, R., Figus, A., Troccola, A., Cocco, V., Saggini, A., & Scuderi, N. (2008) Extracorporeal shock wave therapy for management of chronic ulcers in the lower extremities. *Ultrasound in medicine & biology*, 34(8), 1261–1271.

Salcedo-Jiménez, R., Koenig, J. B., Lee, O. J., Gibson, T. W. G., Madan, P., & Koch, T. G. (2020) Extracorporeal Shock Wave Therapy Enhances the In Vitro Metabolic Activity and Differentiation of Equine Umbilical Cord Blood Mesenchymal Stromal Cells. *Frontiers in veterinary science*, 7(1), 554306.

Salvetti, E., Campedelli, I., Larini, I., Conedera, G., & Torriani, S. (2021) Exploring Antibiotic Resistance Diversity in Leuconostoc spp. by a Genome-Based Approach: Focus on the lsaA Gene. *Microorganisms*, 9(3), 491.

Sandoval-Denis, M., Gené, J., Sutton, D. A., Wiederhold, N. P., Cano-Lira, J. F., & Guarro, J. (2016) New species of Cladosporium associated with human and animal infections. *Persoonia*, *36*, 281–298.

Schaden, W., Thiele, R., Kölpl, C., Pusch, M., Nissan, A., Attinger, C. E., Maniscalco-Theberge, M. E., Peoples, G. E., Elster, E. A.. & Stojadinovic, A. (2007) Shock wave therapy for acute and chronic soft tissue wounds: a feasibility study. *The Journal of surgical research*, 143(1), 1–12.

Schlecht, L. M., Peters, B. M., Krom, B. P., Freiberg, J. A., Hänsch, G. M., Filler, S. G., Jabra-Rizk, M. A., & Shirtliff, M. E. (2015) Systemic Staphylococcus aureus infection mediated by Candida albicans hyphal invasion of mucosal tissue. *Microbiology*, *161*(1), 168–181.

Scott, R. A., Langenberg, C., Sharp, S. J., Franks, P. W., Rolandsson, O., Drogan, D., van der Schouw, Y. T., Ekelund, U., Kerrison, N. D., Ardanaz, E., Arriola, L., Balkau, B., Barricarte, A., Barroso, I., Bendinelli, B., Beulens, J. W., Boeing, H., de Lauzon-Guillain, B., Deloukas, P., & Wareham, N. J. (2013) The link between family history and risk of type 2 diabetes is not

explained by anthropometric, lifestyle or genetic risk factors: the EPIC-InterAct study. *Diabetologia,* 56(1), 60–69.

Selway, C. A., Eisenhofer, R., & Weyrich, L. S. (2020) Microbiome applications for pathology: challenges of low microbial biomass samples during diagnostic testing. *Journal of Pathol Clin Res*, 6(2), 97-106.

Sen, C. K. (2021) Human Wound and Its Burden: Updated 2020 Compendium of Estimates. *Advances in wound care*, 10(5), 281–292.

Sereika, M., Kirkegaard, R. H., Karst, S. M., Michaelsen, T. Y., Sørensen, E. A., Wollenberg, R. D., & Albertsen, M. (2022) Oxford Nanopore R10.4 long-read sequencing enables the generation of near-finished bacterial genomes from pure cultures and metagenomes without short-read or reference polishing. *Nature methods*, 19(7), 823–826.

Serra, M. B., Barroso, W. A., Silva, N. N., Silva, S. N., Borges, A. C. R., Abreu I. C. & Borges, M. R. (2017) From Inflammation to Current and Alternative Therapies Involved in Wound Healing. *International Journal of Inflammation*, 12(8), 340-621.

Shaabani, E., Sharifiaghdam, M., Faridi-Majidi, R., De Smedt, S. C., Braeckmans, K., & Fraire, J. C. (2022) Gene therapy to enhance angiogenesis in chronic wounds. *Molecular therapy*, *Nucleic acids*, 29(1), 871–899.

Shah, J. M. Y., Omar, E., Pai, D. R., & Sood, S. (2012) Cellular Events and Biomarkers of Wound Healing. Indian Journal of Plastic Surgery: *Official Publication of the Association of Plastic Surgeons of India*, 45(13), 220-228.

Shen, B., Cao, Z., Wu, Y., Yi, W., Zhu, Z., Lv, Z., Zhu, C., & Yu, Y. (2020) Purlisin, a toxin-like defensin derived from clinical pathogenic fungus Purpureocillium lilacinum with both antimicrobial and potassium channel inhibitory activities*. FASEB journal : official publication of the Federation of American Societies for Experimental Biology*, 34(11), 15093–15107.

Sidiq, T., Yoshihama, S., Downs, I., & Kobayashi, K. S. (2016) Nod2: A Critical Regulator of Ileal Microbiota and Crohn's Disease. *Frontiers in immunology*, 7(1), 367.

Silvestre-Ryan, J., & Holmes, I. (2021) Pair consensus decoding improves accuracy of neural network basecallers for nanopore sequencing. *Genome biology*, 22(1), 38.

Simanski, M., Dressel, S., Gläser, R., & Harder, J. (2010) RNase 7 protects healthy skin from Staphylococcus aureus colonization. *The Journal of investigative dermatology*, 130(12), 2836–2838.

Simplicio, C. L., Purita, J., Murrell, W., Santos, G. S., Dos Santos, R. G., & Lana, J. F. S. D. (2020) Extracorporeal shock wave therapy mechanisms in musculoskeletal regenerative medicine. *Journal of clinical orthopaedics and trauma*, 11(3), S309–S318.

Simpson, C. L., Kojima, S., & Getsios, S. (2011) RNA interference in keratinocytes and an organotypic model of human epidermis. *Methods in molecular biology*, 585(1), 127–146.

Singh, S., Singhm S. K., Chowdhury, I., & Singh, R. (2017) Understanding the Mechanism of Bacterial Biofilms Resistance to Antimicrobial Agents. *The Open Microbiology Journal*, 11(2), 53-62.

Singer, M. E., Dorrance, K. A., Oxenreiter, M. M., Yan, K. R., & Close, K. L. (2022) The type 2 diabetes 'modern preventable pandemic' and replicable lessons from the COVID-19 crisis. *Preventive medicine reports*, 25, 101636.

Snyder, R. J., Lantis, J., Kirsner, R. S., Shah, V., Molyneaux, M., & Carter, M. J. (2016) Macrophages: A review of their role in wound healing and their therapeutic use. *Wound repair and regeneration*, 24(4), 613–629.

Spencer, J. D., Schwaderer, A. L., Dirosario, J. D., McHugh, K. M., McGillivary, G., Justice, S. S., Carpenter, A. R., Baker, P. B., Harder, J., & Hains, D. S. (2011) Ribonuclease 7 is a potent antimicrobial peptide within the human urinary tract. *Kidney international*, 80(2), 174–180.

Srinivasan, R., Karaoz, U., Volegova, M., MacKichan, J., Kato-Maeda, M., Miller, S., Nadarajan, R., Brodie, E. L., & Lynch, S. V. (2015) Use of 16S rRNA gene for identification of a broad range of clinically relevant bacterial pathogens. *PloS one*, *10*(2), e0117617.

Stein, R. R., Bucci, V., Toussaint, N. C., Buffie, C. G., Rätsch, G., Pamer, E. G., Sander, C., & Xavier, J. B. (2013) Ecological modeling from time-series inference: insight into dynamics and stability of intestinal microbiota. *PLoS computational biology*, 9(12), e1003388.

Steuernagel, B., Taudien, S., & Gundlach, L. *(2009) De novo* 454 sequencing of barcoded BAC pools for comprehensive gene survey and genome analysis in the complex genome of barley. *BMC Genomics,* 10(1), 547.

Stojadinovic, A., Elster, E. A., Anam, K., Tadaki, D., Amare, M., Zins, S., & Davis, T. A. (2008). Angiogenic response to extracorporeal shock wave treatment in murine skin isografts. *Angiogenesis,* 11(4), 369–380.

Suga, H., Sugaya, M., Fujita, H., Asano, Y., Tada, Y., Kadono, T., & Sato, S. (2014) TLR4, rather than TLR2, regulates wound healing through TGF-β and CCL5 expression. *Journal of dermatological science*, 73(2), 117–124.

Sugimoto, S., Iwamoto, T., Takada, K., Okuda, K. I., Tajima, A., Iwase, T., & Mizunoe, Y. (2013) *Staphylococcus epidermidis* Esp Degrades Specific Proteins Associated with *Staphylococcus aureus* Biofilm Formation and Host-Pathogen Interaction. *Journal of Bacteriology*, 195(8), 1645-1655.

Surana, N. K., & Kasper, D. L. (2017) Moving beyond microbiome-wide associations to causal microbe identification. *Nature*, *552*(7684), 244–247.

Sundaram, S., Sellamuthu, K., Nagavelu, K., Suma, H. R., Das, A., Narayan, R., Chakravortty, D., Gopalan, J., & Eswarappa, S. M. (2018) Stimulation of angiogenesis using single-pulse low-pressure shock wave treatment. *Journal of molecular medicine*, *96*(11), 1177–1187.

Takahashi, M., Umehara, Y., Yue, H., Trujillo-Paez, J. V., Peng, G., Nguyen, H. L. T., Ikutama, R., Okumura, K., Ogawa, H., Ikeda, S., & Niyonsaba, F. (2021) The Antimicrobial Peptide Human β-Defensin-3 Accelerates Wound Healing by Promoting Angiogenesis, Cell Migration, and Proliferation Through the FGFR/JAK2/STAT3 Signaling Pathway. *Frontiers in immunology*, 12(4), 712781.

Takeo, M., Lee, W., & Ito, M. (2015) Wound healing and skin regeneration. *Cold Spring Harbor perspectives in medicine*, 5(1), 023267.

Tang, Q., Xue, N., Ding, X., Tsai, K. H., Hew, J. J., Jiang, R., Huang, R., Cheng, X., Ding, X., Yee Cheng, Y., Chen, J., & Wang, Y. (2023) Role of wound microbiome, strategies of microbiota delivery system and clinical management. *Advanced drug delivery reviews*, 192(11), 114671.

Thakkar, J. R., Sabara, P. H., & Koringa, P. G. (2017) Exploring Metagenomes Using Next-Generation Sequencing. *Understanding Host-Microbiome Interactions - An Omics Approach*, 10(3), 29-40.

Tieu, D. D., Peters, A. T., Carter, R. G., Suh, L., Conley, D. B., Chandra, R., Norton, J., Grammer, L. C., Harris, K. E., Kato, A., Kern, R. C., & Schleimer, R. P. (2010) Evidence for diminished levels of epithelial psoriasin and calprotectin in chronic rhinosinusitis. *The Journal of allergy and clinical immunology*, 125(3), 667–675.

Tipton, C. D., Wolcott, R. D., Sanford, N. E., Miller, C., Pathak, G., Silzer, T. K., Sun, J., Fleming, D., Rumbaugh, K. P., Little, T. D., Phillips, N., & Phillips, C. D. (2020) Patient genetics is linked to chronic wound microbiome composition and healing. *PLoS pathogens*, 16(6), e1008511.

Tomic-Canic, M., Burgess, J. L., O'Neill, K. E., Strbo, N., & Pastar, I. (2020) Skin Microbiota and its Interplay with Wound Healing. *American journal of clinical dermatology*, 21(1), 36–43.

Trengove, N. J., Stacey, M. C., McGechie, D. F., & Mata, S. (1996) Qualitative bacteriology and leg ulcer healing. *Journal of wound care*, 5(6), 277–280.

Trindade, B. C., & Chen, G. Y. (2020) NOD1 and NOD2 in inflammatory and infectious diseases. *Immunological reviews*, 297(1), 139–161.

Trinh, X. T., Long, N. V., Van Anh, L. T., Nga, P. T., Giang, N. N., Chien, P. N., Nam, S. Y., & Heo, C. Y. (2022) A Comprehensive Review of Natural Compounds for Wound Healing: Targeting Bioactivity Perspective. *International journal of molecular sciences*, 23(17), 9573.

Trøstrup, H., Laulund, A., & Moser, C. (2020) Insights into Host-Pathogen Interactions in Biofilm-Infected Wounds Reveal Possibilities for New Treatment Strategies. *Antibiotics*, 9(7), 396.

Tsikopoulos, K., Drago, L., Koutras, G., Givissis, P., Vagdatli, E., Soukiouroglou, P., & Papaioannidou, P. (2020) Radial Extracorporeal Shock Wave Therapy Against Cutibacterium acnes Implant-Associated Infections: An in Vitro Trial. *Microorganisms*, 8(5), 743.

Tyler, A. D., Mataseje, L., Urfano, C. J., Schmidt, L., Antonation, K. S., Mulvey, M. R., & Corbett, C. R. (2018) Evaluation of Oxford Nanopore's MinION Sequencing Device for Microbial Whole Genome Sequencing Applications. *Scientific reports*, 8(1), 10931.

Uitto, J., Li, Q., & Urban, Z. (2013). The complexity of elastic fibre biogenesis in the skin--a perspective to the clinical heterogeneity of cutis laxa. *Experimental dermatology*, *22*(2), 88–92.

Unnikrishnan, A. G., Sahay, R. K., Phadke, U., Sharma, S. K., Shah, P., Shukla, R., Viswanathan, V., Wangnoo, S. K., Singhal, S., John, M., Kumar, A., Dharmalingam, M., Jain, S., Shaikh, S., & Verberk, W. J. (2022) Cardiovascular risk in newly diagnosed type 2 diabetes patients in India. *PloS one*, *17*(3), e0263619.

Van Batenburg, A. A., Kazemier, K. M., van Oosterhout, M. F. M., van der Vis, J. J., Grutters, J. C., Goldschmeding, R., & van Moorsel, C. H. M. (2021) Telomere shortening and DNA damage in culprit cells of different types of progressive fibrosing interstitial lung disease. *ERJ open research*, 7(2), 00691-2020.

Velnar, T., Bailey, T., & Smrkolj, V. (2009) The wound healing process: an overview of the cellular and molecular mechanisms. *The Journal of international medical research*, 37(5), 1528–1542.

Veith, A. P., Henderson, K., Spencer, A., Sligar, A. D., & Baker, A. B. (2019). Therapeutic strategies for enhancing angiogenesis in wound healing. *Advanced drug delivery reviews*, 146, 97–125.

Verbanic, S., Shen, Y., Lee, J., Deacon, J. M., & Chen, I. A. (2020) Microbial predictors of healing and short-term effect of debridement on the microbiome of chronic wounds. *NPJ biofilms and microbiomes*, 6(1), 21.

Viigimaa, M., Sachinidis, A., Toumpourleka, M., Koutsampasopoulos, K., Alliksoo, S., & Titma, T. (2020) Macrovascular Complications of Type 2 Diabetes Mellitus. *Current vascular pharmacology*, 18(2), 110–116.

Viigimaa, M., Sachinidis, A., Toumpourleka, M., Koutsampasopoulos, K., Alliksoo, S., & Titma, T. (2020) Macrovascular Complications of Type 2 Diabetes Mellitus. *Current vascular pharmacology*, 18(2), 110–116.

Wagner, F. W. (1981) The dysvascular foot: a system for diagnosis and treatment. *Foot Ankle*, 2(1), 64-122.

Wang, C. J. (2003) An overview of shock wave therapy in musculoskeletal disorders. *Chang Gung medical journal*, 26(4), 220–232.

Wang, C. J., Kuo, Y. R., Wu, R. W., Liu, R. T., Hsu, C. S., Wang, F. S., & Yang, K. D. (2009) Extracorporeal shockwave treatment for chronic diabetic foot ulcers. *The Journal of surgical research*, 152(1), 96–103.

Wang, Z., Gerstein, M., & Snyder, M. (2009) RNA-Seq: a revolutionary tool for transcriptomics. *Nature reviews. Genetics*, 10(1), 57–63.

Wang, Z., Choi, J, E., Wu, C. C., & Di Nardo, A. (2013) Skin commensal bacteria Staphylococcus epidermidis promote survival of melanocytes bearing UVB-induced DNA damage, while bacteria Propionibacterium acnes inhibit survival of melanocytes by increasing apoptosis. *Photodermatology, Photoimmunology and Photomedicine*, 34(6), 405-414.

Wang, G. (2014) Human antimicrobial peptides and proteins. *Pharmaceuticals*, 7(5), 545–594.

Wang, M., Noor, S., Huan, R., Liu, C., Li, J., Shi, Q., Zhang, Y. J., Wu, C., & He, H. (2020) Comparison of the diversity of cultured and total bacterial communities in marine sediment using culture-dependent and sequencing methods. *PeerJ*, 8(3), e10060.

Wangoye, K., Mwesigye, J., Tungotyo, M., & Twinomujuni Samba, S. (2022) Chronic wound isolates and their minimum inhibitory concentrations against third generation cephalosporins at a tertiary hospital in Uganda. *Scientific reports*, 12(1), 1195.

Weihs, A. M., Fuchs, C., Teuschl, A. H., Hartinger, J., Slezak, P., Mittermayr, R., Redl, H., Junger, W. G., Sitte, H. H., & Rünzler, D. (2014) Shock wave treatment enhances cell proliferation and improves wound healing by ATP release-coupled extracellular signal-regulated kinase (ERK) activation. *The Journal of biological chemistry*, 289(39), 27090–27104.

Weirather, J. L., de Cesare, M., Wang, Y., Piazza, P., Sebastiano, V., Wang, X. J., Buck, D., & Au, K. F. (2017) Comprehensive comparison of Pacific Biosciences and Oxford Nanopore Technologies and their applications to transcriptome analysis. *Faculty of 1000 Research*, 6(100), 33-99.

Weilguny, L., De Maio, N., Munro, R., Manser, C., Birney, E., Loose, M., & Goldman, N. (2023) Dynamic, adaptive sampling during nanopore sequencing using Bayesian experimental design. *Nature biotechnology*, 10(1), 483-492.

Weledji, E. P., & Fokam, P. (2014) Treatment of the diabetic foot - to amputate or not?. *BMC surgery*, 14(83, 1-5.

Whitney, J. D. (2005) Overview: Acute and Chronic Wounds. *Nursing Clinics of North America*, 40(2), 191-205.

Wilkinson, H. N., & Hardman, M. J. (2020) Wound healing: cellular mechanisms and pathological outcomes. *Open biology*, 10(9), 200223.

Wilkinson, H. N., Iveson, S., Catherall, P., & Hardman, M. J. (2018) A Novel Silver Bioactive Glass Elicits Antimicrobial Efficacy Against Pseudomonas aeruginosa and Staphylococcus aureus in an ex Vivo Skin Wound Biofilm Model. *Frontiers in microbiology*, 9 (1), 1450.

Wilkinson, H. N., Kidd, A. S., Roberts, E. R., & Hardman, M. J. (2021) Human Ex vivo Wound Model and Whole-Mount Staining Approach to Accurately Evaluate Skin Repair. *Journal of visualized experiments : JoVE*, 5(1), 168-172.

Williams, H., Crompton, R. A., Thomason, H. A., Campbell, L., Singh, G., McBain, A. J., Cruickshank, S. M., & Hardman, M. J. (2017) Cutaneous Nod2 Expression Regulates the Skin Microbiome and Wound Healing in a Murine Model. *The Journal of investigative dermatology*, 137(11), 2427–2436.

Wolcott, R. D., Gontcharova, V., Sun, Y. & Dowd, S. E. (2009) Evaluation of the bacterial diversity among and within individual venous leg ulcers using bacterial tag-encoded FLX and titanium amplicon pyrosequencing and metagenomic approaches. *BMC microbiology*, *9(4)*, 226.

Wong, W. F., & Santiago, M. (2017) Microbial approaches for targeting antibiotic-resistant bacteria. *Microbial Biotechnology*, 10(5), 1047-1053.

Wu, X. M., Zhang, J., Li, P. W., Hu, Y. W., Cao, L., Ouyang, S., Bi, Y. H., Nie, P., & Chang, M. X. (2020) NOD1 Promotes Antiviral Signaling by Binding Viral RNA and Regulating the Interaction of MDA5 and MAVS. *Journal of immunology*, 204(8), 2216–2231.

Wu, Y., Li, D., Wang, Y., Liu, X., Zhang, Y., Qu, W., Chen, K., Francisco, N. M., Feng, L., Huang, X., & Wu, M. (2018) Beta-Defensin 2 and 3 Promote Bacterial Clearance of Pseudomonas aeruginosa by Inhibiting Macrophage Autophagy through Downregulation of Early Growth Response Gene-1 and c-FOS. *Frontiers in immunology*, 9(18), 211.

Wuerfel, T., Schmitz, C., & Jokinen, L. L. J. (2022) The Effects of the Exposure of Musculoskeletal Tissue to Extracorporeal Shock Waves. *Biomedicines*, *10*(5), 1084.

Xia, x., Liu, K., Wu, Y., Jiang, D., & Lai, Y. (2016) Staphylococcal LTA-Induced miR-143 Inhibits Propionibacterium acnes-Mediated Inflammatory Response in Skin. *Journal of Investigative Dermatology,* 136(3), 621-630.

Xiao, H., Chen, X., Liu, X., Wen, G., & Yu, Y. (2023) Recent advances in decellularized biomaterials for wound healing. *Materials today. Bio,* 19(3), 100589.

Xu, Z. & Hsia, H. C. (2018) The Impact of Microbial Communities on Wound Healing: A Review. *Annals of Plastic Surge*ry, 81(1), 113-123.

Yamasaki, K., & Gallo, R. L. (2008) Antimicrobial peptides in human skin disease. *European journal of dermatology*, 18(1), 11–21.

Yan, X., Zeng, B., Chai, Y., Luo, C., & Li, X. (2008) Improvement of blood flow, expression of nitric oxide, and vascular endothelial growth factor by low-energy shockwave therapy in random-pattern skin flap model. *Annals of plastic surgery*, 61(6), 646–653.

Yang, X., Guo, J. L., & Han, J. (2020) Chitosan hydrogel encapsulated with LL-37 peptide promotes deep tissue injury healing in a mouse model. *Military Med Res* 7(1), 20-24.

Yao, W., Kuan, E. C., Francis, N. C., St John, M. A., Grundfest, W. S., & Taylor, Z. D. (2017) Laser-generated shockwaves enhance antibacterial activity against biofilms in vitro. *Lasers in surgery and medicine*, 49(5), 539–547.

Yap, M., Feehily, C., Walsh, C. J., Fenelon, M., Murphy, E. F., McAuliffe, F. M., van Sinderen, D., O'Toole, P. W., O'Sullivan, O., & Cotter, P. D. (2020) Evaluation of methods for the reduction of contaminating host reads when performing shotgun metagenomic sequencing of the milk microbiome. *Scientific reports*, *10*(1), 21665.

Yeaman, M. R., & Yount, N. Y. (2003) Mechanisms of antimicrobial peptide action and resistance. *Pharmacological reviews*, 55(1), 27–55.

Younes, N. A., & Albsoul, A. M. (2004) The DEPA scoring system and its correlation with the healing rate of diabetic foot ulcers. *The Journal of foot and ankle surgery, 43*(4), 209–213.

Youseif, S. H., Abd El-Megeed, F. H., Humm, E. A., Maymon, M., Mohamed, A. H., Saleh, S. A., & Hirsch, A. M. (2021) Comparative Analysis of the Cultured and Total Bacterial Community in the Wheat Rhizosphere Microbiome Using Culture-Dependent and Culture-Independent Approaches. *Microbiology spectrum*, 9(2), e0067821.

Zackular, J. P., Chazin, W. J., & Skaar, E. P. (2015) Nutritional Immunity: S100 Proteins at the Host-Pathogen Interface. *The Journal of biological chemistry*, 290(31), 18991–18998.

Zanger, P., Holzer, J., Schleucher, R., Steffen, H., Schittek, B., & Gabrysch, S. (2009) Constitutive expression of the antimicrobial peptide RNase 7 is associated with Staphylococcus aureus infection of the skin. *The Journal of infectious diseases*, 200(12), 1907–1915.

Zhao, X., Jiang, L., Fang, X., Guo, Z., Wang, X., Shi, B., & Meng, Q. (2022) Host-microbiota interaction-mediated resistance to inflammatory bowel disease in pigs. *Microbiome*, 10(1), 115.

Zhu, S., Yu, Y., & Ren, Y. (2021) The emerging roles of neutrophil extracellular traps in wound healing. *Cell Death Dis*, 12 (1), 984.

Zins, S. R., Amare, M. F., Tadaki, D. K., Elster, E. A., & Davis, T. A. (2010) Comparative analysis of angiogenic gene expression in normal and impaired wound healing in diabetic mice: effects of extracorporeal shock wave therapy. *Angiogenesis*, 13(4), 293–304.

8 Appendices

8.1 Goods Coverage Estimations

Goods coverage estimations describe the coverage estimation of present sample taxa i.e., OTUs with ≥ 1 sequence (Good, 1953). Good's coverage estimator is defined according to the formula: 1 − ($F1/N$) whereby F1 represents the number of singletons OTUs, and N is the total number of counts (Table 8.1). From this value, a percentage is calculated that delineates how many reads in that sample are from OTUs which appear more than once. I.e., a Goods coverage of 96% would indicate that 4% of your reads in that sample are from OTUs that appear only once in that sample.

Table 8.1: Summary of Goods coverage estimation for all samples (Chapter 3).

DONOR	TIMEPOINT	NUMBER OF SINGLETONS (F1)	NUMBER OF SEQUENCES (N)	GOODS COVERAGE (%)
DONOR 01	Wound (A)	25	66	62.1212121
DONOR 01	Wound (B)	1264	53953	97.6572202
DONOR 02	Wound (A)	751	11133	93.2542891
DONOR 02	Wound (B)	1069	19786	94.5971899
DONOR 02	Peri-Wound	1221	24886	95.0936269
DONOR 03	Wound	112	769	85.4356307
DONOR 03	Peri-Wound	71	1565	95.4632588
DONOR 04	Wound (A)	974	33809	97.1191103
DONOR 04	Peri-Wound	24	73	67.1232877
DONOR 04	Wound (B)	33	91	63.7362637
DONOR 05	Skin	35	92	61.9565217
DONOR 05	Peri-Wound	10	41	75.6097561
DONOR 05	Wound	17	86	80.2325581
DONOR 06	Skin	453	11167	95.9434047
DONOR 06	Wound (A)	52	13964	99.6276139
DONOR 06	Peri-Wound (A)	66	1410	95.3191489
DONOR 06	Wound (B)	232	1862	87.5402793
DONOR 06	Peri-Wound (B)	954	47157	97.9769706
DONOR 07	Skin	229	6078	96.2323133
DONOR 07	Wound	13	5338	99.7564631
DONOR 08	Skin	23	131	82.4427481
DONOR 08	Peri-Wound	133	2365	94.3763214
DONOR 08	Wound	644	18898	96.592232
DONOR 09	Wound	395	1689	76.6133807
DONOR 09	Peri-Wound	24	62	61.2903226
DONOR 09	Skin	74	211	64.92891
DONOR 10	Wound	89	16531	99.4616176
DONOR 10	Skin	58	1564	96.2915601
DONOR 11	Wound	251	8703	97.115937
DONOR 11	Peri-Wound	68	3195	97.8716745

DONOR 11	Skin	45	1806	97.5083057
DONOR 12	Skin	64	6727	99.0486101
DONOR 12	Peri-Wound	48	20091	99.7610871
DONOR 12	Wound	43	16270	99.7357099
DONOR 13	Skin	27	246	89.0243902
DONOR 13	Peri-Wound	90	1143	92.1259843
DONOR 13	Wound	43	125	65.6
DONOR 14	Skin	30	1077	97.2144847
DONOR 14	Wound	14	45	68.8888889
DONOR 15	Wound	73	1529	95.2256377
DONOR 15	Skin	12	222	94.5945946
DONOR 16	Wound	41	441	90.7029479
DONOR 16	Peri-Wound	669	18723	96.4268547
DONOR 17	Wound	937	15948	94.1246551
DONOR 17	Skin	80	543	85.267035
DONOR 18	Wound (A)	80	424	81.1320755
DONOR 18	Wound (B)	54	202	73.2673267
DONOR 19	Wound	821	84054	99.023247
DONOR 20	Wound	593	3213	81.5437286
DONOR 20	Skin	658	3842	82.8735034
DONOR 21	Wound	859	158398	99.4576952
DONOR 22	Wound	72	5114	98.5921001
DONOR 23	Wound	580	1201396	99.9517228
DONOR 24	Wound	49	222	77.9279279
DONOR 24	Peri-Wound	41	243	83.127572
DONOR 25	Wound (A)	43	5272	99.1843703
DONOR 25	Wound (B)	130	519	74.9518304
DONOR 25	Skin	6	9	33.3333333
DONOR 25	Peri-Wound	11	33	66.6666667
DONOR 26	Peri-Wound	7	140	95
DONOR 26	Skin	262	14633	98.2095264
DONOR 26	Peri-Wound	1000	107991	99.0739969
DONOR 26	Wound	1019	106401	99.0423022
DONOR 27	Skin	29	866	96.6512702
DONOR 27	Wound	1093	38970	97.1952784
DONOR 28	Wound	36	5057	99.2881155
DONOR 28	Peri-Wound	518	6140	91.5635179
HEALTHY DONOR 01	Skin	1197	495011	99.7581872
HEALTHY DONOR 02	Skin	775	374398	99.793001
HEALTHY DONOR 03	Skin	1448	50182	97.1145032
HEALTHY DONOR 04	Skin	1073	223532	99.5199792
HEALTHY DONOR 05	Skin	1166	136562	99.1461754
HEALTHY DONOR 06	Skin	1166	136562	99.1461754

8.2 Donor Metadata Summary

Table 8.2: Comprehensive summary of study participants.

Donor	Age	Sex	Diabetic Status	HTN	CCF	CKD	Dialysis	Antiplatelet	Anticoagulant	Statin	Diabetic Medication
Donor 01	63	F	Db	Y	N	Y	N	Clopidogrel	N	Y	Liraglutide, insulin, Metformin
Donor 02	75	F	Db	Y	N	N	N	N	N	N	Sitagliptin
Donor 03	73	M	Db	Y	Y	N	N	Clopidogrel	Rivaroxaban	Y	Insulin
Donor 04	51	M	Db	N	N	N	N	Clopidogrel	N	Y	Metformin, Insulin
Donor 05	57	M	Db	N	N	N	N	N	N	N	Insulin
Donor 06	61	F	Db	N	Y	Y	Y	Aspirin and clopidogrel	N	Y	Insulin
Donor 07	58	F	nDb	Y	N	Y	Y	Aspirin	N	Y	N
Donor 08	73	M	Db	N	N	N	N	N	N	N	Insulin
Donor 09	66	M	Db	N	N	N	N	N	N	N	N
Donor 10	84	M	Db	Y	N	N	N	Clopidogrel	N	Y	Insulin
Donor 11	79	F	nDb	Y	N	N	N	N	Warfarin	Y	N
Donor 12	75	M	Db	Y	N	N	N	N	Y	Y	Metformin
Donor 13	75	F	nDb	Y	Y	N	N	Aspirin	N	Y	N
Donor 14	75	F	Db	N	Y	N	N	N	Rivaroxaban	N	N
Donor 15	69	M	nDb	Y	N	N	N	Aspirin	Warfarin	Y	Metformin, insulin

Donor 16	79	M	Db	Y	N	Y	N	Clopidogrel	N	Y	Insulin
Donor 17	64	M	Db	Y	N	N	N	Aspirin	N	Y	Glicazide,Empaglifozin,Insulin
Donor 18	86	M	nDb	N	N	N	N	Aspirin	N	Y	N
Donor 19	66	M	Db	N	N	N	N	aspirin	N	Y	Gliclazide
Donor 20	36	M	Db	N	N	N	N	N	N	Y	Gliclazide,metformin, insulin
Donor 21	83	M	nDb	Y	Y	Y	N	aspirin	apixaban	Y	N
Donor 22	69	M	Db	Y	N	N	N	aspirin	edoxaban	Y	metformin,insulin
Donor 23	82	M	nDb	Y	Y	Y	N	Clopidogrel	edoxaban	Y	N
Donor 24	76	M	Db	Y	Y	N	N	N	Rivaroxaban	Y	metformin,dapaglifozin,insulin
Donor 25	85	M	nDb	Y	N	N	N	N	N	N	N
Donor 26	67	M	Db	N	N	N	N	Clopidogrel	N	Y	metformin,insulin
Donor 27	66	M	Db	N	N	N	N	Clopidogrel	N	Y	metformin,dapaglifozin,insulin
Donor 28	67	M	nDb	N	N	N	N	N	Y	Y	N

8.3 Donor Wound Summary Details

Table 8.3: Study Participant Wound Details.

Donor	Infection Status	Description	Previous Intervention	Wound duration	Date of operation
Donor 01	I	Calcaneum necrosis	Ipsilateral debridement and minor amputation. Contralateral BKA	Over 12 months (Long)	12/09/2019
Donor 02	I	Necrosis and infected	Debridement and angioplasty (PTA)	3 Months (Medium)	29/10/2019
Donor 03	I	Severe heel ulcer	Debridement	3 Months (Medium)	30/12/2019
Donor 04	NI	Plantar ulcer and erythema	Minor amputation (forefoot amputation)	Over 12 months (Long)	11/02/2020
Donor 05	I	Pain relating to previous forefoot amputation	Forefoot amputation. Contralateral BKA	NA	09/02/2020
Donor 06	I	Infected toes, heel ulcer, forefoot gangrene.	Minor amputation and angioplasty (PTA). Contralateral minor amputation	3 months (Medium)	10/03/2020
Donor 07	I	Deep seated infection/lymphoedema	Debridement	NA	11/03/2020
Donor 08	I	Plantar ulcer, osteomyelitis	Minor amputation	6 months (Medium)	14/09/2020
Donor 09	I	Severe necrotising infection	None	NA	21/09/2020
Donor 10	I	Leg ulcer	Angioplasty (PTA). Contralateral BKA	5 years (Long)	25/10/2020
Donor 11	NI	Dry gangrene	None	3 weeks (Short)	02/11/2020
Donor 12	NI	Dry necrotic calcaneal ulcer	Debridement, FA stent Contralateral minor amputation	6 months (Medium)	13/01/2021

Donor 13	I	Open wound and cellulitis	Minor amputation	4 months (Medium)	10/02/2021
Donor 14	I	Open ankle fracture	Left ankle fixation	2 weeks (Short)	10/02/2021
Donor 15	NI	Stump necrosis	Major amputation (BK)	NA	16/02/2021
Donor 16	I	Heel Ulcer	Angioplasty (PTA)	3 months (Medium)	31/03/2021
Donor 17	I	Calcaneal osteomyelitis	None	1 month (Short)	07/06/2021
Donor 18	NI	Non healing toe-amputation site	Femoropopliteal bypass thrombectomy, fasciotomy, minor amputation	6 weeks (Short)	10/06/2021
Donor 19	I	Stump Infection	Debridement, Angioplasty (PTA), previous major amputation (BKA)	2 months (Short)	28/06/2021
Donor 20	I	Infected heel ulcer	Debridement, calcaneal shaving, minor amputation	Over 12 months (Long)	21/07/2021
Donor 21	I	Infected foot ulcer	Debridement	2 months (Short)	03/09/2021
Donor 22	NI	Foot ulcer	None. Contralateral major amputations (AKA)	3 months (Medium)	22/09/2021
Donor 23	NI	Non-healing stump	Debridement, Femoropopliteal bypass	2 Months (Short)	07/10/2021
Donor 24	NI	Medial malleolus non-healing ulcer	Laser ablation, debridement	3 Months (Medium)	07/10/2021
Donor 25	NI	Ischemia	Embolectomy	NA	20/10/2021
Donor 26	NI	Venous ulcers, foot	Debridement, Angioplasty (PTA).	1 Month (Short)	12/11/2021
Donor 27	NI	Toe gangrene, achilleas ulcer	Angioplasty (PTA).	Over 12 Months (Long)	12/11/2021
Donor 28	NI	Forefoot gangrene	None	5 weeks (Short)	11/12/2020

8.4 Donor Blood Summary Results

Table 8.4: Donor Summary Blood Panel Results

Donor	Hb	WCC	Neutrophils	PLT	NA	K	Urea	Albumin	Bilirubin
Donor 01	76	10.3	7.9	335	128	5.5	14	24	3
Donor 02	91	15.7	13.13	361	137	3.6	7.4	17	7
Donor 03	116	11.2	8.9	366	134	4.3	12.4	21	15
Donor 04	100	10.5	6.9	366	133	5.3	13.6	25	5
Donor 05	84	4.5	2.5	381	135	4.2	3.3	16	3
Donor 06	87	18	15.7	455	128	5.9	14.3	19	9
Donor 07	82	13.3	11.6	249	134	4.1	14.3	14	5
Donor 08	126	7.6	5.2	279	137	4.5	4	32	8
Donor 09	112	18.9	15.3	489	130	3.5	1.6	15	6
Donor 10	128	9.7	7.5	281	127	4.4	7.8	32	9
Donor 11	108	18.3	15.09	410	134	4.4	2.4	17	13
Donor 12	100	17.5	13.62	398	134	5.1	4.7	19	7
Donor 13	93	5.1	2.2	314	138	4.5	5.5	34	11
Donor 14	98	6.4	4.1	145	128	3.5	4.4	25	42
Donor 15	105	7.5	5.5	339	138	4.3	7.1	32	6
Donor 16	102	5.4	3.54	167	137	4.8	8.1	25	5
Donor 17	106	9.7	5.8	358	138	4.5	3.7	25	8

Donor 18	108	13.4	8.71	362	132	4.7	5.9	20	5
Donor 19	92	14.5	12.27	521	131	4.6	4.5	20	7
Donor 20	83	7.9	3.76	587	124	4	2.9	19	6
Donor 21	95	15.9	13.95	216	135	4	10.9	13	11
Donor 22	119	9.1	7.3	392	121	5.6	12.6	30	7
Donor 23	124	17.3	14.3	475	125	4.5	4.6	23	19
Donor 24	93	24.7	19.8	483	129	5	8.2	28	5
Donor 25	150	11.2	10.67	181	139	5.2	14.8	25	13
Donor 26	114	18.9	16.74	330	135	4.4	9.1	23	12
Donor 27	122	9.5	6.7	263	137	5.1	5.1	31	7
Donor 28	117	10	7.4	606	138	4.5	3.8	25	7

8.5 Human qPCR Primer Sequences

Table 8.5: qPCR Primer Sequences

qPCR Primer Sequences (*Housekeeping genes)	
*Glyceraldehyde 3-phosphate dehydrogenase (GAPDH)	Left: TGCACCACAACTGCTTAGC Right: GGCATGGACTGTGGTCATGAG
*YWHAZ	Left: ACTTTTGGTACATTGTGGCTTCAA Right: CCGCCAGGACAAACCAGTAT
Homo sapiens S100 calcium-binding protein A7 (S100A7)	Left: ATTGAGAAGCCAAGCCTGCT Right: CCATGGCTCTGCTTGTGGTA
Homo sapiens S100 calcium-binding protein A8 (S100A8)	Left: CGAGCTGGAGAAAGCCTTGA Right: ACGGCATGGAAATTCCCCTT
Homo sapiens S100 calcium-binding protein A9 (S100A9)	Left: TCAAAGAGCTGGTGCGAAA Right: CAGCTGCTTGTCTGCATTTG
Nucleotide-binding oligomerization domain 2 (NOD2)	Left: GATGAAATCAGGTTGCCGAT Right: TAGAAGGAAGGCAGCCAATC
Human β-defensin-1 (hBD-1)	Left: CAGGTGGTAACTTTCTCACAGG Right: GGAGACCACAGGTGCCAATT
Toll like receptor 2 (TLR2)	Left: TCTCCCATTTCCGTCTTTTT Right: GGTCTTGGTGTTCATTATCTTC
C-type lectin domain family 7 member A(CLEC7A)	Left: CTTTCTCGGCCCCCAGACT Right: TTGGGTAGCTGTGGTTCTGA
Myeloid differentiation primary response 88(MYD88)	Left: CGGCAACTGGAGACACAAG Right: TCTGGAAGTCACATTCCTTGC
Ribonuclease A family member 7(RNASE7)	Left: GGAGTCACAGCACGAAGACCA Right: CATGGCTGAGTTGCATGCTTGA
Vascular Endothelial Growth Factor A (VEGFA)	Left: CTTGCTGCTCTACCTCCACC Right: ACTTCGTGATGATTCTGCCC
Cluster of differentiation 31 (CD31)	Left: TCCGGATCTATGACTCAGGG Right: CACTCCTTCCACCAACACCT

8.6 qPCR Product Primer Melt Curve

Primer specificity is demonstrated via melt curve analysis. During this process, the production of a single peak confirmed the amplification of a single product (**Figure 8.1**).

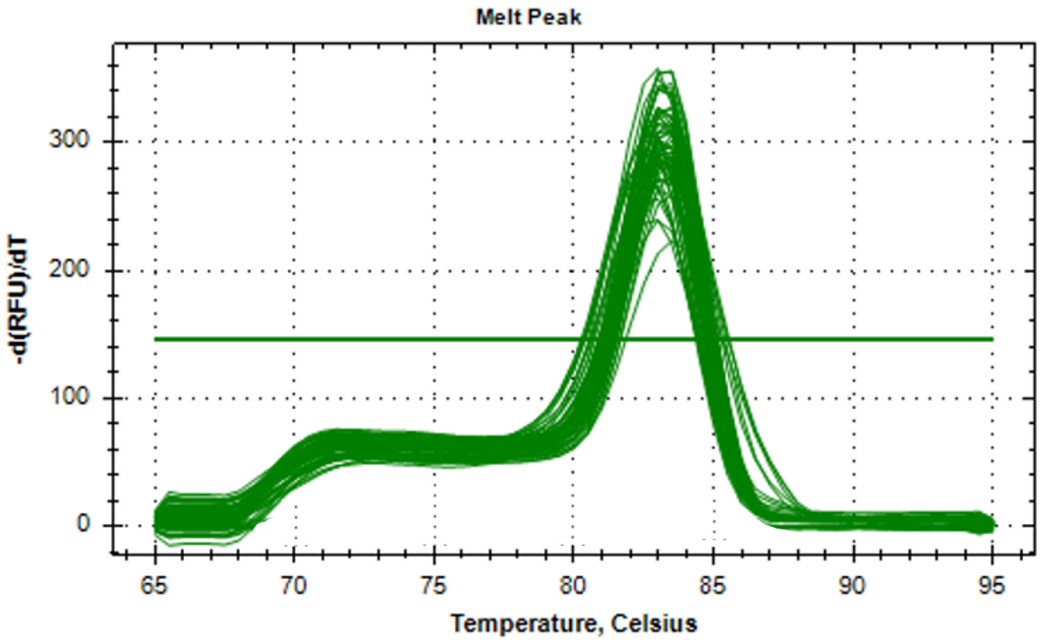

Figure 8.1: Consistent and single melt curve demonstrating primer specificity. Melt peaks demonstrate the alterations in fluorescence (y-axis) in combination with cycling temperature (x-axis). The formation of a single melt curve peak is consistent with the annealing of the primer at a set temperature and the amplification of a single product. qPCR data obtained from runs with multiple melt curve peaks were excluded from the analysis.

8.7 Goods Coverage Estimations

Goods coverage estimations describe the coverage estimation of present sample taxa i.e., OTUs with ≥ 1 sequence (8.1) (Table 8.6)

Table 8.6: Summary of Goods coverage estimation for all samples (ESWT pilot study).

DONOR	TIMEPOINT	NUMBER OF SINGLETONS (F1)	NUMBER OF SEQUENCES (N)	GOODS COVERAGE (%)
DONOR 01	Baseline (0 Weeks)	10	7	100
DONOR 01	Week One	3	59	94.91525424
DONOR 01	Week Six	6	536	98.88059701
DONOR 01	Week Twelve	24	1060	97.73584906
DONOR 02	Baseline (0 Weeks)	53	4758	98.88608659
DONOR 02	Week One	51	6371	99.19949772
DONOR 02	Week Six	48	27486	99.82536564
DONOR 02	Week Twelve	39	354	88.98305085
DONOR 03	Baseline (0 Weeks)	28	435	93.56321839
DONOR 03	Week One	8	21	61.9047619
DONOR 03	Week Six	2	11	81.81818182
DONOR 03	Week Twelve	21	1670	98.74251497
DONOR 04	Baseline (0 Weeks)	10	146284	100
DONOR 04	Week One	10	402742	100
DONOR 04	Week Six	55	12326	99.55378874
DONOR 04	Week Twelve	39	354	88.98305085
DONOR 05	Baseline (0 Weeks)	4	330284	99.99878892
DONOR 05	Week One	10	546874	100
DONOR 05	Week Six	43	582	92.61168385
DONOR 05	Week Twelve	42	67259	99.93755483
DONOR 06	Baseline (0 Weeks)	10	351	97.15099715
DONOR 06	Week One	7	207	96.61835749
DONOR 06	Week Six	12	8788	99.86345016
DONOR 06	Week Twelve	25	13897	99.82010506

8.8 Reagent Recipes

Dulbecco's phosphate-buffered saline (DPBS)

4.8g DPBS (Gibco, Thermo Fisher Scientific)

1L dH_2O

Autoclave to sterilise and store at 4°C

Mueller-Hinton agar (MHA)

19g Mueller-Hinton (OXOID) agar powder

500mL dH_2O

Autoclave at 121°C for 15 minutes then leave to cool until approximately 45-50°C

Pour to a depth of 4mm in Petri dishes (Thermo Fisher Scientific)

Mueller-Hinton broth (MHB)

Resuspend 2.1g Mueller-Hinton broth (OXOID)

100mL dH_2O

Autoclave at 121°C for 15 minutes

Tissue Fixation Solution

4.5g NaCl (Sigma-Aldrich)

0.25g ceramide (Sigma-Aldrich)

10ml acetic acid (Sigma-Aldrich)

40ml formaldehyde (Thermo Fisher Scientific)

500ml dH^2O

Citrate Buffer Recipe

180ml of dH^2O

3.18g of Citric Acid Monohydrate (Thermo Fisher Scientific)

Sodium Hydroxide to adjust to pH 6 (Thermo Fisher Scientific)

***Ex-vivo* staining wash buffer**

0.5% (v/v) Triton X-100 (Sigma-Aldrich)

500mL of PBS (Thermo Fisher Scientific)

***Ex-vivo* blocking buffer**

0.5% (v/v) Triton X-100 (Sigma-Aldrich)

0.2% (w/v) sodium Azide (Sigma-Aldrich)

2% (v/ v) goat serum (Sigma-Aldrich)

500mL of PBS (Thermo Fisher Scientific)

Standard HDF media

High glucose, no glutamine, no phenol red Dulbecco's Modified Eagle Medium (Gibco™)

10% heat-inactivated foetal bovine serum (v/v) (Gibco™)

1% L-glutamine (v/v) (Gibco™)

1% Penicillin-streptomycin (v/v) (Gibco™)

Standard HaCaT media

High glucose, no glutamine, no calcium Dulbecco's Modified Eagle Medium (Gibco™)

10% heat-inactivated foetal bovine serum (v/v) (Gibco™)

1% L-glutamine (v/v) (Gibco™)

1% Penicillin-streptomycin (v/v) (Gibco™)

1mM calcium chloride (Gibco™)

8.9 Neo-epidermal Length Quantification

Throughout the ex-vivo tissue analysis, the quantification of neo-epidermal length according to Keratin 6 was conducted by directly measuring the length of positive K6 IHC staining. Throughout, images of both the wounded area and the surrounding epidermal area were captured using the Nikon E400 Polarizing Light Microscope with SPOT camera and corresponding software. For neo-epidermal K6 tissue analysis, a X20 graticule image was used to set an accurate scale using the 'set scale' tool of Image J 1.5.2 software. Following this, the overall length and area measurement of both the right and left re-epithelised area surrounding the wound was measured (Figure 8.2).

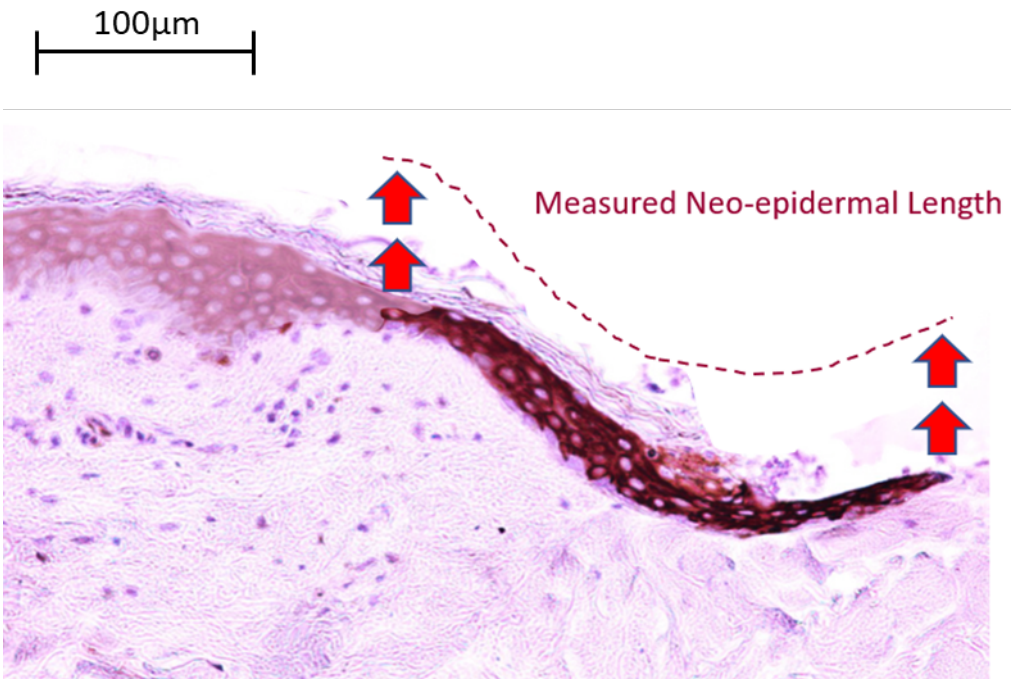

Figure 8.2: Method of quantifying neo-epidermal formation in the epidermis of *ex-vivo* wound tissue. Representative microphotographs (x200 total magnification) of FFPE tissue following staining for the presence of the Keratin 6 in ex-vivo wound biopsy tissue sections. Red arrows represent positive neo-epidermal IHC staining.